Master's thesis

NTNU
Norwegian University of Science and Technology
Faculty of Engineering
Department of Energy and Process Engineering

Martin Klevjer

Thermodynamic modelling of a water injected twin screw compressor for high temperature heat pumps

Master's thesis in Mechanical Engineering
Supervisor: Trygve M. Eikevik and Ruzhu Wang
October 2020

NTNU
Norwegian University of Science and Technology

Martin Klevjer

Thermodynamic modelling of a water injected twin screw compressor for high temperature heat pumps

Master's thesis in Mechanical Engineering
Supervisor: Trygve M. Eikevik and Ruzhu Wang
October 2020

Norwegian University of Science and Technology
Faculty of Engineering
Department of Energy and Process Engineering

NTNU
Norwegian University of
Science and Technology

Problem Description

Background and objective:
Combined cooling, heating and power generation system meets the need of low-carbon neighborhood to fully absorb renewable energy. A development of load peak-shaving technology of renewable energy based on solar energy with thermal energy storage (TES), as well as the new solar-thermal converting devices, with high-temperature heat pump and compact energy storage system (PCM). At the scenario of 100% clean energy, to achieve a high proportion of renewable energy acceptance by energy supply system in large public buildings or small-scale neighborhoods. In such systems it is necessary to develop high temperature electric heat pump using green or natural working fluid, which the hot side outlet temperature can reach 100°C, the temperature rise can exceed 50°C, and the COP of the heating system can exceed 3.5. A system using a water injected twin-screw compressor has been developed and fits this purpose. The results have been promising, and to further optimize this system, an accurate thermodynamic model should be developed. This project will focus on developing this model or simulation and compare the results with experimental data.

The following tasks are to be considered:
1. Literature review about compressors in high temperature heat pumps
2. Make a survey of the availability of compressors regarding pressures and temperatures
3. Define a case study for compressor in high temperature operation
4. Make a simulation program for the compressor dynamics
5. Compare simulation result with experimental results
6. Study the optimal design of the water-injected twin-screw compressor
7. Make a draft paper of the main results from the work
8. Propose further work

Summary

High-temperature heat pumps (HTHPs) are predicted to be an integral part of a more energy-efficient industry sector in the future (IEA, 2020). The main challenge in HTHP research is to find reliable, efficient compressors that can operate with low-global warming potential and zero ozone depletion potential refrigerants. This was investigated closely in this thesis. Consequently, a literature review of compressors used in HTHPs and the availability of compressors regarding temperature and pressure. The main task in the thesis was to make a simulation program for the compressor dynamics. A specific compressor from a research project at SJTU was investigated. The system has received international attention and is a very high-temperature heat pump (VHTHP) system with a water injected twin-screw compressor operated with water vapor as the refrigerant. One of the reasons why this project was chosen is that water is a natural, environmentally friendly refrigerant that is safe and reliable in operation due to its well known thermodynamic properties.

The twin-screw compressor with water injection shows good promise, and a thermodynamic model was developed to optimize the operation of the compressor. A study on the optimum amount of liquid injected, along with the distribution of liquid injected on three injection nozzles has been conducted. The thermodynamic model was developed in the Modelica programming language. It was based on another model used for an ammonia-water compressor. This makes the model more adaptable and allows for further modifications to fit other applications.

The model was validated against experimental data before the liquid-injection optimization study was conducted. The results indicate that when the compressor is investigated as an individual component, a higher amount of liquid injected leads to less compressor work. However, the output named compressor work is not the only indicator of how well the compressor is performing. The enthalpy of the discharged fluid is an important indicator of the heat capacity of the heat pump system. The model is used to perform a thermodynamic analysis to find the optimum amount of injection, which reduces compressor work without compromising heat capacity. Furthermore, the study indicates that the compressor performance differs depending on the distribution of the liquid injected. The general trend shows that a larger amount of liquid injection early in the process is beneficial for the performance of the compressor.

Sammendrag

Det anslås at høytemperaturs varmepumper skal være en vesentlig del av en grønn industrisektor i fremtiden (IEA, 2020). Hovedutfordringen for høytemperaturs varmpepumper er å finne pålitelige og effektive kompressorer som kan drives med kjølemedium som har lavt GWP og null ODP. Denne oppgaven undersøker hvordan man kan overkomme denne utfordringen. I den forbindelse har et literaturstudie på kompressorer brukt i høytemperaturs varmepumper blitt utført, samtidig som begrensingene til dagens kompressorer i forhold til trykk og temperatur har blitt undersøkt. Hoveddelen av oppgaven var å lage en simuleringsmodel for en kompressors dynamikk. En spesifikk kompressor utviklet i et forskningsprosjekt ved SJTU ble undersøkt. Høytemperaturs varmepumpesystemet har fått internasjonal annerkjennelse og er et veldig-høytemperaturs varmepumpesystem som bruker en vanninjeksjons skruekompressor, og drives med vanndamp som kjølemedium. En av åraskene til at dette systemet ble valgt er at vann og vanndamp er et naturlig, miljøvennlig kjølemedium som kan drives trygt og pålitelig. Vanndamp har veldig kjente og utforskede termodynamiske egenskaper.

Skurekompressoren med vanninjeksjon er en lovende teknologi, og en termodynamisk model ble utviklet for å kunne optimalisere driften av kompressoren. Et studie for å finne den optimale mengden vanninjeksjon, samt et studie for å finne fordelingen av injeksjonstrømmen i tre injeksjonsdyser i kompressoren ble utført. Den termodynamiske modellen ble laget i simuleringsprogrammet Modelica. Modellen er basert på en tidligere utviklet ammonium-vannkompressor. Dette øker fleksibiliteten til modellen og kan åpne for at modellen lett kan justeres til å passe andre kompressorer.

Modellen ble validert mot eksperimentelle data før optimaliseringstudiene av vanninjeksjon ble utført. Injeksjonsstudien indikerer at dersom kompressoren er analysert som en enkeltstående komponent vil høyere vanninjeksjon redusere kompressorarbeidet. Dersom et helt varmepumpesystem er analysert kommer det fram at det er noen nedsier ved store mengder vanninjeksjon som ikke kommer fram dersom man bare fokuserer på kompressorarbeid fra simuleringen. Dersom man studerer de termodynamiske betingelsene i fluidet som kommer ut av kompressoren kan man finne en optimaltilstand og derfor en optimal mengde med vanninjeksjon. Studiet for å finne fordelingen av vanninjeksjonstrømmer viser at dette er en faktor som er påvirker både kompressorarbeidet og de termodynamiske betingelsene for fluidet som går ut av kompressoren. Trenden viser at mer vann injesert tidlig i kompressoren fører til lavere kompressorarbeid.

摘要

高温热泵（HTHPs）预计将成为未来能效更高的工业部门的重要部分（IEA，2020）。就高温热泵而言，其研究的主要挑战是研发能够匹配低 GWP 和零 ODP 制冷剂的可靠、高效的压缩。由此，本文对此展开了深入研究。

因此，本文对对应温区下的的压缩机以及压缩机的高温热泵应用场景下可用性进行了文献综述。本文的主要任务是压缩机动态仿真程序的编制，主要基于上海交通大学某研究项目中的一种特殊压缩机展开研究。该系统是一种以水为制冷剂、采用喷水双螺杆压缩机的超高温热泵系统，也受到了国际上的广泛关注。水是一种天然环保的制冷剂，其热力学性质优异且运行安全可靠，这也是我们选择该研究的原因。采用液态水喷射技术的双螺杆压缩机具有良好的应用潜力，由此我们建立了对应的热力学模型用于优化压缩机的运行性能。具体而言，本文研究了三种喷嘴的最佳注液量及其分布情况，其中热力学模型是基于 Modelica 语言开发的。该模型是基于另一个用于氨水压缩机的模型。经过修改，这个模型变得更具适应性和拓展性。

在进行喷液优化前，我们首先采用实验数据对构建模型进行了验证。结果表明，将压缩机作为一个单独的部件进行研究时，其压缩腔内注入的液体量越大，所对应的压缩功就越小。然而，压缩功并不是唯一一个可以反应压缩性能的指标，排出蒸汽的焓值也是衡量热泵制热量的重要指标。该模型可以进一步用于热力学分析，以确定最佳的喷射量，在不影响整机制热量的情况下降低压缩功。此外，研究还表明，喷射水的分布情况将进一步影响压缩机的性能。总体趋势表明，在压缩机运行早期，大量喷射水的注入有助于提升压缩机的性能。

Preface

This master thesis is the final part of a 2.5-year dual-master degree program at Shanghai Jiao Tong University (SJTU) and Norwegian University of Science and Technology (NTNU). The work was conducted at the Institute of Refrigeration and Cryogenics at SJTU, and the Department of Energy Process and Engineering at NTNU. My supervisors have been Prof. Ruzhu Wang (SJTU) and Prof. Trygve M. Eikevik (NTNU).

The main objective of the thesis was to make a thermodynamic model of a water-injected twin-screw compressor used for high-temperature heat pump applications. This model can be used to investigate and optimize the thermodynamic performance of a twin-screw compressor. It has been an interesting project, and I have been lucky to get to work on a state of the art project with excellent scholars and researchers. I hope that this work can be used to further optimize the operation of compressors used in high-temperature heat pumps.

In addition to thanking my supervisors for providing me the opportunity to work on an interesting project, I would like to thank my co-supervisor from SJTU Dr. Bin Hu, and Ph.D. candidate Wu Di for support and help with both practical and technical questions. Furthermore, Marcel Ahrens' support, understanding, and encouragement have been outstanding. I would also like to thank my fellow dual-degree student Signe Truyen Ryssdal for supporting me throughout the entire project. Lastly, I appreciate that my family has supported me throughout my education.

Table of Contents

List of Figures

List of Tables

Nomenclature

Symbols		**Units**
$\dot{Q}$	Heat transfer rate	$\frac{J}{s}$
$\dot{V}$	Volume flow rate	$\frac{m^3}{s}$
$\dot{W}$	Power	$\frac{J}{s}$
$\dot{m}$	Mass flow rate	$\frac{kg}{s}$
h	Specific Enthalpy	$\frac{J}{kg}$
t	Time	s
A	Cross-sectional area	m^2
C	Specific Heat or Coefficient	$\frac{J}{Kg*K}\ or -$
D	Diameter	(m)
N	Number of (rotations)	$-$
Q	Thermal Energy	J
R	Gas constant	$-$
T	Temperature	K
V	Volume	m^3
W	Work	J
der	Derivative of	$-$

m	Mass or number of lobes	$kg\ or -$
p	Pressure	Pa
q	Heat exchange	$\frac{J}{kg}$
u	Specific internal Energy	$\frac{J}{kg}$
x	Mass fraction of second fluid	$-$

Greek Symbols		**Units**
Δ	Difference between two conditions (Temperature)	$-$
Π	Volume ratio	$-$
α	Heat transfer coefficient	$\frac{W}{m^2K}$
β	Angle	$^0\ or\ rad$
η	Efficiency	$-$
θ	Rotational angle	rad
κ	Isentropic exponent	$-$
ν	Specific volume	$\frac{m^3}{kg}$
π	Constant number (3.14)	$-$
ρ	Density	$\frac{kg}{m^3}$
τ	Rotation (twist)	^{0}
ψ	Aspect ratio	$-$
ω	Rotational speed	$\frac{^0}{s}$

Subscripts

0	Total volume (of the compressor)
1	Suction condition or male (lobe)
2	Discharge condition
$high$	High (highest out of two comparable)
A	Area of use
act	Actual
bod	Compressor body
c	Constituent of the working fluid
cav	Cavity
$comp$	Compressor
$cond$	Condenser
$dish$	Discharge

eff	Effective
f	Fraction
$ideal$	Ideal
inj	Injection
is	Isentropic
$isen$	Isentropic
$leading$	Leading (cavity)
$leak$	leakage
$loss$	Loss
low	Low (lowest out of two comparable)
p	Constant pressure
$port$	Inlet or outlet port of a component
rpm	Rotations per minute
$shaft$	Shaft
$suct$	Suction
th	Theoretical
$trailing$	Trailing (cavity)
v	Volumetric
v	Constant Volume
w	Wrap angle
φ	Twist angle

Abbreviations

CFC	ChloroFluoroCarbon
CFD	Computational fluid dynamics
COP	Coefficient of performance
GWP	Global warming potential
$HACHP$	Hybrid absorption compression heat pump
$HCFC$	HydroChloroFluoroCarbon
HFC	HydroFluoroCarbon
HFO	HydroFluoroOlefins
$HTHP$	High-temperature heat pump
HTS	High temperature stage

IHX	Internal heat exchanger
LTS	Low temperature stage
MVC	Mechanical vapor compression
MVR	Mechanical vapor recompression
$MVRHP$	Mechanical vapor recompression heat pump
ODP	Ozone depletion potential
SRM	Svenska rotor maskiner
VCC	Vapor compression cycle
$VHTHP$	Very high-temperature heat pump

1 Introduction

1.1 Motivation

Global energy demand is on the rise (Equinor ASA, 2019), and at the same time, climate change is becoming more and more prominent. The need for energy effective solutions is a focus in all energy-consuming sectors. Heat demand represents about 50% of the energy end-use, larger than any other category. Over half of this is consumed in the industry; process heat, drying, and industrial hot water are some examples of heat used in industry (IEA, 2020). Keeping in mind that energy production accounts for 72% of greenhouse gas emissions (World Resources Institute, 2017), increasing the energy efficiency in the industrial sector will have a major impact on greenhouse gas emissions. Heat pumps are the most energy-efficient heat providing technology on the market today. Almost 80% of heat provided comes from fossil-fuel or less efficient conventional electric heating while heat pumps cover only 5% of the heat demand. According to (IEA, 2020) heat pumps should cover 22% of the heating demand in 2030 to stay on track with the sustainable development scenario. Consequently, heat pump technology must be further developed so the market share increases.

Another reason to implement heat pumps in the industry is that most green and renewable energy resources create electrical energy (solar PV, wind, and hydro). This will lead to an increase in the overall efficiency of the electrically driven heat pumps. In today's fossil-fueled society, a lot of energy is lost in the process of creating electricity from fossil fuel. The average coal-based power plants operate with an efficiency of under 40% (LLC, 2017). Renewable power plants like wind-, hydro-, and solar PV plants produce electricity directly, which indicates that heat pump technology will become even more desirable when implemented with green renewable energy sources. Heat pumps are already integrated into residential buildings all around the world. In recent times the research on high-temperature heat pumps(HTHPs) for industrial purposes has received a lot of attention, but there are still some challenges that need to be solved before heat pumps become the go-to heating technology in most industrial applications.

Technical improvements must be made to ensure safe, reliable, and efficient operation of heat pumps. Economically viable components must be developed to handle the high temperatures and pressures that are required for HTHP-operation. The component with the highest power consumption and also the highest potential for energy savings in a heat pump system is the compressor (Haugland, 1993). One step in the process of improving today's compressor technology is to investigate the thermodynamic operation of cutting edge HTHP-application compressors. In this thesis, a thermodynamic model of a water-injected twin-screw compressor with water vapor will be developed and verified against experimental data. This will increase the understanding of the operating challenges in the compressor. Furthermore, the model can be used as a cheap and efficient measure to optimize the operation of said compressor.

1.2 Objectives

This report will focus on compressors used in HTHP systems. The principle behind heat pumps will be described. The advantages and disadvantages of twin-screw compressors in heat pumps together with their compatibility of operating in high temperatures range is presented. An overview of the limitations and possibilities of various compressors in HTHPs together with a literature review of research groups implementation of various compressors in HTHP application will be provided. Systems using safe, low GWP (Global Warming Potential) and low ODP (Ozone Depletion Potential) refrigerants will be the main focus of the report. A preliminary case study of a water-injected twin-screw compressor with water as a refrigerant is then carried out. A thermodynamic model of a water-injected twin-screw compressor has been developed and will be thoroughly described. The model is then verified against experimental data from a prototype twin-screw compressor from Shanghai. The model is then used to test various injection parameters to see if the injection can be optimized to lower the compressor power consumption.

2 Working Principle and Components of High-Temperature Heat Pumps

2.1 High-temperature heat pump theory

The definition of a high-temperature heat pump varies slightly, but in general, it can be defined as a heat pump with a condensation temperature exceeding 80ºC. As technology is advancing, the need for further specification of heat pumps is necessary. The term very high-temperature heat pump (VHTHP) is currently defined as heat pumps with heat sink temperatures over 100ºC (Arpagaus, Bless, Uhlmann, Schiffmann, & Bertsch, 2019) and (Mateu-Royo, Navarro-Esbrí, Mota-Babiloni, Molés, & Amat-Albuixech, 2019). This report will not distinguish between HTHP and VHTHP in any other way than what a system is defined as in its source. Heat pumps with condensation temperatures exceeding 80ºC will be referred to as HTHPs in this report. The categorization of heat pumps can be seen in Figure 2.1.

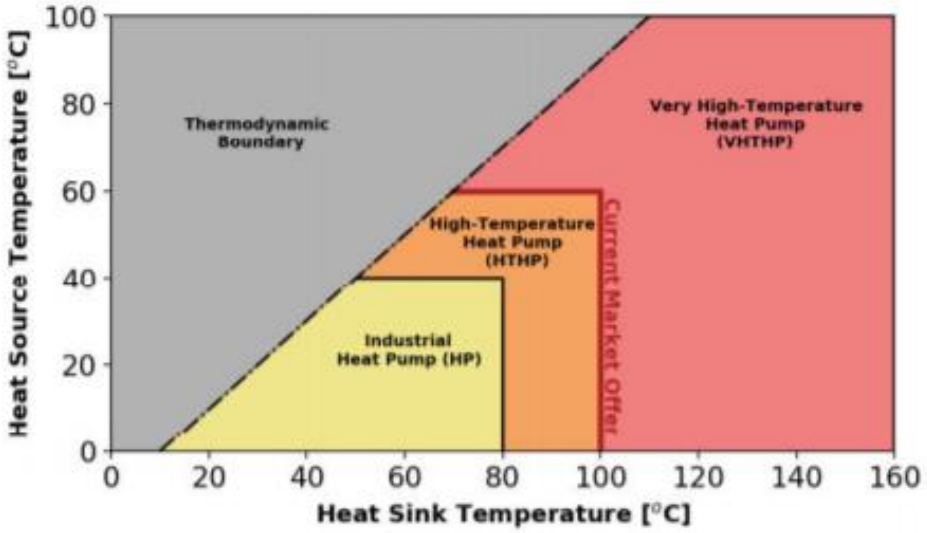

Figure 2.1 Categorizing of Heat Pump temperature zones (Mateu-Royo, Navarro-Esbrí, Mota-Babiloni, Molés, & Amat-Albuixech, 2019).

When designing a heat pump system, many considerations must be made. A heat pump should not only perform in a highly efficient manner, but safe and reliable operation without high maintenance costs is important. Furthermore, there are many requirements for the refrigerant used in the system. Specific volume, critical point (temperature and pressure), chemical composition, and latent heat are some of the thermodynamic properties that must be considered when selecting a refrigerant. Ideally, the system should operate with a fourth-generation refrigerant. Fourth-generation refrigerants have low or zero GWP and ODP.

The compressor is the heart of a heat pump. This is where the majority of the energy is provided to the system. However, this is also where the lowest efficiencies occur, and consequently, compressors represent a limiting factor in HTHPs. High discharge temperatures and high pressure may lead to extra material constraints. High superheat also leads to lower operating efficiency of a heat pump system. If regular compressors are run outside of their specified operating range (temperature and pressure) damage is likely to occur (Bamigbetan O. , Eikevik, Nekså, Bantle, & Schlemminger, 2019). These issues must be solved by adjusting already existing compressors or designing new compressors. There are various compressor technologies and finding the most suitable technology for high temperature and pressure application is therefore a priority.

For HTHP systems to increase their market share of today's heating applications in industry, there are more barriers than just the technical challenges: There is currently a low level of awareness of HTHP solutions and applications in the industry. To change this HTHP solutions must be presented to costumers, along with consultants and investors (Arpagaus, Bless, Uhlmann, Schiffmann, & Bertsch, 2019). Since the technology is relatively new, standard solutions for specific applications is yet to be made, each system must be tailor-made for the application in question. This leads to increased costs, which again results in a longer pay-back period. Consequently, HTHPs experience a competitive disadvantage, especially when the pay-back period of competing technologies is short (typically less than three years). It can be difficult to compare HTHP with fossil-fueled technologies from an economic point of view, due to the ever-changing oil-, coal- and electricity price. Changing from traditional heat sources will also lead to re-training of employees which is an additional cost. It is therefore of importance that new heat pump systems are economically viable while being more energy-efficient and sustainable than today's solutions.

2.2 Working Principle of a vapor compression heat pump

A heat pump is a system that takes heat from one space with relatively low temperature (heat source) and uses energy to increase the temperature and deliver heat to a space with higher temperature (heat sink). A heat pump can be used both to cool the heat source and provide heat to the heat sink. While air and water are the two most common heat sources and heat sinks, various mediums can be used. A variety of heat pumps exists, and they can be categorized as capacity enhancing heat pumps or temperature lifting heat pumps. They can also be categorized as electrically driven (Vapor compression heat pump) or thermally driven (absorption heat pump or adsorption heat pump). Vapor compression heat pumps for heating applications are the focus in the report and will be further described here.

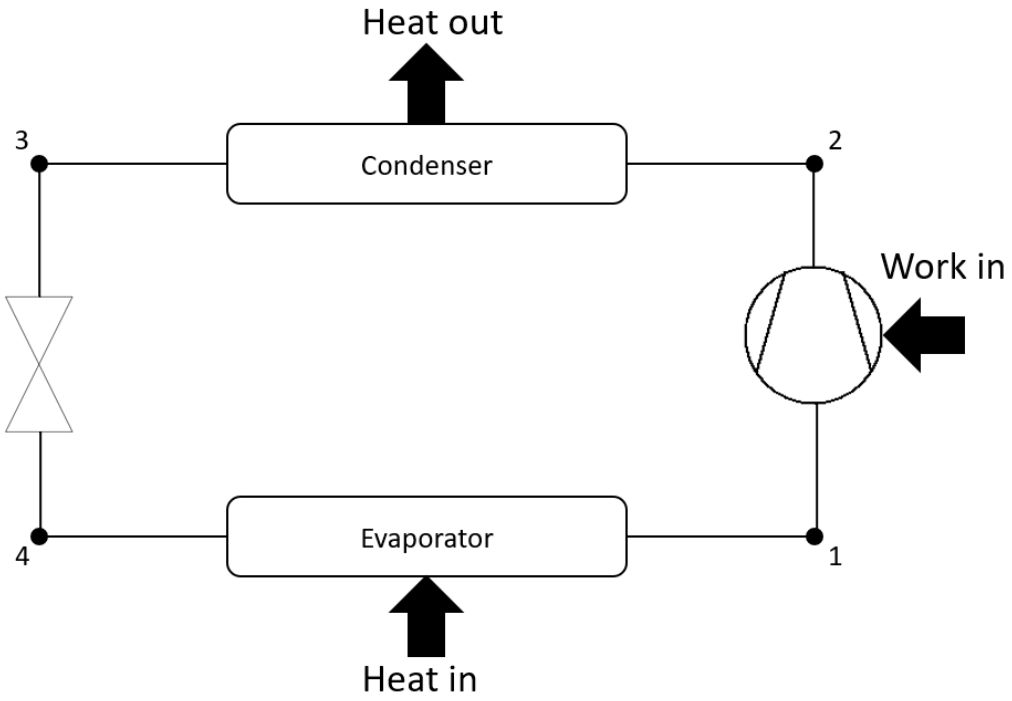

Figure 2.2 Compression heat pump schematic

Vapor compression cycle (VCC) is the most commonly used heat pump system. It utilizes the latent heat of phase change in a closed cycle to enhance the heat transfer, a schematic of a basic VCC can be seen in Figure 2.2. The refrigerant enters the evaporator at a lower temperature than the heat source. Heat is transferred from the heat source and the refrigerant evaporates, before exiting the evaporator in a vapor state (state 1). The refrigerant is then compressed to a higher pressure and temperature level by a compressor and it remains in vapor condition (state 2). The refrigerant will then deliver heat to a heat sink with a lower temperature than the refrigerant through a condenser (heat exchanger). Heat is transferred from the refrigerant; it will cool back into liquid-phase (state 3). Before it is expanded back to the initial pressure level (state 4) by a pressure decreasing device, typically a valve. This describes the most basic closed vapor compression heat pump cycle, and although many different heat pump configurations take advantage of a variety of components, all vapor compression cycles are built on the same principle.

The performance of a heat pump is typically measured in COP (Coefficient of Performance). This is the ratio of heat supplied by a heat pump (Q_{cond}) to the work input (W_{comp}) to the heat pump (Eq 2.1). As long as the COP is higher than one the system itself is more efficient than traditional heating methods. However, when the total efficiency of the heat supplied is calculated, it is necessary to keep in mind how the electricity is generated. If it is obtained from fossil-fueled sources the efficiency of the power plant must be considered as well. This will naturally mean a lower overall performance of the heat provided.

$$\boldsymbol{COP = \frac{Q_{cond}}{W_{comp}}} \ (-) \qquad \textbf{Eq 2.1}$$

Figure 2.3 shows the vapor compression cycle in a temperature-enthalpy diagram. The losses associated with the components along with the thermodynamic processes are labeled. It is worth noting that the heat provided to the heat sink (Q_{cond}) will be at the interception line between the upper part of the minimum theoretical work and the heat exchanger loss.

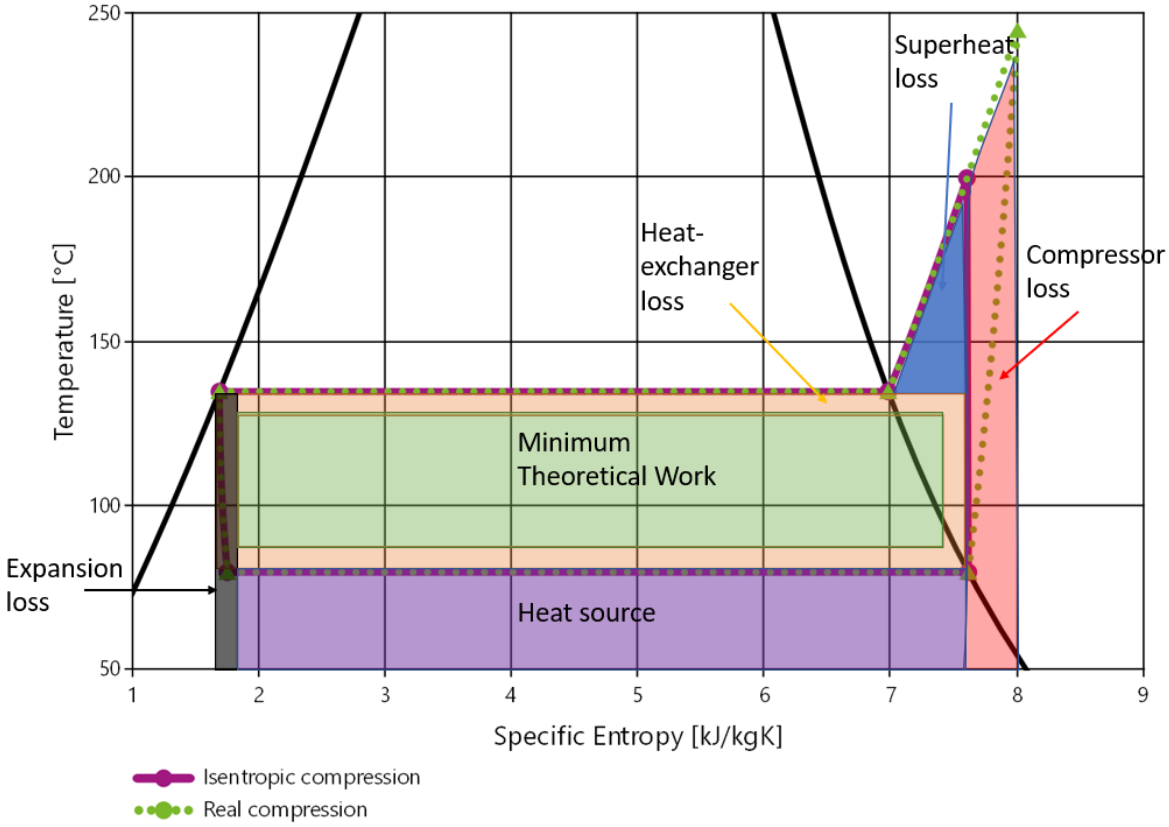

Figure 2.3 Temperature-entropy diagram showing losses associated with heat pump

2.3 Compressor Theory

A compressor is one of the main components of a heat pump. The purpose of a compressor in a heat pump is as mentioned to compress the refrigerant so that the pressure increases from the evaporation pressure to the desired condensation pressure.

2.3.1 Compressor categorization

There are various configurations of compressors in heat pumps. They depend on the temperature lift, range, and refrigerant. Compressors can be split into three different groups: hermetic, semi-hermetic, and open compressors. The hermetic compressor is completely enclosed by a welded casing. A semi-hermetic compressor also is enclosed by a casing, but this casing is screwed together. An open compressor is naturally not enclosed by a casing and has the motor as an open part. There are disadvantages and advantages to all three kinds. The main reason to have a compressor enclosed by a casing is to avoid shaft seal leakage. All maintenance and repair work is more challenging in a hermetic and semi-hermetic compressor (Eikevik, 2019).

From an operational point of view, compressors are typically categorized as either positive displacement compressors or dynamic working compressors, depending on the working principle (Eikevik, 2019). Positive displacement compressors increase the pressure of a gas by mechanically decreasing the volume the gas is encapsulated in. Common examples of positive displacement compressors are piston compressors, screw compressors, and scroll compressors. All positive displacement compressors suffer from similar losses. However, the magnitude of the losses depends on the type of compressor (Woolatt & Heidrich, 2001). Dynamic working compressors elevate the pressure of a gas by accelerating gas into high velocity before the kinetic energy is transformed into pressure energy in a device (typically a diffuser). A turbo compressor is an example of a dynamic working compressor.

2.3.2 Theoretical work and discharge temperature of an ideal gas

As the pressure and temperature of any fluid are lifted from one level to another, certain thermodynamic laws apply to the process. The main part of these laws is outlined here:

The isentropic exponent (κ) can be shown accordingly.

$$\boldsymbol{\kappa = \frac{C_p}{C_v}\ (-)} \qquad \textbf{Eq 2.2}$$

Where C_p is the specific heat at constant pressure, while C_v is the specific heat at constant volume. The specific heat varies depending on the gas. The gas constant (R) is dependent on these coefficients according to the following relationship:

$$\boldsymbol{R = C_p - C_v\ (\frac{J}{Kg * K})} \qquad \textbf{Eq 2.3}$$

Figuring out the theoretical work (W_{th}) needed to compress the fluid is necessary to calculate the efficiency of the compressor.

$$\boldsymbol{W_{th} = p * V\ (J)} \qquad \textbf{Eq 2.4}$$

Work is the product of the change in pressure (p) and volume (V). The volume of interest is the working chamber volume. The volume is the product of the area and length. Work is performed in three different parts of the cycle. The main part is the compression itself from evaporation pressure to condensing pressure, the volume of the chamber changes with time and is therefore described as an integral. The second part is when the gas is pushed out of the working chamber, and the third part is the gas getting sucked into the working chamber. The three parts are included in Equation 2.5. Suction and discharge are represented by subscript 1 and 2 respectively.

$$\boldsymbol{W = \int_1^2 p\, dv - p_2 * V_2 + p_1 * V_1 (\frac{J}{cycle})} \qquad \textbf{Eq 2.5}$$

Once the integral is carried out the work can be found as followed.

$$W = -\frac{k}{k-1} * p_1 * V_1 * \left[\left(\frac{p_2}{p_1}\right)^{\frac{k-1}{k}} - 1\right] \left(\frac{J}{cycle}\right) \quad \textbf{Eq 2.6}$$

Eq 2.6 shows work per cycle. To make work per cycle into work per second, the equation should be divided by mass per cycle and multiplied with mass per second.
One of the limiting factors in high-temperature heat pumps is the discharge temperature. High discharge temperatures may lead to extra constraints in material selection, and superheating the refrigerant is inefficient from a thermodynamic perspective. The discharge temperature can be calculated by applying the gas laws.

$$T_2 = T_1 * \left(\frac{p_2}{p_1}\right)^{\frac{k-1}{k}} (K) \quad \textbf{Eq 2.7}$$

Combining the equations above makes the specific work (w) equation the following.

$$w = -\frac{k}{k-1} * p_1 * V_1 * \left(\frac{T_2}{T_1} - 1\right) \left(\frac{J}{kg}\right) \quad \textbf{Eq 2.8}$$

2.3.3 Efficiencies and actual work

Several efficiencies affect the performance of a compressor. Isentropic efficiency of a compressor is defined as work input in an isentropic process over the work input in an actual process. An isentropic process is an ideal thermodynamic process that is both adiabatic and reversible. Volumetric efficiency is also a very important factor when analyzing a compressor. This efficiency is a result of the geometric configuration of the compressor. In a screw compressor, the leakage between an enclosed cavity or discharge chamber to the suction chamber is a volumetric loss.

Furthermore, there are mechanical losses in a compressor. These losses are taken into account by mechanical efficiency and consist of mechanical friction that slows down the speed of the compressor compared to the energy input. Depending on how the compressor is run, an electrical efficiency from an electric motor could affect the total efficiency/losses. Neither of these two efficiencies will be discussed in detail in this paper. The actual work can easily be measured in a prototype or a finished compressor. Several models and simulations can estimate the actual work input to a compressor. The model and simulation approach should be selected based on what type of compressor is to be evaluated.

2.3.4 Screw Compressor

Screw compressors can be further divided into two categories, traditional twin-screw compressors and more recently developed mono-screw compressors. This chapter will look at the traditional twin-screw compressor. The twin-screw is more mature and has a higher market share than the mono-screw compressor, and it is also the screw compressor most widely used in high-temperature heat pumps. Both the twin-screw and mono-screw compressors fall under the sub-category rotary compressors of positive displacement.

Working principle

The main components in a twin-screw compressor are two helically geared rotors, surrounded by a casing. The rotors are called male (rotor with lobes) and female (rotor with concave cavities) rotors. Gas is trapped between the male lobe, the female cavity,

and the casing. In the first half of the compressor, the volume, which will be filled with fluid, will increase. In the second half of the process, the pressure of the gas will increase as the enclosed volume decreases. The pressure field varies with time and location within each gas pocket. A visual representation of the compression side of a twin-screw compressor can be seen in Figure 2.4.

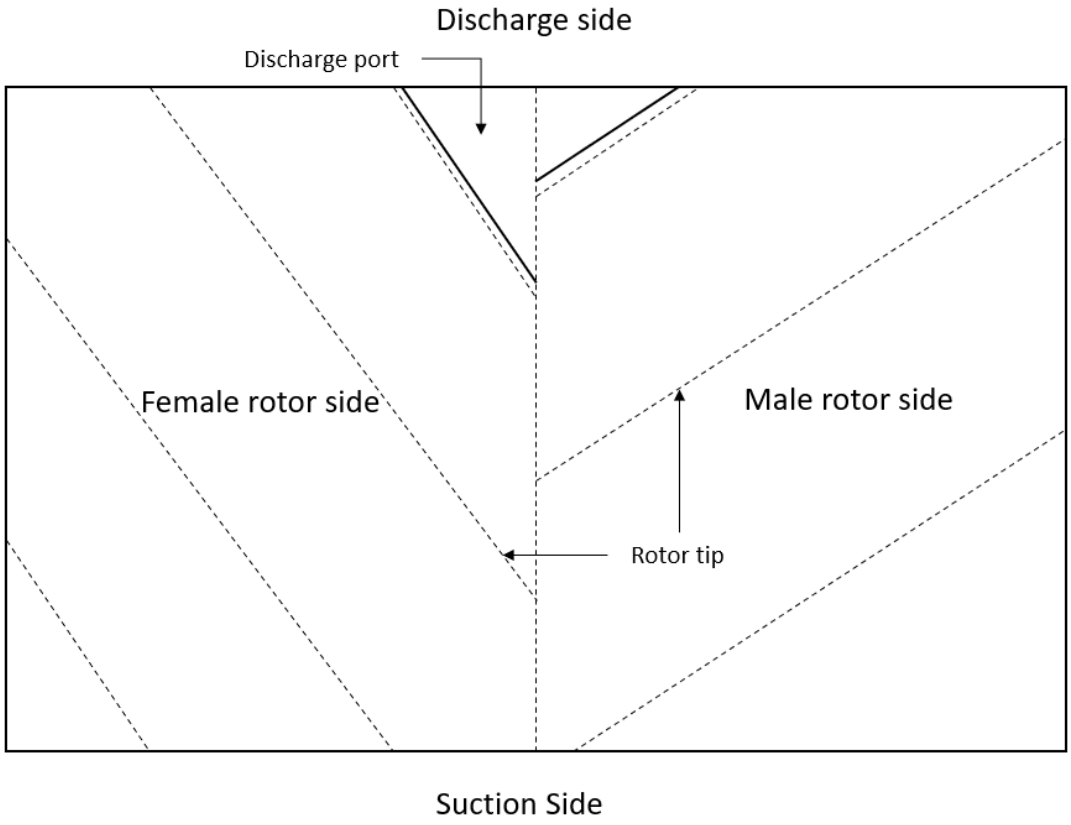

Figure 2.4 Compression side of the twin-screw compressor

Screw compressors are typically divided into oil-free and oil-injected compressors. There are advantages and disadvantages to both types. The compressor preferred is dependent on the operating working fluid, temperature, and pressure. If a refrigerant that should not be contaminated with oil is used, an oil-free compressor should be selected. In an oil-free compressor, there is a need for a matching gear between the female and male rotor, as direct contact between the two will lead to deformation or damage of the rotors, which again will lead to a decreased performance of the compressor. If there is an oil film between the rotors, as it is in oil-injected rotors, the female rotor can be driven by the male rotor, with a protective film of oil preventing direct contact between the rotors. Oil-injected screw compressors are also more sensitive to the formation of liquid in the screw compressor. If liquid refrigerant is accumulated in the screw compressor, it may dilute the oil and prevent the sealing effect and even worse, the lubrication (Horn & Scharf, 1976).

Performance

Screw compressors have a built-in volume ratio or internal compression ratio (Π). The ratio is the volume at the inlet port (V_1) over the volume at the outlet port (V_2). There is no clearance volume, which means that all gas that enters the compressor will ideally leave the compressor at a higher pressure. However, if the suction pressure is low, the

compressor can experience gas flowing back through the suction port. Leakage from high-pressure or discharge chamber to low-pressure cavities or suction chamber will also decrease the efficiency (Fleming & Tang, 1995).

$$\boldsymbol{\Pi} = \frac{\boldsymbol{V_1}}{\boldsymbol{V_2}} (-) \qquad \textbf{Eq 2.9}$$

The most significant thermofluidic loss is internal gas leakage (Fleming & Tang, 1995). Due to manufacturing tolerances, there must be a clearance between the two rotors, as well as between the rotors and the casing. Without this clearance, the rotors can make contact with each other or the casing which will lead to higher power consumption and noise. More significantly, it may lead to damage to the rotor or casing. As mentioned, injected oil has a significant sealing effect. Oil injected compressors can, therefore, achieve higher volumetric efficiencies without affecting the lifetime of the equipment. The volumetric efficiency (η_v) is the actual volume flow rate ($\dot{V}_{act}$) divided by the ideal volumetric flow rate ($\dot{V}_{Ideal}$). Where the ideal volumetric flow rate can be seen in Eq 2.11.

$$\boldsymbol{\eta_v} = \frac{\dot{\boldsymbol{V}}_{\boldsymbol{act}}}{\dot{\boldsymbol{V}}_{\boldsymbol{ideal}}} \textbf{(-)} \qquad \textbf{Eq 2.10}$$

$$\dot{\boldsymbol{V}}_{\boldsymbol{ideal}} = \boldsymbol{C_\varphi C_A \omega \psi D^3} \textbf{(m}^\textbf{3}\textbf{/s)} \qquad \textbf{Eq 2.11}$$

$C\varphi$= Coefficient of the twist angle (-)

C_A= Coefficient of the usage area (-)

ω= rotational speed (degree/s)

ψ=aspect ratio (-)

D= Diameter (m)

Another important efficiency is isentropic efficiency (η_{is}) and can be calculated according to Eq 2.12 and Eq 2.13 (Hsieh, Shih, Lin, & Tsai, 2011). Where Eq 2.13 is similar to Eq 2.6, but with volumetric flow rate instead of volume per cycle.

$$\boldsymbol{\eta_{is}} = \frac{\dot{\boldsymbol{W}}_{\boldsymbol{is}}}{\dot{\boldsymbol{W}}_{\boldsymbol{shaft}}} \textbf{(-)} \qquad \textbf{Eq 2.12}$$

$$\dot{\boldsymbol{W}}_{\boldsymbol{is}} = \frac{\boldsymbol{k}}{\boldsymbol{k-1}} \boldsymbol{P_1 \dot{V}_{act}} \left(\left(\frac{\boldsymbol{P_2}}{\boldsymbol{P_1}} \right)^{\frac{\boldsymbol{k-1}}{\boldsymbol{k}}} - \boldsymbol{1} \right) \textbf{(W)} \qquad \textbf{Eq 2.13}$$

Finding the right clearance is important to make sure that the leakage is limited without unwanted contact between parts in the assembly. Due to the development of manufacturing technologies, clearances can be tighter now than ever. It is also cheaper to produce high precision rotors and casing. As the clearance is tighter, the assembly is more vulnerable to deformation. Consideration of deformation is especially important a high pressure and temperature applications, as thermal deformation is more likely to occur (Husak, Kovacevic, & Karabegovic, 2019).

One of the main advantages of screw compressors is that they can achieve relatively high efficiencies at high-pressure ratios. One of the reasons for this is that fluid (either refrigerant or oil) can be injected in several places throughout the compression. Since the temperature is controlled by the injection, the amount of superheat is limited and the compression will be closer to an isothermal process (Guangbin, et al., 2019). This can both increase the seal between the separate cavities and control the temperature of the compressed fluid. Another advantage compared to a piston compressor is that a screw compressor has a continuous flow of the medium which leads to less pulsation of the discharged refrigerant. Screw compressors are therefore a better fit when continuous operation is desirable.

If the condensing or evaporating temperature fluctuates, the compressor may be required to operate at off-design pressure ratios. Since a screw compressor has a built-in volume ratio it can be challenging to operate at off-design conditions. For example, if the gas is over-compressed (i.e. the gas is compressed to a higher pressure than the condensing pressure) the compressor performs more work than necessary, which leads to lower efficiency of the compressor. Similarly, if the compressor under compresses the gas, the pressure in the condenser is higher than the discharge pressure, and the gas will flow back into the compressor. The gas will then be compressed again, which leads to extra work as a result of more mass flow rate in the compressor (Eikevik, 2019). Ideal-, over-, and under-compression are visualized in Figure 2.5. For all of the cases visualized the condensation pressure is 2.5 bar and the evaporation pressure is 0.6 bar. The pressure ratio changes from approximately 2 (green dashed line), 4.17 (blue solid line), and 6 (red dotted line).

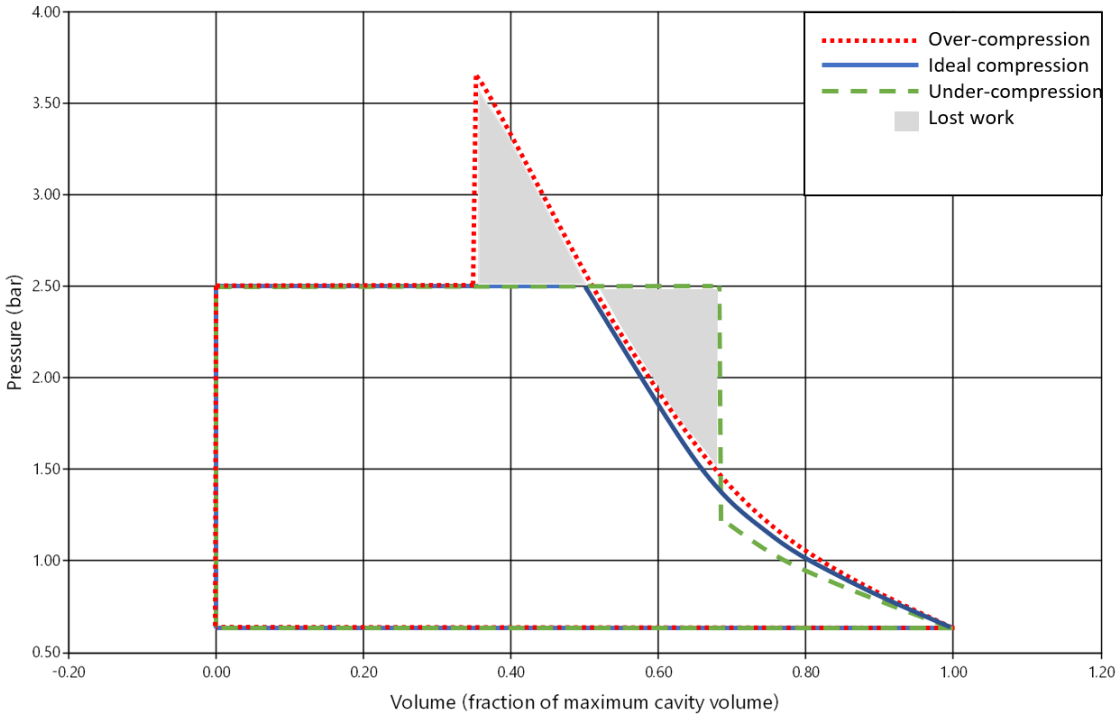

Figure 2.5 Pressure-volume diagram of over-compression, ideal compression, and under-compression

A compressor may also have to operate in a variety of capacities. There are several ways to do this for a screw compressor. If several screw compressors are working in parallel,

the capacity can be regulated by switching on or off compressors, similarly to all other compressor types. Another solution is slide regulation. If the screw compressor has a slide regulation option (by-pass valve at the inlet) it can decrease the capacity down to about 10% of the designed capacity. The efficiency of the compressor will be reduced as a result of under compressed gas since the volume ratio decreases with the capacity. There is also another slide than can be installed in a screw compressor called a variable volume ratio slide. The slide can control the stage at which the gas is discharged from the compressor, and therefore also the volume ratio. The last capacity control mechanism is speed control, which typically can reduce the capacity to 50% (due to oil lubrication) (Eikevik, 2019).

Increased manufacturing precision and higher expectations of the overall efficiency of compressors lead to a need to understand more of the exact operation of twin-screw compressors. Research done on modeling and simulation of all kinds of compressors is of interest. Sub-Chapter 4.3 is dedicated to the research done to improve the modeling, simulation, and therefore also the performance of twin-screw compressors.

Liquid injection in twin-screw compressors

As mentioned previously, one way to reduce the superheat in a twin-screw compressor is to inject liquid directly into the compressor. This can be done at one or multiple injection points. The latent heat of the liquid will decrease the temperature of the gas, which will lead to less superheat and therefore a more efficient thermodynamic performance. The extra mass injected will lead to additional compressor work, but if implemented correctly this will be outweighed by the increased efficiency. The process is described in a log p-h diagram in Figure 2.6.

Log p-h diagram of compression processes

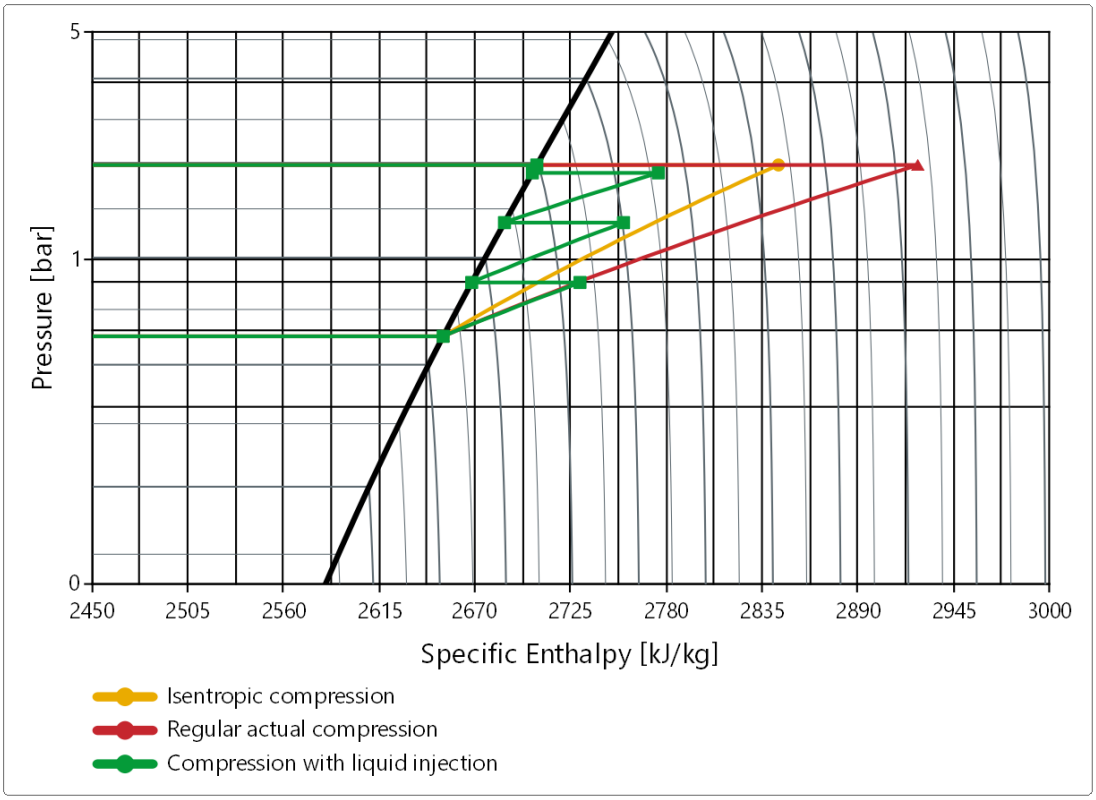

Figure 2.6 Pressure-Enthalpy Diagram water showing various compressor processes

An interesting question that rises along with the injection of liquid, is the amount of fluid that should be injected. Ideally, there should be no liquid present at the end of the compression phase as the fluid is discharged from the compressor. This is because the latent heat of condensation is an important part of the heat pump principle. At the same time, there should be enough liquid to work as a protective seal between the rotors to minimize leakage and a liquid film on the rotors will keep the equipment from reaching high temperatures or colliding with each other. The theoretical amount of liquid water that is needed to reach saturation state at the discharge of the compressor in a randomly decided temperature lift will be calculated below.

The known values are temperature (364.55K), pressure (0.642 bar) and mass flow rate (0.125kg/s) at suction along with the discharge temperature (391.57K), pressure (1.957 bar), and injected mass flow rate (0.011kg/s), with the corresponding temperature (290.43K) and pressure (1.023 bar). REFPROP is used to find any thermodynamic data in all calculations.

1. Enthalpy is found at suction and injection based on pressure and temperature.
2. Entropy is found at suction based on temperature and vapor condition (Tvap function in REFPROP.)
3. Isentropic enthalpy is found at discharge (found by using discharge pressure and constant entropy from the suction condition)
4. Isentropic efficiency is assumed (0.7, (Arpagaus, Bless, Uhlmann, Schiffmann, & Bertsch, 2019)) and used to calculate a more realistic enthalpy at discharge.

$$\boldsymbol{h_{dish} = \frac{h_{isen,dish} - h_{suct}}{\eta_{isen}} + h_{suct}} \qquad \textbf{Eq 2.14}$$

5. Enthalpy at the saturation line of water at the discharged pressure is found (enthalpy at discharge using Pvap condition at discharge temperature)
6. Conservation of mass and energy in a control volume surrounding the discharge chamber is done to find the injected mass flow rate if the liquid is fully evaporated. It is assumed that the compressed flow is mixed with liquid to fit the enthalpy value of the fluid at discharge pressure without any superheat. Work and heat loss are assumed negligible at this stage as it only assumes that there is a mixing process in a discharge chamber not in the compressor itself.

$$\boldsymbol{\dot{m}_{suct} + \dot{m}_{inj} = \dot{m}_{dish}} \qquad \textbf{Eq 2.15}$$

$$\boldsymbol{\dot{m}_{suct} * h_{dish} + \dot{m}_{inj} * h_{inj} = (\dot{m}_{suct} + \dot{m}_{inj}) * h_{th,dish} + \dot{W} - \dot{Q}_{loss}} \qquad \textbf{Eq 2.16}$$

This gave a theoretical injected mass flow of 0.00655 which is approx. 42% lower than the amount injected at the same operating conditions in an experiment conducted on a water-injected twin screw compressor. This indicates that in theory there should be liquid left at the end of the discharge phase. This is considering a highly theoretical amount of liquid where all liquid will be evaporated instantaneously, which is not the case in real applications as droplets or film on a surface of liquid requires higher heat over time to evaporate. The

time it takes for liquid to evaporate is dependent on the size and shape of the droplets(i.e. how the liquid is injected). If atomized liquid is sprayed in the compressor it will evaporate relatively quickly compared to large droplets and liquid film. Leakage and the sealing layer of liquid are not taken into consideration when doing this theoretical calculation. The sealing effect from a liquid layer is desirable and is therefore an argument for having a higher liquid injection in real applications than in theory. This calculation is, as mentioned, a simplified process where the mixture of compressed vapor and liquid water takes place and is done to see whether the experimental injection levels can be justified. The calculation can be extracted further if the compressor work is calculated.

$$(\boldsymbol{h_{dish}} - \boldsymbol{h_{suct}}) * \dot{\boldsymbol{m}}_{\boldsymbol{suct}} + \left(\boldsymbol{h_{dish}} - \boldsymbol{h_{inj}}\right) * \dot{\boldsymbol{m}}_{\boldsymbol{inj}} = \dot{\boldsymbol{W}} \qquad \textbf{Eq 2.17}$$

The work can then be included in Eq 2.16, which implicates that this is an iterative process that can be continued until the change of injected mass flow rate from step to step is within a set error.

2.4 Limitations in high temperature and pressure compressors

Only a few high-temperature heat pumps have been introduced to the commercial market, and as a result, not many components are tailor-made for high-temperature heat pump applications. In 2015, Ommen et al. published a technical and economic analysis of limitations in components in a high-temperature heat pump. Compressors were a part of this analysis. There are natural limitations in the high-pressure side of a compressor as the temperature and pressure levels are high and this imposes challenges for material selection. Suction pressure may also impose limitations, especially if the suction pressure is lower than atmospheric pressure, which tends to be the case with water vapor as a refrigerant. (Ommen, Jensen, Markussen, Reinholdt, & Elmegaard, 2015)

A literature study has been carried out to describe the general characteristics of four types of compressors. This was done to figure out what type of compressor could be suitable for HTHP-applications. Table 2.1 includes a brief introduction to the findings. The main take-outs are as follows: the adiabatic efficiency is high with piston compressors, but these compressors are limited by inefficient operation at high compressor ratios and unbalanced forces cause noise and higher maintenance costs. Screw compressors have the lowest adiabatic efficiencies but can handle high pressure ratios and are insensitive to gas composition. Centrifugal Turbo compressors can operate at a large range of pressure ratios at relatively high adiabatic efficiencies. However, the efficiency drops significantly once operated outside of the design conditions. Lastly, the scroll compressor can achieve very high adiabatic efficiencies but are limited in their displacement volume and by expensive maintenance.

Table 2.1 Compressor characteristics

Compressor type:	*Displacement (m^3/h) **	*Adiabatic Efficiency***	*Pressure ratio*	*capacity control*	*Advantages*	*Disadvantages*
Piston	1-10^3	80-90	Peak efficiency at pressure ratios around 3-5	Mechanically controlled valves are a good option	- High peak efficiency. - Relatively good capacity control**	- unbalanced forces, pulsation, and vibration. - Sensitive to liquid. - High maintenance. **
Screw	10^2-10^4	55-70	Can tolerate higher pressure ratios 6-10	slide or lift regulation, not as efficient as piston compressor	- High efficiency at high-pressure ratios. - insensitive to gas composition**	- Noisy **- relatively low efficiency
Centrifugal Turbo	10^3 -10^5	70-87	wide range of pressure ratios	Efficiency falls pretty quickly when operating in off-design conditions	- Can obtain a high-pressure ratio. - High efficiency at the design condition. - Low maintenance**	- Instability at reduced flow. - rotor dynamic problems **
Scroll	1-60	Slightly higher than piston***	Peak efficiency at pressure ratios around 3-5	Bad capacity control, incremental capacity control if several compressors applied	- High efficiency. - Low noise and vibration ****	- Low displacement - Expensive maintenance ****

** (Eikevik, 2019)*

*** (Process Industry Practices, 2013)*

**** (Sarbu & Serbarchievici, 2016)*

***** (Carrier Corporation, 2004)*

Another limitation found in compressors is oil degradation. According to Nekså et al. oil degradation can be avoided for temperatures up to 180ºC if mineral oils or polyglycol lubricants are used (Nekså, Rekstad, Zakeri, & Schiefloe, 1998). A market survey of available compressors manufactured by large companies was carried out. Price and operating limits were considered, compressor type one, two, and three(in Table 2.2) are similar compressors. Type one should be run with HFCs, type two can handle flammable refrigerants like propane (R290) and isobutane (R600a). While type three is made specifically for ammonia (R717). Type four is also made for ammonia but in a high-pressure cycle. Type 5 is a transcritical CO_2 (R744) compressor (Ommen, Jensen, Markussen, Reinholdt, & Elmegaard, 2015). It is interesting to note that all compressors have similar limits in terms of maximum pressure, temperature, and capacity, except for the compressor made for the high-pressure ammonia cycle and transcritical CO_2 operation where the maximum pressure limit naturally has to be higher. The capacity is lower in these two compressors, especially in the CO_2 compressor.

Table 2.2 Available compressor technology with current operating limits (Ommen, Jensen, Markussen, Reinholdt, & Elmegaard, 2015)

Working fluid	*Type*	*Pressure limit (bar)*	*Lubrication max. temp (°C)*	*Capacity (1500RPM) m^3/h*
R134a	1	28	180	5-280
R290	2	28	180	5-280
R600a	2	28	180	5-280
R717-LP	3	28	180	5-280
R717-HP	4	50	180	90-200
R744	5	140	180	6-25

Furthermore, (Bamigbetan O. , Eikevik, Nekså, & Bantle, 2017) made a review of high-temperature VCCs using natural refrigerants. In this publication, an extensive review of what challenges varying systems with their respective working fluids would impose. In addition to naming the challenges, existing solutions and improvement possibilities were presented. The challenges, solutions, and improvements of water as a high-temperature natural refrigerant will be further discussed in Sub-Chapter 2.5.3.

Table 2.3 Challenges, solutions, and suggested improvements for various natural refrigerants in high-temperature heat pump operation (Bamigbetan O. , Eikevik, Nekså, & Bantle, 2017)

Working System	*Challenges for HTHP*	*Existing Solutions*	*Possible Improvement*
Water	Sub atmospheric suction pressure	The heat source at or above 100°C	Cascade in HTC with other working fluid
	High discharge temp	Intercooling between stages/injection	Process integration with intercooler
	Low-temperature lift	Multi-staging	-
	High volume flow rate	Turbo compressors or parallel compressors	-
Ammonia	Material compatibility	Steel and aluminum	Enhanced material properties
	High discharge temperature	Multi-stage, intercooler integration/injection	Cascade system with other fluids
	High discharge pressure	60 bar discharge pressure	-
	High toxicity	Machine room safety, secondary cycle (glycol)	-
	Compressor cooling	Heat sink integrated as coolant	High-temperature lubricant research
	High refrigerant inventory	Plate heat exchangers, machine room, charge mass optimization	-
	low performance	Flooded type evaporation, multi-staging	
CO2	High gas cooler exit temperature	Temperature glide matching HX optimization	integration with secondary heat sink
	High compressor discharge pressure	150 bar compressors	Material or compressor technology improvement
	Expansion device losses	Vapor compression, expanders, ejectors	Further research in ejectors
	low performance	Evaporator overfeeding	-
	Low heat sink outlet temperature	Multiple vertical tanks for stratification	-
	Low critical temperature	-	combined cycle with other working fluid
Hydrocarbons	Flammability	Leak detection ventilation explosive unit	-
	High discharge temperature	-	Lubricant or cooling system research, mixture properties
	High discharge pressure	-	Compressor technology research
	Charge mass reduction	Multiple units to meet charge requirement	-
	Sub atmospheric suction pressure	-	Mixture properties
HACHP systems	Large heat exchangers	-	Further research in heat transfer
	High discharge temperature	Multi-stage, intercooler integration/injection	-
	low performance	Internal heat exchangers	Wet compression

There has also been done some research on the durability of operation of a compressor in very high-temperature heat pump range. Research showed that a reciprocating compressor can run at temperatures over 100ºC for over 1000h in a bypass cycle without reporting issues (Oh, et al., 2016). The consensus is that there are challenges with the operation of compressors in HTHP-applications, but there are several promising solutions to the challenges for a wide range of system configurations.

2.5 Water vapor as a heat pump refrigerant

2.5.1 Historical review of the development of refrigerants

Various refrigerants have been used in heat pumps. Throughout history, the requirements for refrigerants have changed significantly, and are typically divided into four generations. When refrigeration applications first emerged around 1830 the only thought was to use whatever refrigerant that could perform the desired task. This generation consisted of many naturally occurring refrigerants, like CO_2, NH_3, ethers, etc. The second-generation refrigerants focused on safety and reliability, CFCs (chlorofluorocarbons) and HCFCs (hydrochlorofluorocarbons) were common at the time. However, it was later discovered that HCFCs and CFCs harm the ozone layer. This led to laws and regulations which banned these refrigerants. The effect of this was that a new generation of refrigerants emerged. The main factor to consider next to efficiency and economy was the ODP (Ozone Depletion Potential). HFCs (Hydrofluorocarbons) generally have a lower ODP than CFCs and HCFCs, and as a result, the market share of HFCs increased. As global warming became a serious concern, HFCs were no longer desirable as they in general have a relatively high Global Warming Potential (GWP). The fourth-generation are refrigerants that have low ODP, GWP, and are safe to use. If the refrigerant is cheap and accessible this will be an advantage as the economy is always a factor. HFOs (Hydrofluoroolefins) are a group of refrigerants that has low GWP and no ODP (Linde, 2020). HFOs have increased their market share in recent years and are especially popular when looking at the research stage of high-temperature heat pumps.

As HFOs are getting more accepted as refrigerants, more research is being conducted on the consequences of utilizing these low GWP, no ODP refrigerants. The main reason for their low GWPs is their short atmospheric lifetime, for example, HFO-1234yf(R-1234yf) which is approximately 6 days (Luecken, et al., 2010). This is very short compared to more traditional refrigerants such as HFC-134a(R-134a), which has an atmospheric lifetime of 14 years (Solomon, et al., 2016). The quick degradation of HFOs means that the degradation products return to the earth as participation. Degradation products include HF, HCl, formic acid, and carbon dioxide. The effect of small concentrations of these products in water sources, wildlife, and human health is yet to be determined with high certainty (RPA and Anthesis-Caleb, 2017). This is an argument to limit the use of HFOs in the future and chose natural refrigerants where applicable. Currently, there is no consensus of a fifth-generation refrigerant in literature, but if pollution of water as a result of the degradation of HFOs becomes a serious issue, it may be the case in the future (see Figure 2.7).

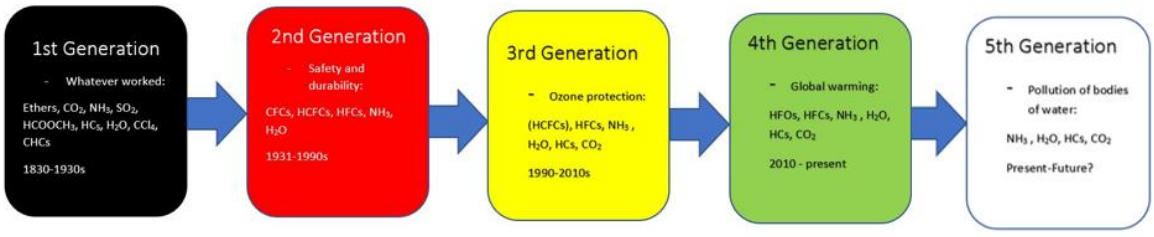

Figure 2.7: Development of refrigerants

Water vapor has been considered for compression systems several times throughout history; it was used in an air conditioning system already in 1934. It has never taken a significant market share due to water being outperformed by other refrigerants. Now that sustainability is a more important factor than ever, water is once again attracting a lot of attention (Hu, Wu, & Wang, 2018).

2.5.2 Water vapor refrigeration properties

Water vapor is a very attractive refrigerant based on its low ODP (=0) and GWP (<1) values. Furthermore, it is non-toxic and non-flammable and will, therefore, receive a safety classification of A1 (Calm & Hourahan, 2011).

Table 2.4 Physical, Safety and Environmental Characteristics of Water (R718)

Physical data						
Molecular mass	NBP		Tc		Pc	
	(°C)	(°F)	(°C)	(°F)	(MPa)	(psia)
18.02	100	212	373.9	705.02	22.06	3200
safety data				Environmental data		
OEL	LFL	HOC	safety classification	Atmospheric life (yr)	ODP	GWP
PPMv	(%)	(MJ/kg)				100 yr
-	none	-	A1		0	<1

Water is also stable from a chemical point of view, making it a very durable and reliable refrigerant. Since there is no chemical change in the structure of the refrigerant and no bi-product, disposal is not an issue. The latent heat of vaporization of water is high. It outperforms ammonia, propane, and carbon dioxide in this aspect at 20°C (Hu, Wu, & Wang, 2018). Water vapor also has a high theoretical COP and can be utilized with direct heat exchangers. Physical properties like high molecular weight, large specific volume, and high adiabatic index limit the application of water vapor. Large pressure ratio, small differential pressure, high exhaust temperature, large volume flow rate, and small capacity characterizes water as a refrigerant.

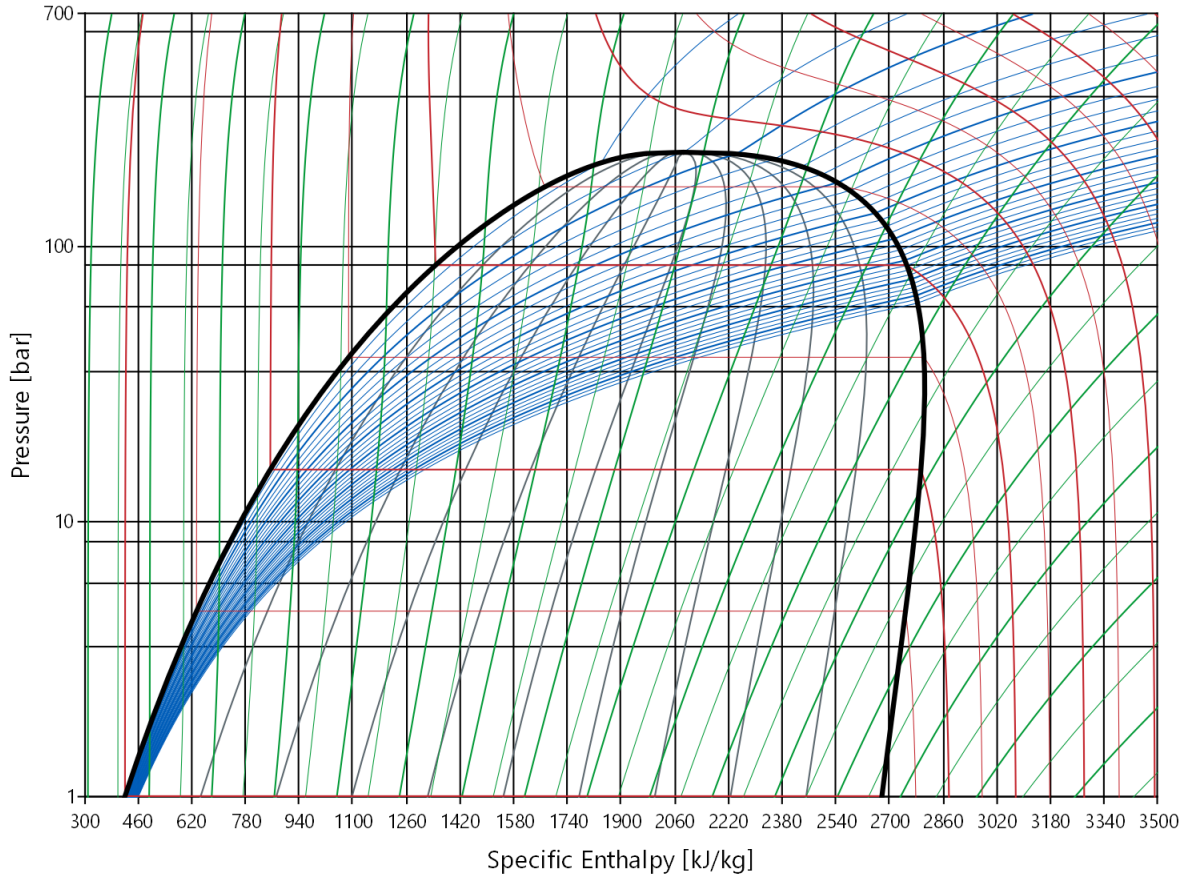

Figure 2.8: Log P-h diagram for R718 (water)

2.5.3 Water vapor in HTHP applications

Recent studies have indicated that water is the most promising natural refrigerant for heat range above 110ºC (Bergamini, Jensen, & Elmegaard, 2019), & (Wu, Hu, Wang, Fan, & Wang, 2020). As seen in Table 2.5, water has a high critical temperature and pressure of 373.9ºC and 22.06 MPa. This is higher than all the other currently available natural refrigerants. The operating pressure and temperature limits are discussed in (Ommen, Jensen, Markussen, Reinholdt, & Elmegaard, 2015) and (Nekså, Rekstad, Zakeri, & Schiefloe, 1998). The table shows that R718, is not limited in by a maximum pressure nor temperature limit, but rather a pressure ratio limit.

Table 2.5: Applied Operation limits and critical point of various natural working fluids (Ommen, Jensen, Markussen, Reinholdt, & Elmegaard, 2015)

Working fluid	*Pressure limit (bar)*	*Temperature limit (°C)*	*Pressure ratio limit (-)*	*Critical Pressure (bar)*	*Critical Temperature(°C)*
R290	28	180	-	42.5	96.7
R600a	28	180	-	36.5	134.6
R717	76	180	-	111.3	132.4
R718	-	-	22.1	217.7	373.9

Looking at the thermophysical properties of water, the latent heat will decrease with increased temperature. This change is relatively small in temperatures around the range in which VHTHPs operate today. The specific volume of water vapor decreases significantly with increased pressure. The decreased specific volume will lead to more compressor work

as the volume flow rate is the same, and therefore the mass flow rate is increased (Shen, Xing, Zhang, He, & Wang, 2016). Other challenges water has at high-temperature applications along with high volumetric flow rate include sub-atmospheric suction pressure, high discharge temperature, and low temperature lift.

In the compressor developed by Shanghai Jiao Tong University and Hanbell Precise Machinery, the high discharge temperature is dealt with by injecting water at several stages throughout the compression. Even though the injected water leads to a higher volumetric flow rate, the phase change i.e. latent heat exchange will lower the temperature significantly. From a thermodynamic perspective, this is a similar solution to the intercooling between stages proposed by Bamigbetan et al in Table 2.3. Suction pressure correlates directly with the temperature of the heat source. If heat can be supplied at temperatures close to 100 ^{0}C the operation will be at near-atmospheric operation at the suction side. This may eliminate the sub-atmospheric operation issue. Heat can be supplied at these temperatures either with high-temperature waste heat or by a cascade system that uses another refrigerant in the low-temperature cycle. However, if heat cannot be provided at these temperatures a purging system should be implemented to get rid of air and other gases that are leaked into this side of the compressor or evaporator. If leakage occurs, the performance of the cycle will decrease (Chamoun M. , Rulliere, Haberschill, & Berail, 2012). The suggested solution to deal with the high density is a low pressure ratio and high volume flow compressor. This limits the options when selecting compressor types. Screw and centrifugal turbo compressors are the two types that fit this application and are therefore most frequently used in HTHP systems with water as the refrigerant.

There are plenty of industrial applications for high-temperature heat pumps, and some of the applications are especially well-suited for water vapor as the refrigerant. Superheated steam drying (SSD) is one application where a water-vapor high-temperature heat pump is suitable. Traditionally the steam generation in an SSD has been provided by an electrical steam generator or fossil fuel combustion, the energy efficiency can be improved by using VCC heat pumping technology instead. An "open" and "closed" three-stage SSD system was analysed for pet-food drying (Tolstorebrov, Bantle, Hafner, Kuz, & Eikevik, 2014). The difference between the open and closed systems is that the open system utilizes superheat steam directly from the main flow of steam, while the closed system absorbs energy from the surplus steam through an evaporator. This indicates that there is an extra heat exchanger in the closed system that will decrease the overall efficiency. The analysis was conducted with radial turbo compressors modified from a supercharger. The experiment reported that the technology is promising, with huge energy saving potential, with the open system being the most efficient with a COP of 3.84.

Distillation is another industrial process where a water-vapor heat pump is seen as a good fit. A mechanical vapor recompression heat pump (MVRHP) used for distillation purposes has been proposed to be an energy-efficient alternative to traditional distillation. Simulation of four distillation systems was used to find the most energy-efficient way of separating water and N, N-Dimethylacetamide. The systems simulated were conventional distillation, top MVRHP distillation, double-effect distillation, and lastly a double effect distillation with double MVRHPs. The analysis showed that the double effect distillation with double MVRHPs is the most energy-efficient distillation process and offers energy savings of 78.4%. It should be mentioned that the investment cost is for this system is significantly higher than for a conventional distillation system (Gao, et al., 2015).

To sum up, water is a refrigerant with very interesting properties for high-temperature operation. Some challenges arise, but several solutions have been proposed to combat most of these challenges. The most mature solutions have also been implemented successfully. An advantage with water vapor as a refrigerant is that it can be used in a variety of applications, it is expected to earn a significant market share of the future HTHP-market.

3 Literature review of high-temperature heat pumps and their compressors

There is currently a lot of research on high-temperature heat pumps. The number of publications including "high-temperature heat pumps" has previously correlated well with the crude oil price. In the past few years, the number of publications has increased independently of the crude oil price (Figure 3.1). This is due to the demand for more efficient energy utilization.

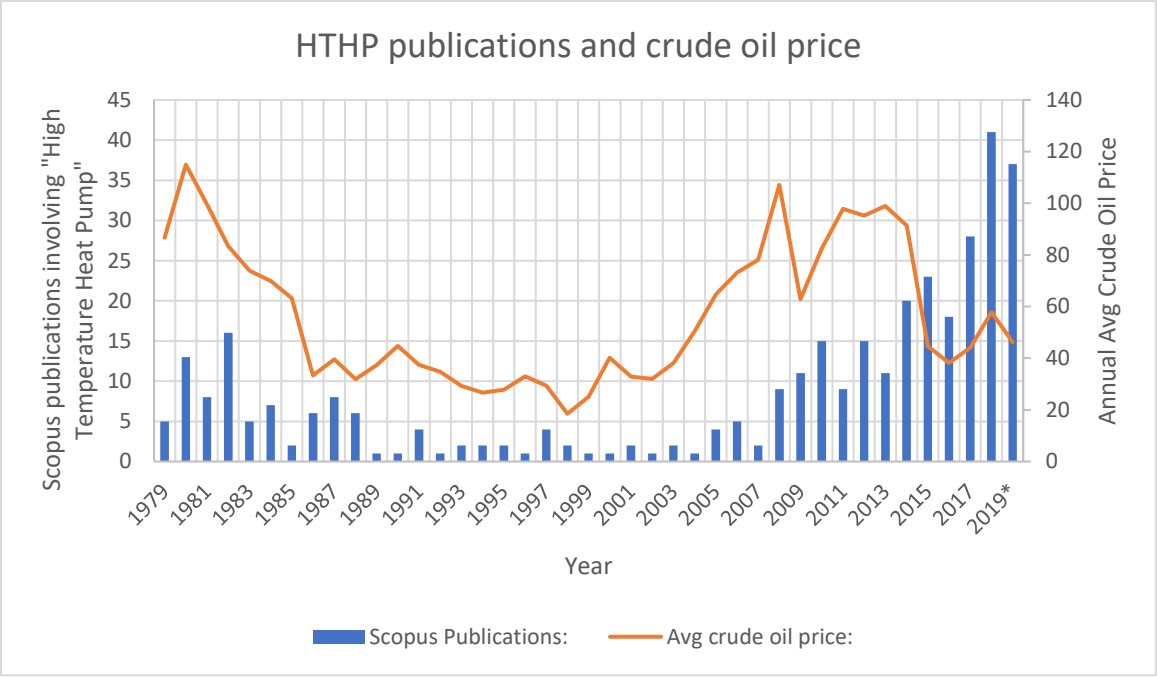

Figure 3.1: Number of Scopus publications about "High-Temperature Heat Pump"(www.scopus.com) and inflation-adjusted annual average crude oil price (McMahon, 2020) over the past 40 years. (* = data not available throughout the entire year)

3.1 High-Temperature Heat Pumps Research Stage

Even though there are about 20 commercialized HTHPs or VHTHPs available on the market today, the research in the area is exploding. It is therefore of interest to investigate what solutions are currently being researched. Research teams spread around the world, but mainly in Europe and Asia, are currently leading the way in HTHP research. There are exciting new publications in the area every year.

Table 3.1 Overview of research on HTHP

The organization, Project Partners	*Compressor*	*Refrigerant*	*ODP*	*GWP*	*Safety classification*	*Cycle type*	*Heat source and heat sink temperatures [°C]*	*Heating capacity [kW]*	*Authors (year)*
Danmarks Tekniske Universitet, SINTEF, EPCON, Norway/Denmark	Compressor 1: Turbo Compressor 2: Turbo	R718	0	<1	A1	Two-stage	Source: 80-110°C Sink: 134-176°C		(Zühlsdorf, Schlemminger, Bantle, Evenmo, & Elmegaard, 2018)
Tianjin University, China	LTS: scroll HTS: Piston	LTS: BY3B HTS: BY6	LTS: 0.03 HTS: 0.08	LTS:2125 HTS:670	A1, A1	water source cascade	Source: 55°C sink: 100-170°C	22.45	(Li, et al., 2019)
Austrian Institute of Technology, Vienna, Chemours, Blitzer	Piston	R1336mzz(Z)	0	2	A1	Single-stage with IHX	Source: 50-110°C Sink:75-160°C	12	(Helminger, Kontomaris, Pfaffl, Hartl, & Fleckl, 2016)
Norwegian University of Science and Technology, SINTEF, Norway	Piston	R600	0	4	A3	Cascade	Source: 50°C Sink: 115°C (128-132?)	20	(Bamigbetan, Eikevik, Nekså, Bantle, & Schlemminger, 2019)
Seoul National University, Republic of Korea	Piston	R245fa	0	1030	A1	Single-stage with IHX	source: 60-70°C sink: 115-125°C	9	(Kang, Na, Yoo, Lee, & Kim, 2019)
Viking Heat Engines, Norway Chemours Fluorochemicals, USA	Piston	R1336mzz(Z)	0	2	A1	Single-stage with recuperator	source: 60-95°C sink: 110-150°C	35	(Nilsson, Rislå, & Kontomaris, 2017)
Norwegian University of Science and Technology, SINTEF, Norway, Officine Mario Dorin	Piston	LTS: R290 HTS: R600	LTS:0 HTS:0	LTS:0 HTS:4	LTS: A3 HTS:A3*	water source cascade	source: 67-95°C sink: 102-118°C	20	(BAMIGBETAN, et al., 2018)
Shanghai Jiao Tong University, China	Screw	R718	0	<1	A1	water-injected screw compressor	Heat Source: 75-85°C Heat Sink: 110-150°C	285	(Wu, Hu, & Wang, 2019)
Paco, University Lyon, EDF Electricité de France	Screw	R718	0	<1	A1	Flash tank	Source: 75-95°C Sink: 120-145°C	30	(Chamoun, Rulliere, Haberschill, & Peureux, 2014)
Jiangsu University of Science and Technology, China	Scroll	LTS: R22, HTS: R134a	LTS:0.055 HTS:0	LTS:1810 HTS:1430	A1, A1*	Dual-mode, single-stage, and cascade	Source: 0-20°C Sink: 70°C	10.5	(Shen, Guo, Tian, & Xing, 2018)
ISTENER, Universitat Jaume I, Spain	Scroll	R245fa	0	1030	A1*	Single-stage with IHX	Heat Source: 60-80°C Heat Sink: 90-140°C	17.5	(Mateu-Royo, Navarro-Esbrí, Mota-Babiloni, Molés, & Amat-Albuixech, 2019)
Tianjin University, China, MOE key laboratory	Scroll	NBY-1	0	523		Single-stage	Source: 80°C Sink: 130°C	15.36	(Deng, et al., 2020)
Kysushu University, Japan	twin rotary	R1234ze(Z)	0	7	A2L	Single-stage	Source: 50°C Sink: 75°C (125°C simulated)	1.8	(Fukuda, Kondou, Takata, & Koyama, 2014)

* (Linde, 2020)

Table 3.1 shows the current research groups and their work. Older contributions to the field have not been included in this table, and they can be found in a similarly structured table provided by (Arpagaus, Bless, Uhlmann, Schiffmann, & Bertsch, 2019). Some of the research teams in the HTHP field have several different approaches to solve the current challenges. These approaches may include a variety of compressors with different configurations.

3.2 Compressor Research Stage

A large variety of HTHP systems have been developed, some are already in commercial use, while most are in the research stage. As mentioned in Chapter 2, the compressor requirements vary greatly with the temperature, pressure, refrigerant, and cycle. Because most high temperature heat pump configurations are still in the research stage, no specific system is superior in high temperature applications. In more mature heat pumping technology, there is room for several solutions as the requirements for capacity and operating range varies a lot. It is therefore beneficial to keep exploring and developing various system configurations.

Piston Compressors

The piston compressor is the oldest kind of compressor and represents a very mature technology. It has shown promising research results in high-temperature applications. It is the compressor that is used in most HTHP research projects, especially for lab scale. The disadvantage with piston compressors is that the efficiency is at the maximum at a pressure ratio of about 3-5. A single-stage piston compressor is limited in what temperature glide it will operate efficiently, as a limitation for the compressor is low efficiency at high pressure ratios. However, if designed correctly, it can operate at high temperatures and is therefore seen as a good fit for high-temperature applications.

Helminger et al. tested a simple single-stage system for HTHP application in 2016. An improved system was developed by adding an IHX (internal heat exchanger). The compressor used in the system was a modified semi-hermetic piston compressor from BITZER. Isentropic and volumetric efficiencies of 0.58-0.67 and 0.75-0.9 respectively were used for calculations. The system was tested for source and sink temperatures ranging from 30-90ºC and 75-160ºC respectively and delivered COPs ranging from 2.67-5.81 (Helminger, Kontomaris, Pfaffl, Hartl, & Fleckl, 2016).

Viking Heat Engines adapted a piston expander used in a small-scale Rankine cycle system to a compressor. This was simply done by adjusting the expander valve system. The expander had been thoroughly tested and provided high efficiencies at high temperatures. Viking Heat Engines has put a lot of effort into the development of expander/compressor technology that can operate efficiently at high temperatures. It was used with a POE lubricant that could sustain high temperatures and was miscible with the refrigerant (R1336zz(Z)). The hermetic piston compressor is designed to operate at speeds up to 1500 rpm with an electrical power of 10 kW. Their system includes a recuperator to prevent any liquid from entering the compressor. The refrigerant was in a superheated state at this point in the process. The system was able to provide a temperature lift of 20-60K with

COPs ranging from 2.5-7.8 dependent on operating temperatures. (Nilsson, Rislå, & Kontomaris, 2017)

Another research group that has researched HTHP systems with piston compressors is a group at NTNU. Piston cascade systems show a lot of promise and (Bamigbetan O. , Eikevik, Nekså, Bantle, & Schlemminger, 2019) proved that a specifically designed piston compressor can handle discharge temperatures up to 132ºC. The average total and isentropic efficiencies in their simulation were assumed to be 74% and 83% respectively. The assumption of the compressor efficiency is trustworthy because a prototype of a piston cascade system was built and tested. This prototype heat pump delivered 20kW. The piston compressor prototype averaged an overall efficiency of 74% while delivering heat at 115ºC. The semi-hermetic one-stage 4-cylinder compressor had a displacement of 48.82m^3/hr. at 50 Hz. The modifications done to cope with the high temperatures were an external manifold at discharge, 25% larger electrical motor, thermal protection set at 140ºC with a discharge temperature of 160ºC, and a high-pressure safety switch at 28.6 bar (BAMIGBETAN, et al., 2018).

(Kang, Na, Yoo, Lee, & Kim, 2019) did an experimental study with a single-stage piston compression system with an Internal Heat Exchanger. The main purpose of the experiment was to prove how various system configurations improved the performance of the heat pump system. The system, which had a four-cylinder piston compressor managed to lift temperatures from 60-70ºC up to 115-125ºC with reasonable COPs (1.83-3.24).

(Li, et al., 2019) set up a prototype heat pump system with a piston compressor as the HTS (high-temperature stage) cycle. The piston compressor was used with a high-temperature resistant lubricant called POE68 which properties can be found in (Ma, et al., 2018). The compressor specifications in the system was a semi-hermetic piston compressor with a displacement volume of 18.4m^3/h. It rotated at 1450 rev/min with a rated power of 3.75 kW (Li, et al., 2019).

Screw Compressors

Screw compressors have shown a lot of promise in HTHP applications. The ability to control the temperature throughout the process with injection allows the compressor to give a high-pressure ratio in one stage. This is due to compression being closer to an isothermal process as losses due to superheat is limited. In 2014 (Chamoun, Rulliere, Haberschill, & Peureux, 2014) rebuilt an air compressor to fit the purpose of high-temperature heat pump application. Some of the modifications were to fix sealing and water injection. Adiabatic and volumetric efficiencies were estimated to be 57% and 82% respectively. The pressure ratio represents a temperature glide of 40-50K, by using 90 kW of electrical power running at 4700rpm.

(Wu, Hu, & Wang, 2019) designed and constructed a VHTHP system using a water vapor screw compressor with water injection. Having water injection throughout the compression process makes the superheat significantly lower than what would be expected from another compressor. The disadvantage with water compared to oil is that the lower viscosity leads to a worse seal, and therefore a lower volumetric efficiency of the compressor. The experiment was conducted at a variety of evaporation and condensation temperatures. The highest adiabatic efficiency was 58% at evaporation and condensation temperatures of 85ºC and 125ºC. The volumetric efficiency has a negative correlation with the condensation

temperatures if the evaporation temperature is set as a constant. The highest volumetric efficiency reported was 73% at T_{evap}=85ºC and T_{cond}=117ºC. The compressor has an internal compressor ratio of 7 and operated at 5000rpm with a volumetric flow rate of $30.8\frac{m^3}{min}$.

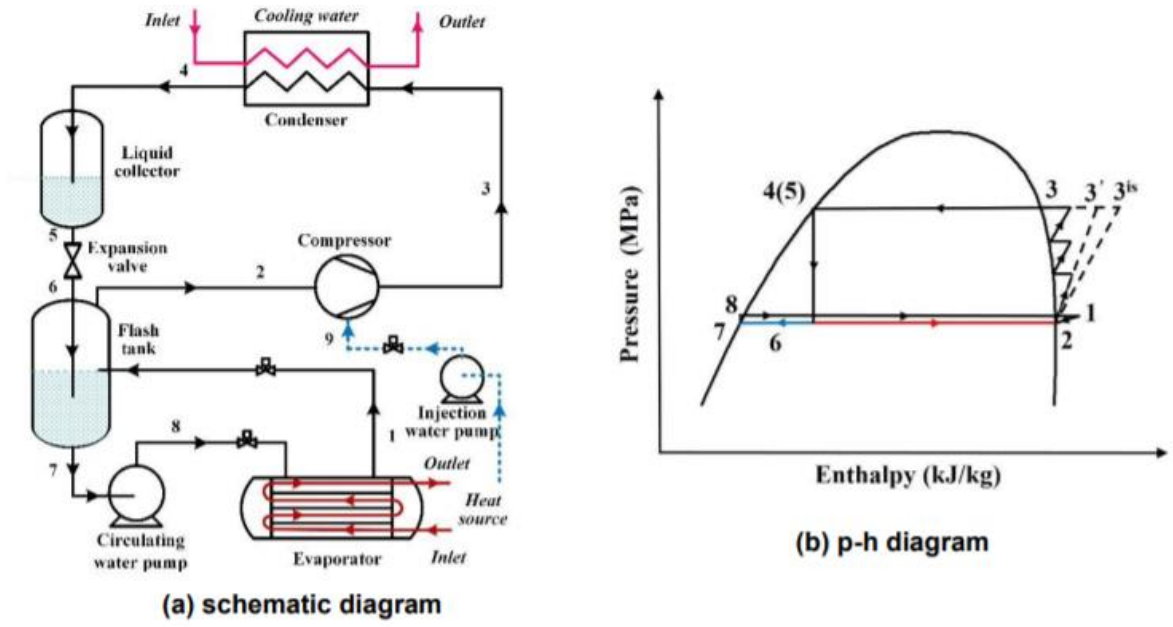

Figure 3.2: VHTHP water vapor screw compressor system (Wu, Hu, & Wang, 2019)

Turbo Compressor

Turbo compressors have a high displacement capacity. It has been suggested that a turbo compressor is a good fit when utilizing R718 (water) as the refrigerant. According to (Sarevski & Sarevski, 2017) the pressure ratio (Π) is limited to 2.8-4.8 with temperature lifts of 20-38 K for one stage centrifugal turbo compressors with water as a refrigerant, depending on the assumed inlet temperatures.

Rotrex AS patented design of a turbo compressor specifically manufactured for HTHP applications. A radial turbocharger used in the automotive industry was taken as the starting point. The impeller was made in titanium, while the rest of the casing was aluminum. To prevent leakage between the compression chamber and the planetary traction drive, the carbon seal was enhanced. These changes were made to ensure that the compressor could sustain high temperature and pressure operation over a long time. The importance of durability and reliability of compressors cannot be stressed enough. The compressor was able to deliver a temperature lift of 25 Kelvin at high temperatures with a high COP and a maximum isentropic efficiency of 72% (90’000 rpm, pressure ratio of 2.4, and a mass flow of 450kg/h) (Madsboell, Weel, & Kolstrup, 2014), (Bantle M. , 2017).

A two-stage turbo-compressor system with water vapor as the working fluid was designed and simulated for HTHP applications (Zühlsdorf, Schlemminger, Bantle, Evenmo, & Elmegaard, 2018). The compressors were modeled based on the abovementioned previous work. With isentropic efficiencies of 74%, compressors 1 and 2 had pressure ratios of 3.2 and 2 respectively. The two-stage turbo compressor simulations showed the potential of a

temperature lift from 110ºC atmospheric pressure and up to 250ºC at 6.5 bar(a). Water spray cooling at 120ºC was also introduced to control the superheat (Bantle M. , 2017). A test rig with an MVR heat pump system with two-stage turbo-compressors with inter-stage spray cooling was set up. The experimental investigation of the test rig showed that both stages could deliver an isentropic efficiency of 74%, for a combined pressure ratio of 3.0. For a condensation temperature of 133ºC, the system delivered 300 kW with a COP of 5.9 (Bantle, Schlemminger, Gabrielii, & Ahrens, 2019).

Scroll Compressor

The scroll compressor has many beneficial characteristics. It has low noise and vibration, high efficiency and reliability, and is easy to install. However, some issues arise from high temperatures. The main issue is the thermal deformation. Thermal deformation leads to a decreased clearance between the fixed and orbiting scroll. This will lead to a shorter lifetime as a result of wear. To enhance the axial tightness without leading to the tip of scroll and baseplate contact, lubricant can work as a seal on the flanks. However, this leads to an extra constraint since the lubricant must be able to handle the operating temperature and pressure. In Ma et al.'s HTHP system with a cascade scroll compression system, they used POE68. Due to changes made in the scroll compressor, the heat sink temperature could reach 142ºC (Ma, et al., 2018).

In Spain, the ISTENER research group, helped by Expander Tech S.L, modified an open scroll compressor to fit the purpose of an HTHP system. The modifications consisted of internal adjustments and magnetic coupling. A polyester oil that can handle high temperatures was used to ensure proper lubrication. The compressor used a motor with a nominal power of 7.5kW. The displacement was 121.1 cm^3/rev (2900 rpm at 230V and 50Hz). The highest heat sink temperature was 140ºC. The project concluded that the compressor was the component with the highest potential for improvement. This is due to the high irreversibility of the compression process. It was pointed out that lubrication and mechanical design changes of the compressor could increase the efficiency of the system drastically (Mateu-Royo, Navarro-Esbrí, Mota-Babiloni, Molés, & Amat-Albuixech, 2019).

Other compressors used in HTHP configurations

(Fukuda, Kondou, Takata, & Koyama, 2014) made an experimental setup with a hermetic twin rotary compressor (rolling piston compressors). The experiment was able to produce heat at a condensation temperature of 75ºC with rpm varying between 1500-1600. The volume was 24cm^3 on the suction side. The lubricant used was POE VG68. This experimental setup was mainly conducted to verify a simulation and to compare two refrigerants (R1234ze(E) and R1234ze(Z)). The simulation was carried out at higher condensation temperatures (105ºC and 125ºC). It was not experimentally verified at these temperatures. There have been no reports of any further testing of a rolling piston compressor at high temperatures from the author.

There also exist high-temperature heat pumps that take advantage of other thermodynamic principles than vapor compression heat pumps (VCHPs), namely hybrid absorption-compression heat pumps (HACHPs). There are implemented HACHPs (Nordtvedt & Horntvedt, 2019) in industry, and research supports the potential for HACHPs in high-temperature applications (Jensen, Ommen, Markussen, Reinholdt, & Elmegaard, 2015), (Ahrens, Hafner, & Eikevk, 2019), (Tønsberg, 2020).

Devices that are used to improve the performance of HTHPs

The greatest concern in HTHPs and VHTHPs may be the superheat loss. The superheat occurs in and can be limited by the compressor. The literature review shows that energy-efficient, simplistic, and economically viable de-superheating techniques have been evaluated and attempted implemented in prototypes. Several of the research groups who have proposed HTHP-systems have incorporated devices to increase the efficiency of the system. Some of the common de-superheating techniques include liquid injection, open-intercooling, and surface absorption.

Liquid injection:
Liquid injection can be implemented in several ways. While all compressor-configurations with compressors in series can have liquid injection in the pipe between an LP and HP compressor, twin-screw compressors allow for liquid injection directly into the compressor. If liquid injection is implemented between dry compressors all liquid must be evaporated before the next compressor, which may lead to a significant length of pipe and therefore also pressure drop between the compressors. To boost the evaporation process, liquid can be injected with an atomizer which will decrease the necessary pipe length.

The direct injection into the compressor does not have the disadvantage of pressure drop due to an extended pipe length, but this technique is limited to twin-screw compressors and turbo-compressors. As seen from the literature review, liquid injection is a popular technique when water is the working fluid.

Open intercooling:
A component that can be added to a system to decrease the superheat is an open intercooler. This is naturally only possible in configurations where compressors are in series. The open intercooler works in an intuitive way where the compressed gas from the low-pressure compressor is cooled down in a tank(intercooler) together with the liquid that has passed through a throttling valve after the condenser. The gas will go from the intercooler to the high-pressure compressor. The disadvantage of this configuration is the increased complexity in the system. More components will lead to a more expensive and comprehensive initial- and operational cost. From a thermodynamic point of view, the open intercooler may lead to a need for additional superheat from the first compressor to ensure that there is enough fluid in the gas phase for the second compressor.

Surface absorption:
The surface absorption technique is a compact alternative to liquid injection. The concept was developed by (Shutte & Koerting, 2017). The process injects liquid into vapor through a duct of wetted reaction rings. The disadvantage compared to the liquid injection is the larger pressure drop (90mbar).

Internal Heat Exchanger:
An internal heat exchanger is a commonly used device in the research status of HTHPs. And even though it is not a de-superheating technique it is seen fit to describe its function here. The purpose of an IHX is to ensure sub-cooling of the refrigerant after the condenser and superheat after the evaporator. It is simply done by placing a heat exchanger with high-pressure liquid on one side, and low-pressure gas on the other. This will increase the overall performance of the system as the pressure ratio of the compressor can be lower.

This can be illustrated by an example: A theoretical scenario where a waste heat source of 83°C shall be used together with a water-vapor twin-screw compressor to provide heat at 125°C. The evaporation temperature should then be approximately 80°C, as the heat exchanger does require some temperature difference between the heat source and evaporation temperature. This indicates that the suction pressure of the compressor cannot be higher than 0.47 bar to ensure vapor. If an internal heat exchanger was used after the evaporator, the temperature of the fluid going into the compressor may be as high as 85°C, which means that the suction pressure can be 0.58 bar. The discharge pressure should be approximately 2.54 bar which gives a saturation temperature of 127.92°C. The implementation of an internal heat exchanger will then decrease the pressure ratio from 5.40 to 4.38.

One important thing to keep in mind when looking at all devices that can improve a heat pump system performance is the additional investment and maintenance costs. Higher complexity leads to more uncertainty and a higher risk of something not working properly.

Discussion

There is no doubt that there are many potential solutions to high-temperature heat pump systems. Natural refrigerants have been used in many studies for HTHP, and they are reported to perform at a similar level compared to synthetic refrigerants. Water, propane, and butane are some of the natural refrigerants used in HTHP research. There are several promising piston compressor systems, but the main challenges with piston compressor in HTHPs are the inefficient operation at high pressure ratios and the lack of inter-stage injection in the compression process to limit superheat. A compressor that in turn delivers higher efficiencies at high pressure ratios and inter-stage injection is the twin-screw compressor. However, there are some challenges with twin-screw compressors as well. The superheat is not completely fixed by injecting liquid in the compression process, and the injection leads to higher power consumption. The twin-screw compressor is especially compatible with water, which leads to a sub-atmospheric pressure operation at the evaporation side. Centrifugal turbo-compressors experience advantages and disadvantages that are similar to the twin-screw compressor. Both are reported to be a good fit for water-vapor compression. Turbo-compressors can be designed to fit a large range of pressure ratios, but only turbo-compressors with relatively low pressure ratios have been tested for high-temperature heat pump applications. Lastly, scroll compressors are the least mature compressor technology in this comparison. They are known to have small displacement volumes but have the potential for the highest efficiencies. The technology has been tested in some laboratory-scale HTHPs, where it was reported that more research on the technology could drastically improve the operation of the compressor.

To sum up, water seems to be a viable option at a VHTHP operating range. As mentioned previously the main challenges with water are low suction pressure, high volumetric flow rate, and low-pressure ratio. However, several different research groups have reported very promising results with systems that incorporate various solutions to these challenges.

4 Design considerations of a HTHP water-injected twin-screw water vapor compressor

This thesis will describe a model of a water-injected twin-screw compressor. Reading into the state of the art research on the field of twin-screw compressors is therefore an important task. Optimizing water vapor injection screw compressors is of increasing importance if these compressors are to take a leading role in the HTHP market. However, the concept is relatively new, and research on the specific compressor is limited. A lot of research has been done on oil-injected screw compressors and the design of rotor compressors in general. Even though this is not directly research on water-injected twin-screw compressors, the research is transferrable and highly relevant for the development of a high-temperature screw compressor with liquid injection. This chapter is dedicated to the development of liquid-injected twin-screw compressors.

4.1 Special considerations of water vapor

As mentioned previously, there are some challenges regarding water vapor as a refrigerant. The most obvious challenge is the high specific volume of water vapor. Since heat exchange is directly proportional to the mass flow (Eq 4.1), the volume flow rate needs to be relatively high, to ensure a sufficient mass flow rate. Twin-screw compressors can handle high volumetric flow rates.

$$q = \dot{m} C \Delta T \qquad \textbf{Eq 4.1}$$

Since water is corrosive there are special materialistic requirements when using water as a refrigerant and making parts compatible with water may lead to extra costs. To make good use of water vapor in high-temperature applications there is a need for a high pressure ratio. This high pressure ratio is currently an important constraint. This is both due to a large amount of work needed to perform the compression and the high discharge vapor temperature. Ensuring a low discharge vapor temperature, or superheat, is of importance (Tian, Shen, Wang, Xing, & Wang, 2017)

The abovementioned concerns have been dealt with by some of the research groups mentioned in Chapter 3.2. Corrosion in turbo-compressors can be dealt with by changing the material of vital parts like the impeller. Corrosion has not been reported as a significant issue in screw compressors. The problem with superheat in screw compressors can be solved by direct liquid injection into the working chambers of the compressor.

4.2 Rotor profile research

Screw compressors have seen a variety of profile designs throughout history (Figure 4.1). Until recent time profile research was almost exclusively conducted by manufacturers. This led to few publications of papers to maintain the competitive advantage of the various manufacturers. SRM (Svenska Rotor Maskiner) made patents on rotor profiles in 1946

(symmetric SRM), 1970 (asymmetric SRM), and 1982 ("D" profile). It was not given enough information to reproduce these designs, which hindered the development of rotor profiles, but led SRM to keep their competitive advantage. Since the 1980s there have been numerous papers on screw machines, but few of them go in detail on profile design (Stosic & Hanjalic, 1997). The method for generating the "N"-profile was also explained. It provided valuable insight for the common mechanical engineering designer on how to generate a rotor profile. In addition to publishing a rotor design, a numerical model of the fluid flow and thermodynamic processes of the rotor were published in the second part of the paper (Hanjalic & Stosic, 1997). The "N"-profile has later been subject to minor modifications to fit whatever purpose the screw compressor shall serve.

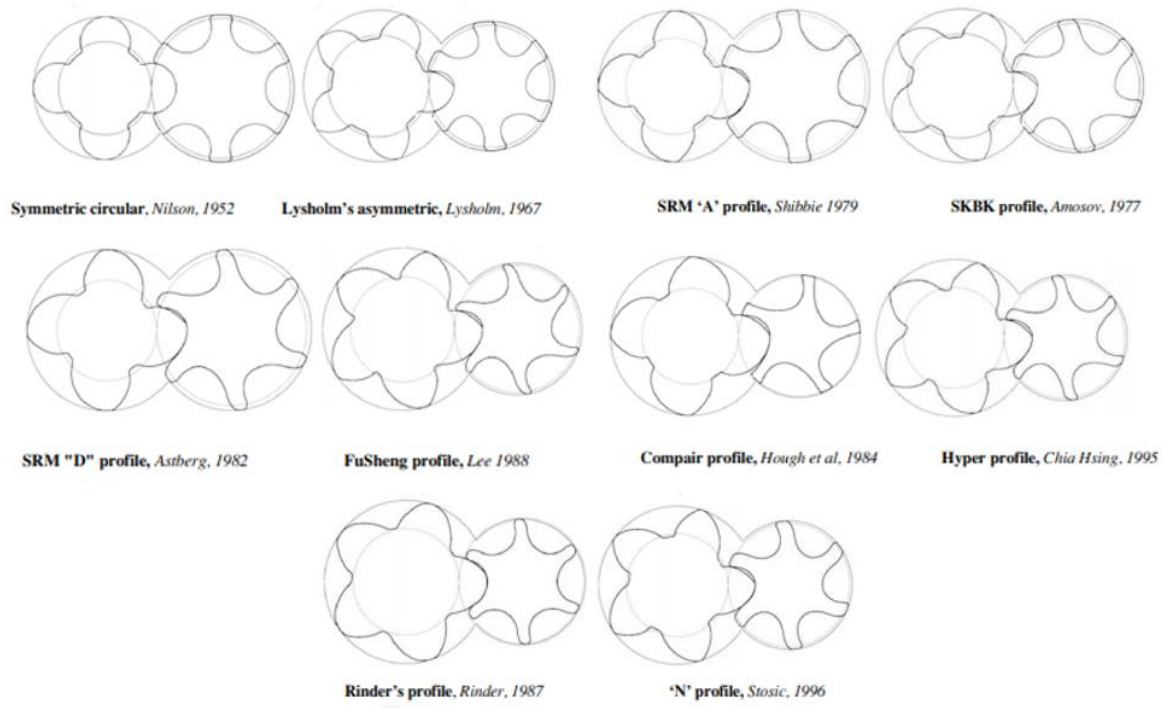

Figure 4.1 Historical screw compressor rotor profiles (Stosic, Smith, & Kovacevic, 2005)

Stosic et al (2019) proved how the depth of the rotor profile affects the performance of the compressor both in terms of displacement and efficiency (Stosic, Smith, & Kovacevic, 2019). The experimental set-up was one oil-free and three oil-flooded screw compressors, with different configurations of the number of lobes on the male and female rotors (3/5 & 4/5, 4/6, 5/6 respectively). The same inlet temperature and pressure (20ºC and 1 bar) was set for all compressors. All oil-flooded compressors had an outlet pressure of 8 bar, while the outlet pressure of the oil-free compressor was set to 3.5 bar. The working fluid was air. All configurations were made with both nominal and deeper profiles. The center distance had to be reduced to maintain the outer diameter of the male rotor. The results show that all configurations with a deeper profile deliver a higher flow rate with higher adiabatic and volumetric efficiencies. The study also showed that for the pressure levels tested, the configuration with fewer lobes was more efficient than ones with more lobes (4/5 is more efficient and cheaper to manufacture than 5/6).

When a commercialized HTHP with a twin-screw compressor is to be developed, and the operating conditions of the compressor are known, the rotor profile research is highly relevant. Optimizing the depth, the number of lobes and the profile type are all parameters

that will affect the performance of a compressor. The model developed in this thesis is made to accurately simulate an already manufactured prototype. The geometry of the rotor-profile is therefore pre-determined, and will not be a part of the optimization work in this thesis.

4.3 Simulation and numerical modeling of twin screw compressors

Being able to accurately predict a compressor's performance in various operating conditions is important. If the performance is significantly off the predicted value, the consequence will be an inefficient operation of the equipment or in the worst case, an expensive modification or replacement of the compressor. Prototypes can be used to predict the performance of a compressor, but they are expensive to manufacture, so it is often desired that a model is developed as a pre-study for a prototype. There is therefore a need for accurate and reliable screw compressor models. Furthermore, the development of high precision manufacturing along with the need for compressors to operate in higher temperatures and pressures results in a need for a better understanding of the deformation of the parts in a twin-screw compressor. This leads to a need for more precise models and simulations of screw compressors than what was expected earlier. Numerical, analytical, and empirical methods are most frequently used. In the past couple of decades, several models have been developed that test geometrical and thermodynamic variations of a twin-screw compressor. CFD technology, which uses numerical analysis along with data structures to model fluid flow, has also improved drastically in the past couple of years. CFD technology has been used to model twin-screw compressors (Casari, Kovacevic, & Ziviani, 2018); (Rane S. , 2105).

This thesis will focus on the thermodynamic modeling of screw compressors. Thermodynamic models are not seen as more important than a CFD-model, and the reason why a thermodynamic model is chosen for this thesis is that a CFD analysis of the very same compressor is developed in parallel. The two independently developed models can therefore be used to enhance the understanding of the twin-screw compressor and further optimization of the compressor design and operation.

A dynamic model of a high-temperature heat pump using water as a refrigerant was developed in 2012 (Chamoun M. , Rulliere, Haberschill, & Berail, 2012). The entire heat pump system was modeled using Modelica modeling language. The compressor is based on a model provided by (Browne & Bansal, 2002). Isentropic and volumetric efficiencies were provided by manufacturers. The model uses basic equations (Equation 4.2 and Equation 4.3) to obtain the mass flow rate ($\dot{m}$) and work ($\dot{W}$) needed to fulfill the compression of the refrigerant.

$$\dot{m} = \eta_v \rho_1 V_1 \frac{N_{rpm}}{60} \left(\frac{kg}{s}\right) \qquad \textbf{Eq 4.2}$$

$$\dot{W} = \dot{m} \frac{h_{2is} - h_1}{\eta_{is}} \ (W) \qquad \textbf{Eq 4.3}$$

ρ_1 = density of the fluid at the inlet of the compressor (kg/m^3)

V_1 = Compression volume per rotation (m^3/rotation)

N_{rpm} = rotations per minute of the compressor (rotation/min)

η_{is} = isentropic efficiency (-)

h = enthalpy of the fluid (J/g), where the inlet of the compressor and the outlet of an isentropic compressor is represented by subscript 1 and 2is.

The mathematical model of the compressor was verified experimentally both for single and twin-screw compressors by Browne and Basal. In a later publication (Chamoun, Rulliere, Haberschill, & Peureux, 2014) experimentally verified the precision of their dynamic model of the heat pump system. There are some delays and inaccuracies in the model of the system due to the assumptions made, these delays are mainly from other components than the compressor.

A model originally developed by (Zaytsev, 2003) was modified as (Bommel, 2016) made a thermodynamic model of a twin-screw compressor with ammonia-water injection. Van Bommel's model was made in MATLAB and SIMULINK, the model used geometrical parameters of the rotor to create a volume function. After the volume function was made the thermodynamic modeling was dealt with using conservation equations. Various leakage paths were implemented in the model. The model was later validated, and parameter studies were done to optimize the model. It is noted that the geometrical model, conservation equation, and experimental data were gathered from Zaytsevs previous work.

(Tian, Shen, Wang, Xing, & Wang, 2017) published a paper explaining their thermodynamic model of a mechanical vapor compression (MVC) heat pump system. Their mechanical vapor compression uses water both as a refrigerant and as an injection medium. This leads to a special need for calculating mass and heat transfer. The model takes the control volume between the male and female rotors and the casing, which means that the control volume is moving while shrinking as the pressure is increased. Their model is comprehensive and includes leakage, water flashing, and heat transfer. The model was later on verified experimentally within an error of 8%.

A 3D numerical analysis of a twin-screw compressor was made in 2018. The software SCORG was used to generate the mesh used in the CFD. Some simplifications had to be made to the compressor. A low wrap angle and short axial dimensions were the results of the simplifications. The CFD-analysis has yet to be validated against other simulation tools or an actual application of twin-screw compressors (Casari, Kovacevic, & Ziviani, 2018).

As mentioned in Chapter 3.2, (Husak, Kovacevic, & Karabegovic, 2019) made a model trying to predict how deformation of the rotor and casing affects the clearance and the importance of understanding this effect. If this is further validated, it will be a precise, cheap, and fast method of predicting the change in clearance due to deformation. This, in turn, can lead to better design and significant enhancement in the performance of screw compressors.

Making accurate models of both the thermodynamic performance, deformation, heat, and mass distribution of the compressor is important. However, there will always be a need to verify the functionality and result of the proposed methods. There is work being done to make verification of different compressor design more feasible. An ejector-based detection

system has been proposed by (Li, et al., 2020). This can save economic investment costs up to 94.5% for manufacturers in need of a compression detection system.

Modeling is without a doubt an important part of developing and optimizing efficient twin-screw compressors that can operate in high temperature and pressure conditions. Understanding all processes inside every chamber at all times would make the optimization work of a twin-screw compressor relatively easy. With increasing computational power and competence in the area, the development of accurate models will continue to grow rapidly.

4.3.1 Research and modeling of leakage

In all positive displacement compressors, leakage is an important factor when considering the overall performance. A literature study on the topic was carried out by (Patel & Lakhera, 2020). In Table 4.1, the key findings of a literature view can be found. This is to give a quick overview of the current research status.

Table 4.1 Key findings from a literature review of leakage research in twin-screw compressors (Patel & Lakhera, 2020)

Researcher(s)	*Leakage type investigated*	*Work completed*	*Key findings*
(Prins & Ferreira, Leakage experiments on a running twin screw compressor, 2002)	Rotor tip housing	Indicated diagram analysis to study the influence of leakages on the compression line at different pressure ratings and different speeds.	Both the isentropic and volumetric efficiencies decreased as the gap size increased.
(Zamfirescu & Ferreira, 2004)	End plate	Identification of leakages at the beginning of the compression process.	ASR model gave a better prediction of the work done, discharge mass flow rate, isentropic efficiency (4-5%). The flow coefficient value found 1.2 against the range of 0.5-0.7 used by (Zaytsev, 2003)
(Prins, On the structure of compressor gas leakage flow, 2006)	Rotor tip housing	The qualitative aspect of leakage flows with consideration of friction and pressure recovery parameters.	The "Class D" representing high friction and low-pressure recovery was found to have the lowest leakages in comparison to the rest of the three classes (having a different combination of friction and pressure recovery).
(Buckney, Kovacevic, & Stosic, 2011)	Rotor tip housing	Estimation of operational clearances to derive the operating envelope of a specific application.	This approach found useful to design the manufacturing or cold clearances for the most severe and anticipated operating conditions of a specific application
(Rane, Kovacevic, & Stosic, 2015)	Interlobe and Blowhole	Analytical grid generation procedure formulated for mesh refinement in the interlobe area.	The approach provided flexibility to enhance the resolution of the rotor geometry which resulted in more accurate leakage flow prediction.

The major finding in this literature review indicates that there is limited research done on leakage in twin-screw compressors. In addition to the papers presented in Table 4.1, there is other work in the area. For instance, a similar approach to Zaytsev's approach was done by (Bommel, 2016). There are models on leakage, which can predict the leakage of a specific compressor after being compared to experimental data. But these models often have significant assumptions. Accurately predicting the leakage is a complex task, and there is still room for improvement. If all leakage paths are fully understood and modeled satisfyingly, it should be possible to decrease the leakage in a twin-screw compressor. Minimizing leakage will directly decrease the power consumption and therefore increase the performance of a screw compressor. This should therefore be a prioritized area for further research.

An analysis of leakages in a twin-screw air compressor using water as the refrigerant was carried out in 2019. The analysis was done in a mathematical model where the liquid water was modeled as droplets or film against a surface. The research concluded that the sealing line (rotor tip) clearance and the discharge end-face clearance have the most significant effects on the compressor performance. On the other side, the effect of the contact line clearance along with the start blow hole and suction end-face clearance was deemed negligible (Wang, Xing, Chen, Sun, & He, 2019). This paper was discovered after the work on the model was concluded, and is therefore not taken into consideration when it was decided which leakage paths should be prioritized.

4.4 Injection research

Injection of liquid in a screw compressor can as previously mentioned lower the discharge temperature without affecting the discharge pressure. There is a limitation to the amount of liquid that can be injected in a screw compressor. Ideally, there should be no liquid in the fluid that leaves the compressor as too much liquid at the end of the compressor is harmful to the equipment and may decrease the enthalpy of the mixture going into the condenser. The injected liquid will also lead to more compressor work as the mass flow rate will increase.

A test rig was set up to find the optimum amount of water injected. The experiment was set up for a process-gas screw compressor. It concluded that the optimum amount of water injected was 2-3 L/m^3 for the application tested (Yang, et al., 2018). This study is limited as the amount of water injected in a screw compressor is highly dependent on the operating conditions, placement of injection, and the refrigerant.

A case study on the effect of oil-injection diameter was conducted by (Basha & al, 2018). The injection was done with a variety of diameters and with an atomizer. The rotational speed and discharge pressure were also varied throughout the experiment. For two cases with relatively low discharge pressure, a reduction in the average oil flow resulted in a significant improvement of the specific power, however in two cases with higher discharge pressure a reduction in the average oil flow resulted in higher specific power of the compressor. Furthermore, the optimal diameter of the nozzle was dependent on the operating conditions (discharge pressure and shaft speed). An atomizer nozzle did, for most cases, decrease the specific power compared to the same operation with a single hole nozzle of comparable diameter. This is supported by previous research (Paepe, Bogaert, & Mertens, 2005).

The most comprehensive study done on liquid injection in twin screw compressors found in literature was done by (Tian, Yuan, Wang, Wu, & Xing, 2017). A numerical model of an ammonia compressor was made. The model, which considers a heterogenous mixture of ammonia and water, was validated against the experimental results of an ammonia refining system. The model concluded that there should be a pressure difference between the injected liquid and the vapor, to create a flashing effect of the liquid which will lead to atomization of the droplets. This is important to enhance the heat transfer of the liquid injected. An optimization method was carried out to figure out the ideal placement of injection points along with the amount of liquid injected. The study showed that it was beneficial for a liquid-injected twin-screw compressor to have two injection points (compared to one) and that the extra point should be in the part of the compression phase that has the highest temperature glide. The study also concluded that the proportion of

the second injection nozzle should be 70% to minimize the compressor work per unit of ammonia production.

There is a limited amount of research done on liquid injection in twin-screw compressors, which makes this an interesting part of the analysis of the operation of the twin-screw compressor. The benefit of introducing injection to limit the temperature glide seems to have a very desirable impact on the power consumption of the compressor. Atomizing the injected liquid to enhance the heat transfer, along with adding several injection points in the compression phase seems to have a positive impact on the performance of the screw compressor. Finding the right amount of liquid to inject, along with the ideal placement, the diameter of the droplet, pressure, and temperature of the liquid are just some of the many factors that can and should be optimized for liquid injection in screw compressors.

5 Thermodynamic modelling of a water injected twin screw compressor

A thermodynamic model of a water-injected screw compressor was developed based on an ammonia-water compressor model (Tønsberg, 2020). Ideally, any model should have limited assumptions, without sacrificing accuracy. If this is done satisfyingly, reliability will be ensured. Furthermore, a simplistic model that can easily be adjusted with regards to geometric variables, injection, and working fluid is beneficial. An adaptable model can be verified against experimental data from various compressors and therefore reassure the accuracy of the simulation based on a large sample size. It is also beneficial if the model can be implemented in a larger scheme to model an entire heat pump system.

As mentioned, the model is adapted from an ammonia-water compressor model. This model was built in the Modelica modeling language using Dymola. Modelica is an object-oriented programming language. This means that functions and data can be stored in objects and that these objects can be connected. Dymola consists of several commercial libraries containing various pre-made objects or data. In this model, TIL and TILMedia from TIL Suite are the two commercial libraries used. TIL is a model library for thermal components and systems, it contains steady-state and transient simulation. TILMedia on the other hand is a library that provides thermophysical properties. TILMedia can utilize external databases such as REFPROP (Frohböse, 2020), which is done in this model. The previous model was not based on an existing compressor but rather developed as a part of a pre-study for a compressor prototype that is set to be manufactured at a later stage. Validating the water-vapor compressor model with experimental results will be an indication of whether the ammonia-water compressor model is accurate and reliable for further use.

5.1 Assumptions

To verify that the modeled developed can be used as a reliable tool for simulating a twin-screw compressor it has to be verified against experimental data. To run the model, certain assumptions were made. This leads to some inaccuracies, however, most assumptions made in the model can be justified, due to their small or negligible impact on the simulation results.

Assumptions:

1. Negligible heat transfer from the compressor body to the surroundings. The model has a function for heat transfer from the compressor body to the surroundings. However, the literature indicates that the heat transfer between the working fluid and the machine parts has a negligible impact on the compressor performance (Stosic N. , 2015), and the heat transfer coefficient is therefore set to zero.
2. Homogenous fluid state at all times. This may be the most significant assumption in the model as there will be liquid and vapor present throughout the compression

process. When the liquid is injected into the compressor it will not evaporate instantaneously, and as the compression process is very fast the amount of injected water in the late stage of the compressor should be limited to avoid a lot of liquid in the discharged fluid. This is a consideration that needs to be kept in mind when evaluating the results from the simulations.

3. Homogenous pressure and temperature in a control volume at any instant. Similarly to assumption 2, this affects the performance and is not realistic as there will significant variations in the temperature and pressure.
4. Negligible kinetic and potential energy. This is a justifiable assumption in most screw compressor models. The change in both kinetic and potential energy is insignificant in an energy-equation of a screw-compressor.
5. Water is treated as an incompressible fluid.
6. Only two leakage paths are modeled. (Zaytsev, 2003) modeled five leakage paths, while (Fleming & Tang, 1995) identified and modeled six paths. This is a simplification that can be changed if the model is to be further developed. The two leakage paths taken into consideration is the contact line leakage between the two rotors and the sealing line leakage between the tip of the rotors and the compressor housing. These are, according to (Fleming & Tang, 1995) the leakages with the most significant impact on the volumetric efficiency of a screw compressor.

5.2 Model description

As mentioned, Modelica is an object-oriented programming language that can contain several objects containing functions or data. These objects can be combined into sub-systems, or as they are referred to in this model, components. The four different components utilized in the model will be described underneath. The components are connected through connection ports (green dots in the graphical view).

5.2.1 Component 1 – Control Volume

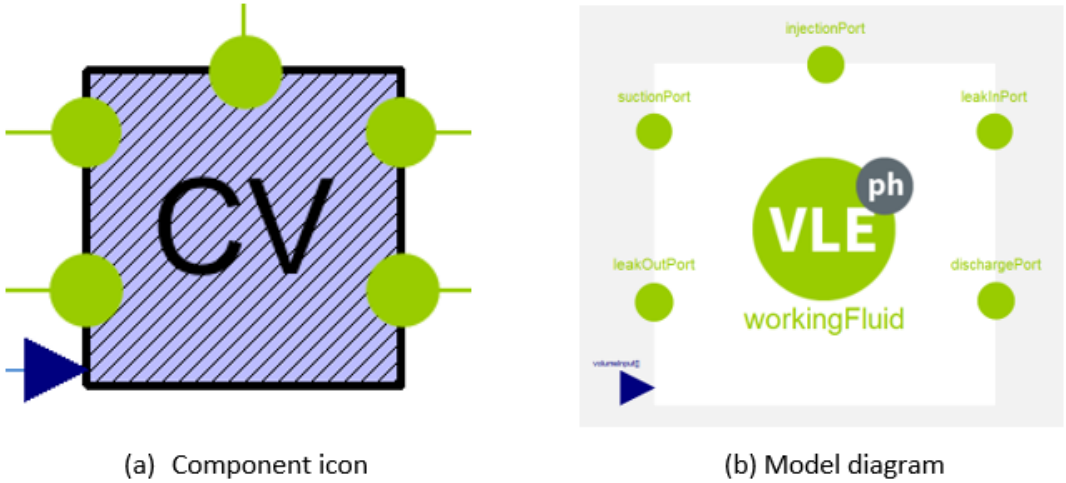

(a) Component icon (b) Model diagram

Figure 5.1 (a) shows the component icon as it is represented in the complete model. (b) shows the model diagram of the control volume including the elements the component is made of.

The most important component in the screw compressor model is the control volume. Each separate control volume represents one volume cavity in the actual screw compressor. A similar approach has been conducted in previous work described in the literature (Chamoun M. , Rulliere, Haberschill, & Berail, 2012) and (Tian, Shen, Wang, Xing, & Wang, 2017). The number of control volumes is dependent on geometrical factors like wrap angle, the number of male lobes, the length of the rotors, and the rotor profile. The water-injected screw compressor under consideration has 5 and 7 male and female lobes respectively. This is modeled by 10 control volumes, which rotate a total of 733° per complete cycle. To evenly distribute the control volumes, they rotate with 73.3° intervals. If the model is to be adapted to another compressor with other geometrical factors the number of control volumes and the angle between the control volumes can easily be modified. Eq 5.1 shows how the shaft rotational angle per cycle can be calculated (Bommel, 2016).

$$\boldsymbol{shaft\ rotation\ angle} = \left(\boldsymbol{2\pi + \tau_w + \frac{2\pi}{m_1} + \beta}\right) * \boldsymbol{\frac{180}{\pi} + 1} \qquad \textbf{Eq 5.1}$$

τ_w = wrap angle of the male rotor (°)
β = geometrical angle between the male rotor and centerline between the rotors (°)
m_1 =number of male lobes (-)

The number of control volumes can be calculated by

$$\boldsymbol{\#of\ CVs} = \frac{\dfrac{\boldsymbol{shaft\ rotational\ angle}}{\boldsymbol{360}} * \boldsymbol{V_0}}{\boldsymbol{V_{cav}}} \qquad \textbf{Eq 5.2}$$

V_0 = volume of the compressor (given in manufacture manual)
V_{cav} = Max volume of one cavity (calculated by information given by manufacture manual)

The control volume contains five connection ports as seen in Figure 5.1 (b): suction-, discharge-, injection-, leak in-, and leak out-, ports. The ports come from the TIL library and contain four variables that describe the state of the flow at each port. The variables are pressure at the port (p), mass flow rate at the port ($\dot{m}$), enthalpy of the flow if it flows out of the control volume ($h_{outflow}$) and the mass fraction out from the port of one of the fluids at the outflow ($x_{outflow}$) in a two substance model. The concentration will always be set to one in a single fluid compressor like the water-injected water vapor compressor modeled. The mass fraction is a factor that is left intentionally from the ammonia-water model to keep the adaptability of the model.

As seen in the model diagram in Figure 5.1 (b) there is a working fluid element called VLE (vapor-liquid equilibrium). This is taken from the TILMedia library and calculates the thermodynamic state of the fluid at the given conditions. The VLE needs two input parameters to calculate the other properties at the given conditions. In this model pressure and enthalpy are chosen as input parameters. However, pressure and entropy (ps), density and temperature (ρT) or pressure and temperature (pT) could have been used instead. The implementation of the VLE leads to an assumption that a cavity, i.e. control volume, is in equilibrium between vapor and liquid at all times (assumption 2 in 5.1). This is not the case for a twin-screw compressor as the injection of water at certain locations leads to different pressure and temperature in some areas in the cavity at a variety of stages throughout the process.

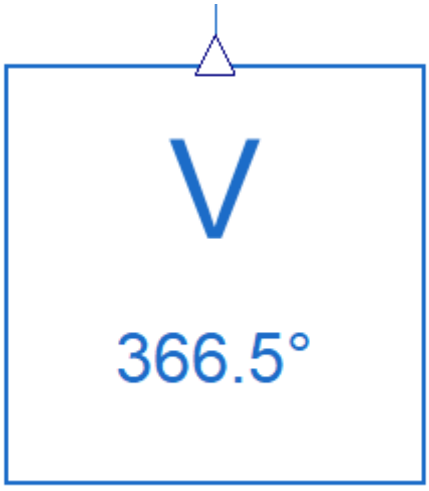

Figure 5.2 The volume function icon as it is represented in the complete model. The angle (366.5°) indicates at what angle this particular volume function starts at.

The change of the volume in the control volume is given by the volume function. The icon can be seen in Figure 5.2 and the corresponding code can be found in "Appendix D.8 Volume function". As this is a function containing information regarding the geometry of the screw, and not the fluid or flow, the connection port does not appear as a green dot but rather a blue arrow. The parameters that shape the volume curve is V, $\frac{dV}{dt}$ and θ where V is the volume of the cavity, $\frac{dV}{dt}$ is the time derivative of the volume while θ represents the rotational angle. The compression angle will go from 0 to the end of the cycle, so θ says where in the compressor the cavity volume is a certain value. The entire volume function

is a sub-model, and the input parameter is simply the angle at which volume starts for the specific cavity. As seen in Figure 5.3, the different cavities are represented by volume curves at different stages. The angle between the curves is determined based on the total rotation of the cycle divided by the number of cavities. In the water-injected screw compressor modeled in this report, there are 10 cavities. The volume curve (Figure 5.3) is created by a mathematical function and is identical to the volume curve provided by the manufacturer of the prototype modeled in this thesis.

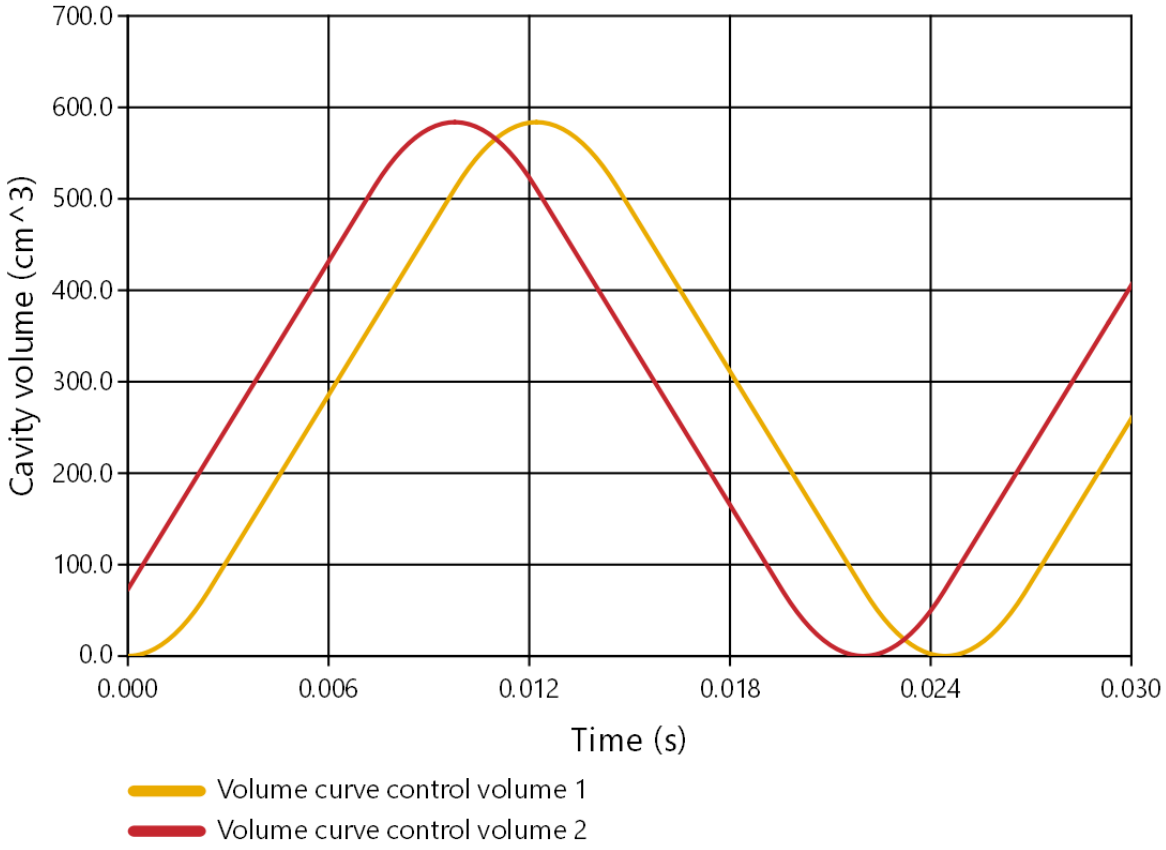

Figure 5.3 Volume functions of control volume 1 and 2. They represent the cavities in the twin-screw compressor.

In any control volume, certain conservation equations must be followed. For the control volume surrounding a cavity, the following conservation equations are applicable. Note that the built-in derivation operator in Modelica is $der()$,

$$\boldsymbol{der(m) = \sum \dot{m}_{port}} \qquad \textbf{Eq 5.3}$$

In Eq 5.3 the derivative of the mass inside a control volume is the summation of the mass flow in and out of the fluid ports, keep in mind that as mass goes out of a port the value will be negative.

$$\boldsymbol{der(mx_c) = \sum \dot{m}_{port} x_{c,port}} \qquad \textbf{Eq 5.4}$$

Eq 5.4 is an equation that was introduced when the model was developed for ammonia-water compression. It is in place to make sure that the mass balance is taken care of for the separate fluids. This equation is kept as a part of the model to keep the adaptability of the model to work with fluid mixtures, and not only single-fluid compression.

$$\boldsymbol{der(mu) = \dot{W}_{comp} - \dot{Q}_{loss} + \sum \dot{m}_{port} h_{port}} \qquad \textbf{Eq 5.5}$$

Eq 5.5 is the energy-balance equation, where the compressor work is calculated from Eq 5.6 and the heat loss rate is calculated from Eq 5.7.

$$\boldsymbol{\dot{W}_{comp} = -p \frac{dV}{dt}} \qquad \textbf{Eq 5.6}$$

It is noted that Dymola solver can produce a time derivative of the volume, but when it is introduced as an input, as it is in this model, the computational time and the possibility of numerical errors are reduced.

$$\boldsymbol{\dot{Q}_{loss} = \alpha V^{\frac{2}{3}} (T - T_{bod})} \qquad \textbf{Eq 5.7}$$

The heat loss equation was developed by (Chamoun M. , Rulliere, Haberschill, & Peureux, 2013).
Furthermore, the specific enthalpy and the total fluid mass of the control volume can be calculated using Eq 5.8 and Eq 5.9:

$$\boldsymbol{h = u + \frac{p}{\rho}} \qquad \textbf{Eq 5.8}$$

$$\boldsymbol{m = \rho V} \qquad \textbf{Eq 5.9}$$

m = Mass (kg)
$\dot{m}$ = Mass flow rate (kg/s), subscript port implies that it is the mass flow rate at an inlet or outlet port
x = Mass concentration of a fluid in a mixture (kg/kg), subscript c represents a specific fluid
u = Specific internal energy (kJ/kg)
h = Specific enthalpy (kJ/kg)
p = Pressure (kPa)
$\frac{dV}{dt}$ = time derivative of volume (m^3/s)
V = Volume (m^3)
α = Heat transfer coefficient (W/m^2K)
T = Temperature (K), subscript bod represents the compressor body
ρ = density (kg/ m^3), calculated from TILMedia library

As each compression cycle comes to an end the volume goes to zero and the cavity is emptied from any fluid. The cycle will be reinitialized by the built-in Modelica operator

$reinit()$. This means that all physical properties will be set back to their initial values. The code for the control volume can be found in "Appendix D.4 Control volume component".

5.2.2 Component 2 – Flow Restrictor

Figure 5.4 (a) shows the flow restrictor icon as it is represented in the complete model. (b) shows the model diagram of the flow restrictor including the elements the component is made of.

The fluid must follow a path as it moves through the compressor from suction to discharge. Fluids may also go through one of the leakage paths which exists in a twin-screw compressor. All of these paths are modeled by the flow restrictor component.

The blue arrow in the component icon and model diagram in Figure 5.4 indicates that an input function controls the behavior of the flow restrictor. The green dots in Figure 5.4 indicates that the TILMedia library is used in this component as well. The purpose of the fluid elements is to calculate the density of the flow, which of the two elements used is dependent on the direction of the flow. If the direction of the flow is into port A, element A will calculate the density upstream of the flow restrictor, and if the flow runs in the other direction, element B will calculate the density. The component is considered isenthalpic. It has two ports, A and B which can be used as inlet/outlet ports interchangeably dependent on the pressure. The mass flow rate is calculated by Eq 5.10

$$\dot{m} = A_{eff}\sqrt{2\rho(p_{high} - p_{low})} \qquad \textbf{Eq 5.10}$$

$\dot{m}$ = Mass flow rate (kg/s)

A_{eff} = effective cross-sectional area of the path (m^2)

ρ = density of the fluid (kg/m^3)

p = pressure (kPa)

The discharge and suction ports are two areas that are controlled by flow restrictors. The model icon representing these functions is shown in Figure 5.5 with their output functions dependent on time is shown in Figure 5.6. This is a vital part of the model to ensure that the ports are open at the right rotational angle, and therefore also at the right stage of the compression.

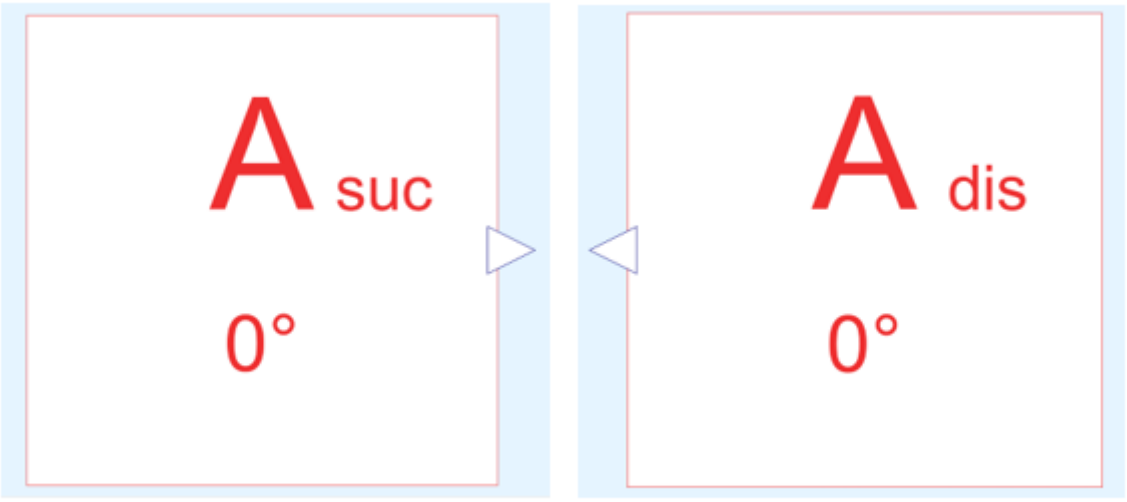

Figure 5.5 (a) and (b) Icon representing the suction area function and discharge area function in the diagram of the model. The number below represents the angle where the function starts and varies dependent on the control volume.

The effective cross-sectional area (A_{eff}) is described by a function that varies depending on what path is being dealt with. This function is connected to the flow restrictor as an input function. For the suction and discharge path, A_{eff} is calculated with a mathematical function that is closely fitted to the suction and discharge function portrayed in (Bommel, 2016), where the discharge and suction functions are results of a geometrical model. The suction port is only open up until the compression phase starts, this is to ensure that no compressed gas will leak out of the suction port. The discharge port is only open for a brief time when the pressure is at the desired level. The opening size and time of the discharge port are significantly lower than the suction port, this a natural consequence of the increased pressure and therefore decreased specific volume of the mass flow.

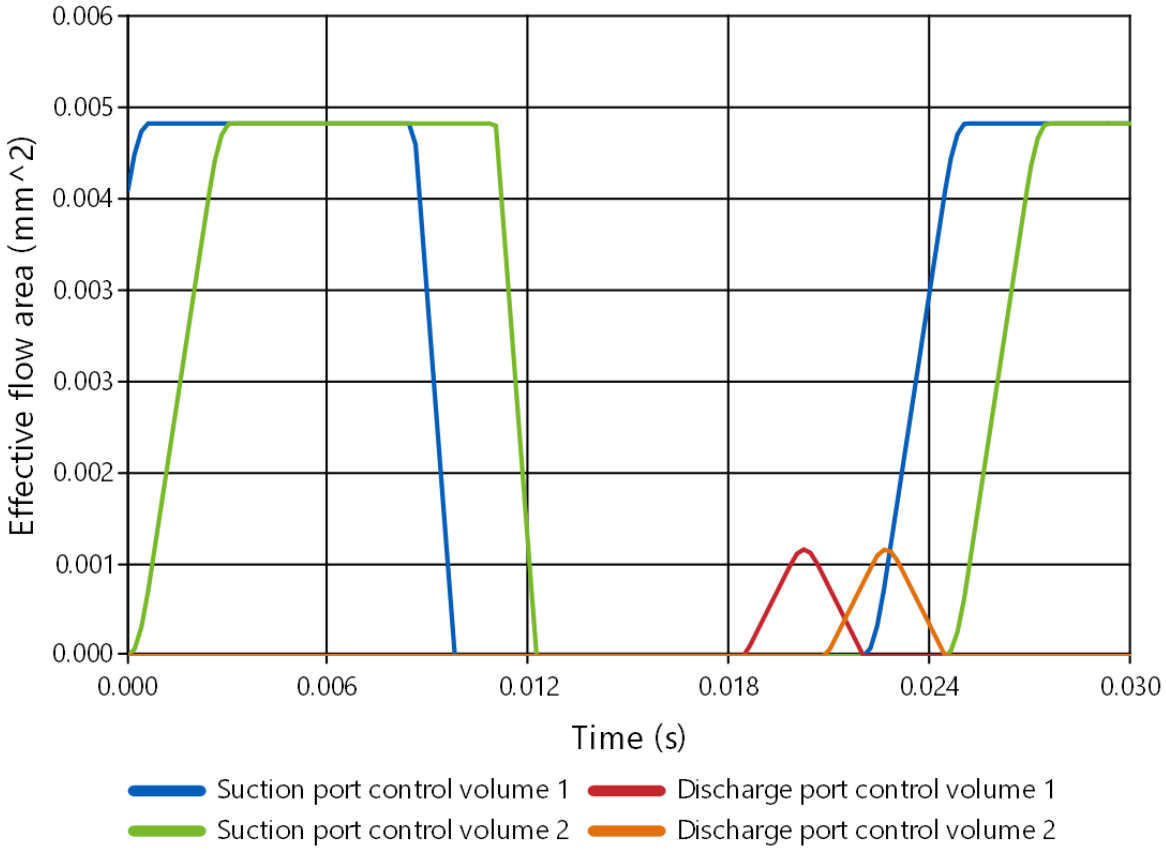

Figure 5.6 Effective flow area of the suction port and discharge port, for two consecutive control volumes.

The flow restrictor component is also used for leakage paths 1 and 2, which is the sealing line leakage (between rotor tips and casing) and the contact line leakage (between the two rotors) respectively. The effective area of the leakage is calculated by Eq 5.11.

$$A_{eff} = C_{leak} * \min(V_{trailing}, V_{leading}) \qquad \textbf{Eq 5.11}$$

$V_{trailing}, V_{leading}$ = volume of the trailing and leading cavity

C_{leak} = Leakage coefficient

It is assumed that the suction line leakage is proportional to the cavity volume in the separate cavities. A proportionality coefficient is introduced to manage the influence of the leakage and ensure that it is within a reasonable value. The proportionality coefficient is decided based on a linear function which is dependent on the evaporation temperature and the volumetric efficiency calculated from the experimental data. This is done to make sure that the model can be used to predict the performance of the compressor outside of the operating ranges tested in the experimental data. The reason why the leakage coefficient function is based on experimental data is to compensate for the lack of other leakages in the model. Ideally, all leakage paths should have been modeled, and been dynamic dependent on the input in a way that no coefficient function had to be implemented. This can also be solved if a precise geometrical model of the compressor is developed.

Figure 5.7 Icon representing the leakage function in the compressor diagram

As discussed in the assumptions, there are 5 or 6 leakage paths according to literature. In this model, only the two most significant leakage paths are considered. As seen in Figure 5.8 the first leakage path is the sealing line leakage between the rotor tips and the housing. This leakage is only in the compression phase when the pressure is larger in the leading cavity than in the trailing cavity. The second leakage path modeled, the contact line leakage, is between the two rotors. Fluid leaks from the compression side to the suction side. Both of these leakages are modeled to reflect the leakages reported in (Bommel, 2016) which again was found based on a geometrical model of a twin-screw compressor.

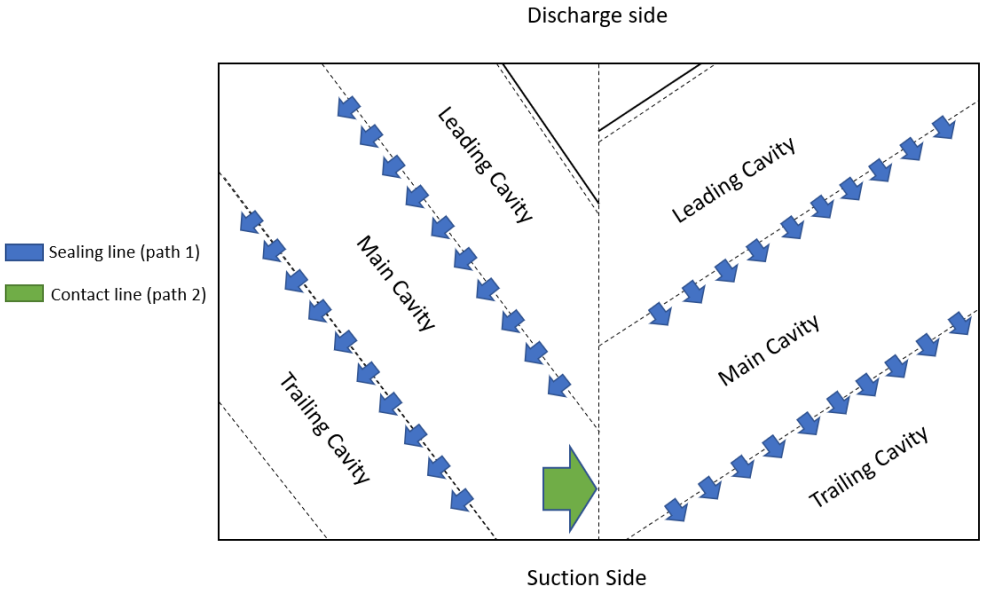

Figure 5.8 Illustrated sealing- and contact line leakage paths

The graphical results of the leakage path functions can be seen in Figure 5.9. The leakage area y-axis is on the right, while the control volume is on the left. The control volume is shown in the graph so that it can be seen where in the process the leakage paths are relevant. The contact line leakage is only relevant in the compression phase when there is a significantly lower pressure in a trailing cavity compared to the leading one. The sealing

line leakage happens both in the suction phase and in the compression-/discharge phase. The relationship between the leakage paths is constant as there is only one leakage coefficient. In previous iterations of the simulation, both leakage paths were controlled by separate input coefficients. If there is data showing the exact effective leakage area, two separate leakage coefficient can be reintroduced to enhance the accuracy of the model.

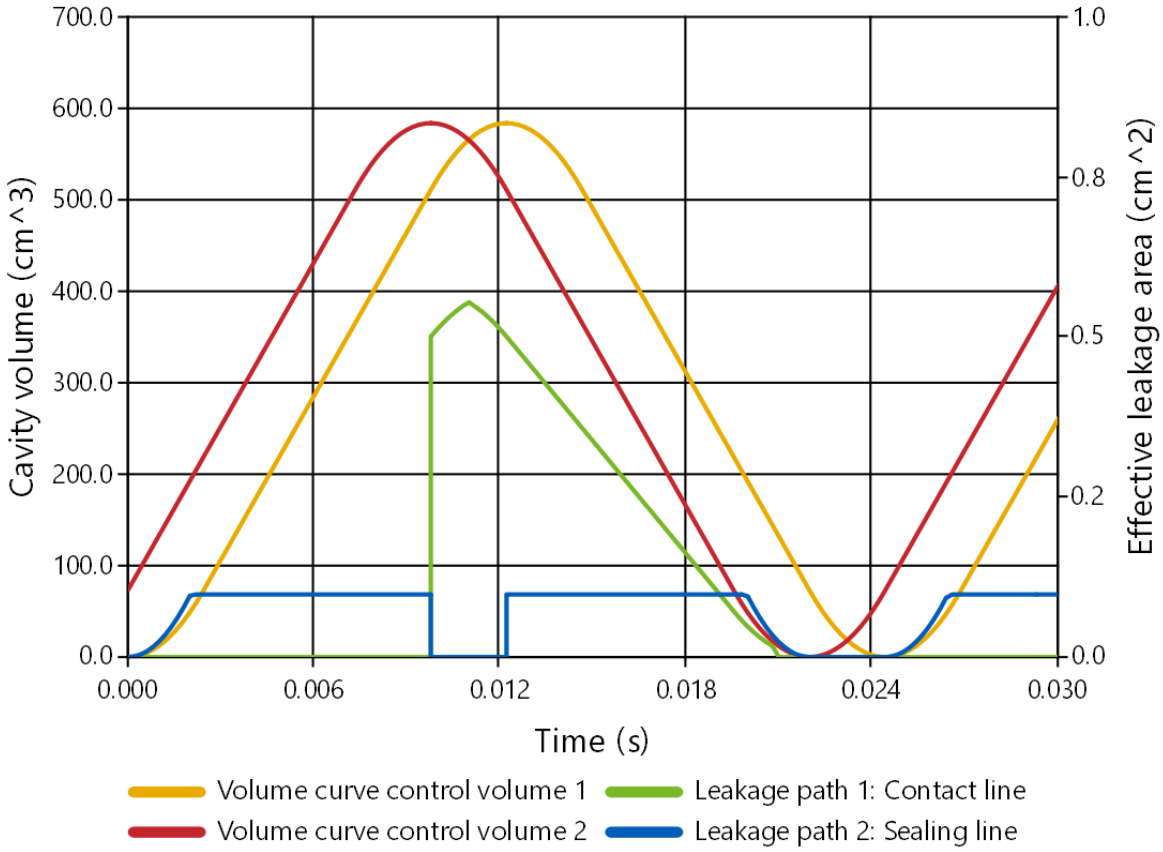

Figure 5.9 Effective flow area of leakage paths 1 and 2. Cavity volume is shown to better understand when leakage occurs in the two leakage paths modeled.

5.2.3 Component 3 – Injector

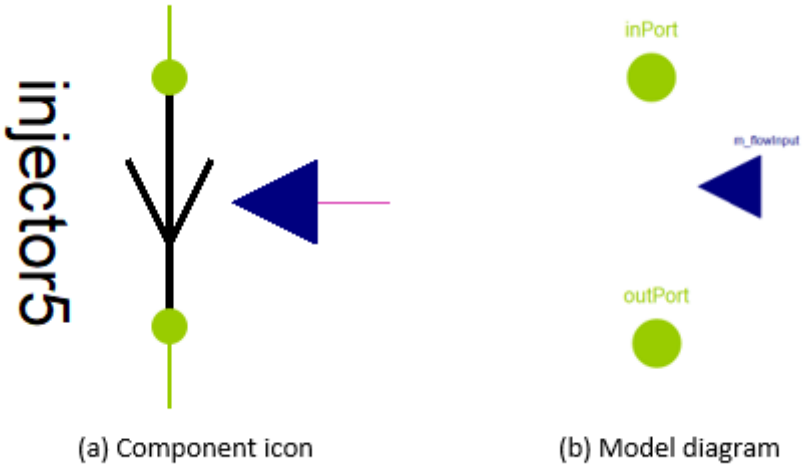

Figure 5.10 (a) shows the injector icon as it is represented in the complete model, the label "injector5" indicates that this injector is fitted with the fifth control volume. (b) shows the model diagram of the injector including the elements the component is made of.

The injector is the third component (Figure 5.10). The injector is used to inject liquid into each control volume. The component consists of three elements. There are an inlet and an outlet port, and an input injection function. The inlet and outlet port lets the working fluid (liquid water in the cases presented in this thesis) flow in and out of the component, while the injection function controls the mass flow rate of the liquid injected. There are 10 injectors in the model, one for each control volume. The phase change between the control volumes must be specified for each injection function as well. The inlet flow port is controlled by an input signal, so the liquid appears from an external source. The outlet port must be connected to its corresponding control volume to make sure that the injection happens at the right time.

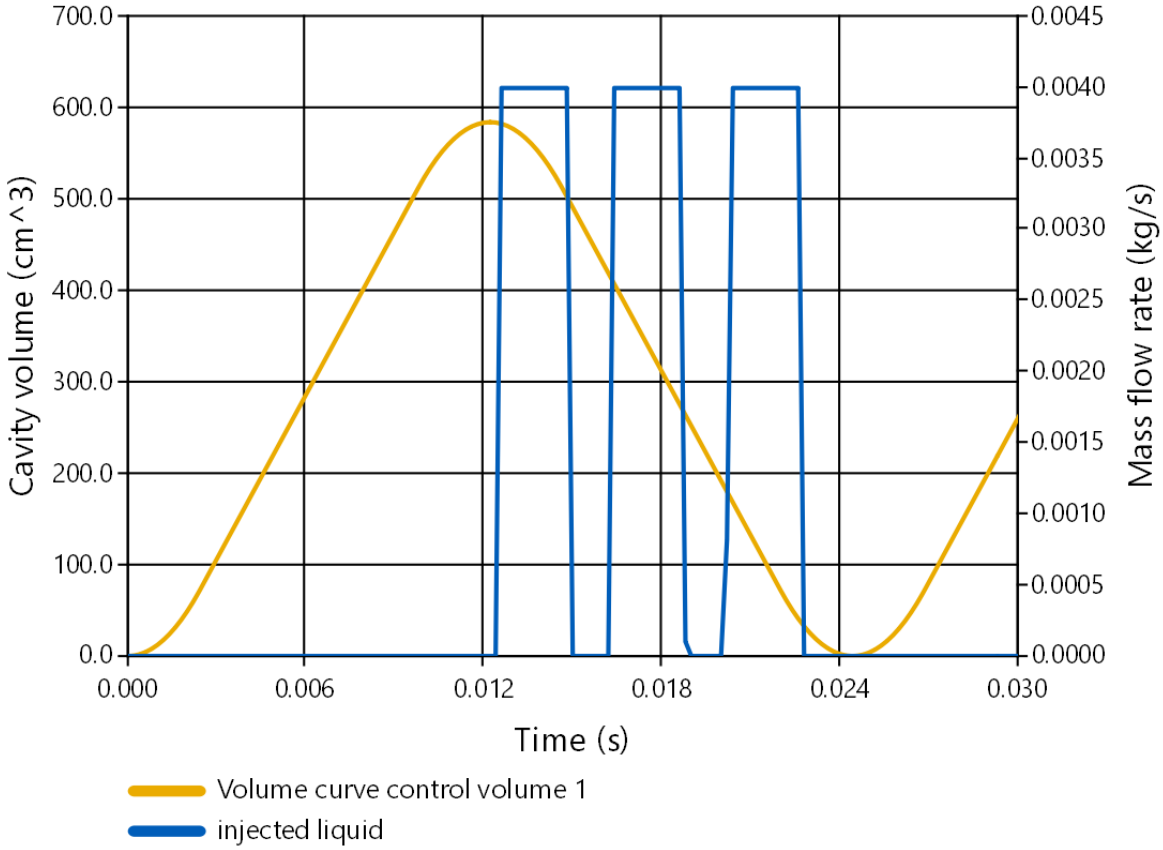

Figure 5.11 Injection function. The volume curve is shown to view at what stage the injection is done

The input signal is controlled by a function called an injection flow function. The function used in this simulation contains three injection points all in the compression phase. The maximum injected liquid mass flow rate (kg/s) is controlled by a constant input. The angle of the injections(rad) in the cycle are also set from as constant inputs. The model does consider the change in angle between the control volumes, so the injection angles are consistent in the cycle regardless of control volume or iteration. As seen in Figure 5.11 the three injection nozzles in the compression phase of the model. The maximum injection point is set to the maximum injection at one nozzle since there are three nozzles', the value is must be multiplied with three if it shall be compared to the experimental data.

5.2.4 Component 4 – Junction

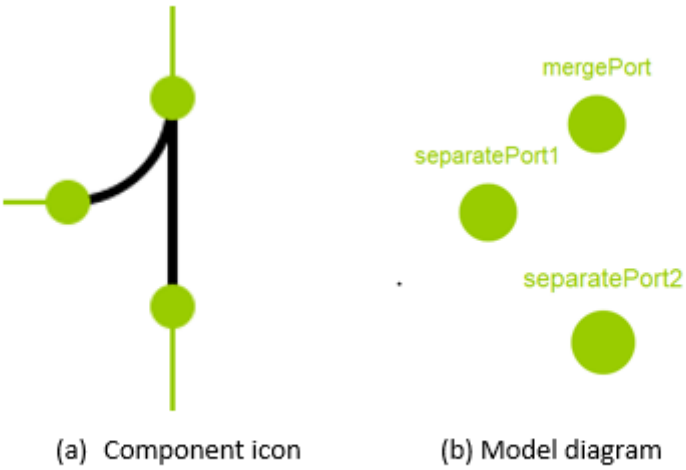

Figure 5.12(a) shows the injector icon as it is represented in the complete model. (b) shows the model diagram of the injector including the elements the component is made of.

The final Component is a junction component (Figure 5.12). The purpose is to separate one fluid flow path into two or merge two fluid flow paths into one. As there are only two input ports (suction port and injection port) of flow and one outlet port (discharge port), and ten control volumes, the flow needs to be separated before the suction and injection functions and merged after the compression part of the cycle. The component consists of one merged and two separated ports. The mass in the junction component is set at a low constant value of $m = 1 * 10^{-8} kg$, which dictates that as mass flows into the component, the mass flow must exit the component simultaneously in a similar magnitude.

$$\sum \dot{\boldsymbol{m}}_{\boldsymbol{port}} = \mathbf{0} \qquad \textbf{Eq 5.12}$$

The model is developed to handle a variety of working fluids including mixtures, for instance, ammonia and water. The junction function is set up so that the mass fraction can vary in the individual ports.

$$\sum \dot{\boldsymbol{m}}_{\boldsymbol{port}} \boldsymbol{x}_{\boldsymbol{f,port}} = \boldsymbol{m}\ \boldsymbol{der}(\boldsymbol{x}_{\boldsymbol{f}}) \qquad \textbf{Eq 5.13}$$

Energy conservation is taken care of by balancing the energy equation by

$$\boldsymbol{m}\ \boldsymbol{der}(\boldsymbol{h}) = \sum \dot{\boldsymbol{m}}_{\boldsymbol{port}} \boldsymbol{h}_{\boldsymbol{port}} \qquad \textbf{Eq 5.14}$$

.

$$\boldsymbol{m}\ \boldsymbol{der}(\boldsymbol{h}) = \sum \dot{\boldsymbol{m}}_{\boldsymbol{port}} \boldsymbol{h}_{\boldsymbol{port}} \qquad \textbf{Eq 5.14}$$

$x_{f,port}$ = mass fraction of fluid f at the inlet or outlet port

h_{port} = specific enthalpy at a port

The pressure is the same at all ports, so it is assumed no pressure drop in the component.

5.2.5 The complete model

The complete model is shown in Figure 5.13. The various components are connected to represent the entire screw compressor. Three connections ports are the input and output of the model (represented as green dots on the border between the white square and the grey background). The one on the left is the suction port, the port on top is the injection port and the one on the right represents the discharge port. All of the green lines represent paths the fluid flows through, while the other coloured (pink, red, and blue) lines represent input signals. As mentioned, the control volumes are set to run the different functions 73.3° apart. This can be modified in the graphics by changing "theta start" also known as the start value for the rotational angle.

Between all of the control volumes, there are flow restrictors, these represent the leakage from one control volume to the next. A red input line goes from each separate leakage function to the leakage flow restrictor. The other flow restrictors are at the suction and discharge phase, where the suction area function and discharge area function are input signals following red lines.

Furthermore, the injector component can be found in the upper part of the model, downstream of the injection port. The input signal here is the injection function and is represented by a pink line.

The junction component is used at all major ports(suction-, injection- and discharge port) of the model. After the inlet ports (suction and injection) the junction is used to split the stream into 10 separate streams who all lead to each control volume. While at the outlet port the component is used to merge the 10 streams from the control volumes into 1 before entering the discharge port. It is worth mentioning that the junction components are upstream of the suction area and injection flow restrictors and downstream of the discharge area flow restrictors.

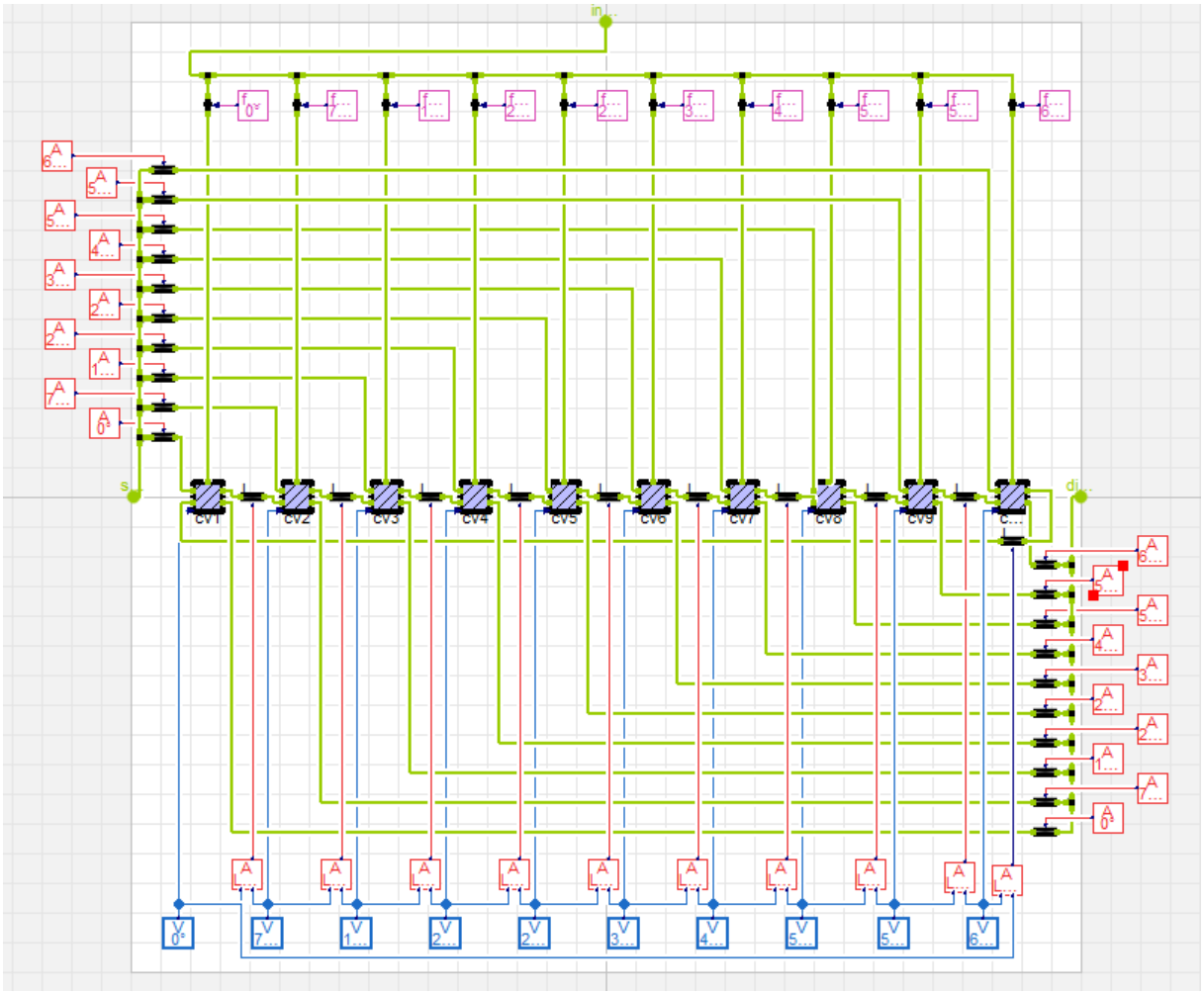

Figure 5.13 A diagram of the entire screw compressor model

One of the aims of the model is that it should be implementable in larger systems with more heat pump components than just the compressor. If a model of an entire heat pump is to be developed in Dymola, the compressor model can easily be implemented with the other components by connecting lines between the components. The model icon is shown in Figure 5.14, and the three green dots on the edge of the icon which represents the suction, injection, and discharge port can be connected to for instance a flash tank, liquid injection pump, and a condenser.

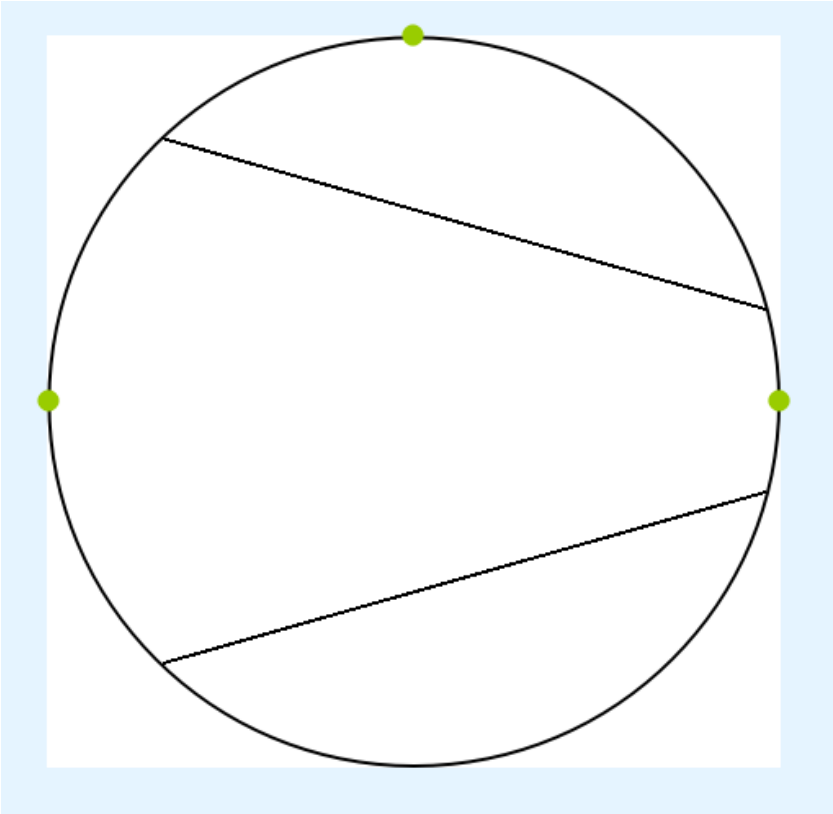

Figure 5.14 The icon of the compressor model

5.3 Simulation settings for validation against experimental data

5.3.1 Settings and input parameters

As one of the purposes of the model is to be easy to modify, some input parameters can change the operating conditions of the screw compressor without doing any changes to the actual code. The input parameters can simply be changed by double-clicking the

compressor icon of the simulation model. A pop-up window similar to Figure 5.15 will then appear. The input parameters are described below.

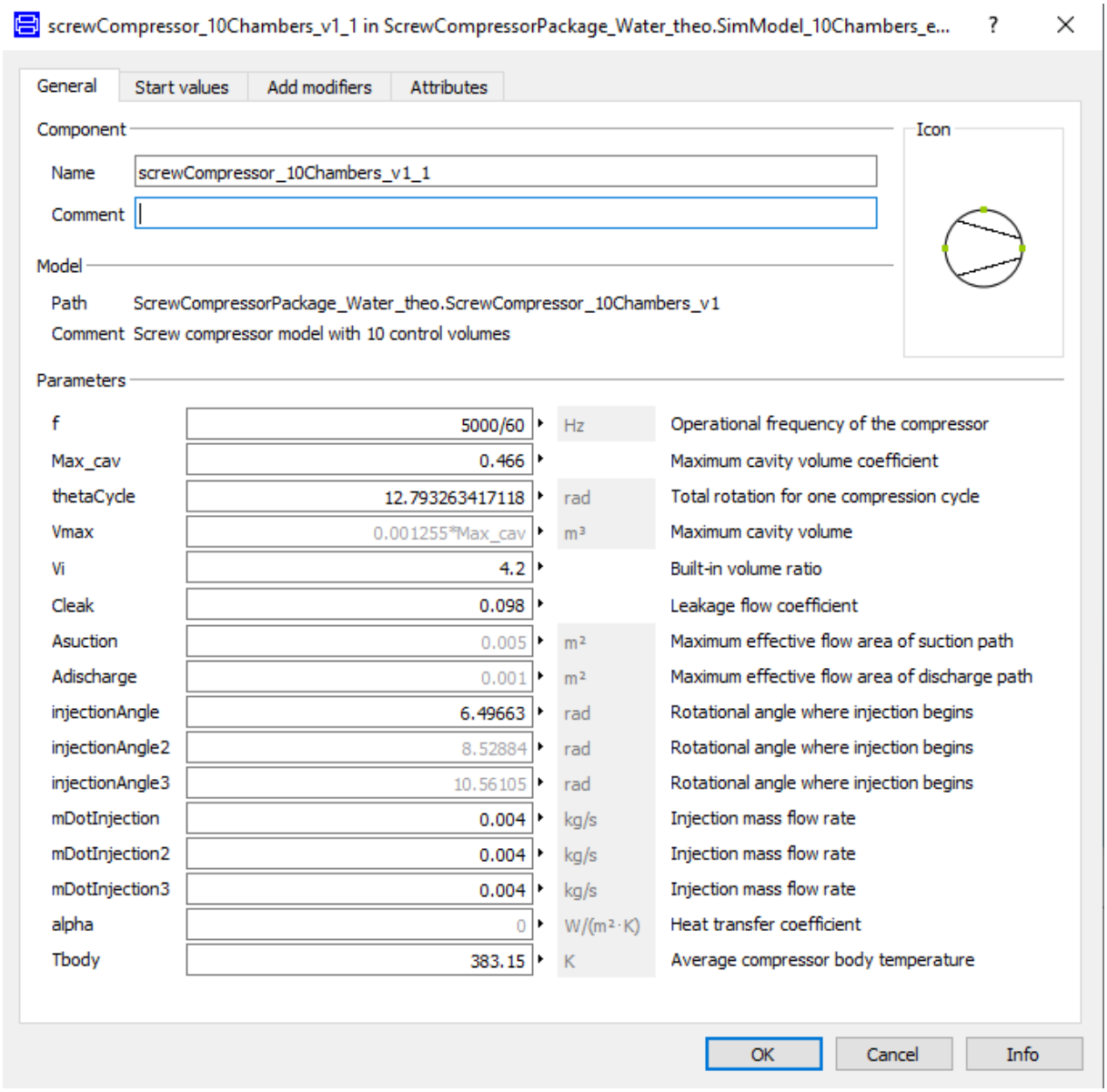

Figure 5.15 Input parameters in a simulation model

f = Operational frequency of the compressor (Hz). This is simply the number of 360° rotations per second. It is here calculated by 5000rpm/60Hz which is the operational speed of the twin-screw compressor at SJTU divided by the AC frequency in China. This value is further used to determine the angular velocity of the compressor.

Max_cav = Maximum volume per cavity coefficient (-). This is a way of compensating for the volumetric efficiency of the compressor. As the experimental data were analyzed, the volumetric efficiency was calculated based on the theoretical operational speed/ actual operational speed. As can be seen in Vmax, this value limits the maximum volume per cavity. The value here is the same or in the range of being the same as the calculated volumetric efficiency based on the experimental results.

θ_{cycle} = Total rotation for one compression cycle (rad). This is quite self-explanatory, and the calculations for the total rotation for one compression cycle is carried out in section 1.1.1.

V_{max} = Maximum cavity volume (m^3). This is constant for a compressor. This is calculated based on the geometrical parameters of the compressor that is found in the manufacturer's handbook. As the volumetric efficiency is implemented as a limitation of max value, it is here expressed as $V_{max} = V_{max,geomtrical} * Max\_cav$

v_i =Built-in volume ratio (-). This is constant for a compressor as long as the compressor does not have a sliding valve. Value is typically given by the manufacturer.

C_{leak} = Leakage flow coefficient for path 1 and 2 per cavity (-). A proportionality constant which is implemented to calculate the effective flow area for the separate leakage paths per control volume. The limit of the effective area of leakage area for path 2 is also based on this value to ensure that the relationship between the leakage paths is reasonable.

$A_{suction}\ and\ A_{discharge}$ = Maximum effective flow area for suction and discharge (m^2). The cross-sectional area of the fluid path of suction and discharge flow per control volume.

$Injection\ Angle, Injection\ Angle\ 2, Injection\ Angle\ 3$ = Rotational angle where injection begins (rad). The angle from the start of the suction phase until each liquid injection starts per control volume (rad).

$mDotInjection, mDotInjection2, mDotInjection3$ = Injection mass flow rate (kg/s). This is the maximum amount of liquid injected per injection nozzle.

α= Heat transfer coefficient (W/m^2K). Heat transfer coefficient for heat transfer from compressor body to surroundings.

T_{body}= Average compressor body temperature (K). The assumed average temperature of the compressor body in heat transfer from a compressor to its surroundings.

Dymola has a wide range of integration methods that can be used to solve a numerical problem. The default integration method is Dassl, the model can be simulated with acceptable results when this integration method is utilized. However, in some conditions, a warning flag saying the model is stiff is raised. This can be dealt with by solving the simulation with Esdirk23A instead. Esdirk23A is slower, as it requires more computational power than Dassl. However, it is less sensitive to step size and is therefore recommended in this application. When developing the model, Dassl was used to save time, but during all results, Esdirk23A was used (Tønsberg, 2020). In "Appendix D.14 Comparison between integration methods", the pressure development with both integration methods can be seen. There is no noticeable difference in the result.

5.3.2 Initialization

To start a simulation procedure start values have to be inserted in the programming text. Dymola is not able to guess initial values in the range of what it should be before the simulation start, so this has to be done manually. TILMedia needs to calculate the thermodynamic properties of the fluid in each control volume at each iteration step also at

t = 0s. The initialization parameters are $p_{start,cv}$, $h_{start,cv}$ and $x_{start,cv}$. The last parameter, the concentration, is a result of this model being adapted from an ammonia-water compressor and is kept to keep the model's adaptability. The value is naturally 0 at all times, including the initial values for a single fluid compression. The first 50% of the control volumes starts in the suction phase, the initial pressure, and enthalpy value is determined by the suction condition. For the last 50% of the control volumes, the initial value for the pressure and enthalpy is increasing the further into the compression phase the control volume starts. The values are a rough estimate and are not changed dependent on the operating conditions of the simulation. There is a preliminary simulation that will calculate more accurate start values. The number of preliminary simulations can be chosen, and will naturally decide the accuracy of the start values, as many simulations will reassure a good starting value.

Furthermore, there have to be starting values for the junction component as well. Eq 5.13 and Eq 5.14 requires an initial guess of h and x_c. Once again the mass concentration will be set to 0 for single fluid compression. The start values for the junction immediately after the suction and injection port are decided based on the values for the suction-($h_{start,suc}$) and injection-($h_{start,inj}$)port respectively. The discharge starting values must be estimated manually, but the mass in each junction is low ($m = 1 * 10^{-8} kg$), this allows a rapid change in the state of the fluid.

5.4 Simulation Procedure

The experimental data consisted of one sheet of raw data. The first step of the validation was to decide which parameters were known (inputs) and which parameters were desired outputs. It was decided that the input parameters were the thermodynamic state(pressure and temperature) of the refrigerant (water) at suction, injection, and discharge along with the injected mass flow rate. This meant that the output is the mass flow rates and the compressor power consumption. It is also important to check that the simulation can meet the thermodynamic states desired. For example, if there is not enough liquid injection the simulation could potentially not be able to keep the temperature within an accepted error of the desired discharge temperature.

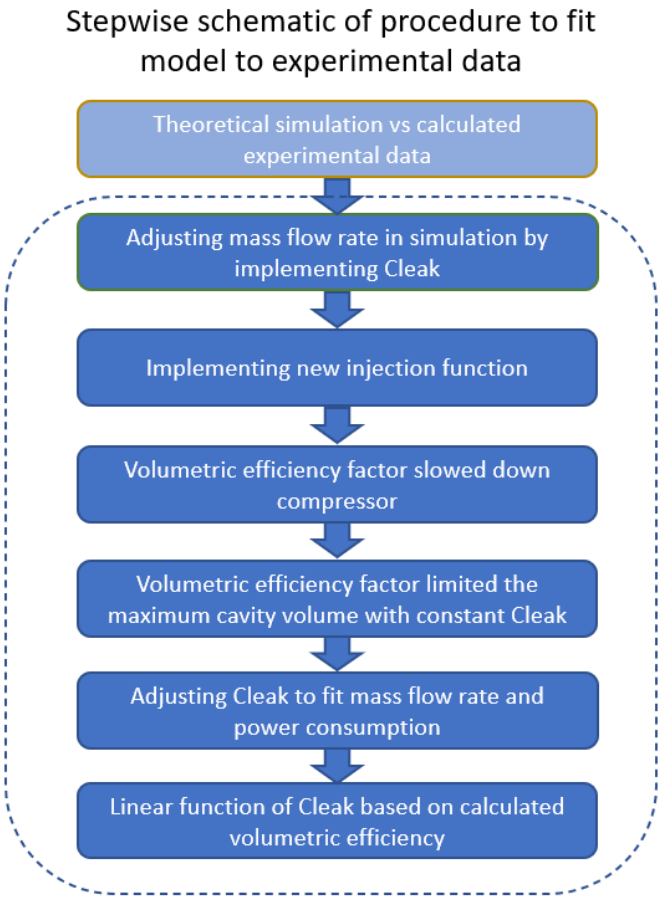

Figure 5.16 Schematic of major changes done to match simulation and experimental data (inside dotted lines are against experimental data, while outside is against theoretical calculations)

The first step towards verification of the model was based on a theoretical operation of the screw compressor. A theoretical operation of a screw compressor is here seen as a screw compressor with a volumetric efficiency of 1 and zero leakage. The ideal mass flow rate at suction and discharge was calculated based on the operational speed of the compressor. It is, as discussed in Chapter 2.3.4, difficult to calculate the theoretical work of a twin-screw compressor with liquid injection. If the isentropic enthalpy or an enthalpy calculated with reasonable isentropic efficiency is used, the compressor work is unreasonably high. If the enthalpy at the saturated vapor line, or based on the thermodynamic state at the discharge point is used, the compressor work is low. Therefore, the theoretical simulation is mainly done to assure that the mass flow rates are accurate in ideal operation. The model was only tested for 9 operating settings, spread equally between the 3 evaporation temperatures with varying pressure ratios.

After the theoretical simulation was done, the job of figuring out fitting values for C_{leak} started. The same 9 operating conditions were simulated, and the C_{leak} value was tuned to fit the experimental data, the mass flow rate was still the main concern as the compressor work was not very accurate at this point. A correlation study was done to see what operating parameter correlated best with the C_{leak} input value, but with only 9 operating points, the sample size was not large enough to draw a reliable conclusion.

Before increasing the sample size, a new injection function was developed. Up until this point, there had only been one injection nozzle, while the experiment was set up with three injection nozzles. 22 experimental data points were simulated with the new injection function. The C_{leak} was adjusted for each point to make sure the mass flow rate matched the experimental data. The mass flow rate had a decent fit, but the compressor work was way off. It was decided that a volumetric efficiency parameter had to be implemented to deal with the inaccurate compressor power consumption. The first volumetric efficiency was simply a coefficient that slowed down the compressor speed. It was then decided that a more accurate representation of the volumetric efficiency loss would be to limit the maximum volume in a control volume. The new parameter was called Max_cav, and the factor (based on the volumetric efficiency from experimental results) was multiplied by the maximum cavity volume in the model.

In parallel with the simulations carried out with the new Max_cav parameter, a new leakage function was developed. To better simulate the real case, the new leakage function included two leakage paths instead of one. The new path modeled represented the leakage over the contact line between the two rotors. This is according to literature the leakage path with the largest influence on volumetric efficiency (Fleming & Tang, 1995).

After all of the functions and variables were implemented in the model, there was still an unacceptably large error for the compressor power consumption. The main concern was the input values for C_{leak} and Max_cav. All 22 operating conditions were simulated with a constant C_{leak} value, where the Max_cav value was adjusted until the simulation was as close to the experimental data for mass flow rate and power consumed by the compressor as possible. Then all 22 data points were simulated with a constant C_{leak} and a Max_cav equal to the volumetric efficiency. Lastly, all 22 operating conditions were tuned with both of the abovementioned parameters as changeable parameters. All of this data was used in a correlation study to figure out how to make functions for Max_cav and C_{leak} based on the inputs (thermodynamic state of the operating conditions). The functions had to be implemented to make sure that the simulation was a close fit for the experimental data for all operating conditions.

Several functions were made, and polynomial functions for the C_{leak} had a good fit. However, it was a priority to be able to explain the function from a thermophysical point of view. It was therefore decided that the C_{leak} should be based on a linear function with the volumetric efficiency as a coefficient and the evaporation temperature as added constant. The Max_cav was offset by a constant of 0.01 from the volumetric efficiency. The functions, along with the data it was based on can be found in "Appendix C.2 Pearson Correlation and Linear approximation calculation". The justification of the function can be found in Chapter 7.2.1.

5.5 Further studies based on the simulation

5.5.1 Injection-optimization study

Figuring out how injection can be optimized for a water-injected twin-screw compressor is of interest as this may drastically improve the performance of such a compressor. There are several ways to differ the injection conditions other than changing the total mass flow injected. Some of them include placement of injection, number of injection points,

distribution of mass flow in the injection points, temperature and pressure of the liquid injected, and how the liquid is injected (diameter of stream, atomized, sprayed, etc.). In this thesis, various injection amounts and distribution were tested at several operating conditions to see how this would affect the simulated performance of the compressor.

The variable injection amount was tested at operating conditions with an evaporation temperature of 80°C and a suction pressure of 0.47 bar and a pressure ratio of 6.2. The same evaporation temperature was then tested with a pressure ratio of 3.9 and 9.5 which are the lowest and highest-pressure ratios from the experimental data. To see how if the results would be similar with different evaporation temperatures, simulations with similar pressure ratios to the original case was ran for evaporation temperatures of 75°C and 85°C. The reason why these cases are chosen is to see if the trends are similar both in the horizontal and vertical direction from the original case as seen in Figure 5.17. All operating conditions were first simulated with the same amount of liquid injected as the experimental case before 8 other amounts were tested. Two cases were pre-determined (0 and 0.01kg/s maximum injection per nozzle) while the other cases were determined based on the experimental injection value. The pre-determined cases are not realistic to run in an experiment as these conditions are likely to damage the equipment in the system. If no liquid water is injected, the protective seal between the rotors is expected to vanish, and the superheat will reach temperatures higher than the specifications of the compressor. Too much liquid water will make the compressor operate more like a pump, which is an inefficient operation of the system as the condenser will be filled with water, and the latent heat of condensation will not be utilized.

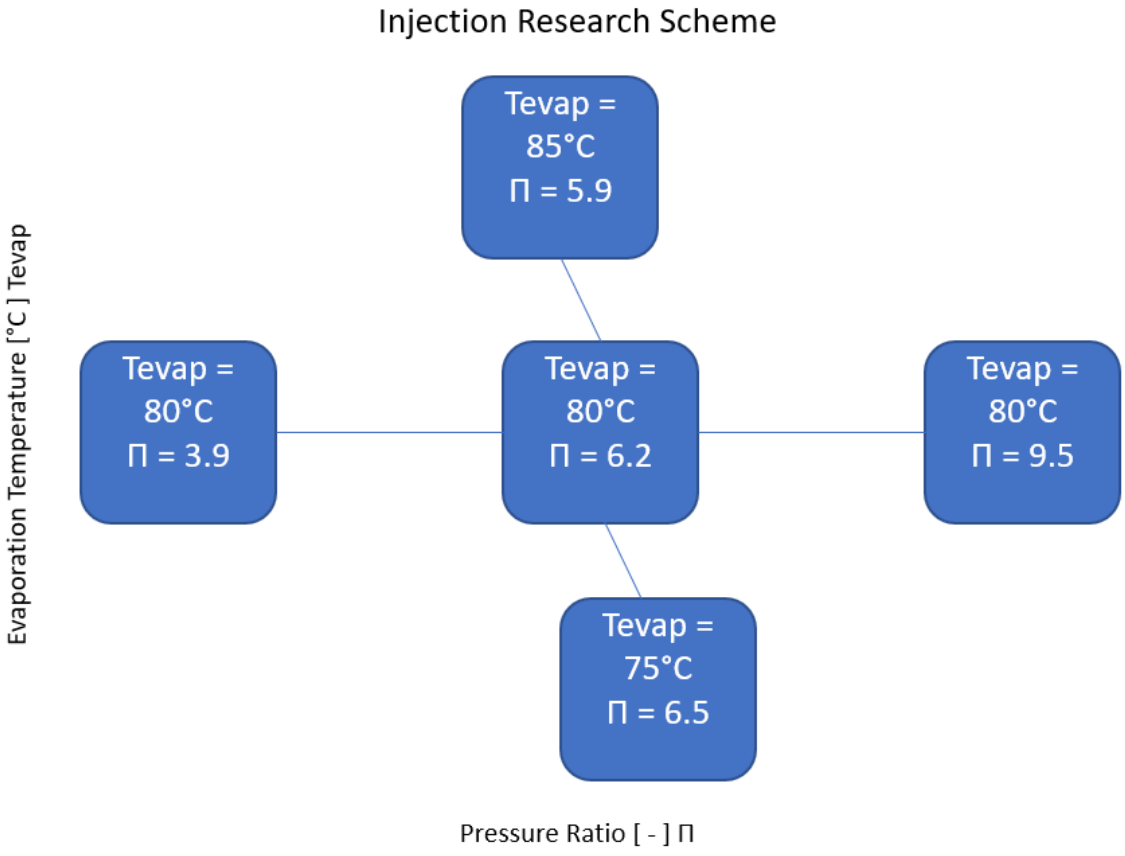

Figure 5.17 Injection testing settings

As mentioned, many injection variables could be interesting to look at. The second variable investigated in this thesis is the distribution of the liquid injection. In the experimental data, the liquid injected is spread equally on the three injection points. The five operating conditions shown in Figure 5.17 were all considered for this part of the study. Firstly, the original mass flow rate from the experimental data was used. Then the same amount of liquid was injected but with 5 different distributions of mass flow in the injection points. Furthermore, the same temperature and pressure condition was simulated with lower and higher mass flow rates for all of the distribution settings, this was done to see whether the trend was independent of the amount of mass flow for every operating condition. In all, 15 different mass flow rates were tested for all the operating conditions. The distributions can be seen in Table 5.1. The bolded font indicates that the total mass flow rate injected is the same as in the experimental investigation.

Table 5.1 Liquid injection distribution

Temperature and pressure settings:	Average injected mass flow (kg/s)	Distribution (%)				
Tevap = 80, П = 3.9	0.006	30, 30, 40	20, 20, 60	40, 40, 20	40, 30, 30	50, 30, 20
	0.008					
	0.010					
Tevap = 80, П = 6.2	0.008	30, 30, 40	20, 20, 60	40, 40, 20	40, 30, 30	50, 30, 20
	0.012					
	0.016					
Tevap = 80, П = 9.5	0.015	30, 30, 40	20, 20, 60	40, 40, 20	40, 30, 30	50, 30, 20
	0.017					
	0.019					
Tevap = 75, П = 6.5	0.008	30, 30, 40	20, 20, 60	40, 40, 20	40, 30, 30	50, 30, 20
	0.010					
	0.013					
Tevap = 80, П = 9.5	0.010	30, 30, 40	20, 20, 60	40, 40, 20	40, 30, 30	50, 30, 20
	0.014					
	0.018					

5.5.2 Simulation of new operating conditions

One of the reasons why an accurate, reliable thermodynamic model of a twin-screw compressor is beneficial is to see how the compressor should perform in new operating conditions. Using linear interpolation or extrapolation of experimental data can indicate how the compressor may perform at these conditions. However, many thermodynamic factors will affect the performance of the compressor, so it is not realistic to expect a linear performance curve. The thermodynamic model takes all of the changing properties of the refrigerant into consideration at all conditions evaluated and is therefore expected to be more reliable and accurate than a linear prediction.

The model was, therefore, run with evaporation temperatures in between (Tevap = 78°C and 83°C) the experimentally tested conditions to see how the compressor would operate

at these conditions. The pressure ratios were set to be within the range of the experimentally tested ratios. The model was also run at operating conditions outside of the tested conditions. Experimentally testing of operating ranges outside of the specification may damage the equipment. This may lead to an expensive try-and-fail method, the simulation may predict whether the conditions tested will be outside of what is expected of the equipment to handle.

For the operating conditions, some decisions have to be made. For C_{leak} and Max_cav, the linear prediction function will decide the input values for these functions. When it comes to the liquid injection it has not been made a function that decides what amount should be injected at the various operating conditions. However, there is a clear trend on how much is injected at the operating points from the experimental data. For the simulations in between experimental data points, a quick approximation can result in very reliable input conditions. There is a larger uncertainty regarding the amount of liquid injection when simulating conditions outside of the experimental data, one way to solve this is the exact reason why a thermodynamic model is beneficial in the first place. If a try-and-fail approach is used to simulate varying amounts of injection for a case until the compression phase is exactly at the saturation line, the compressor should be in ideal operation from a thermodynamic perspective.

5.6 Experimental Setup

A prototype VHTHP with water-injection has been set up in a laboratory in Shanghai, China. This is the same system by Di Wu et al. which is explained in Chapter 3.2. The system schematics are properly represented in Figure 3.2. The prototype was developed to experimentally investigate how a water-injected twin-screw compressor using water vapor as the refrigerant would operate at several VHTHP conditions. The prototype was operated at varying operating conditions (both evaporating and condensing conditions were changed throughout the experiment). The liquid water injected is at a constant pressure of 3 bars. Even though the compressor is the main focus of this paper, the other components in the experimental setup are listed in Table 5.2. Note that an expansion valve is electronically controlled with the condensation pressure as the control signal. More information about the experimental setup can be found in the Experimental investigation on the performance of a very high-temperature heat pump with water refrigerant published by (Wu, Jiang, Hu, & Wang, 2020).

Table 5.2 The components of the water-injected VHTHP

Component	*Type*	*Model*	*Parameter*
Compressor	Twin-Screw	Prototype	30.8m^3 *min^{-1}
Evaporator	Falling film	ES1855STL	240 kW
Condenser	Plate	111B1508	300 kW
Expansion valve	Electrically controlled	GBH6015X	/
Flash tank	Vacuum	GB127	2.5 m^3
Liquid collector	High pressure	GB126	0.6 m^3
Circulating water pump	Self-priming	YKZX12	1.5 kW
Injection water pump	Centrifugal	CR1S-7	0.37 kW

The twin-screw water-vapor compressor was developed by Shanghai Hanbell Precise Machinery co., LTD. The prototype was developed from an air-compressor. It consists of

five male lobes and seven female lobes (concave cavities). It has three injection points which are spread equally far apart in the compression phase of the screw-compressor. As mentioned several times throughout this report, water-injection serves both as a seal to prevent leakage, but also as a coolant to limit superheat which is one of the main challenges by using water as a refrigerant in heat pumps at these operating conditions. Further specifications of the prototype are listed in Table 5.3.

Table 5.3 Specification of prototype compressor developed by Shanghai Hanbell Precise Machinery co., LTD

Specifications of the current compressor			
	Rotor:		unit:
	Male:	Female:	
Injection points	3	3	[-]
Lobes	5	7	[-]
Diameter	205	192	[mm]
Wrap angle	300		[^{o}]
Center length	160		[mm]
Length of rotor	330		[mm]
Internal compression ratio	7		[-]
rated rotational speed	5000		[rpm]
rated suction volume flow	30.8		[m^3/min]
oil rate in the compression chamber	0		[-]

6 Results

6.1 Experimental Results

The experimental research was carried out at a laboratory in Shanghai, China. The evaporation temperature was set at three different levels, 85°C, 80°C and 75°C. The raw data from the experimental work is shown in Table 6.1. To get units and specifications that are comparable to the simulated data some calculations were made from the raw data. These calculations can be seen in "Appendix A: Experimental results". An in-depth analysis of the experimental data can be found in (Wu, Jiang, Hu, & Wang, 2020).

Table 6.1 Experimental data

	Suction temperature (℃)	Suction pressure (bar)	Discharge temperature (℃)	Discharge pressure (bar)	Discharge volume (m3/min)	Injected-water temperature (℃)	Injected-water pressure (bar)	Injected-water volume flow rate (L/H)	Compressor power consumption (kW)
Evaporation temperature =85℃	91.40	0.64	118.42	1.96	7.41	14.63	0.75	41.05	46.70
	90.02	0.61	121.61	2.22	6.33	14.11	0.72	38.60	49.25
	88.88	0.59	126.44	2.46	5.10	13.73	0.70	38.30	53.46
	88.66	0.58	135.78	2.88	4.12	13.70	0.71	42.04	58.98
	88.47	0.58	136.67	3.44	3.38	13.71	0.75	51.26	64.16
	87.84	0.57	146.66	3.85	2.73	14.67	0.76	58.71	70.49
	87.33	0.56	152.20	4.42	2.14	14.85	0.80	62.93	76.80
	87.09	0.56	151.22	5.10	1.76	14.04	0.83	62.87	82.72
	Suction temperature (℃)	**Suction pressure (bar)**	**Discharge temperature (℃)**	**Discharge pressure (bar)**	**Discharge volume (m3/min)**	**Injected-water temperature (℃)**	**Injected-water pressure (bar)**	**Injected-water volume flow rate (L/H)**	**Compressor power consumption (kW)**
Evaporation temperature =80℃	84.85	0.49	117.07	1.85	5.66	17.28	1.02	28.65	42.92
	84.50	0.48	125.99	2.10	4.56	17.27	1.04	30.16	46.65
	83.98	0.49	129.79	2.52	3.62	17.20	1.18	33.54	51.33
	82.99	0.48	135.11	2.93	3.02	17.15	1.82	41.84	55.81
	82.26	0.46	140.80	3.36	2.42	16.74	1.72	45.67	62.64
	81.62	0.47	144.52	3.87	2.04	17.05	2.34	57.84	68.07
	81.55	0.47	150.01	4.48	1.66	16.49	2.82	62.55	75.30
	Suction temperature (℃)	**Suction pressure (bar)**	**Discharge temperature (℃)**	**Discharge pressure (bar)**	**Discharge volume (m3/min)**	**Injected-water temperature (℃)**	**Injected-water pressure (bar)**	**Injected-water volume flow rate (L/H)**	**Compressor power consumption (kW)**
Evaporation temperature =75℃	79.04	0.40	112.43	1.61	4.59	16.40	1.11	35.35	38.21
	80.15	0.39	116.42	1.79	4.03	16.30	1.12	36.45	40.61
	79.92	0.38	121.63	2.15	3.26	16.30	1.10	35.66	44.82
	78.99	0.39	131.40	2.54	2.60	16.39	1.05	35.76	49.38
	77.28	0.39	131.01	2.89	2.21	16.51	1.43	42.04	54.14
	76.04	0.40	154.68	3.31	1.86	16.62	1.92	49.76	58.66
	75.85	0.42	150.14	3.79	1.58	16.34	2.23	57.53	64.16

As seen in the raw experimental data, the compressor was operated at 8 different pressure ratios when the evaporation temperature was 85°C. 7 pressure ratios were investigated for an evaporation temperature of 80°C and 75°C. The temperature of the injected liquid was between 13.70 and 16.62 for all cases. The general trend was that while both the amount injected and the compressor power consumption increased with an increasing

pressure ratio, the displacement volume decreased. The compressor ran at 5000 rpm throughout the entire experiment according to the reported data. It is worth noting that the discharge temperature was not always consistent with the discharge pressure in the various experiments. To clarify, this means that the thermodynamic state of the discharge fluid (vapor or liquid-vapor mixture) can vary between the experiments.

6.2 Simulation Results

6.2.1 Validation of model against experimental data

All experimentally tested conditions were simulated with a linear function for C_{leak} based on the calculated volumetric efficiency and evaporation temperature. Max_cav was also based on the calculated volumetric efficiency. All simulated results for the compressor power consumption were inside +-5% margin of the experimental results excluding the two simulations with the lowest compression ratio with an evaporation temperature of 85°C.

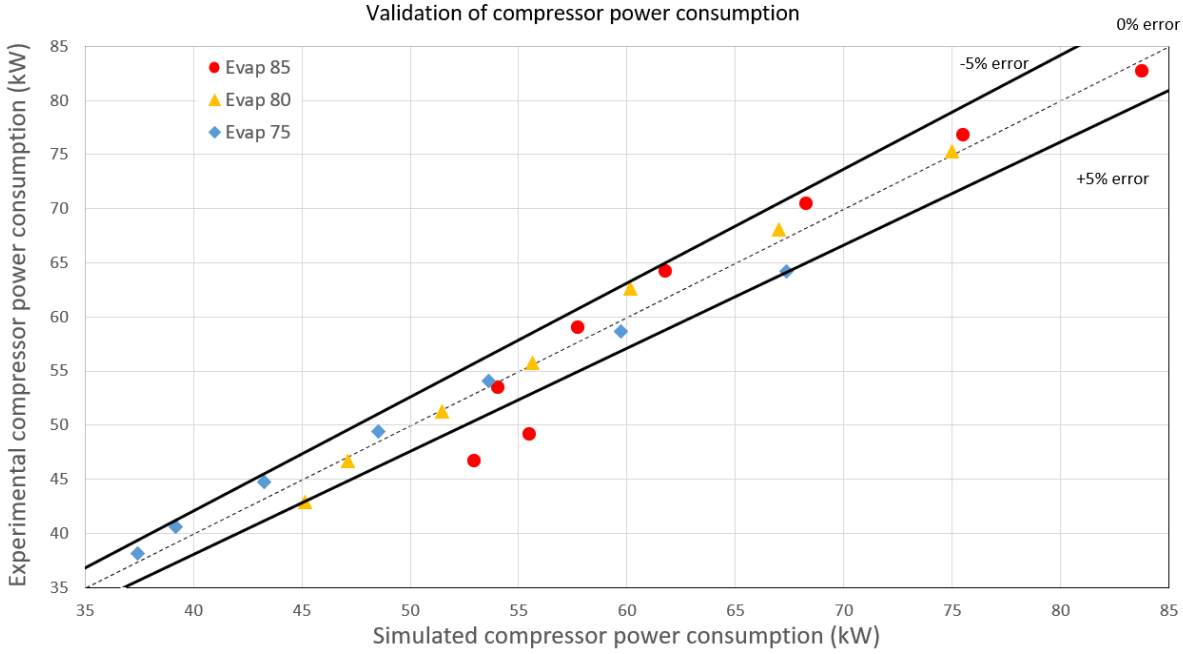

Figure 6.1 Simulated compressor power consumption vs experimental compressor power consumption. Solid lines indicate an error of +-5%

The mass flow rate was checked at all the three major ports of the compressor for the same simulations. The simulated results for suction mass flow rate deviated less than +-5% from the experimental data for all but one condition. The outlier had an error of -6.6% and had the second-highest pressure ratio when the evaporation temperature was 80°C. There is a general trend that a higher suction mass flow rate correlates with a higher percentage error of the simulated suction mass flow rate compared to the experimental data.

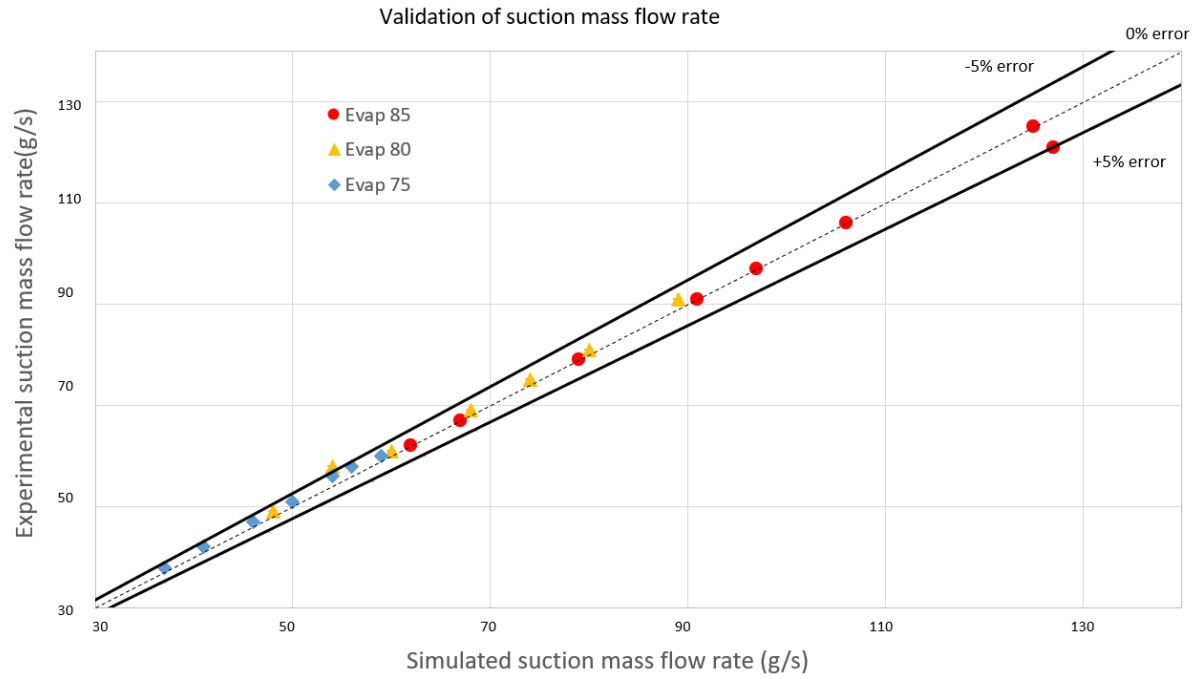

Figure 6.2 Simulated suction mass flow rate vs Experimental suction mass flow rate. Solid lines indicate an error of +-5%

The injection mass flow rate is an input variable in the simulation and is therefore changed to fit each experimental value. This is why the simulated data correlate so well to the experimental data.

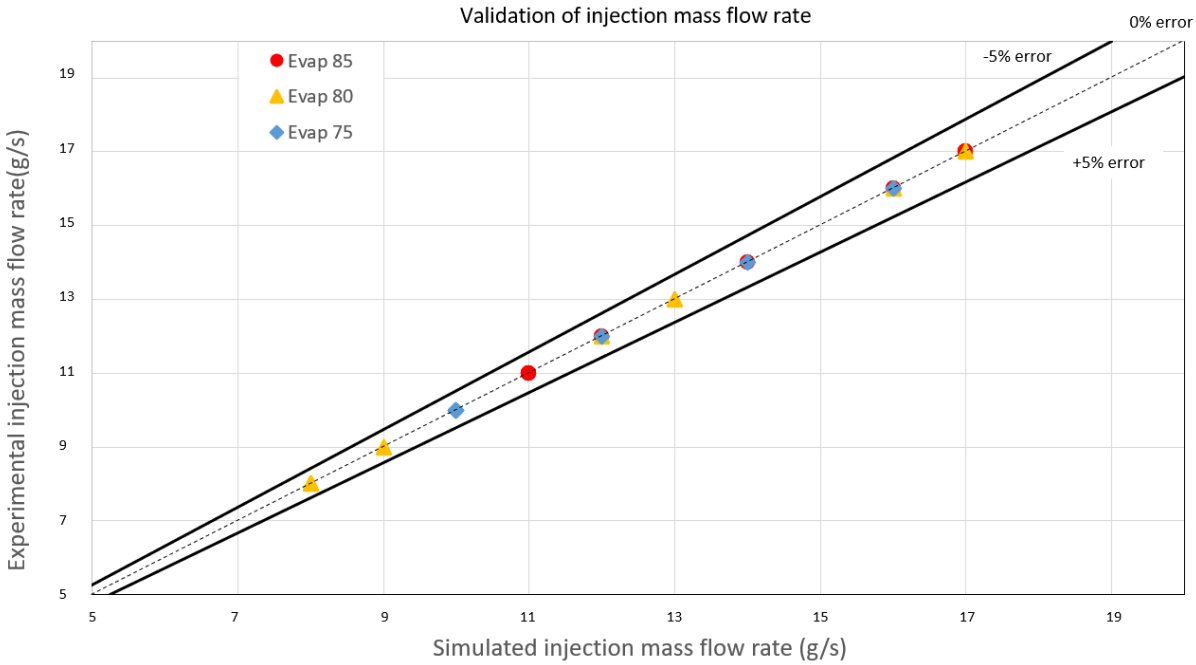

Figure 6.3 Simulated injection mass flow rate vs Experimental injection mass flow rate. Solid lines indicate an error of +-5%. Many of the points are on top of each other

When it comes to the discharge mass flow rate the simulation is quite good. The one condition where the mass flow rate was outside of the +-5% error is at evaporation temperature of 85°C with the second-lowest pressure ratio. This is one of the two

conditions not taken into consideration when the linear function to determine the inputs was made.

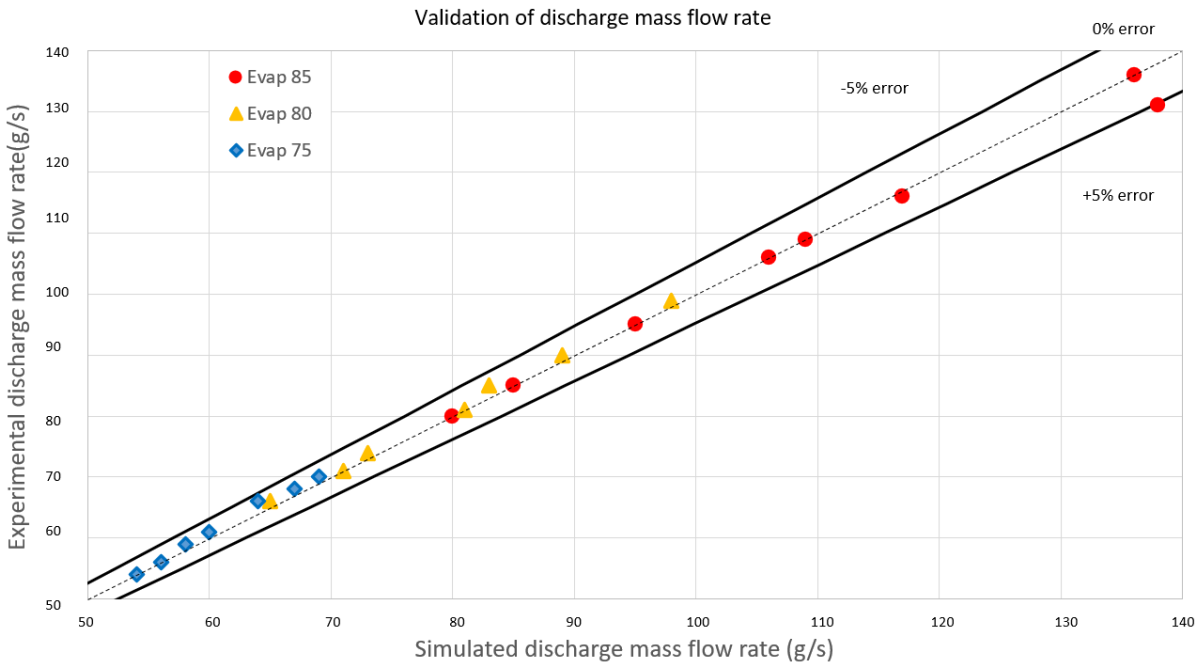

Figure 6.4 Simulated discharge mass flow rate vs Experimental discharge mass flow rate. Solid lines indicate an error of +-5%

6.2.2 Injected mass flow rate optimization study

The injection study in this thesis is split into two parts, the first looks at the optimal amount of liquid injected, while the second looks at how the liquid should be distributed. The results from the first part showed that increasing the amount of injected liquid would decrease the work used by the compressor. The power consumptions reported here are not comparable to the experimental data, as the volumetric efficiency is not compensated for in these simulations. The study is only done to compare the simulated settings against each other.

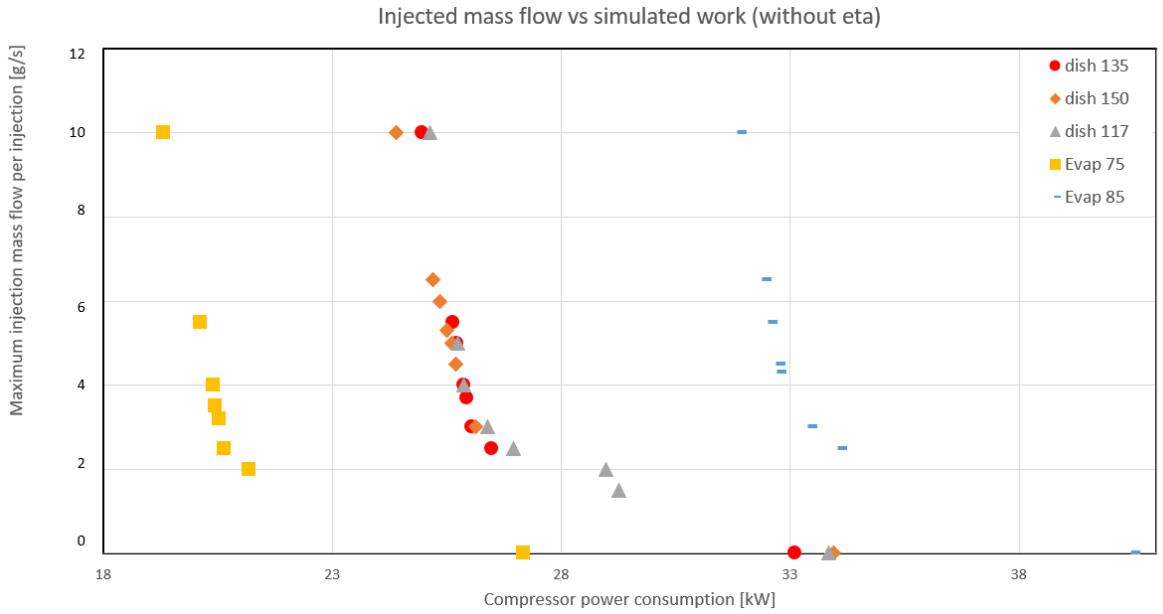

Figure 6.5 Injected mass flow vs power consumption for 5 operating conditions

Based on the graph in Figure 6.5 it looks like the compressor will converge to some value if the injected mass flow reached high enough values. This was tested by simulating an injected mass flow rate 27 times higher than the value used in the experimental data. The simulation showed that the compressor power consumption decreased with an increased amount of liquid injection.

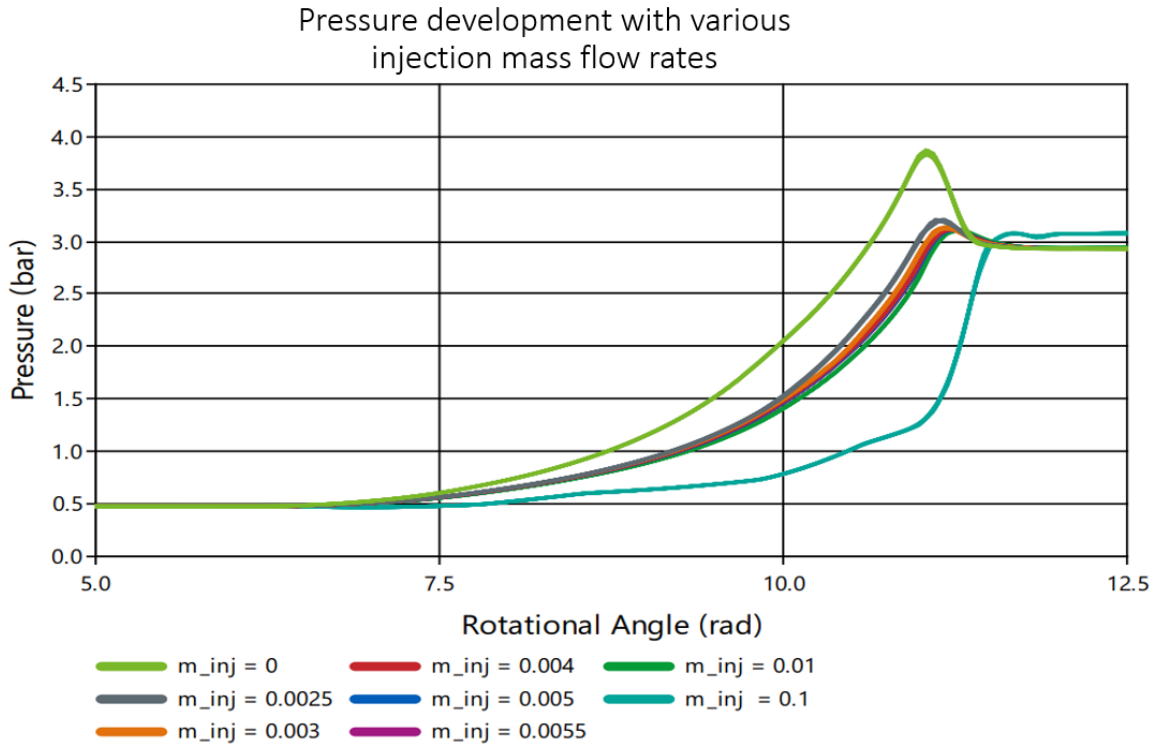

Figure 6.6 Pressure development with various amounts of injection for an evaporation temperature of 85°C (suction pressure of 0.47 bar) and an attempted discharge pressure of 2.93

Figure 6.6 is a good representation of how the pressure develops throughout the compression process with various amounts of liquid injection. It can be seen that with no

injection, maximum pressure during compression greatly exceeds the discharge pressure. This indicates an unideal operation of the compressor, as the compressor work to reach this pressure is higher than necessary. Furthermore, it appears that with higher injection mass flow rates, the pressure peaks at lower values.

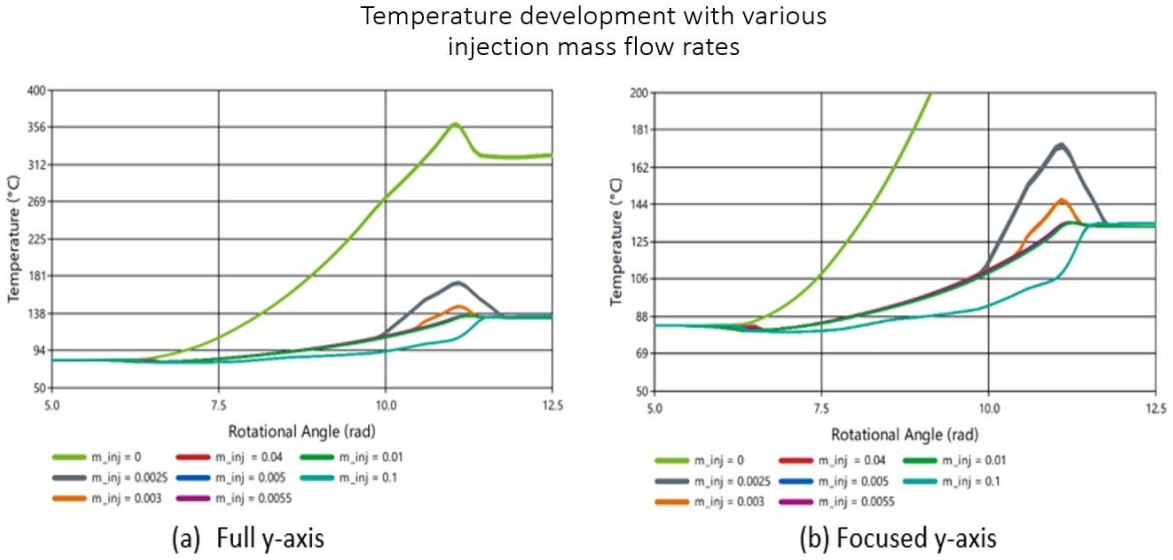

Figure 6.7 Temperature development with various amounts of injection for an evaporation temperature of 85°C (suction pressure of 0.47 bar) and discharge pressure set to 2.93 bar. (a) shows all amounts of injections tested. (b) ignores the high-temperature value of zero injection

The thermodynamic argument for why compressor work decreases when liquid is injected is that the amount of superheat in the compressor is reduced. Figure 6.7 shows how increased injected liquid mass flow rate will lower the temperature throughout the compression process. For the zero injection case, the outlet temperature is much higher than desired. Furthermore, a very high injection mass flow rate has a temperature curve below what can be expected from a compressor, which indicates that the compressor operates more like a pump.

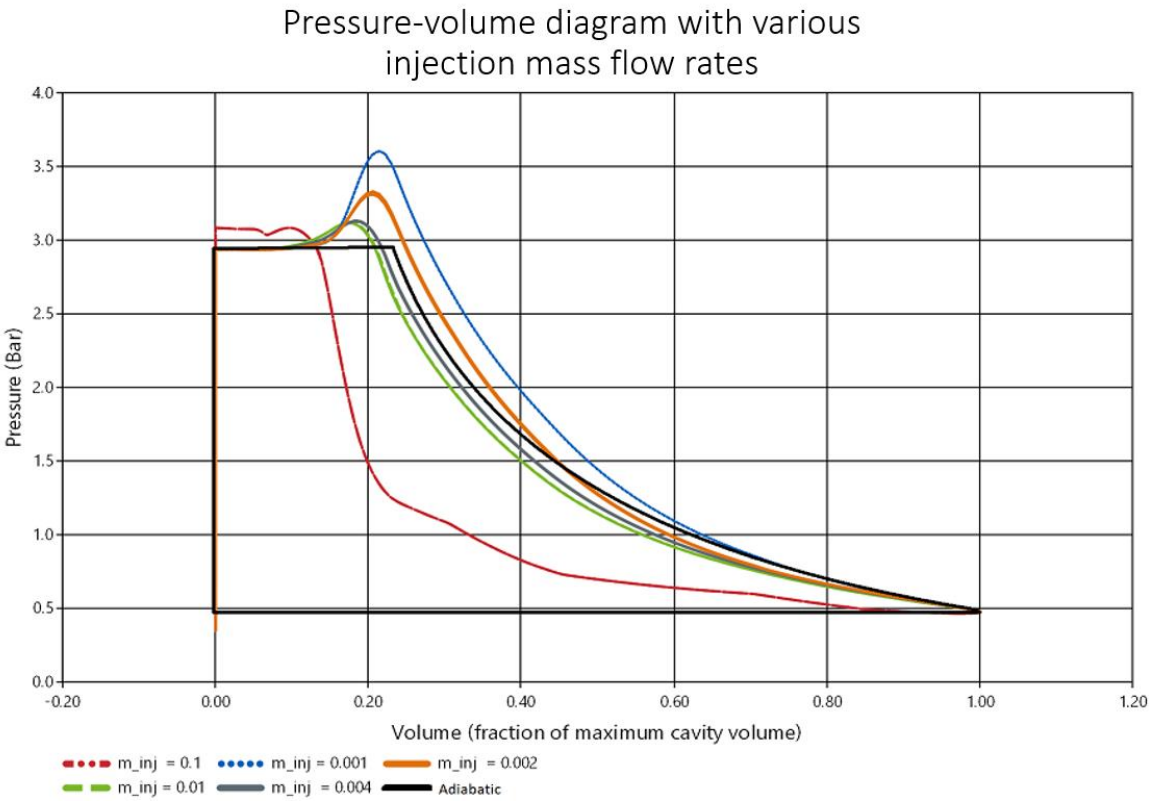

Figure 6.8 pressure-volume diagram with various amount of liquid injection

A pressure-volume diagram of the same process, with some of the same injection conditions, show that a high amount of liquid injection results in a close to adiabatic compression. A small liquid injection leads to over-compression, while too much liquid injection leads to under-compression. The adiabatic process in Figure 6.8 is included to illustrate how an adiabatic compression is expected to look like for these conditions and is not a part of the simulation results.

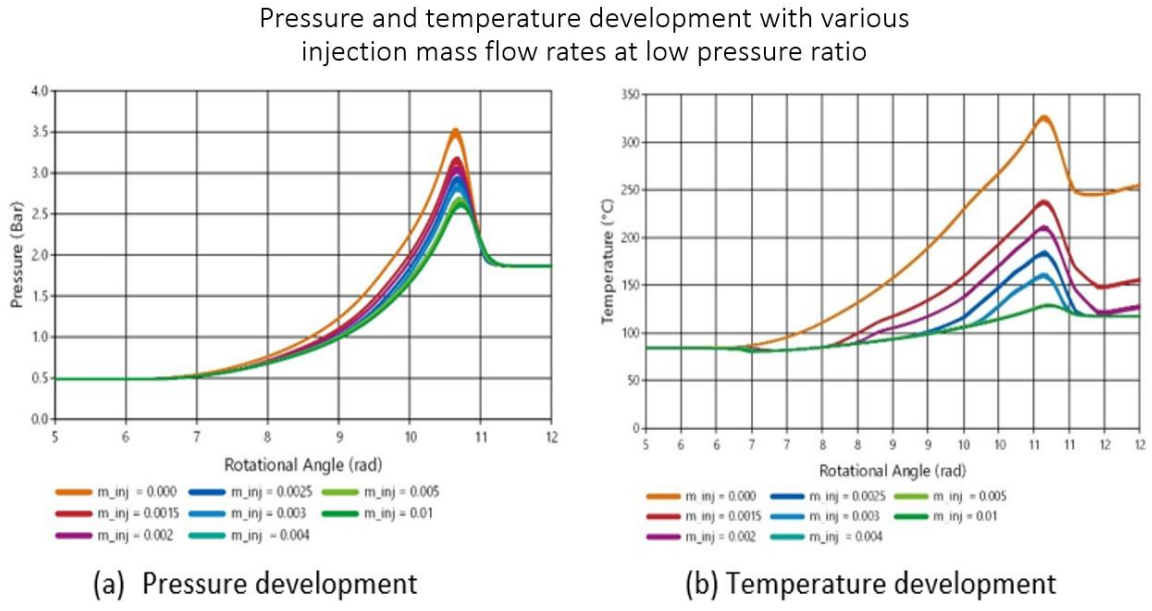

Figure 6.9 Pressure (a) and temperature (b) development of the compressor simulated at a low-pressure ratio with various amounts of injection

Figure 6.7 shows a case where the compressor is set to operate with a pressure ratio of 6.2 and with an evaporation temperature of 80°C, which is close to the design parameters of the compressor. It is therefore of interest to investigate other operating conditions, to see if the compressor is sensitive to change. In Figure 6.9 it can be seen that when the pressure ratio is lower, the compressor over-compresses the water vapor. The amount of liquid injected is lower with a smaller pressure ratio, and the compressor is therefore more likely to suffer from superheat. It is important to note that the amount of liquid injected varies between Figure 6.7 and Figure 6.9, this is due to the difference in the amount injected in the experimental results of the two cases. The graphs are therefore considered comparable.

So far a liquid injection study of a medium-and low pressure ratio case has been presented. A high pressure ratio case was also studied, but a higher pressure ratio leads to less sensitive operation regarding superheat. Since the experimental data shows that the amount of liquid injected increases with increasing pressure ratio, the simulation of injection in the same range as the experimental data does not differ much. The results from the high pressure ratio liquid injection investigation can be seen in "Appendix C.6 Pressure and temperature development with various amounts of liquid injection at a high pressure ratio".

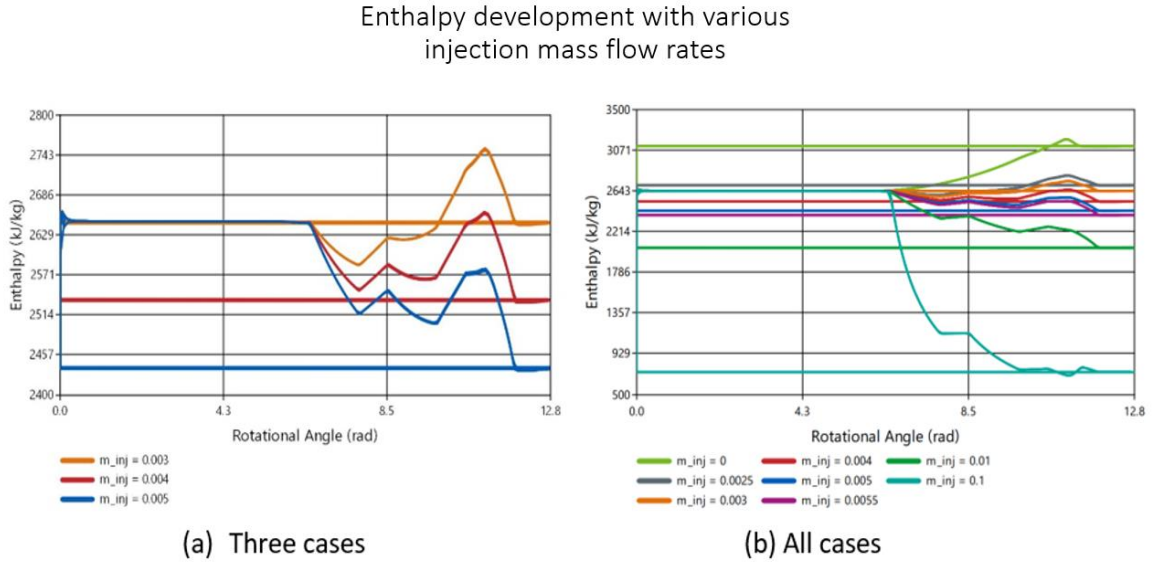

Figure 6.10 Enthalpy development with various amounts of injection for an evaporation temperature of 85°C (suction pressure of 0.47 bar) and a discharge pressure set to 2.93 bar. (a) shows the three most relevant cases. (b) shows all amounts tested

To further understand why the simulation model responds so well to liquid injection, an analysis of the enthalpy development was conducted. It can be seen that as the amount of liquid injection increases the enthalpy decreases before the small peak at the end. When the simulation calculates the work needed to reach these enthalpies the compressor work will decrease.

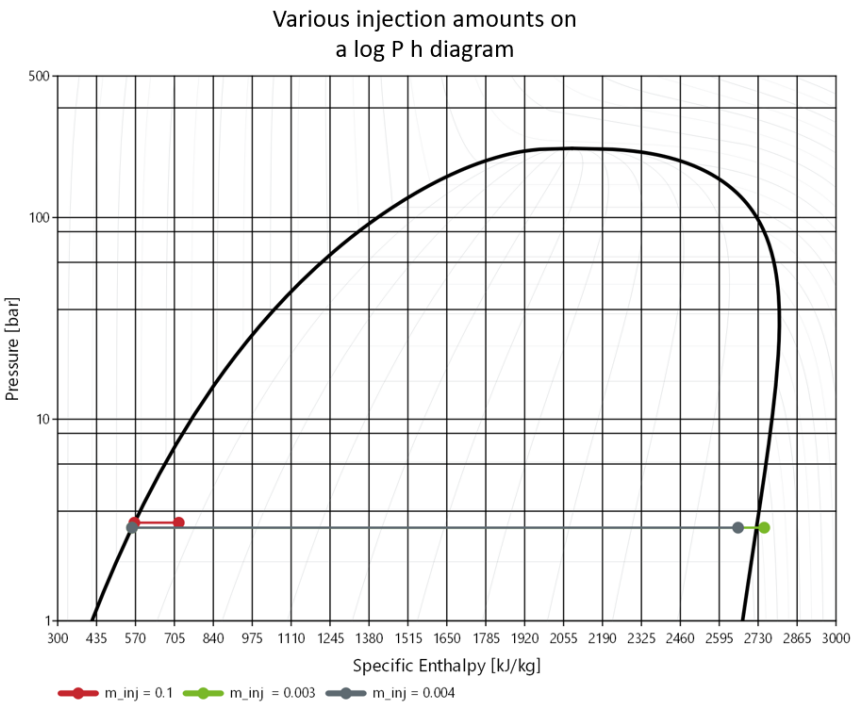

Figure 6.11 log P-h diagram showing the discharge points of three different injected mass flows

The question that naturally arises is then how much of an impact too much liquid injection has on the thermodynamic performance of the screw compressor. To understand the amount of specific latent heat available in the condenser, a log p-h diagram is provided. Three different liquid injection mass flow rates are shown, where two are realistic amounts that correlate to a total amount of liquid injected of 0.009kg/s and 0.012kg/s, while the last case shows an unrealistic large amount of liquid injected. It is clear that when the injected liquid is too large, the discharged fluid is far inside the saturation dome. This leads to a small latent heat utilized per fluid mass that is going through the heat pump.

6.2.3 Distribution of liquid injection optimization study

The second part of the injection optimization study looks at how changing the distribution of the injection mass flow rate in the three injection points affects the compressor performance.

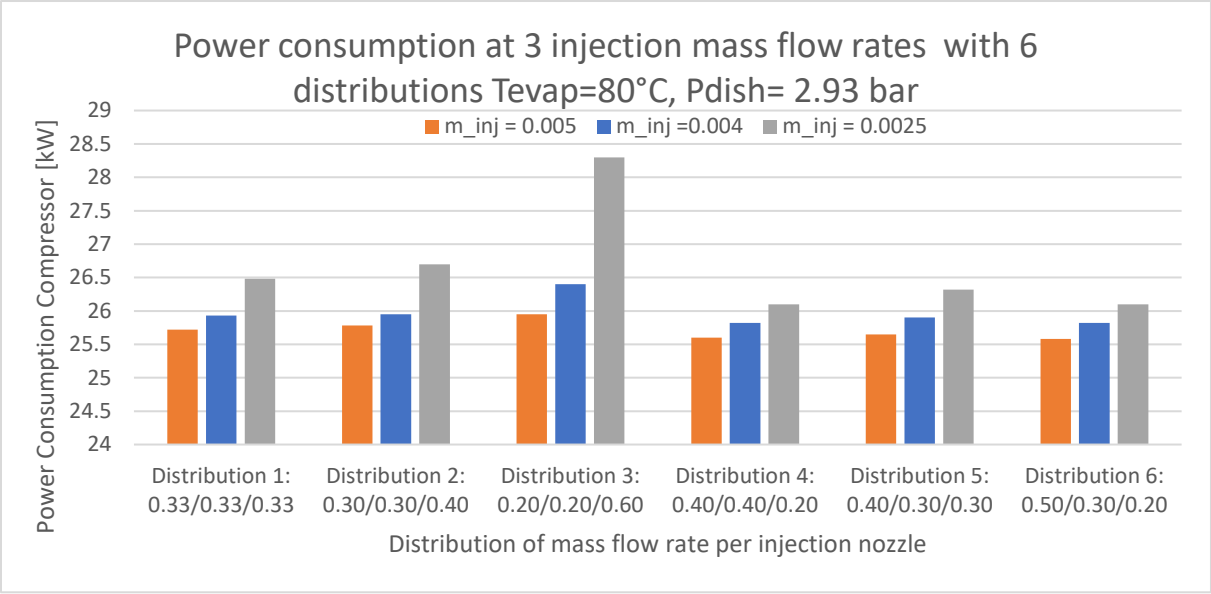

Figure 6.12 Power consumption at 3 different liquid injection mass flow rates with 6 distributions per mass flow rate (Tevap = 80°C, Pdish = 2.929)

The general trend from Figure 6.12 is that the higher percentage of the liquid is injected at the start of the compression process, the lower the power consumption of the compression is. Similarly to the previous study, a higher injection mass flow rate has a negative correlation with the compression power consumption. Based on the results in Figure 6.12, it appears that the distribution has a larger impact when the injected mass flow rate is low. Distribution 3 has the worst performance, while distribution 6 has the best performance for all injected flow rates.

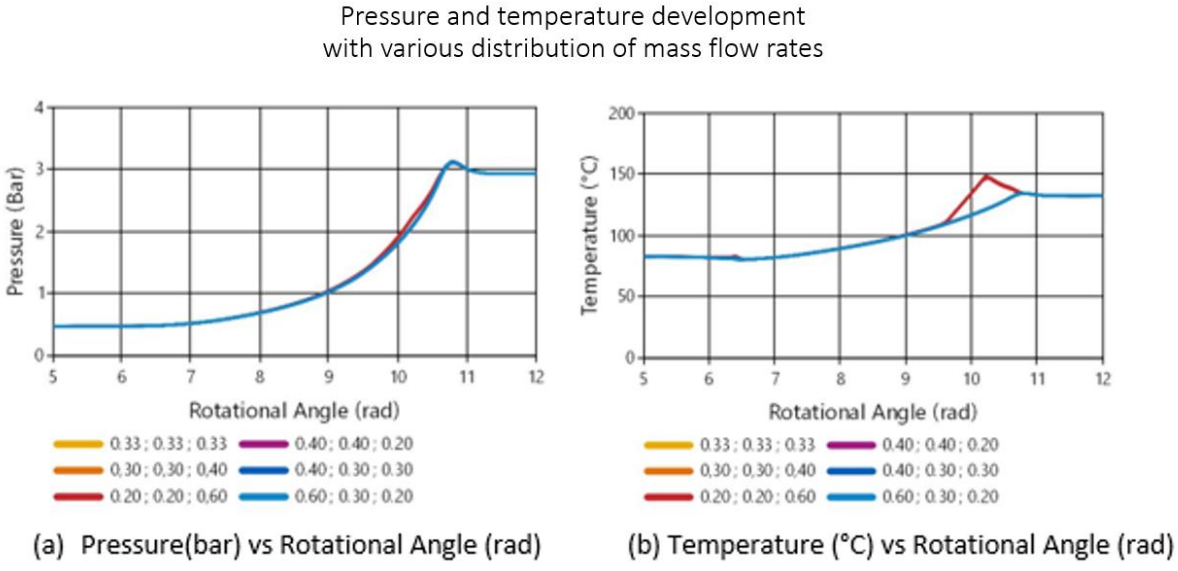

Figure 6.13 Pressure and temperature graphs of various distributions of m_inj at Tevap 80°C and Pdish = 2.929 with a total liquid injection of 0.012 kg/s

Due to the variations in compressor work for the different injection distributions, pressure, and temperature graphs for the previously described cases were made (Figure 6.13). The pressure curves vary slightly, the only mention-worthy difference is that the distribution with 60% of the liquid injected in the third nozzle shows a higher pressure rise earlier than

the other cases. This case stands out from the temperature graph as it is the only case with superheat. The rest of the conditions tested show similar results. They are shown on top of each other in the graph.

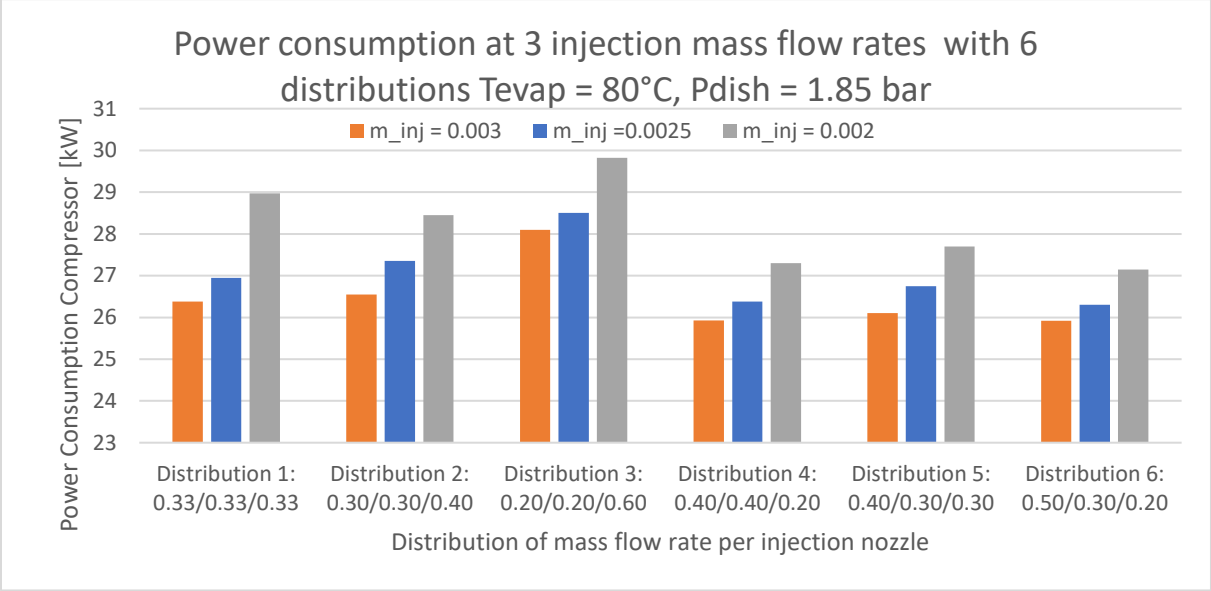

Figure 6.14 Power consumption at 3 different liquid injection mass flow rates with 6 distributions per mass flow rate (Tevap = 80°C, Pdish = 1.85)

As the compressor is thought to be more sensitive to superheat and over-compression at lower pressure ratios, the same study was carried out with an evaporation temperature of 80°C and a discharge pressure of 1.85 bar, which is approximately 1 bar lower than the previous case and yields a pressure ratio of 3.9. A higher percentage of liquid injection early in the compression process correlates with a low compressor power consumption for this operating condition as well(Figure 6.14). The trends concerning the effect of distribution on power consumption seen in Figure 6.12 is confirmed.

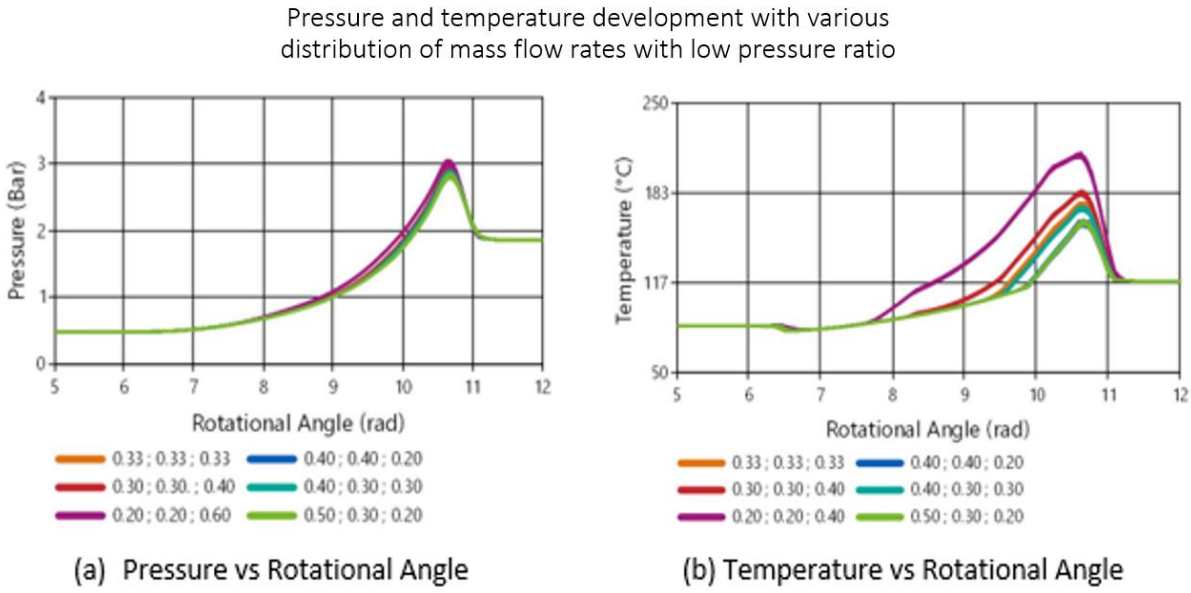

Figure 6.15 Pressure and temperature graphs of various distributions of m_inj at Tevap 80°C and Pdish = 1.85 with a total liquid injection of 0.008 kg/s

The pressure and temperature graphs of the operating conditions in Figure 6.14 are shown in Figure 6.15. Both the pressure and temperature graphs show a larger spread in over-compression and superheat, respectively compared to Figure 6.13. The trend is again that a higher percentage injected earlier in the compression process is ideal for the thermodynamic performance of the compressor.

In both optimization studies presented, the main factor that has been used to measure performance has been the power consumption of the compressor. However, it has become clear that enthalpy is also a very important factor when the performance of the system is to be evaluated.

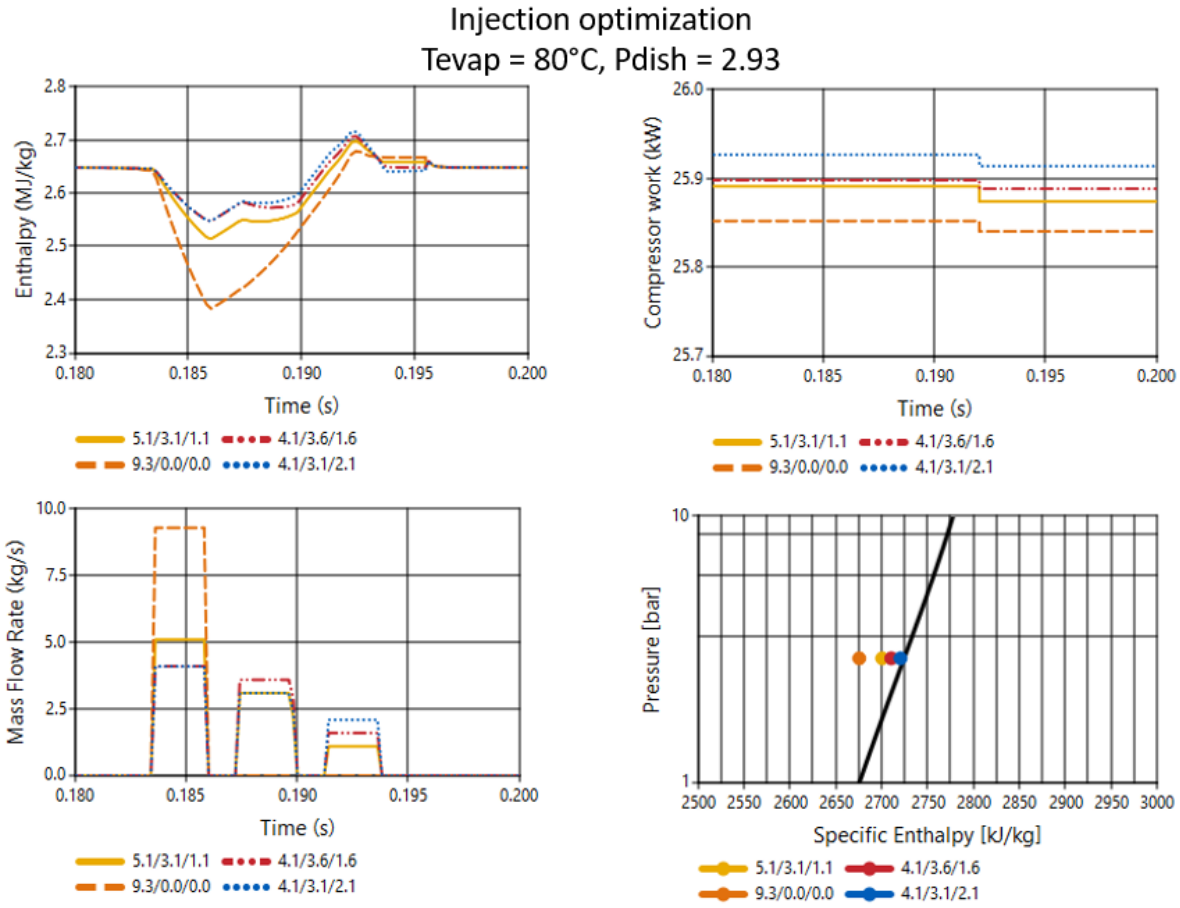

Figure 6.16 Injection optimization approach

Figure 6.16 shows how a thermodynamic model can be used to find the optimal liquid injection settings. In addition to compressor work, the thermodynamic state of the discharged fluid was taken into consideration. Discharging a fluid in an optimal thermodynamic state takes full advantage of the latent heat in the condenser, while there still is some liquid to protect the equipment. Even though the blue dotted case has the highest compressor power consumption, there is a small difference between the highest and lowest compressor power consumption for the distributions considered. The additional enthalpy, and therefore latent heat of condensation is thought to outweigh the additional power consumption. The blue case with a 4.1/3.1/2.1 distribution is therefore seen as the ideal injection case for this operating condition.

6.2.4 Simulation of untested operating conditions

So far, operating conditions in the simulation have been identical to the experimental settings. One of the purposes of making a thermodynamic model of a twin-screw compressor is to see how the performance changes at new conditions. Operating points in between the experimental operating points were therefore tested. It is difficult to evaluate the accuracy of these points by simulation, as there is no experimental operating point to compare them with. One of the results is presented with the two closest cases above and below it. In Figure 6.17 the pressure and temperature development of a case with an evaporation temperature of 83°C and a pressure ratio of 2.4 are shown in between two experimental cases (Tevap = 85°C, Pdish = 2.46 bar and Tevap = 80°C, Pdish=2.1 bar). As expected the results of the new simulation are between the experimental cases throughout the entire compression process. All cases presented here are simulated with the same injection rate of 0.009 kg/s for the three nozzles combined. The injection mass flow rate was the same for all simulated cases presented here, even though it varied in the experiments. This was done to ensure comparable simulation settings.

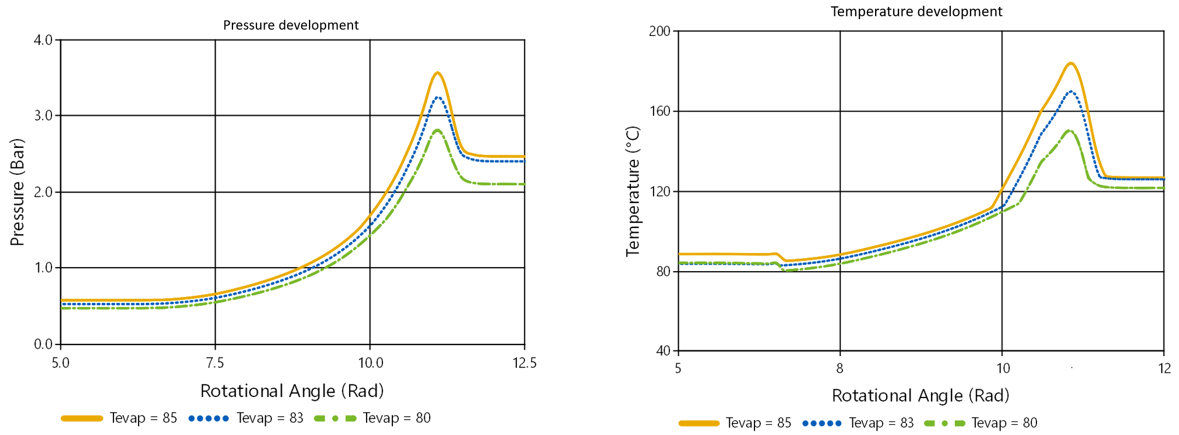

(a) Pressure development (b) Temperature development

Figure 6.17 (a) Pressure development and (b) Temperature development of a data point at Tevap = 83°C with discharge pressure of 2.4 bar

The compressor work of the new data point simulated goes in between the two surrounding cases. This along with other data points can be seen in "APPENDIX C.7 Compressor power consumption of new operational settings".

For the simulation points outside of the experimental data points, it is a little bit harder to predict exactly how much liquid should be injected as this requires extrapolation instead of interpolation of the experimental settings. Instead of doing this mathematically, the amount of liquid injected was found by simulating various amounts of injection until it was clear what value would lead the simulation to be at the saturation line. This was done for a case where the evaporation temperature was set to 87°C with a discharge pressure of 5.18 bar, which means that both temperature and pressure were higher than in any of the experiments. The results of the approach can be seen in Figure 6.18.

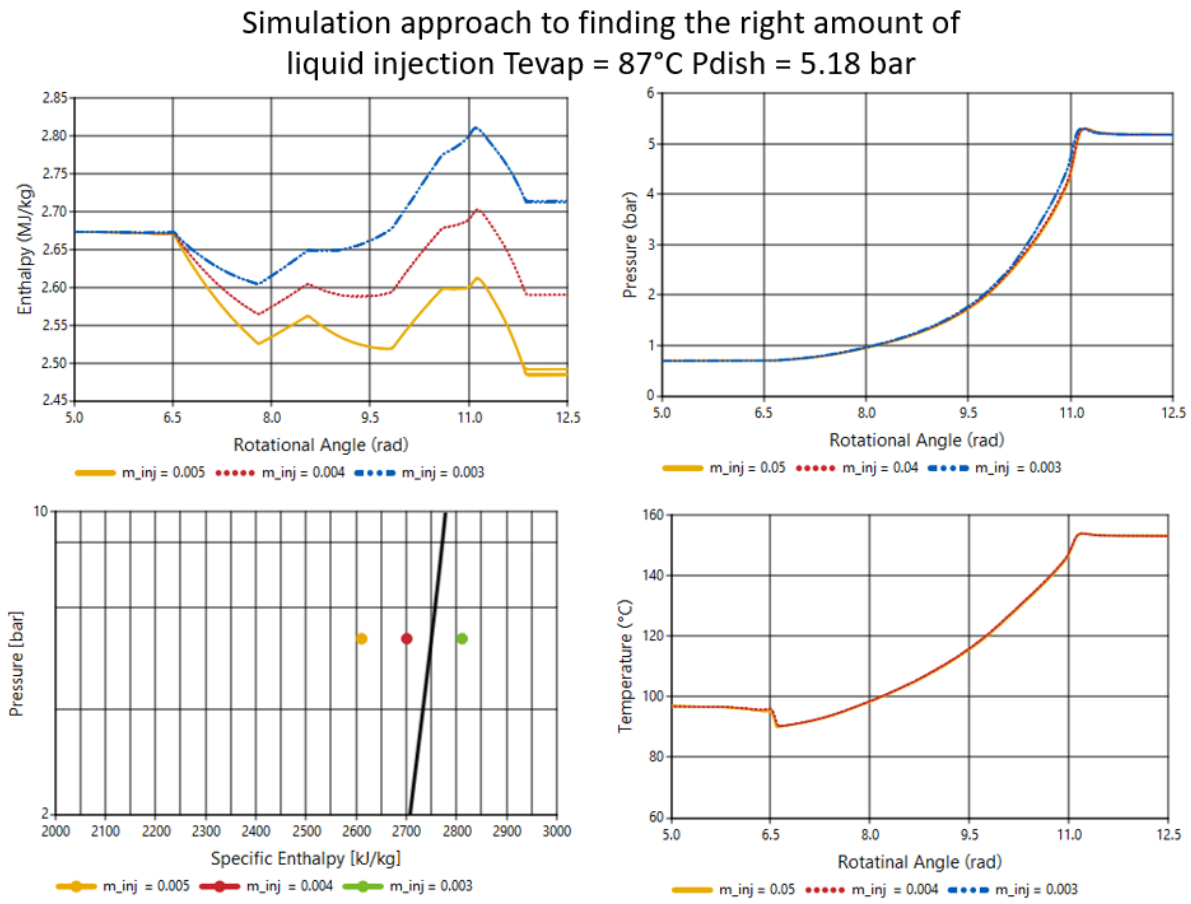

Figure 6.18 Simulation approach to finding the right amount of liquid injection

This highlights the advantage of having a thermodynamic model of a twin-screw compressor as new operating conditions can be tested without expensive experiments. In this case, the simulation suggests that the amount of liquid injected should be 0.0036kg/s per nozzle or 0.0108kg/s for the three nozzles combined for the optimal thermodynamic operation at this condition. The simulation can be used to see if the operating conditions are safe with regards to the equipment.

7 Discussion

7.1 Experimental results

The experiment was as mentioned conducted in a laboratory in Shanghai. Based on the experimental data, a few concerns were raised. Firstly, the phase of the water at discharge is an issue. As there is no measurement of the state of the fluid in the discharge state, there is an uncertainty in the amount of liquid going into the condenser. Liquid could reduce the heat transfer resulting in increased pressure in the condenser, which is hurtful for the overall performance of the system since the latent heat of condensation is crucial to the vapor compression cycle. Because a discharge temperature below the saturated vapor line for the discharge pressure was reported in two of the conditions tested, liquid water likely entered the condenser. However, this does not necessarily mean that liquid dominates the discharged liquid. The lower experimental temperature can be explained either by a droplet at the temperature sensor, or an error in the temperature or pressure measurement. It can be argued that some liquid in the discharge phase is necessary because a liquid sealing film can limit the leakage and protect the rotors from colliding.

On the other side, the experimental data indicated some superheat in a few of the experiments. Naturally, some superheat will occur as it is very difficult to inject the perfect amount of liquid to be precisely at the saturated vapor line. Even though the temperature indicates superheat, there may still be enough liquid in the fluid at the discharge gate to work as a sealing line. This is due to an uneven distribution of pressure and temperature in a compression chamber and the fact that the evaporation process requires some time.

Another mention-worthy concern based on the experimental data is the low volumetric efficiency. High volumetric efficiency is seen as one of the main advantages of a twin-screw compressor, so it is a concern that the volumetric efficiency is calculated to be as low as 0.285 for the experiment with the highest pressure ratio. At the condition with the best volumetric efficiency, it is 0.635. The volumetric efficiency has a clear negative correlation with an increasing pressure ratio, especially when the pressure ratio exceeds the built-in volume ratio of 4.2. Reduction of volumetric efficiency with an increased pressure ratio is also found in literature. When a twin-screw compressor operates with under-compression, the pressure in the compressor is lower than the pressure in the discharge chamber. As a result, the refrigerant flows back into the compressor from the discharge chamber, and the volumetric flow rate decreases. If the volumetric efficiency calculated is correct, there is room for improvement if the compressor is designed for specified operating conditions. Another possible reason for why the volumetric efficiency is so low for the high pressure ratio cases is that there is a lot of liquid injected at these operating conditions. The pressure of the liquid injected is 3 bars, so if the first injection point is placed in a cavity that is connected to the suction gate it may lead to an additional leakage through the suction gate and therefore lower the volumetric efficiency.

Furthermore, according to the experimental analysis, the adiabatic efficiency is reported to peak for all the evaporating temperatures at volume ratios around 4. This is a natural

consequence of the built-in volume ratio being 4.2. It is also noted that the adiabatic efficiency is highest at the evaporation temperature of 85°C. This may happen due to the generally lower pressure ratio for these cases.

An error analysis, based on the Kline and McClintock method, of the experimental setup, can be found in *Experimental investigation on the performance of a very high temperature heat pump with water refrigerant* (Wu, Jiang, Hu, & Wang, 2020). The results of the analysis show that the largest uncertainty is found when the pressure ratio is at its largest. The uncertainty is within +-5% for the heating capacity, COP, volumetric-, and adiabatic efficiency.

7.2 Simulation

7.2.1 Validation of model against experimental data

Simulations with inputs using the linear prediction function are a good fit when compared to the experimental results as seen in Chapter 6.2. In the process of tuning the simulation, some difficulties at certain conditions were noted. Especially the two simulations with the lowest pressure ratios at the evaporation temperature of 85°C. The issue was that the simulated work became too large compared to the experimental data at these conditions. As these conditions did not match well with the other data, the points were disregarded when the prediction function was tuned in. The thought behind the decision was that it is better to have a good prediction of most conditions, with a limited operating range where the simulation model is reliable than to sacrifice the accuracy of the entire simulation model to extend the range where the current input function is reliable.

When analyzing the linear function to determine the leakage coefficient(C_{leak}), it is natural that the higher pressure ratios lead to more leakage between the control volumes. This is compensated, to some degree, by the flow restrictor function (Eq 5.1), as the pressure difference between the control volumes will lead to a larger leakage mass flow rate. However, this is not sufficient according to the results from the experimental data, so C_{leak} must increase with an increased pressure ratio. This may be a result of only implementing two of the five or six actual leakage paths in the screw compressor. Even though the leakage paths implemented are the most significant leakage paths from a mass flow rate perspective, other leakage paths may have an impact on the power consumption of the compressor. This theory may have been confirmed by the discovery of a new paper on leakage paths. The paper claimed that the discharge end-phase clearance leads to a leakage path that has a significant impact on compressor performance. The increased leakage coefficient is supported by a literature review of leakage modeling found in (Patel & Lakhera, 2020). The linear prediction function also compensates for a higher leakage coefficient at lower evaporation temperatures.

For the simulated result of the compressor power consumption, suction-, injection- and discharge mass flow rate, the value throughout each cycle varies. A function to determine the average value per cycle was made to deal with the variation. There is also a variation in output results between one cycle to the next. To cope with this, a visual inspection was used to determine a reasonable value of the simulation. The variation between the cycles was not constant, but in most cases the difference from cycle to cycle was negligible. The largest variation between the cycles was found in the discharge mass flow rate, so these

are the numbers with the lowest confidence. The simulation was always performed for a minimum of 8 cycles to ensure that the simulation was stable. For cases where the simulation did not look entirely stable, the simulation time was extended to ensure stable results. The potential error in readings that came as a result of variation in the results was considered smaller than the uncertainty introduced by the assumptions.

Looking at the temperature graphs of the simulation, there is an issue with superheat and over-compression for all cases with a low pressure ratio. This is not surprising considering the built-in pressure ratio of the compressor. The occurring superheat and over-compression indicate that the adiabatic efficiency is low at these conditions. This finding is supported by the experimental analysis carried out by (Wu, Jiang, Hu, & Wang, 2020).

7.2.2 Injected mass flow rate optimization study

The injection research was carried out to investigate if the model can be used to optimize the current operation of the twin-screw compressor. From theory, it was known that there should be an optimal amount of injected liquid. This is because more injected liquid leads to less superheat, and therefore less work. At the same time, more liquid injection leads to a higher mass flow rate in the compressor and therefore higher power consumption. These considerations are true when the compressor is seen as a standalone component. When taking the rest of the system into consideration there is another downside by a high rate of liquid injected since this can lead to liquid in the condenser, and therefore less available latent heat during condensation.

The simulation results indicate that more liquid injected into the compressor leads to lower power consumption. This was tested with an unreasonable high amount of liquid injected to see if the model was able to see the downside with the extra mass flow rate. Even with 27 times higher liquid injection than what was reported in the experimental result, the power consumption was lower than at an injected flow rate of 2.5 times the experimental case. A hypothesis of why this is the case is the enthalpy of the mixture. If there is a large enough amount of liquid injected, the compressor will work as a pump. The specific enthalpy at the discharge conditions in the simulation with 27 times more liquid injected than the actual amount is less than 800 kJ/kg, the saturation line at these pressures are approximately 2750 kJ/kg. Another downside to injecting a large amount of liquid is that the power consumption of the pump used to supply the injected liquid will increase. The power consumption of this pump has not been taken into consideration in the simulations (or the experiments). Normally the power consumed in the pump is negligible, but for the unreasonable amount of injected liquid in this simulation, this will contribute to a significant amount of power consumed and should therefore be taken into consideration before justifying injecting too much liquid water.

Intuitively, a higher mass flow rate should lead to higher compressor power consumption. Looking at the thermodynamic perspective of liquid injection, the temperature and pressure graphs for the various injections indicate that there is no thermodynamic downside to high liquid-injection mass flow rates. When considering the enthalpy of these simulations, along with the heat pump system performance, the thermodynamic downside of the liquid injection is clear. The enthalpy indicates that the discharge phase of the compressor is almost at the bubble point (see Figure 6.11), which means that the latent heat of condensation will not be utilized. From the log p-h diagram it can be seen that from

a thermodynamic point of view, the most ideal injection mass flow rate distribution of the mass flow rates simulated with equal distribution is $m_{inj} = 0.003\ kg/s$ per injection nozzle.

7.2.3 Study on the optimal distribution of liquid injection

In recent years, research in the field of the distribution of liquid injection on twin-screw compressors has been conducted (Tian, Yuan, Wang, Wu, & Xing, 2017). The results from the study done here agree with the previous finding that there is a benefit to distributing the liquid unevenly. There is a clear trend that indicates that a high liquid injected mass flow rate early in the compression phase is beneficial for compressor performance. This trend was true for all three amounts of injection at all five operating conditions. A large amount of liquid injection early in the process is an efficient measure to avoid superheat. This can be explained by the fact that if there is not enough liquid injected at the beginning of the compression phase, the temperature will rise quickly, and the power consumption will therefore be high. When the log p-h diagram is studied it is evident that the entropy lines are close to diagonal far out in the superheated area, and more vertical inside and around the dome (See green lines in Figure 2.8). When the liquid is injected early in the compression phase, the fluid will stay close to the saturation line, and the entropy increase is small when compared to an identic pressure rise of fluid in the superheated area. The increase in enthalpy (work needed) is, therefore, lower for a compressor with early injection as the enthalpy change is small for an increase in the pressure close to the saturation line. If the same compressor with the same isentropic efficiency and pressure rise shall compress the same working fluid at a higher starting entropy value, further in the superheated area, the enthalpy difference will increase more, and the compressor work will increase.

Another benefit to large amounts of liquid injection early in the compression process is that the liquid will have enough time to evaporate completely. This process does not happen instantaneously, and it is of importance to ensure that the entire cooling effect of evaporation will be utilized. Furthermore, this indicates that cases with a lower total amount of liquid injection should be more sensitive to unideal distributions, as they are more likely to run high into the superheated region. The simulation results support this theory as, in general, the difference in power consumption between the worst and best distributions of the liquid is largest for the low injection flow rate case. The only exception of this is the high pressure ratio case. This might be a result of an already high amount of liquid injection combined with the pressure ratio being significantly higher than the built-in ratio, so the amount of superheat is not as big of a concern as in lower pressure ratio operation.

To determine the optimal injection, the thermodynamic state of the discharged fluid is taken into consideration along with the compressor work. This is important as both factors have a significant effect on the performance of the system, and not only the compressor. The model can easily be implemented into a larger system as a sub-model, where the importance of the discharge state will be clearer than in the current model. In the current model, it is tempting to assume that the compressor work is the only indicator of the compressor performance, but the investigation of the enthalpy has shown that there are downsides to a large amount of liquid injection even though the compressor work decreases.

The main disadvantage of doing injection research with this model is that it is assumed that the pressure and temperature distributions are uniform in a cavity. This is not the case in a real application, and affects the thermodynamic performance of the compressor, especially at the point of injection. The model indicates that there is a thermodynamic benefit to early liquid injection, something that can be reinforced when considering that the model assumes the evaporation of the liquid happens spontaneously. If the simulation had suggested that late injection would have been beneficial, there had been a reason to question the results as the evaporation process takes a longer time in a real application. The homogenous mixture in the cavity is one of the significant assumptions in the model. The model would therefore not be able to consider a situation with a large concentration of two-phase flow. And as previously discussed, a high concentration of liquid in the discharge phase is not beneficial for the system operation.

7.2.4 Simulation of untested conditions

The simulation of settings in-between the experimental operating conditions shows that the temperature and pressure development is in-between the two experimental data sets. The compressor work is also inside the two closest experimental points above and below the simulation. The work fits inside the two closest experimental cases for five out of the six other cases tested. The one case that is outside of the two closest data points from the experimental results is a simulation with high evaporation temperature and low pressure ratio. This has been seen as an operating range where the linear prediction function is not valid.

As there is no experimental data for these simulations, it is hard to further specify the error of the simulation. However, the simulation results were compared to a linear prediction of the experimental data and showed promising results. If these settings were tried in an experimental setup after the simulations are completed, and the experimental results were within an acceptable range of error, this would strengthen the reliability of the model in this range.

7.3 Further work

An unvalidated ammonia-water twin-screw compressor model has been modified to fit a water-vapor compressor. The model has then been further developed to include more functions while keeping the flexibility of the model intact. The model was validated against experimental data within an error of +-5%. However, the range where the model is considered reliable is limited. To further develop this model and enhance its reliability, both in terms of accuracy and range, the number of assumptions should be reduced or further justified. The most significant assumption in the current model is that there is assumed a uniform distribution of pressure and temperature at all cavities at any instant. Implementing two-phases, and varying pressure and temperature within each cavity will increase the accuracy of the model drastically. One of the advantages of the Modelica programming language is that a model can easily be implemented as a sub-model in a larger system. Based on the liquid-injection optimization study, it is clear that the model should be expanded to include more components of a heat pump cycle. If the entire system is incorporated, it will make the disadvantages of injecting too much liquid clearer. The

heat provided to the heat sink (Q_{cond}) will most likely decrease as a result of the decreased enthalpy value, which will also harm the COP.

More functions can also be added to the model. Currently, only two leakage paths are implemented, when literature indicates that there are 5-6 leakage paths present. One paper indicates that one of the two most significant leakage paths are not included in this thesis. So if more leakage paths are to be modeled, the discharge end-phase leakage should be prioritized. Furthermore, the mechanical efficiency of the compressor can be added to more realistically reflect the compressor power consumption. If the friction, which reduces mechanical efficiency, is modelled correctly, the heat generated in the process can be evaluated. This will give a better picture of the operating efficiency of the compressor. The volumetric efficiency is currently modeled by decreasing the maximum cavity volume to limit the amount of liquid present in each compression chamber. It is possible to implement this function in a way that is based on the geometrical properties of the twin-screw compressor instead of the experimental data. The linear prediction of C_{leak} was based on the experimental data, while it ideally should be a constant value or explained by thermodynamic equations. If the model is to have a predictive functionality, the linear prediction should be replaced by thermodynamic equations. It is reasonable to believe that there will no longer be a need for a function that determines C_{leak} if all leakage paths are implemented. To further validate the model, it would be interesting to experimentally test the new conditions simulated. If the simulated predictions fit well with the experimental data, it would be interesting to test operating ranges outside of what has been done so far. This could expand the range of where the simulation is deemed valid. The model has shown weakness at high evaporation temperature with low pressure ratio, but it could be interesting to go at lower evaporation temperatures. Another way to expand the range where the model is valid is to test higher evaporation temperatures, but with high enough pressure ratios, ensuring that the model does not run into the same issues as in the operating conditions from the experimental data, where the model was considered invalid. If the simulations are verified satisfyingly it would be interesting to see how precise the injection functions are, and if they can be used to precisely determine the correct amount of liquid injection for optimal thermodynamic operation.

The model is very adaptable, and can easily be run with other refrigerants. If the model is verified against a twin-screw compressor with another refrigerant in a similar operating range, the reliability of the compressor model is enhanced. It can then be used to compare a variety of refrigerants and test how various injection can affect the compressor performance. The liquid-injection study conducted in this thesis was also relatively limited. There are many ways to try to optimize the liquid injection. Placement of the injection nozzles, atomizing water droplets, the number of injection nozzles and the thermodynamic condition of the liquid injection are all parameters that should be optimized, and this model can be used to do preliminary tests.

For the experimental setup, it may be beneficial to increase the number of sensors inside the working chamber. This data can be used to get a better understanding of how the temperature and pressure distribution works. The focus should be to place the sensors around the injection nozzles.

8 Conclusion

An extensive literature review regarding compressor used in various high-temperature heat pump systems has been presented together with available compressor technology and its limitations. Together with the basic theory of twin-screw compressors and vapor compression cycles, it will increase the understanding of what challenges the state of the art compressor technology is facing. A further literature review was then conducted, with a focus on liquid-injected screw compressors and water as a refrigerant. Furthermore, the development of a thermodynamic model of a water-injected twin-screw compressor was presented. This development is based on the findings in the literature review and survey of compressors.

The task of developing a thermodynamic model of a water-injected twin-screw compressor is challenging. There are many ways to solve the challenge, and a wide range of programming languages can be utilized. It was decided that the most efficient way of making a reliable model was to adapt an already existing ammonia-water twin-screw compressor with liquid injection to the application needed in this thesis. The previous model was found in literature and was a quasi-one-dimensional numerical model made in the object-oriented modeling language Modelica. Adapting the model required an in-depth investigation of the model's functionality and setup. In the process of adapting the ammonia-water compressor model to a water vapor compressor model, several functions that are relevant for two-fluid flow was intentionally kept in the model even though they were not relevant for single-fluid flow. This was to ensure adaptability so that the model can be used in future research regardless of the choice of refrigerants.

The model was verified against experimental data provided by SJTU and Shanghai Hanbell Precise Machinery co, LTD. A linear function was implemented to change the leakage coefficient of the compressor, dependent on the volumetric efficiency and the evaporation temperature. The model was then within an error of +-5% for the compressor power consumption for all 20 cases considered. 20 of the 22 cases that were run in the experimental data were used to make a linear function of the C_{leak} as the two other sets of data deviated drastically from the other data and implementing these data points would affect the reliability of the entire function. The suction-, injection-, and discharge mass flow rates for all 20 cases were within an error range of +-5% except one.

Based on the liquid-injection study conducted on this model, the amount of liquid injection has a negative correlation with the compressor work, i.e. more liquid injected, leads to lower compressor work. However, based on the thermodynamic principle behind a vapor compression cycle and the thermodynamic properties of water, there is reason to believe that the overall performance of the cycle would drastically decrease with liquid water in the discharge phase. Furthermore, the study showed that injecting a large amount of liquid early in the compression phase is beneficial for compressor performance. This is also something that would limit the liquid water in the discharge phase of the compressor. However, if there is not enough liquid water present at the end of the compression phase, the protective liquid film between the rotors could disappear which could lead to damage

on the rotors. Lack of liquid film between the rotors could also lead to lower volumetric efficiency as a result of more leakage between the cavities.

9 References

Ahrens, M. U., Hafner, A., & Eikevk, T. (2019). Development of ammonia-water hybrid absorption-compression heat pumps. *25th IIR international Congress of Refrigeration* (ss. 4942-4949). Montreal, Canada: ICR2019.

Arpagaus, C., Bless, F., Uhlmann, M., Schiffmann, J., & Bertsch, S. (2019). High temperature heat pumps: Market overview, state of the art, research status, refrigerants, and application potentials. *Science Direct*, ss. 985-10110.

Bamigbetan, O., Eikevik, T. M., Nekså, P., & Bantle, M. (2017). Review of vapour compression heat pumps for high temperature heating using natural fluids. *International Journal of Refrigeration*, 197-211.

Bamigbetan, O., Eikevik, T. M., Nekså, P., Bantle, M., & Schlemminger, C. (2019). Experimental investigation of a prototype R-600 compressor for high. *Science Direct*, ss. 730-738.

BAMIGBETAN, O., EIKEVIK, T. M., NEKSÅ, P., BANTLE, M., SCHLEMMINGER, C., & DALLAI, M. (2018). Experimental Investigation of a Hydrocarbon Piston Compressor for High Temperature Heat Pumps. *24th International Compressor Engineering Conference*, (s. 1607). Purdue.

Bantle, M. (2017). Steam compression and the development of a cost effective turbo compressor. *International Workshop on High* (ss. 134-141). Copenhagen: DTU; SINTEF.

Bantle, M. (2017). Turbo-Compressors: Prototype tests of mechanical vapour re-compression steam driers. *12th IEA Heat Pump Conference .*

Bantle, M., Schlemminger, C., Gabrielii, C., & Ahrens, M. (2019). Turbo-compressors for R-718: Experimental evaluation of a two-stage steam compression cycle. *25th IIR International Congress of Refrigeration.* IIF/IIR.

Basha, N., & al, e. (2018). Effect of oil-injection on twin screw compressor performance. *IOP Conf. Ser.: Mater. Sci. Eng.*, (s. 425 012009).

Bergamini, R., Jensen, J. K., & Elmegaard, B. (2019, May 31). Thermodynamic competitiveness for high temperature vapor compression heat pumps for boiler substitution. *Energy*, ss. 110-121.

Bommel, L. v. (2016). *Thermodynamic Model of a Screw Compressor.* Delft: Delft University of Science and Technology.

Browne, M., & Bansal, P. (2002). Transient simulation of vapour compression packaged liquid chillers. *International Journal of Refrigeration 25*, ss. 597-610.

Buckney, D., Kovacevic, A., & Stosic, N. (2011). Consideration of clearances in the design of screw compressor rotors. *7th International Conference on Compressors and their Systems* (ss. 401-410). London: City University, London; Woodhead Publishing ltd.

Calm, J., & Hourahan, G. C. (2011). Physical, safety, and environmental data for refrigerants. *ICR 2011.* Prague.

Carrier Corporation. (2004). *Scroll Compressors - High efficiency for commercial and industrial applications.* Syracuse, New York: Carrier.

Casari, N., Kovacevic, A., & Ziviani, D. (2018). Full 3D numerical analysis of a twin screw compressor by employing open-source software. *IOP conf. Ser.: Mater. Sci.Eng.*, (s. 425 012017).

Chamoun, M., Rulliere, R., Haberschill, P., & Berail, J. F. (2012). Dynamic model of an industrial heat pump using water as refrigerant . *International Journal of Refrigeration*, ss. 1080-1091.

Chamoun, M., Rulliere, R., Haberschill, P., & Peureux, J. (2013). Modelica-based modeling and simulation of a twin screw compressor for heat pump applications. *Applied Thermal Engineering*, ss. 479-489.

Chamoun, Rulliere, Haberschill, & Peureux. (2014). Experimental and numerical investigations of a new high temperature heat pump for industrial heat recovery using water as refrigerant. *International Journal of Refrigeration*, 177-188.

Eikevik, T. M. (2019). Compressors. I T. M. Eikevik, *Heat Pumping Processes and Systems* (s. Chapter 11). Trondheim.

Equinor ASA. (2019). *Energy Perspectives 2019.* Stavanger: Equinor.

Fleming, J., & Tang, Y. (1995, March 20). The analysis of leakage in a twin screw compressor and its application to performance improvement. *Proc Instn Mech Engnr Vol 209*, ss. 126-136.

Frohböse, D.-I. I. (2020, Juli 7). *TIL Suite*. Hentet fra tlk.thermo.com: https://www.tlk-thermo.com/index.php/en/til-suite

Fukuda, S., Kondou, C., Takata, N., & Koyama, S. (2014). Low GWP refrigerants R1234ze(E) and R1234ze(Z) for high temperature heat pumps. *International Journal of Refrigeration* , ss. 161-173.

Gao, X., Chen, J., Tan, J., Wang, Y., Ma, Z., & Yang, L. (2015, March 5). Application of Mechanical Vapor Recompression Heat Pump to Double-Effect Distillation of Separating N,N-Dimethylacetamide/Water Mixture. *Industrial & Engineering Chemistry Research*, ss. 3200-3204.

Guangbin, L., Xiaoyan, Z., Liansheng, L., Bin, T., Qichao, Y., & Yuanyang, Z. (2019). Analysis of Performance of Screw Compressor in MVR system. *International Conference on Compressors and their Systems* (s. IOP Conf. Ser.: Mater. Sci. Eng. 604 012002). IOP publishing.

Hanjalic, K., & Stosic, N. (1997, September 1). Development and Optimization of Screw Machines with a Simulation Model - Part 2: Thermodynamic Performance SImulation and Design Optimization . *Journal of Fluids Engineering* , ss. 664-670.

Haugland, K. (1993). *Undersøkelse av Skruekompressorens Arbeidsprocess.* Trondheim : NTH - Institutt for kuldeteknikk.

Helminger, F., Kontomaris, K., Pfaffl, J., Hartl, M., & Fleckl, T. (2016). HOCHTEMPERATUR-WÄRMEPUMPEN-MESSERGEBNISSE EINER LABORANLAGE MIT HFO-1336MZZ-Z BIS 160°C KONDENSATIONSTEMPERATUR.

Horn, J., & Scharf, P. H. (1976). *Design Considerations for Heat Pump Compressors.* Sidney, Ohio: Copeland Corporation.

Hsieh, S., Shih, Y. C., Lin, F. Y., & Tsai, M. J. (2011). Performance analysis of screw compressors - numerical simulation and experimental verification . *IMechE vol 226 part C J. Mech. Engr. Sci.*, 968-980.

Hu, B., Wu, D., & Wang, R. (2018, september 14). Water vapor compression and its various applications. *Renewable and Sustainable Energy Reviews*, ss. 92-107.

Husak, E., Kovacevic, A., & Karabegovic, I. (2019). Calculation of clearances in twin screw compressors. *International Conference on Compressors and their Systems.*

IEA. (2020). *Fuels and technologies - heating.* International Energy Agency.

International Energy Agency. (2014). *Heating without global warming - market overview, state of the art, research status, refrigerants and application potensials.* Paris: IEA.

Jensen, J. K., Ommen, T., Markussen, W. B., Reinholdt, L., & Elmegaard, B. (2015, March 3). Technical and economic working domains of industrial heat pumps: Part 2 - Ammonia water hybrid absorption-compression heat pumps. *International Journal of Refrigeration* , ss. 183-200.

Kang, D. H., Na, S.-I., Yoo, J. W., Lee, J. H., & Kim, M. S. (2019, September 10). Experimental study on the performance of a steam generation heat pump with the internal heat exchanger effect. *International Journal of Refrigeration*, ss. 154-162.

Li, X., Wang, X., Zhang, Y., Fang, L., Deng, N., Zhang, Y., . . . Yao, S. (2020). Experimental and economic analuysis with a novel ejector-based detection system for thermodynamic measurement of compressors. *Applied Energy*.

Li, X., Zhang, Y., Ma, X., Deng, N., Jin, Z., Yu, X., & Li, W. (2019, June 3). Performance analysis of high-temperature water source cascade heat pump. *Applied Thermal Engineering*.

Linde. (2020). *Linde-gas*. Hentet 2020 fra https://www.linde-gas.com/en/products_and_supply/refrigerants

LLC. (2017, Mars 31). *Power: News & Technology for the global energy industry.* Hentet February 2020 fra powermag.com: https://www.powermag.com/who-has-the-worlds-most-efficient-coal-power-plant-fleet/

Luecken, D., Waterland, R., Papasavva, S., Taddonio, K., Hutzell, W., Rugh, J., & Andersen, S. (2010). Ozone and TFA impacts in North America from degradation of 2,3,3,3-Tetrafluoropropene (HFO 1234yf) a potential greenhouse gas replacement. *Environ. Sci. Technol. 44*, 343-348.

Ma, A. l., Zhang, Y., Li, X., Zou, H., Deng, N., Nie, J., . . . Li, W. (2018, June 25). Experimental study for a high efficiency cascade heat pump water heater system using a new near-zeotropic refrigerant mixture. *Applied Thermal Engineering*, ss. 783-794.

Madsboell, H., Weel, M., & Kolstrup, A. (2014). Development of a water vapor compressor for high temperature heat pump applications. *11th IIR Gustav Lorentzen Conference on Natural Refrigerants*, (ss. 891-899). Hangzhou, China.

Mateu-Royo, C., Navarro-Esbrí, J., Mota-Babiloni, A., Molés, F., & Amat-Albuixech, M. (2019, July 15). Experimental exergy and energy analysis of a novel high-temperature heat. *Applied Energy*.

McMahon, T. (2020, January 7). *inflationdata*. Hentet fra Historical crude oil prices: https://inflationdata.com/articles/inflation-adjusted-prices/historical-crude-oil-prices-table/

Nekså, P., Rekstad, H., Zakeri, G. R., & Schiefloe, P. A. (1998, February 3). CO2-heat pump water heater: characteristics, system design and experimental results. *International Journal of Refrigeration*, ss. 172-179.

Nilsson, M., Rislå, H. N., & Kontomaris, K. (2017). Measured performance of a novel high temperature heat pump with HFO-1336mzz(Z) as the working fluid. *12th IEA Heat Pump Conference.* Rotterdam: IEA Energy Technology Network .

Nordtvedt, S., & Horntvedt, B. (2019). Combined Heating and Cooling: Integrated Ammonia-Water Heat Pump in Modern Dairy Production. *2nd Conference on high temperature heat pumps* (ss. 122-133). Copenhagen: DTU.

Oh, S., Lee, G., Lee, B., Ra, H.-S., Cho, J.-H., .Baik, Y.-J., & Lee, Y.-S. (2016). A study on reliability evaluation test of compressor for high temperature heat-pump based on gas bypass cycle. *Proceedings of the Korean Society of Mechanical Engineers - Thermal Engineering Division Spring Conference*, ss. 326-327.

Ommen, T., Jensen, J. K., Markussen, W. B., Reinholdt, L., & Elmegaard, B. (2015, March 4). Technical and economic working domains of. *International Journal of Refrigeration*, ss. 168-182.

Paepe, M. D., Bogaert, W., & Mertens, D. (2005, December). Cooling of oil injected screw compressors by oil atomisation . *Applied Thermal Engineering*, ss. 2764-2779.

Patel, H. L., & Lakhera, V. J. (2020). A critical review of the experimental studies related to twin screw compressors. *Journal of Process Mechanical Engineering*, ss. Vol. 234 157-170.

Prins, J. (2006). On the structure of compressor gas leakage flow. *International Compressor Engineering Conference* (ss. C012 (1-8)). West Lafayette, Indiana, USA: Purdue University.

Prins, J., & Ferreira, C. (2002). Leakage experiments on a running twin screw compressor. *International Compressor Engineering Conference* (ss. C 19-3). West Lafayette, Indiana, USA: Purdue University.

Process Industry Practices. (2013). *Compressor Selection Guidelines.* Austin: PIP machinery.

Rane, Kovacevic, & Stosic. (2015). Analytical grid generation for accurate representation of clearances in CFD for screw machines. *9th International Conference on Compressors and their Systems* (ss. 90: 1-10). London: IOP Conf Series: Materials Science and Engineering.

Rane, S. (2105). *Grid Generation and CFD Analysis of Varialbe Geometry Screw Machines.* London: City, Universit of London Institutional Repository.

RPA and Anthesis-Caleb. (2017). *Study on the enviornmental and health effects of HFO refrigerants.* Loddon, Norfolk, UK: The Norwegian Environment Agency.

Sarbu, I., & Serbarchievici, C. (2016). Types of Compressors and Heat Pumps. I *Ground-Source Heat Pumps* (ss. 47-70). Elsevier Ltd.

Sarevski, M., & Sarevski, V. (2017, February 12). Thermal Characteristics of High-Temperature R718 Heat Pumps with Turbo Compressor Thermal Vapor Recompression. *Applied Thermal Engineering* , ss. 355-365.

Shen, J., Xing, Z., Zhang, K., He, Z., & Wang, X. (2016). Development of a water-injected twin-screw compressor for mechanical vapor desalination system. *Applied Thermal Engineering*, ss. 125-135.

Shutte & Koerting. (2017). *Steam Desuperheater - Brochure and Manual for Design and Selection.* Hentet fra product brochures: https://www.s-k.com/product-brochures.cfm

Solomon, K., Velders, G., Wilson, S., Madronich, S., Longstreth, J., Aucamp, P., & Bornman, J. (2016). Sources, fates toxicity, and risks of trfliuoroacetic acid and its salts: Relevance to substances regulated under the Montreal and Kyoto protocols. . *Journal of Toxicology and Environmental Health Part B, 19*, 289-304.

Stosic, N. (2015). On heat transfer in scew compressors. *International Journal of Heat and Fluid Flow*, 287-297.

Stosic, N., & Hanjalic, K. (1997, September 1). Development and Optimization of Screw Machines With a Sumlation Model - Part 1: Profile Generation . *Journal of Fluids Engineering*, ss. 659-663.

Stosic, P. N., Smith, P. I., & Kovacevic, D. A. (2005). *Screw Compressors - Mathematical Modelling and Performance Calculation* . London : Springer.

Stosic, Smith, & Kovacevic. (2019). Improving Screw Compressor Displacement and Efficiency by Increasing the Rotor Profile Depth. *IOP Conf. Ser.: Mater. Sci. Eng.*, s. 604 011012.

Tian, Y., Shen, J., Wang, C., Xing, Z., & Wang, X. (2017). Modeling and performance study of a Water-injected Twin-Screw Water Vapor Compressor. *International Journal of Refrigeration*, ss. 75-87.

Tian, Y., Yuan, H., Wang, C., Wu, H., & Xing, Z. (2017, June 20). Numerical investiation on mass and heat transfer in an ammonia oil-free twin-screw compressor with liquid injection. *International Journal of Thermal Sciences*, ss. 175-184.

Tolstorebrov, I., Bantle, M., Hafner, A., Kuz, B., & Eikevik, T. M. (2014). Energy efficiency by vapor compression in superheated steam drying systems. *11th IIR Gustavn Lorentzen Conference on Natural Refrigerants.* Hangzhou, China: IIR.

Tønsberg, E. K. (2020). *Modeling Approach for a Liquid-Injected NH3-H20 Screw Compressor.* Norway: NTNU.

Wang, C., Xing, Z., Chen, W., Sun, S., & He, Z. (2019). Analysis of the leakage in a water-lubricated twin-screw air compressor. *Applied Thermal Engineering*, ss. 217-225.

Woolatt, D., & Heidrich, F. (2001). Compressor Performance - Positive Displacement. I P. C. Hanlon, *Compressor Handbook.* New York etc.: McGraw-Hill.

World Resources Institute. (2017). *climate Analysis Indicators Tool*. Hentet fra Climate data explorer: http://cait.wri.org/

Wu, D., Hu, B., Wang, R., Fan, H., & Wang, R. (2020). The performance comparison of high temperature heat pump among R718 and other refrgierants. *Renewable Energy*, 715-722.

Wu, D., Jiang, J., Hu, B., & Wang, R. (2020). Experimental investigation on the performance of a very high temperature heat pump with water refrigerant. *Energy*.

Yang, Q., Liu, C., Zhang, Q., Liu, Q., Zhao, Y., & Li, L. (2018). Experimental investigation of the water-injected process-gas screw compressor. *Journal of Process Mechanical Engineering*, ss. 3-11.

Zamfirescu, C., & Ferreira, C. (2004). A uniform property region method for screw compressor's end-face leakage prediction. *International Compressor Engineering Conference* (ss. C142/1-9). West Lafayette, Indiana, USA: Purdue University .

Zaytsev, D. (2003). *Development of Wet Compressor for Application in Compression-Resorption Heat Pumps.*

Appendix A: Experimental results

Table A.1 Expanded experimental data

Evaporation temperature =85°C	Speed (rpm)	calc. Speed (rpm)	eta_vol (-)	Pressure at saturation temperature(bar)	suction temperature (K)	Suction temperature (°C)	Suction pressure (bar)	Saturation Temperature at given Pressure (°C)	Saturation Temperature at given Pressure (K)	Vapor density at sat cond. (kg/m³)	Suction mass flow (kg/s)	enthalpy (kJ/kg)	Discharge temperature (K)	Discharge temperature (°C)	Discharge pressure (bar)	Saturation Temperature at given Pressure (°C)	enthalpy (kJ/kg)	Discharge volume (m3/min)	Discharge volume (m³/s)	Vapor density at sat cond. (kg/m³)	Discharge mass flow (kg/s)
	5000	3152	0.630	0.058	364.550	91.40	0.642	87.67	360.82	0.386	0.125	2655.82	391.567	118.417	1.957	119.52	2705.34	7.407	0.123	1.105	0.136
	5000	3177	0.635	0.058	363.170	90.02	0.612	86.44	359.59	0.369	0.121	2653.81	394.760	121.610	2.220	123.55	2711.14	6.333	0.106	1.244	0.131
	5000	2900	0.580	0.058	362.026	88.88	0.586	85.34	358.49	0.355	0.106	2651.98	399.588	126.438	2.458	126.85	2715.81	5.104	0.085	1.368	0.116
	5000	2677	0.535	0.058	361.806	88.66	0.584	85.22	358.37	0.353	0.097	2651.79	408.930	135.780	2.875	132.08	2723.04	4.123	0.069	1.585	0.109
	5000	2522	0.504	0.058	361.623	88.47	0.582	85.13	358.28	0.352	0.091	2651.65	409.823	136.673	3.440	138.25	2731.28	3.377	0.056	1.875	0.106
	5000	2219	0.444	0.058	360.992	87.84	0.569	84.58	357.73	0.345	0.079	2650.73	419.813	146.663	3.853	142.26	2736.46	2.734	0.046	2.086	0.095
	5000	1913	0.383	0.058	360.485	87.33	0.563	84.31	357.46	0.342	0.067	2650.28	425.350	152.200	4.422	147.26	2742.72	2.141	0.036	2.374	0.085
	5000	1782	0.356	0.058	360.237	87.09	0.560	84.15	357.30	0.340	0.062	2650.02	424.373	151.223	5.103	152.60	2749.14	1.761	0.029	2.717	0.080

Evaporation temperature =80°C		Speed ?		Pressure at saturation temperature(bar)	suction temperature (K)	Suction temperature (°C)	Suction pressure (bar)	Saturation Temperature at given Pressure (°C)	Saturation Temperature at given Pressure (K)	Vapor density at sat cond. (kg/m³)	Suction mass flow (kg/s)	enthalpy (kJ/kg)	Discharge temperature (K)	Discharge temperature (°C)	Discharge pressure (bar)	Saturation Temperature at given Pressure (°C)	enthalpy (kJ/kg)	Discharge volume (m3/min)	Discharge volume (m³/s)	Vapor density at sat cond. (kg/m³)	Discharge mass flow (kg/s)
	5000	2937	0.587	0.047	357.998	84.85	0.488	80.71	353.86	0.301	0.091	2644.30	390.221	117.0714	1.8503	117.77	2702.77	5.6614	0.094	1.049	0.099
	5000	2656	0.531	0.047	357.647	84.50	0.481	80.35	353.50	0.297	0.081	2643.71	399.144	125.9943	2.0987	121.74	2708.55	4.5553	0.076	1.180	0.090
	5000	2440	0.488	0.047	357.131	83.98	0.486	80.64	353.79	0.301	0.075	2644.18	402.940	129.7903	2.5237	127.72	2717.04	3.6243	0.060	1.402	0.085
	5000	2279	0.456	0.047	356.137	82.99	0.480	80.28	353.43	0.297	0.069	2643.59	408.263	135.1130	2.9290	132.71	2723.89	3.0175	0.050	1.613	0.081
	5000	2087	0.417	0.047	355.405	82.26	0.460	79.26	352.41	0.285	0.061	2641.88	413.950	140.8000	3.3554	137.38	2730.14	2.4205	0.040	1.832	0.074
	5000	1854	0.371	0.047	354.773	81.62	0.468	79.70	352.85	0.290	0.055	2642.62	417.668	144.5176	3.8711	142.43	2736.68	2.0432	0.034	2.095	0.071
	5000	1651	0.330	0.047	354.697	81.55	0.466	79.56	352.71	0.288	0.049	2642.37	423.162	150.0118	4.4778	147.72	2743.28	1.6563	0.028	2.402	0.066

Evaporation temperature =75°C		Speed ?		Pressure at saturation temperature(bar)	suction temperature (K)	Suction temperature (°C)	Suction pressure (bar)	Saturation Temperature at given Pressure (°C)	Saturation Temperature at given Pressure (K)	Vapor density at sat cond. (kg/m³)	Suction mass flow (kg/s)	enthalpy (kJ/kg)	Discharge temperature (K)	Discharge temperature (°C)	Discharge pressure (bar)	Saturation Temperature at given Pressure (°C)	enthalpy (kJ/kg)	Discharge volume (m3/min)	Discharge volume (m³/s)	Vapor density at sat cond. (kg/m³)	Discharge mass flow (kg/s)
	5000	2372	0.474	0.039	352.193	79.04	0.396	75.60	348.75	0.248	0.060	2635.71	385.579	112.4286	1.6055	113.40	2696.30	4.5879	0.076	0.918	0.070
	5000	2333	0.467	0.039	353.300	80.15	0.388	75.14	348.29	0.243	0.058	2634.95	389.573	116.4227	1.7932	116.79	2701.34	4.0348	0.067	1.018	0.068
	5000	2253	0.451	0.039	353.073	79.92	0.384	74.86	348.01	0.241	0.056	2634.46	394.783	121.6325	2.1536	122.57	2709.74	3.2573	0.054	1.209	0.066
	5000	2065	0.413	0.039	352.137	78.99	0.385	74.94	348.09	0.241	0.051	2634.60	404.550	131.4000	2.5390	127.92	2717.31	2.6033	0.043	1.410	0.061
	5000	1870	0.374	0.039	350.427	77.28	0.390	75.26	348.41	0.244	0.047	2635.14	404.164	131.0136	2.8897	132.25	2723.27	2.2108	0.037	1.592	0.059
	5000	1654	0.331	0.039	349.186	76.04	0.398	75.73	348.88	0.249	0.042	2635.94	427.827	154.6773	3.3114	136.92	2729.53	1.8618	0.031	1.809	0.056
	5000	1427	0.285	0.039	348.997	75.85	0.416	76.80	349.95	0.259	0.038	2637.73	423.290	150.1400	3.7885	141.66	2735.70	1.5792	0.026	2.053	0.054

Injected-water temperature (°C)	Injected-water pressure (bar)	Injected-water volume flow rate (L/H)	enthalpy (kJ/kg)	Density (kg/m³)	mass flow rate (kg/s)	Compressor power consumption (kW)	Compression ratio	In	Out	Power		theoretical enthalphy suction	theoretical enthalphy injection	theoretical enthalphy discharge	suction mass flow / eta_vol	discharge mass flow/eta_vol	discharge (suction mass flow/etavol + minj)	Power	
14.625	0.754	41.046	61.48	999.1	0.011	46.7	3.0	332.75	369.06	36.31	77.76%	2655.717	385.0065	2705.229	0.198316	0.216386	0.210	39.93615	0.855226
14.105	0.722	38.600	59.30	999.2	0.011	49.2	3.6	320.65	355.98	35.32	71.73%	2653.709	380.1508	2711.032	0.18981	0.206673	0.201	39.29058	0.797819
13.733	0.699	38.304	57.74	999.3	0.011	53.5	4.2	281.03	316.04	35.01	65.49%	2651.881	376.5403	2715.703	0.182297	0.200627	0.193	39.89434	0.74625
13.700	0.714	42.043	57.60	999.3	0.012	59.0	4.9	258.51	296.54	38.03	64.48%	2651.689	378.9511	2722.929	0.181577	0.203371	0.193	44.04004	0.746646
13.708	0.749	51.258	57.64	999.3	0.014	64.2	5.9	242.95	288.27	45.31	70.62%	2651.55	384.2386	2731.165	0.181069	0.209282	0.195	52.45475	0.817532
14.671	0.757	58.711	61.67	999.1	0.016	70.5	6.8	209.70	260.04	50.33	71.41%	2650.631	385.4225	2736.344	0.177444	0.214168	0.194	58.79232	0.83409
14.846	0.797	62.929	62.41	999.1	0.017	76.8	7.9	179.36	232.39	53.03	69.05%	2650.181	391.2979	2742.601	0.175796	0.221439	0.193	63.05634	0.821094
14.040	0.829	62.869	59.04	999.2	0.017	82.7	9.1	166.10	219.22	53.12	64.21%	2649.915	395.7825	2749.016	0.174802	0.223771	0.192	64.26351	0.776893

Injected-water temperature (°C)	Injected-water pressure (bar)	Injected-water volume flow rate (L/H)	enthalpy (kJ/kg)	Density (kg/m³)	mass flow rate (kg/s)	Compressor power consumption (kW)	Compression ratio	In	Out	Power		theoretical enthalphy suction		theoretical enthalphy discharge	suction mass flow / eta_vol		discharge (suction mass flow/etavol + minj)		
17.2810	1.0230	28.6548	72.63	998.7	0.008	42.9	3.8	241.22	267.45	26.23	61.11%	2747.014		2796.567	0.15493		0.163		
17.2657	1.0429	30.1588	72.57	998.7	0.008	46.7	4.4	215.32	242.65	27.32	58.56%	2746.377		2799.251	0.152876		0.161		
17.1968	1.1834	33.5406	72.29	998.8	0.009	51.3	5.2	200.07	230.17	30.10	58.65%	2746.885		2802.038	0.15451		0.164		
17.1478	1.8196	41.8420	72.15	998.8	0.012	55.8	6.1	184.53	220.90	36.36	65.16%	2746.243		2803.097	0.152451		0.164	40.37015	0.723376
16.7400	1.7177	45.6685	70.43	998.9	0.013	62.6	7.3	162.65	201.75	39.11	62.42%	2744.393		2802.942	0.146675		0.159		
17.0486	2.3428	57.8435	71.78	998.8	0.016	68.1	8.3	147.27	195.24	47.97	70.47%	2745.194		2801.4	0.149146		0.165		
16.4941	2.8155	62.5495	69.51	998.9	0.017	75.3	9.6	130.58	181.93	51.35	68.20%	2744.927		2798.094	0.148319		0.166		

Injected-water temperature (°C)	Injected-water pressure (bar)	Injected-water volume flow rate (L/H)	enthalpy (kJ/kg)	Density (kg/m³)	mass flow rate (kg/s)	Compressor power consumption (kW)	Compression ratio	In	Out	Power		theoretical enthalphy suction		theoretical enthalphy discharge	suction mass flow / eta_vol		discharge (suction mass flow/etavol + minj)		
16.4000	1.1078	35.3489	68.95	998.9	0.010	38.2	4.1	159.90	189.33	29.43	77.02%	2737.56		2792.913	0.127333		0.137		
16.3000	1.1161	36.4526	68.53	998.9	0.010	40.6	4.6	154.49	185.00	30.51	75.12%	2736.7		2795.814	0.125101		0.135		
16.3000	1.1026	35.6621	68.53	998.9	0.010	44.8	5.6	147.50	177.83	30.33	67.68%	2736.154		2799.728	0.123702		0.134		
16.3867	1.0545	35.7604	68.89	998.9	0.010	49.4	6.6	135.76	166.28	30.52	61.80%	2736.316		2802.103	0.124115		0.134		
16.5091	1.4251	42.0428	69.44	998.9	0.012	54.1	7.4	124.67	159.77	35.10	64.84%	2736.921		2803.051	0.125669		0.137		
16.6227	1.9209	49.7618	69.96	998.9	0.014	58.7	8.3	112.56	153.24	40.68	69.36%	2737.811		2803.009	0.127993		0.142		
16.3400	2.2310	57.5262	68.80	998.9	0.016	64.2	9.1	101.53	147.83	46.30	72.16%	2739.82		2801.733	0.133408		0.149		

Appendix B: Compressor Information

Table B.1 Compressor information and calculation

		V,th	30.8	m³/min									
		three injection holes on both sides of the male and female rotor. Free of oil!											
		male to female ratio:	5 to 7									99	°C
		Diameter male	205	mm								0.098	Mpa
		Diameter female	192	mm								165	°C
		Center length	160	mm								0.69	MPa
		Rotor length	330	mm		0.33	m					0.89	t/h
		Male wrap angle	300	°									
		Internal comp. Ratio	7										
		Rated speed	5000	rpm	83.33333								
		V,t	30.85	m³/min	0.514167	0.00617							
		V,t	0.00617	m³/round									
		V,o	6159.99	cm³	0.00616	m³	(used in calculation)						
		Min speed	2000	rpm	0.00617								
		Max speed	5000	rpm									
												m³/min	m³/s
		eta,vol	0.83									3.377	0.056
		eta,ad	0.75										
											rpm	5000	83.33333
		A,cav,male	19.384	cm²	0.001938	m²		0.003802	m²		cycle per	min	s
		A,cav,female	18.636	cm²	0.001864	m²		0.001255	m³			2456	40.92769
												30.79995	0.513333
		injection angle,female	115	°								30.79995	0.513333
		injection angle,male	125	°									

	Ratio 1 = ratio 2 = ratio 3 = ratio 4				
	each V		0.001543		
				6.17	
				1.576	
			0.017453		
2 pi	6.283185	6.283185			
wrap angle	300	5.235988			
male	1.256637	1.256637			
beta	0	0			
180/pi	57.29578	57.29578			
shaft rotation angle		**733**			
		Number of CVs			
V for a full cycle		0.0125			
rounds per full compression cycle		2.0361			
	# of CVs	**10.00**			

Appendix G: Calculation Shaft Rotation Angle

The shaft rotation angle is based on the wrap angle of the male rotor, number of male lobes and the rotor geometry. The inputs as used by Zaytsev [1] and described in chapter 1-4 are used in this appendix as inputs, Table G-0-1.

Table G-0-1 Inputs of the shaft rotation angle calculation used by Zaytsev [1].

Symbols	Description	Value	Units
τ_w	Wrap angle of the male rotor	314/5.48	°/rad
β	Angle between R_1 and A	29/0.513	°/rad
m_1	Number of male rotor lobes	5	-

The shaft rotation angle is necessary in the calculations for the transfer from the shaft angle to the time. The maximum shaft rotation angle is calculated by equation G.1. The input values will be in radians and are multiplied by $\frac{180}{\pi}$ to calculate to angle degrees. The one added in the end of the equation results from the total shaft rotation that starts at 0 whilst Matlab only can start at 1, one extra step needs to be added.

$$Shaft\ Rotation\ Angle = \left(2\pi + \tau_w + \frac{2\pi}{m_1} + \beta\right) \cdot \frac{180}{\pi} + 1 \qquad \text{(G.1)}$$

Four different angles are added to result in the shaft rotation angle, the 360 degrees of the rotor, the wrap angle in the length of the rotor, the angle representing the width of the cavity and β (will be explained next). The shaft rotation angle in this case results in 777°.

In the equation of the shaft rotation angle, angle β is used. Angle β is calculated with the cosine rule, is given in equation G.2 and illustrated in Figure G-1. Angle β represents the angle from the first touch between the male rotor and the female rotor and the 'A-line'. The A-line is line used as start point of the rotation angle of the rotors ($A = r_{1h} + r_{2h}$ in m).

$$\beta = acos\left(\frac{A^2 + {R_1}^2 - {r_{2h}}^2}{2 \cdot A \cdot R_1}\right) \qquad \text{(G.2)}$$

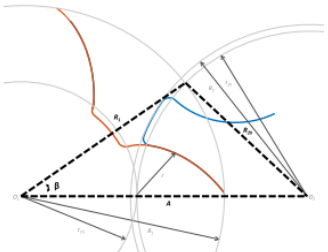

Figure G-1 Illustration of angle β. β is used in the shaft rotation angle calculation.

101

Appendix C: Simulation Results

C.1 Linear function simulation

Table C.1 Results of linear prediction function simulation

C.2 Pearson Correlation and Linear approximation calculation

Table C.2 Pearson correlation and linear approximation calculation

% Error work	9.3	7.5	-4	-7.3	-6.4	-10.4	-10.9	-9	-3.1	-8.3	-8.9
Discharge pressure:	1.96	2.22	2.46	2.88	3.44	3.85	4.42	5.1	1.85	2.1	2.52
vol_eff-excel			0.01	0.025	0.021	0.02	0.01	0.004	0.013	0.024	0.023
Cleak	N/A	N/A	0.05	0.08	0.09	0.1	0.1	0.085	0.03	0.08	0.09
Pressure ratio:	3.05	3.62745098	4.194539249	4.92294521	5.91065292	6.771529	7.854352	9.1125	3.791598	4.363202	5.192798

% Error work	-9.8	-14.2	-13.7	-14	-12.2	-14.6	-14.9	-14.9	-15.2	-14.3	-13.4
Discharge pressure:	2.93	3.36	3.87	4.48	1.61	1.79	2.15	2.54	2.89	3.31	3.79
vol_eff-excel	0.024	0.027	0.039	0.015	0.026	0.033	0.039	0.027	0.026	0.009	0.01
Cleak	0.105	0.13	0.125	0.12	0.13	0.15	0.15	0.155	0.14	0.13	0.115
Pressure ratio:	6.102083	7.294348	8.271581197	9.609013	4.054293	4.621649	5.608333	6.594805	7.409487	8.320101	9.106971

	Evaporation temp:	Discharge temp:	temperature glide:	Volumetric e	% Error work
Evaporation temp:	1				
Discharge temp:	0.17	1			
Temperature Glide:	-0.15	0.949	1		
volumetric efficiency:	0.467	-0.740	-0.89	1	
% Error work	0.649	-0.393	-0.60	0.812	1

Lower volumetric efficiency leads to a to rapid decrase in work. This is seen in the high correlation between volumetric efficiency and % error work.

Cleak vs p.ratio	0.3564
dish p vs vol_eff	-0.46668
dish p vs Cleak	-0.00817
%error work vs Cleak	-0.95715
volumetric efficiency vs Cleak	-0.59927
metric efficiency vs v	0.166044

0.02125

eta =	0.6	Cleak =	0.014	vol_eff =	0.6212
	0.58		0.040		0.6012
	0.56		0.062		0.5812
	0.54		0.080		0.5612
	0.52		0.095		0.5412
	0.5		0.106		0.5212
	0.48		0.115		0.5012
	0.46		0.120		0.4812
	0.44		0.124		0.4612
	0.42		0.126		0.4412
	0.4		0.126		0.4212
	0.38		0.125		0.4012
	0.36		0.123		0.3812
	0.34		0.120		0.3612
	0.32		0.117		0.3412
	0.3		0.114		0.3212
	0.28		0.111		0.3012

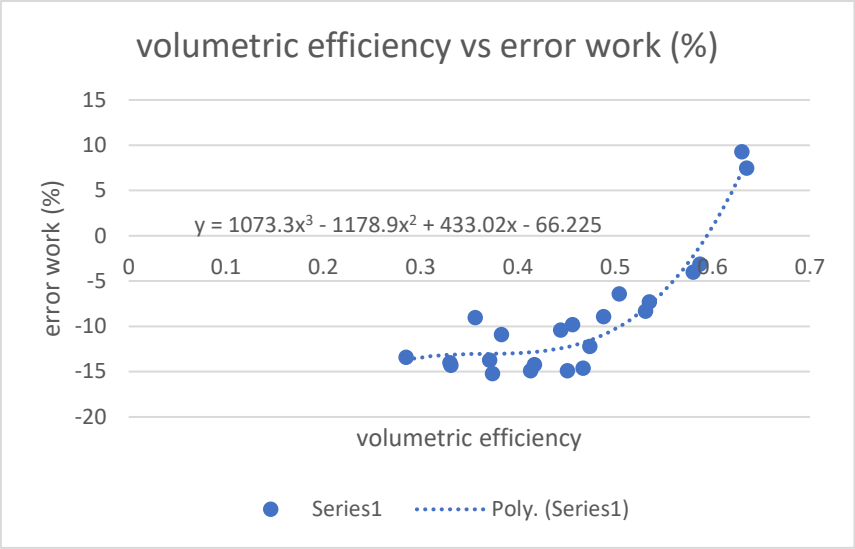

Figure C.1 Preliminary volumetric efficiency vs error work (%)

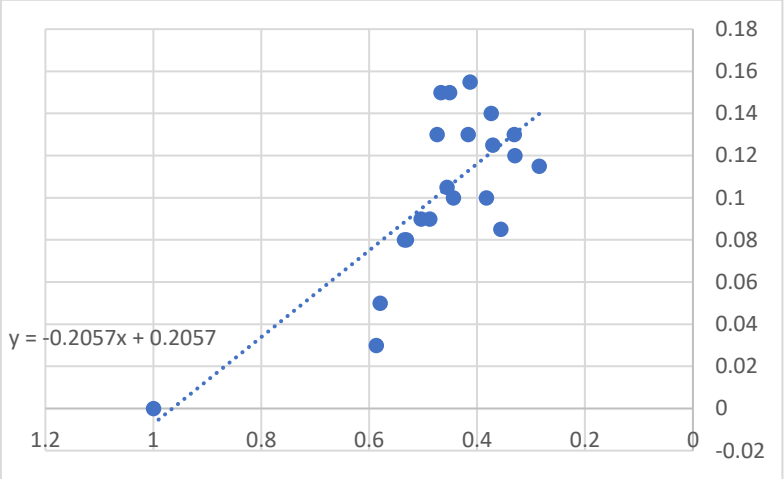

Figure C.2 Linear approximation

Injected mass flow rate	Evap 85								Evap 80								Evap 75							
	Dish 118	Dish 122	Dish 126	Dish 136	Dish 137	Dish 147	Dish 152	Dish 151	Dish 117	Dish 126	Dish 130	Dish 135	Dish 141	Dish 145	Dish 150	Dish 112	Dish 116	Dish 121	Dish 131	Dish 131	Dish 154	Dish 150
simulated	0.011	0.011	0.011	0.012	0.014	0.016	0.017	0.017	0.008	0.008	0.009	0.012	0.013	0.016	0.017	0.0104	0.01	0.01	0.0104	0.012	0.014	0.016
input	0.0035	0.0034	0.0034	0.0037	0.0043	0.0049	0.0052	0.0053	0.0025	0.0025	0.0028	0.0037	0.004	0.005	0.0053	0.0032	0.0031	0.0031	0.0032	0.0037	0.0043	0.005

Figure C.3 Injected mass flow rate

C.3 Theoretical simulation

Table C.3 Results of theoretical simulation

Evap 85 discharge 118.417		temp up to 220	
Parameters:	Suction mass flow	Injected mass flow	discharge mass flow	Wdot
Excel sheet	0.1983	0.011	0.21	46700
Simulation	0.198	0.011	0.21	56500
% error	0.2%	0.0%	0.0%	21.0%
Evap 85 discharge 136.673				
Parameters:	Suction mass flow	Injected mass flow	discharge mass flow	Wdot
Excel sheet	0.181	0.014	0.195	64200
Simulation	0.181	0.014	0.195	63150
% error	0.3%	1.4%	0.2%	-1.6%
Evap 85 discharge 151.223				
Parameters:	Suction mass flow	Injected mass flow	discharge mass flow	Wdot
Excel sheet	0.174802	0.017	0.192	82700
Simulation	0.1745	0.017	0.193	76200
% error	0.2%	0.0%	0.5%	-7.9%

Evap 80 discharge 117			temp up to 220	
Parameters:	Suction mass flow	Injected mass flow	discharge mass flow	Wdot
Excel sheet	0.16493	0.008	0.163	42900
Simulation	0.1528	0.00808	0.161	46300
% error	7.4%	1.0%	1.2%	7.9%
Evap 80 discharge 135.113				
Parameters:	Suction mass flow	Injected mass flow	discharge mass flow	Wdot
Excel sheet	0.152451	0.012	0.164	55800
Simulation	0.151	0.012	0.163	52900
% error	1.0%	0.0%	0.4%	-5.2%
Evap 80 discharge 150				
Parameters:	Suction mass flow	Injected mass flow	discharge mass flow	Wdot
Excel sheet	0.148	0.017	0.166	75300
Simulation	0.147	0.017	0.165	65700
% error	0.6%	0.0%	0.6%	-12.7%

Evap 75 discharge 112				
Paramete	Suction m	Injected n	discharge	Wdot
Excel shee	0.127	0.010	0.137	38200
Simulatio	0.126	0.010	0.136	36550
% error	1.1%	0.0%	0.7%	-4.3%
Evap 75 discharge 131				
Paramete	Suction m	Injected n	discharge	Wdot
Excel shee	0.124	0.010	0.134	49400
Simulatio	0.122	0.010	0.133	44050
% error	1.3%	0.0%	0.7%	-10.8%
Evap 75 discharge 150				
Paramete	Suction m	Injected n	discharge	Wdot
Excel shee	0.133	0.016	0.149	64200
Simulatio	0.133	0.016	0.150	56700
% error	0.4%	0.8%	0.7%	-11.7%

C.4 Optimization study of the mass flow rate of liquid injection

Table C.4 Results of optimization study on the mass flow rate of liquid injection

Injection optimization			Same amount injected in all three injection points. Various magnitude			
Evap 80, Dish 135						
Original simulation						
Cleak = 0.098	vol_eff=	0.466	eta = 0.456	Mass injecte	0.0037	kg/s
Parameters:	Suction mas	Injected mas	discharge mas	Wdot	suct tem	dish temp
Simulation	0.068	0.012	0.081	25930	83.000	132.8
Excel sheet	0.069	0.012	0.081	55800	82.99	135.11
% error	-1.0%	0.0%	-0.6%	-0.3%	0%	-2%
Pressure curve:		OK				
Temperature Curve:		OK				
Cleak = 0.098	vol_eff=	0.466	eta = 0.456	Mass injecte	0.005	kg/s
Parameters:	Suction mas	Injected mas	discharge mas	suct temp	dish tem	Wdot
Simulation	0.068	0.016	0.085	83.000	132.8	25720
original	0.068	0.012	0.081	82.99	135.11	25930
% error	0.0%	34.2%	5.6%	0%	-2%	-0.8%
Pressure curve:		OK				
Temperature Curve:		OK				
Cleak = 0.098	vol_eff=	0.466	eta = 0.456	Mass injecte	0	kg/s
Parameters:	Suction mas	Injected mas	discharge mas	suct temp	dish tem	Wdot
Simulation	0.068	0.000	0.068	83.000	325.5	33100
original	0.068	0.012	0.081	82.99	135.11	25930
% error	0.0%	-100.0%	-15.5%	0%	141%	27.7%
Pressure curve:		Over-compression (almost 4 bar)				
Temperature Curve:		emperatures above 350 deg				
Cleak = 0.098	vol_eff=	0.466	eta = 0.456	Mass injecte	0.0025	kg/s
Parameters:	Suction mas	Injected mas	discharge mas	suct temp	dish tem	Wdot
Simulation	0.068	0.008	0.077	83.000	132.8	26480
original	0.068	0.012	0.081	82.99	135.11	25930
% error	0.0%	-32.5%	-5.0%	0%	-2%	2.1%
Pressure curve:		ok				
Temperature Curve:		ok, highest temp at 160				
Cleak = 0.098	vol_eff=	0.466	eta = 0.456	Mass injecte	0.003	kg/s
Parameters:	Suction mas	Injected mas	discharge mas	suct temp	dish tem	Wdot
Simulation	0.068	0.010	0.078	83.000	132.8	26050
original	0.068	0.012	0.081	82.99	135.11	25930
% error	0.0%	-19.2%	-3.1%	0%	-2%	0.5%
Pressure curve:		ok				
Temperature Curve:		ok				

Cleak = 0.098	vol_eff=	0.466	eta = 0.456	Mass injecte	0.004	kg/s
Parameters:	Suction mas	Injected mas	discharge mas	suct temp	dish tem	Wdot
Simulation	0.068	0.013	0.082	83.000	132.8	25870
original	0.068	0.012	0.081	82.99	135.11	25930
% error	0.0%	8.3%	1.2%	0%	-2%	-0.2%
Pressure curve:		ok				
Temperature Curve:		ok				
Cleak = 0.098	vol_eff=	0.466	eta = 0.456	Mass injecte	0.0055	kg/s
Parameters:	Suction mas	Injected mas	discharge mas	suct temp	dish tem	Wdot
Simulation	0.068	0.018	0.086	83.000	132.8	25620
original	0.068	0.012	0.081	82.99	135.11	25930
% error	0.0%	48.3%	7.2%	0%	-2%	-1.2%
Pressure curve:		ok				
Temperature Curve:		ok				
Cleak = 0.098	vol_eff=	0.466	eta = 0.456	Mass injecte	0.01	kg/s
Parameters:	Suction mas	Injected mas	discharge mas	suct temp	dish tem	Wdot
Simulation	0.068	0.032	0.102	83.000	132.8	24950
original	0.068	0.012	0.081	82.99	135.11	25930
% error	0.0%	170.0%	26.1%	0%	-2%	-3.8%
Pressure curve:		ok				
Temperature Curve:		ok				
Cleak = 0.098	vol_eff=	0.466	eta = 0.456	Mass injecte	0.1	kg/s
Parameters:	Suction mas	Injected mas	discharge mas	suct temp	dish tem	Wdot
Simulation	0.072	0.324	0.400	83.000	132.8	14540
original	0.068	0.012	0.081	82.99	135.11	25930
% error	4.7%	2600.0%	396.9%	0%	-2%	-43.9%
Pressure curve:		ok				
Temperature Curve:		ok				

Injection optimization				Same amount injected in all three		
Evap 80, Dish 150				injection points. Various magnitude		
Original simulation						
Cleak = 0.121	Max_Cav	0.34	eta = 0.3	Mass injected	0.0053	kg/s
Parameters:	Suction mas	Injected mas	discharg	suct temp	dish tem	Wdot
Simulation	0.048	0.017	0.065	81.560	147.8	25500
Excel sheet	0.049	0.017	0.066	82.99	150.01	75300
% error	-1.7%	0.0%	-1.5%	-2%	-1%	-0.4%
Pressure curve:		OK				
Temperature Curve:		little low				

Injection optimization				Same amount injected in all three		
Evap 80, Dish 117				injection points. Various magnitude		
Original simulation						
Cleak = 0.074	Max_Cav	0.597	eta = 0.5	Mass inj	0.0025	kg/s
Parameters:	Suction n	Injected	discharg	suct tem	dish tem	Wdot
Simulation	0.089	0.008	0.098	84.870	118	26950
Excel sheet	0.091	0.008	0.099	84.85	117.07	42900
% error	-1.8%	0.0%	-1.0%	0%	1%	5.2%
Pressure curve:		overcompression (2.9 bar)				
Temperature Curve:		high superheat ~172deg C				

Cleak = 0.121	Max_Cav	0.34	eta = 0.3	Mass injected	0	kg/s
Parameters:	Suction mas	Injected mas	discharg	suct temp	dish tem	Wdot
Simulation	0.047	0	0.047	81.560	443	33950
original	0.048	0.017	0.065	81.560	147.8	25500
% error	-2.8%	-100.0%	-27.7%	0%	200%	33.1%
Pressure curve:		ok				
Temperature Curve:		Temp close to 450 deg C				

Cleak = 0.074	Max_Cav	0.597	eta = 0.5	Mass inj	0	kg/s
Parameters:	Suction n	Injected	discharg	suct tem	dish tem	Wdot
Simulation	0.887	0	0.887	84.880	256	33830
originalsim	0.089	0.008	0.098	84.870	118	26950
% error	892.7%	-100.0%	805.1%	0%	117%	25.5%
Pressure curve:		overcompression 3.5 bar				
Temperature Curve:		superheat over 320 deg C				

Cleak = 0.121	Max_Cav	0.34	eta = 0.3	Mass injected	0.003	kg/s
Parameters:	Suction mas	Injected mas	discharg	suct temp	dish tem	Wdot
Simulation	0.048	0.010	0.058	81.560	147.8	26125
original	0.048	0.017	0.065	81.560	147.8	25500
% error	-0.3%	-42.9%	-10.8%	0%	0%	2.5%
Pressure curve:		ok				
Temperature Curve:		ok				

Cleak = 0.074	Max_Cav	0.597	eta = 0.5	Mass inj	0.0015	kg/s
Parameters:	Suction n	Injected	discharg	suct tem	dish tem	Wdot
Simulation	0.090	0.00483	0.093	84.870	150	29250
originalsim	0.089	0.008	0.098	84.870	118	26950
% error	0.4%	-39.6%	-5.1%	0%	27%	8.5%
Pressure curve:		overcompression 3.17 bar				
Temperature Curve:		superheat over 230 deg C				

Cleak = 0.121	Max_Cav	0.34	eta = 0.3	Mass injected	0.0045	kg/s
Parameters:	Suction mas	Injected mas	discharg	suct temp	dish tem	Wdot
Simulation	0.048	0.015	0.063	81.560	147.8	25700
original	0.048	0.017	0.065	81.560	147.8	25500
% error	-0.1%	-14.1%	-3.1%	0%	0%	0.8%
Pressure curve:		ok				
Temperature Curve:		ok				

Cleak = 0.074	Max_Cav	0.597	eta = 0.5	Mass inj	0.002	kg/s
Parameters:	Suction n	Injected	discharg	suct tem	dish tem	Wdot
Simulation	0.089	0.00649	0.095	84.870	120	28970
originalsim	0.089	0.008	0.098	84.870	118	26950
% error	-0.1%	-18.9%	-3.1%	0%	2%	7.5%
Pressure curve:		overcompression 2.9 bar				
Temperature Curve:		superheat over 200 deg C				

Cleak = 0.121	Max_Cav	0.34	eta = 0.3	Mass injected	0.005	kg/s
Parameters:	Suction mas	Injected mas	discharg	suct temp	dish tem	Wdot
Simulation	0.048	0.016	0.0645	81.560	147.8	25600
original	0.048	0.017	0.065	81.560	147.8	25500
% error	-0.1%	-4.7%	-0.8%	0%	0%	0.4%
Pressure curve:		ok				
Temperature Curve:		ok				

Cleak = 0.074	Max_Cav	0.597	eta = 0.5	Mass inj	0.003	kg/s
Parameters:	Suction n	Injected	discharg	suct tem	dish tem	Wdot
Simulation	0.089	0.0097	0.098	84.870	118	26380
originalsim	0.089	0.008	0.098	84.870	118	26950
% error	0.1%	21.3%	0.0%	0%	0%	-2.1%
Pressure curve:		overcompression 2.8 bar				
Temperature Curve:		superheat over 200 deg C				

Cleak = 0.121	Max_Cav	0.34	eta = 0.3	Mass injected	0.006	kg/s
Parameters:	Suction mas	Injected mas	discharg	suct temp	dish tem	Wdot
Simulation	0.048	0.019	0.068	81.560	147.8	25350
original	0.048	0.017	0.065	81.560	147.8	25500
% error	0.1%	14.1%	4.6%	0%	0%	-0.6%
Pressure curve:		ok				
Temperature Curve:		ok				

Cleak = 0.074	Max_Cav	0.597	eta = 0.5	Mass inj	0.004	kg/s
Parameters:	Suction n	Injected	discharg	suct tem	dish tem	Wdot
Simulation	0.089	0.013	0.102	84.870	118	25875
originalsim	0.089	0.008	0.098	84.870	118	26950
% error	0.1%	61.3%	4.1%	0%	0%	-4.0%
Pressure curve:		ok, max pressure at 2.7				
Temperature Curve:		ok, superheat @ 130				

Cleak = 0.121	Max_Cav	0.34	eta = 0.3	Mass injected	0.0065	kg/s
Parameters:	Suction mas	Injected mas	discharg	suct temp	dish tem	Wdot
Simulation	0.048	0.021	0.069	81.560	147.8	25200
original	0.048	0.017	0.065	81.560	147.8	25500
% error	0.1%	24.1%	6.2%	0%	0%	-1.2%
Pressure curve:		ok				
Temperature Curve:		ok				

Cleak = 0.074	Max_Cav	0.597	eta = 0.5	Mass inj	0.005	kg/s
Parameters:	Suction n	Injected	discharg	suct tem	dish tem	Wdot
Simulation	0.090	0.0162	0.106	84.870	118	25740
originalsim	0.089	0.008	0.098	84.870	118	26950
% error	0.2%	102.5%	8.2%	0%	0%	-4.5%
Pressure curve:		ok, max pressure at 2.7 bar				
Temperature Curve:		ok, superheat below 130				

Cleak = 0.121	Max_Cav	0.34	eta = 0.3	Mass injected	0.01	kg/s
Parameters:	Suction mas	Injected mas	discharg	suct temp	dish tem	Wdot
Simulation	0.048	0.032	0.081	81.560	147.8	24400
original	0.048	0.017	0.065	81.560	147.8	25500
% error	0.4%	90.6%	24.6%	0%	0%	-4.3%
Pressure curve:		ok				
Temperature Curve:		ok				

Cleak = 0.074	Max_Cav	0.597	eta = 0.5	Mass inj	0.01	kg/s
Parameters:	Suction n	Injected	discharg	suct tem	dish tem	Wdot
Simulation	0.090	0.0324	0.122	84.870	118	25130
originalsim	0.089	0.008	0.098	84.870	118	26950
% error	0.4%	305.0%	24.5%	0%	0%	-6.8%
Pressure curve:		ok, max pressure at 2.6 bar				
Temperature Curve:		ok, superheat below 130				

Injection optimization			Same amount injected in all three			
Evap 75, Dish 131			injection points. Various magnitude			
Original simulation						
Cleak = 0.131	Max_cav =	0.423	eta = 0.413	Mass inj	0.0032	kg/s
Parameters:	Suction mas	Injected mas	discharge mas	suct tem	dish tem	Wdot
Simulation	0.0495	0.01	0.06	79	128	20530
Excel sheet	0.051	0.01	0.061	78.99	131.4	49400
% error	-2.9%	3.0%	-1.6%	0%	-3%	-1.8%
Pressure curve:		ok				
Temperature Curve:		ok				

Injection optimization			Same amount injected in all three			
Evap 85, Dish 137			injection points. Various magnitude			
Original simulation						
Cleak = 0.064	Max_cav =	0.514	eta = 0.504	Mass inj	0.0043	kg/s
Parameters:	Suction mas	Injected mas	discharge mas	suct tem	dish tem	Wdot
Simulation	0.091	0.014	0.106	88.52	138.40	32740
Excel sheet	0.091	0.014	0.106	88.47	136.67	64200
% error	0.3%	-0.5%	-0.1%	0%	1%	-0.8%
Pressure curve:		ok				
Temperature Curve:		ok				

Cleak = 0.131	Max_cav =	0.423	eta = 0.413	Mass inj	0	kg/s
Parameters:	Suction mas	Injected mas	discharge mas	suct tem	dish tem	Wdot
Simulation	0.0482	0.00	0.0485	79	359	27170
Originalsim	0.0495	0.01	0.06	79	128	20530
% error	-2.6%	-100.0%	-19.2%	0%	180%	32.3%
Pressure curve:		overcompression > 3.2 bar				
Temperature Curve:		Superheat over 380 degC				

Cleak = 0.064	Max_cav =	0.423	eta = 0.413	Mass inj	0	kg/s
Parameters:	Suction mas	Injected mas	discharge mas	suct tem	dish tem	Wdot
Simulation	0.0906	0.00	0.090	88.52	307.00	40470
Originalsim	0.091	0.014	0.106	88.52	138.40	32740
% error	-0.7%	-100.0%	-15.0%	0%	122%	23.6%
Pressure curve:		highest pressure at 4.5 bar				
Temperature Curve:		highest temperature at 340 deg C				

Cleak = 0.131	Max_cav =	0.423	eta = 0.413	Mass inj	0.002	kg/s
Parameters:	Suction mas	Injected mas	discharge mas	suct tem	dish tem	Wdot
Simulation	0.0493	0.01	0.056	79	128	21170
Originalsim	0.0495	0.01	0.06	79	128	20530
% error	-0.4%	-37.2%	-6.7%	0%	0%	3.1%
Pressure curve:		ok				
Temperature Curve:		ok				

Cleak = 0.064	Max_cav =	0.423	eta = 0.413	Mass inj	0.0025	kg/s
Parameters:	Suction mas	Injected mas	discharge mas	suct tem	dish tem	Wdot
Simulation	0.0912	0.01	0.099	89	147	34050
Originalsim	0.091	0.014	0.106	88.52	138.40	32740
% error	-0.1%	-41.9%	-6.5%	0%	6%	4.0%
Pressure curve:		ok				
Temperature Curve:		highest temperature at 190 degC				

Cleak = 0.131	Max_cav =	0.423	eta = 0.413	Mass inj	0.0025	kg/s
Parameters:	Suction mas	Injected mas	discharge mas	suct tem	dish tem	Wdot
Simulation	0.0495	0.01	0.0578	79	128	20630
Originalsim	0.0495	0.01	0.06	79	128	20530
% error	0.0%	-21.4%	-3.7%	0%	0%	0.5%
Pressure curve:		ok				
Temperature Curve:		ok				

Cleak = 0.064	Max_cav =	0.423	eta = 0.413	Mass inj	0.003	kg/s
Parameters:	Suction mas	Injected mas	discharge mas	suct tem	dish tem	Wdot
Simulation	0.0912	0.01	0.101	89	138.4	33400
Originalsim	0.091	0.014	0.106	88.52	138.40	32740
% error	-0.1%	-30.2%	-4.2%	0%	0%	2.0%
Pressure curve:		ok				
Temperature Curve:		highest temperature at 167.7degC				

Cleak = 0.131	Max_cav =	0.423	eta = 0.413	Mass inj	0.0035	kg/s
Parameters:	Suction mas	Injected mas	discharge mas	suct tem	dish tem	Wdot
Simulation	0.0495	0.01	0.061	79	128	20450
Originalsim	0.0495	0.01	0.06	79	128	20530
% error	0.0%	9.7%	1.7%	0%	0%	-0.4%
Pressure curve:		ok				
Temperature Curve:		ok				

Cleak = 0.064	Max_cav =	0.423	eta = 0.413	Mass inj	0.0045	kg/s
Parameters:	Suction mas	Injected mas	discharge mas	suct tem	dish tem	Wdot
Simulation	0.09127	0.01	0.1065	89	138.4	32710
Originalsim	0.091	0.014	0.106	88.52	138.40	32740
% error	0.0%	4.6%	0.6%	0%	0%	-0.1%
Pressure curve:		ok				
Temperature Curve:		ok				

Cleak = 0.131	Max_cav =	0.423	eta = 0.413	Mass inj	0.004	kg/s
Parameters:	Suction mas	Injected mas	discharge mas	suct tem	dish tem	Wdot
Simulation	0.0496	0.013	0.063	79	128	20390
Originalsim	0.0495	0.010	0.060	79	128	20530
% error	0.2%	25.8%	4.2%	0%	0%	-0.7%
Pressure curve:		ok				
Temperature Curve:		ok				

Cleak = 0.064	Max_cav =	0.423	eta = 0.413	Mass inj	0.0055	kg/s
Parameters:	Suction mas	Injected mas	discharge mas	suct tem	dish tem	Wdot
Simulation	0.0913	0.02	0.1095	89	138.4	32530
Originalsim	0.091	0.014	0.106	88.52	138.40	32740
% error	0.0%	27.8%	3.4%	0%	0%	-0.6%
Pressure curve:		ok				
Temperature Curve:		ok				

Cleak = 0.131	Max_cav =	0.423	eta = 0.413	Mass inj	0.0055	kg/s
Parameters:	Suction mas	Injected mas	discharge mas	suct tem	dish tem	Wdot
Simulation	0.0497	0.02	0.0672	79	128	20110
Originalsim	0.0495	0.01	0.06	79	128	20530
% error	0.4%	72.8%	12.0%	0%	0%	-2.0%
Pressure curve:		ok				
Temperature Curve:		ok				

Cleak = 0.064	Max_cav =	0.423	eta = 0.413	Mass inj	0.0065	kg/s
Parameters:	Suction mas	Injected mas	discharge mas	suct tem	dish tem	Wdot
Simulation	0.091	0.02	0.1125	89	138.4	32400
Originalsim	0.091	0.014	0.106	88.52	138.40	32740
% error	0.1%	50.8%	6.3%	0%	0%	-1.0%
Pressure curve:		ok				
Temperature Curve:		ok				

Cleak = 0.131	Max_cav =	0.423	eta = 0.413	Mass inj	0.01	kg/s
Parameters:	Suction mas	Injected mas	discharge mas	suct tem	dish tem	Wdot
Simulation	0.05	0.03	0.082	79	128	19300
Originalsim	0.0495	0.01	0.06	79	128	20530
% error	1.0%	212.6%	36.7%	0%	0%	-6.0%
Pressure curve:		ok				
Temperature Curve:		ok				

Cleak = 0.064	Max_cav =	0.423	eta = 0.413	Mass inj	0.01	kg/s
Parameters:	Suction mas	Injected mas	discharge mas	suct tem	dish tem	Wdot
Simulation	0.0915	0.03	0.124	89	138.4	31870
Originalsim	0.091	0.014	0.106	88.52	138.40	32740
% error	0.3%	131.9%	17.1%	0%	0%	-2.7%
Pressure curve:		ok				
Temperature Curve:		ok				

C.5 Optimization study of the distribution of liquid injection in the various nozzles

Table C.5 Results of optimization of the distribution of liquid injection in the various nozzles

Low Pressure ratio

Medium Pressure ratio and evaporation temperature

High pressure ratio

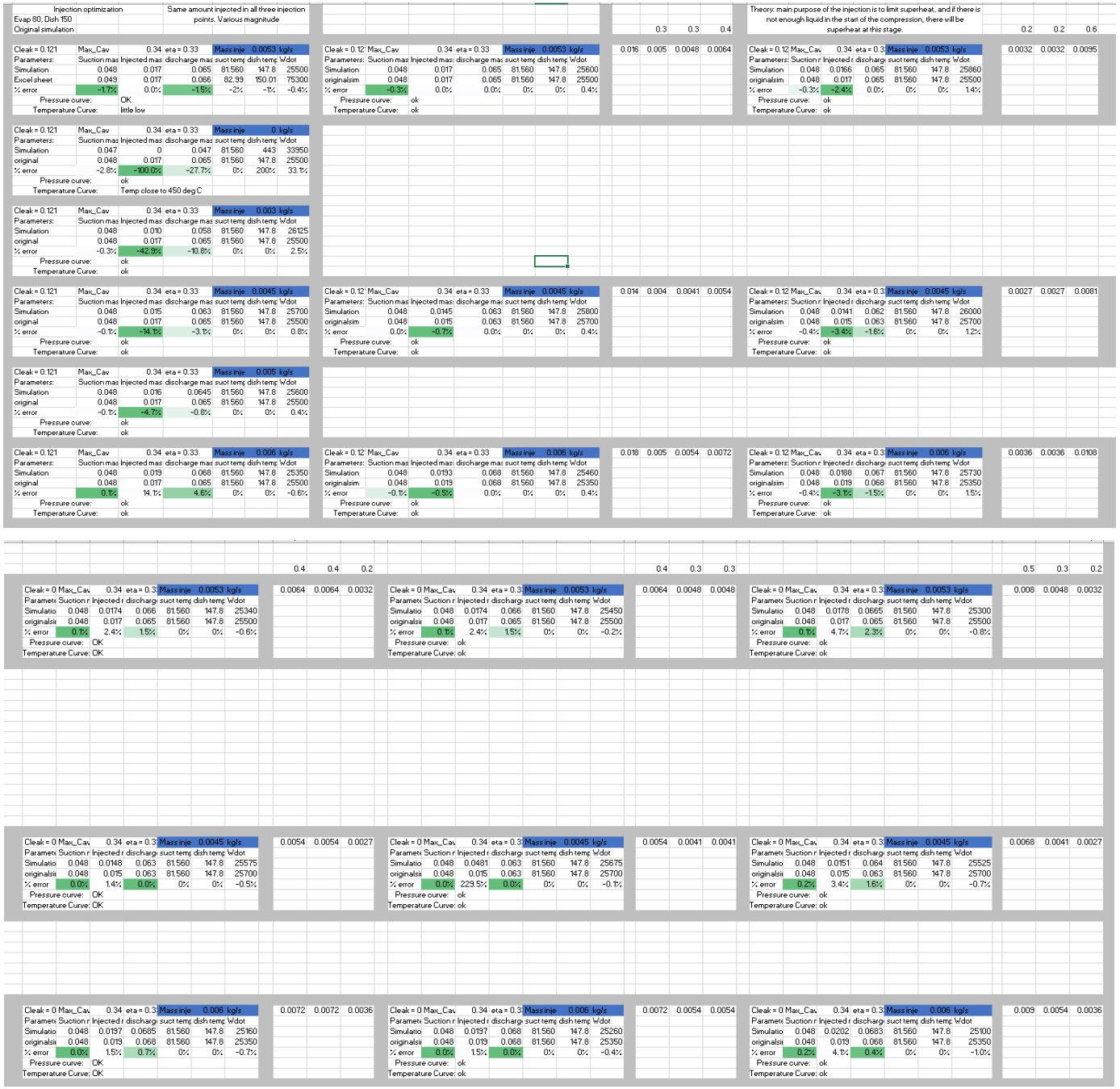

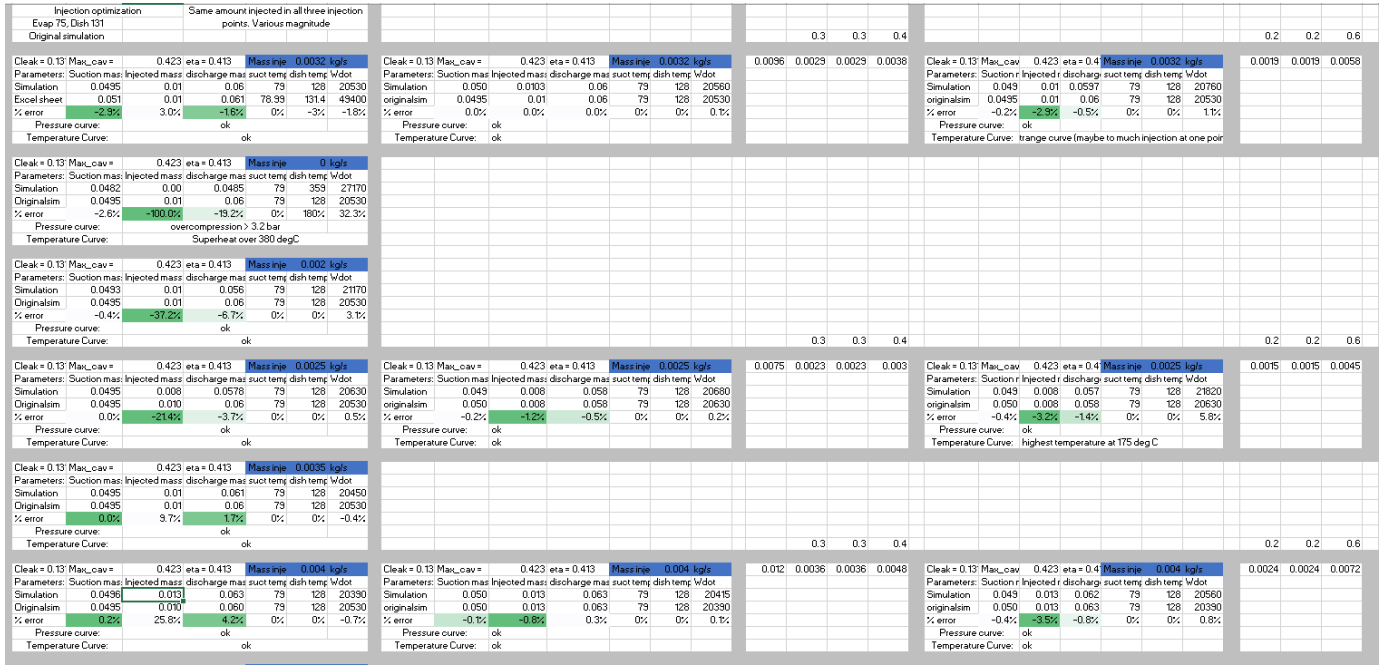

Injection optimization
Evap 75, Dish 131
Original simulation

Same amount injected in all three injection points. Various magnitude

Cleak = 0.13	Max_cav =	0.423	eta = 0.413	Mass inje	0.0032	kg/s
Parameters:	Suction mas	Injected mass	discharge mas	suct temp	dish temp	Wdot
Simulation	0.0495	0.01	0.06	79	128	20530
Excel sheet	0.051	0.01	0.061	78.99	131.4	49400
% error	-2.9%	3.0%	-1.6%	0%	-3%	-1.8%
Pressure curve:	ok					
Temperature Curve:	ok					

Cleak = 0.13	Max_cav =	0.423	eta = 0.413	Mass inje	0.0032	kg/s
Parameters:	Suction mas	Injected mass	discharge mas	suct temp	dish temp	Wdot
Simulation	0.050	0.0103	0.06	79	128	20560
originalsim	0.0495	0.01	0.06	79	128	20530
% error	0.0%	0.0%	0.0%	0%	0%	0.1%
Pressure curve:	ok					
Temperature Curve:	ok					

0.0096 0.0029 0.0029 0.0038

Cleak = 0.13	Max_cav	0.423	eta = 0.4	Mass inje	0.0032	kg/s
Parameters:	Suction r	Injected r	discharg	suct temp	dish temp	Wdot
Simulation	0.049	0.01	0.0597	79	128	20760
originalsim	0.0495	0.01	0.06	79	128	20530
% error	-0.2%	-2.9%	-0.5%	0%	0%	1.1%
Pressure curve:	ok					
Temperature Curve:	trange curve (maybe to much injection at one poir					

0.0019 0.0019 0.0058

Cleak = 0.13	Max_cav =	0.423	eta = 0.413	Mass inje	0	kg/s
Parameters:	Suction mas	Injected mass	discharge mas	suct temp	dish temp	Wdot
Simulation	0.0482	0.00	0.0485	79	359	27170
Originalsim	0.0495	0.01	0.06	79	128	20530
% error	-2.6%	-100.0%	-19.2%	0%	180%	32.3%
Pressure curve:	overcompression > 3.2 bar					
Temperature Curve:	Superheat over 380 degC					

Cleak = 0.13	Max_cav =	0.423	eta = 0.413	Mass inje	0.002	kg/s
Parameters:	Suction mas	Injected mass	discharge mas	suct temp	dish temp	Wdot
Simulation	0.0493	0.01	0.056	79	128	21170
Originalsim	0.0495	0.01	0.06	79	128	20530
% error	-0.4%	-37.2%	-6.7%	0%	0%	3.1%
Pressure curve:	ok					
Temperature Curve:	ok					

0.3 0.3 0.4 0.2 0.2 0.6

Cleak = 0.13	Max_cav =	0.423	eta = 0.413	Mass inje	0.0025	kg/s
Parameters:	Suction mas	Injected mass	discharge mas	suct temp	dish temp	Wdot
Simulation	0.0495	0.008	0.0578	79	128	20630
Originalsim	0.0495	0.010	0.06	79	128	20530
% error	0.0%	-21.4%	-3.7%	0%	0%	0.5%
Pressure curve:	ok					
Temperature Curve:	ok					

Cleak = 0.13	Max_cav =	0.423	eta = 0.413	Mass inje	0.0025	kg/s
Parameters:	Suction mas	Injected mass	discharge mas	suct temp	dish temp	Wdot
Simulation	0.049	0.008	0.058	79	128	20680
originalsim	0.050	0.008	0.058	79	128	20630
% error	-0.2%	-1.2%	-0.5%	0%	0%	0.2%
Pressure curve:	ok					
Temperature Curve:	ok					

0.0075 0.0023 0.0023 0.003

Cleak = 0.13	Max_cav	0.423	eta = 0.4	Mass inje	0.0025	kg/s
Parameters:	Suction r	Injected r	discharg	suct temp	dish temp	Wdot
Simulation	0.049	0.008	0.057	79	128	21820
originalsim	0.050	0.008	0.058	79	128	20630
% error	-0.4%	-3.2%	-1.4%	0%	0%	5.8%
Pressure curve:	ok					
Temperature Curve:	highest temperature at 175 deg C					

0.0015 0.0015 0.0045

Cleak = 0.13	Max_cav =	0.423	eta = 0.413	Mass inje	0.0035	kg/s
Parameters:	Suction mas	Injected mass	discharge mas	suct temp	dish temp	Wdot
Simulation	0.0495	0.01	0.061	79	128	20450
Originalsim	0.0495	0.01	0.06	79	128	20530
% error	0.0%	9.7%	1.7%	0%	0%	-0.4%
Pressure curve:	ok					
Temperature Curve:	ok					

0.3 0.3 0.4 0.2 0.2 0.6

Cleak = 0.13	Max_cav =	0.423	eta = 0.413	Mass inje	0.004	kg/s
Parameters:	Suction mas	Injected mass	discharge mas	suct temp	dish temp	Wdot
Simulation	0.0496	0.013	0.063	79	128	20390
Originalsim	0.0495	0.010	0.060	79	128	20530
% error	0.2%	25.8%	4.2%	0%	0%	-0.7%
Pressure curve:	ok					
Temperature Curve:	ok					

Cleak = 0.13	Max_cav =	0.423	eta = 0.413	Mass inje	0.004	kg/s
Parameters:	Suction mas	Injected mass	discharge mas	suct temp	dish temp	Wdot
Simulation	0.050	0.013	0.063	79	128	20415
originalsim	0.050	0.013	0.063	79	128	20390
% error	-0.1%	-0.8%	0.3%	0%	0%	0.1%
Pressure curve:	ok					
Temperature Curve:	ok					

0.012 0.0036 0.0036 0.0048

Cleak = 0.13	Max_cav	0.423	eta = 0.4	Mass inje	0.004	kg/s
Parameters:	Suction r	Injected r	discharg	suct temp	dish temp	Wdot
Simulation	0.049	0.013	0.062	79	128	20560
originalsim	0.050	0.013	0.063	79	128	20390
% error	-0.4%	-3.5%	-0.8%	0%	0%	0.8%
Pressure curve:	ok					
Temperature Curve:	ok					

0.0024 0.0024 0.0072

Low evaporation temperature

0.4 0.4 0.2 0.4 0.3 0.3 0.5 0.3 0.2

Cleak = 0.13	Max_cav	0.423	eta = 0.4	Mass inje	0.0032	kg/s
Parameters:	Suction r	Injected r	discharg	suct temp	dish temp	Wdot
Simulation	0.050	0.011	0.061	79	128	20460
originalsim	0.050	0.010	0.060	79	128	20530
% error	0.1%	2.2%	0.8%	0%	0%	-0.3%
Pressure curve:	ok					
Temperature Curve:	ok					

0.0038 0.0038 0.0019

Cleak = 0.13	Max_cav	0.423	eta = 0.4	Mass inje	0.0032	kg/s
Parameters:	Suction r	Injected r	discharg	suct temp	dish temp	Wdot
Simulation	0.049	0.011	0.060	79	128	20515
originalsim	0.050	0.010	0.060	79	128	20530
% error	-1.0%	1.9%	0.7%	0%	0%	-0.1%
Pressure curve:	ok					
Temperature Curve:	ok					

0.0038 0.0029 0.0029

Cleak = 0.13	Max_cav	0.423	eta = 0.4	Mass inje	0.0032	kg/s
Parameters:	Suction r	Injected r	discharg	suct temp	dish temp	Wdot
Simulation	0.050	0.011	0.061	79	128	20450
originalsim	0.050	0.010	0.060	79	128	20530
% error	0.3%	4.9%	1.5%	0%	0%	-0.4%
Pressure curve:	ok					
Temperature Curve:	ok					

0.0048 0.0029 0.0019

0.4 0.4 0.2 0.4 0.3 0.3 0.5 0.3 0.2

Cleak = 0.13	Max_cav	0.423	eta = 0.4	Mass inje	0.0025	kg/s
Parameters:	Suction r	Injected r	discharg	suct temp	dish temp	Wdot
Simulation	0.050	0.008	0.006	79	128	20580
originalsim	0.050	0.008	0.058	79	128	20630
% error	0.0%	1.6%	-30.0%	0%	0%	-0.2%
Pressure curve:	ok					
Temperature Curve:	ok					

0.003 0.003 0.0015

Cleak = 0.13	Max_cav	0.423	eta = 0.4	Mass inje	0.0025	kg/s
Parameters:	Suction r	Injected r	discharg	suct temp	dish temp	Wdot
Simulation	0.050	0.008	0.058	79	128	20620
originalsim	0.050	0.008	0.058	79	128	20630
% error	0.0%	1.5%	-0.2%	0%	0%	0.0%
Pressure curve:	ok					
Temperature Curve:	ok					

0.003 0.0023 0.0023

Cleak = 0.13	Max_cav	0.423	eta = 0.4	Mass inje	0.0025	kg/s
Parameters:	Suction r	Injected r	discharg	suct temp	dish temp	Wdot
Simulation	0.050	0.008	0.058	79	128	20600
originalsim	0.050	0.008	0.058	79	128	20630
% error	0.2%	3.7%	0.3%	0%	0%	-0.1%
Pressure curve:	ok					
Temperature Curve:	ok					

0.0038 0.0023 0.0015

0.4 0.4 0.2 0.4 0.3 0.3 0.5 0.3 0.2

Cleak = 0.13	Max_cav	0.423	eta = 0.4	Mass inje	0.004	kg/s
Parameters:	Suction r	Injected r	discharg	suct temp	dish temp	Wdot
Simulation	0.050	0.013	0.063	79	128	20290
originalsim	0.050	0.013	0.063	79	128	20390
% error	0.1%	1.9%	0.8%	0%	0%	-0.5%
Pressure curve:	ok					
Temperature Curve:	ok					

0.0048 0.0048 0.0024

Cleak = 0.13	Max_cav	0.423	eta = 0.4	Mass inje	0.004	kg/s
Parameters:	Suction r	Injected r	discharg	suct temp	dish temp	Wdot
Simulation	0.050	0.013	0.063	79	128	20350
originalsim	0.050	0.013	0.063	79	128	20390
% error	0.1%	1.5%	0.8%	0%	0%	-0.2%
Pressure curve:	ok					
Temperature Curve:	ok					

0.0048 0.0036 0.0036

Cleak = 0.13	Max_cav	0.423	eta = 0.4	Mass inje	0.004	kg/s
Parameters:	Suction r	Injected r	discharg	suct temp	dish temp	Wdot
Simulation	0.050	0.013	0.064	79	128	20260
originalsim	0.050	0.013	0.063	79	128	20390
% error	0.4%	3.4%	2.1%	0%	0%	-0.6%
Pressure curve:	ok					
Temperature Curve:	ok					

0.006 0.0036 0.0024

High evaporation temperature case

C.6 Pressure and temperature development with various amounts of liquid injection at a high pressure ratio

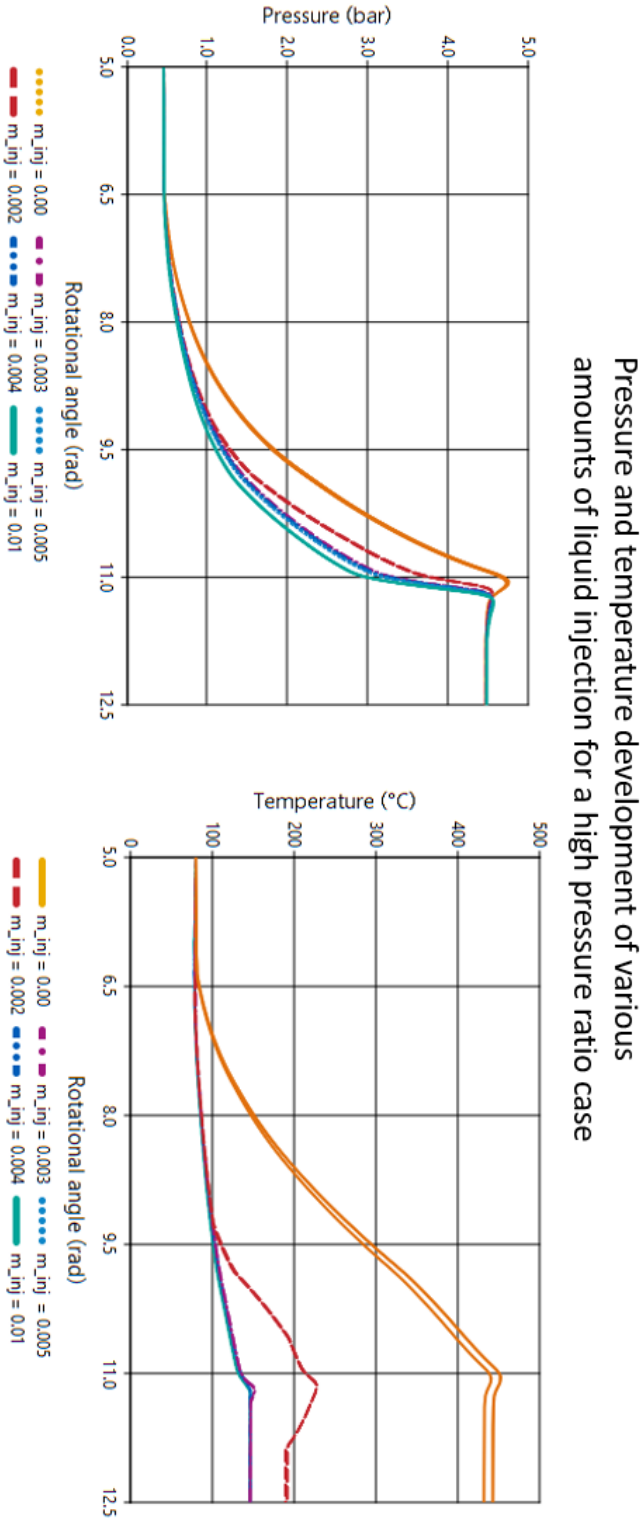

Figure C.4 Pressure and temperature development of various amounts of liquid injection for a high pressure ratio case

C.7 Compressor power consumption of new operational settings

Table C.6 Results of simulations of new operational settings (power consumption)

Evap Temp (C)	Evap temp (K) (+1 in sim)	Suction enthalphy	pressure (Mpa)	pressure bar	Disch Temp	Disch temp (K)	Disch enthalphy	pressure (Mpa)	pressure (pa)	speed (rpm)	calc speed	eta	suction mass flow	vapor density at suction	linearly estimated work	Cleak	Max_cav	new work	New Work/eta	new error%
83	356.15	2648.016	0.053475772	534.75.7718	135	408.15	2726.867	0.28966	289660	5000	2838	0.568	0.096	0.32868	57720	0.063	0.578	32375	56047	-2.9 %
83	356.15	2648.016	0.053475772	534.75.7718	151	424.15	2747.122	0.4444	444400	5000	1774	0.355	0.060	0.32868	76200	0.101	0.365	27730	76033	-0.2 %
83	356.15	2648.016	0.053475772	534.75.7718	118	391.15	2703.007	0.1916	191600	5000	3296	0.659	0.111	0.32868	45180	0.046	0.669	32050	47886	6.0 %
78	351.15	2639.662	0.043702988	437.02.9676	117	390.15	2701.537	0.1814	181400	5000	2794	0.559	0.078	0.271281	41980	0.089	0.569	23600	41488	-1.2 %
78	351.15	2639.662	0.043702988	437.02.9676	131	404.15	2721.454	0.2538	253780	5000	2357	0.471	0.066	0.271281	50540	0.105	0.481	23875	49594	-1.9 %
78	351.15	2639.662	0.043702988	437.02.9676	150	423.15	2745.925	0.383806	383806	5000	1599	0.320	0.045	0.271281	66540	0.132	0.330	22060	66888	0.5 %

Appendix D: Simulation model graphics and code

D.1 Left side of the model diagram

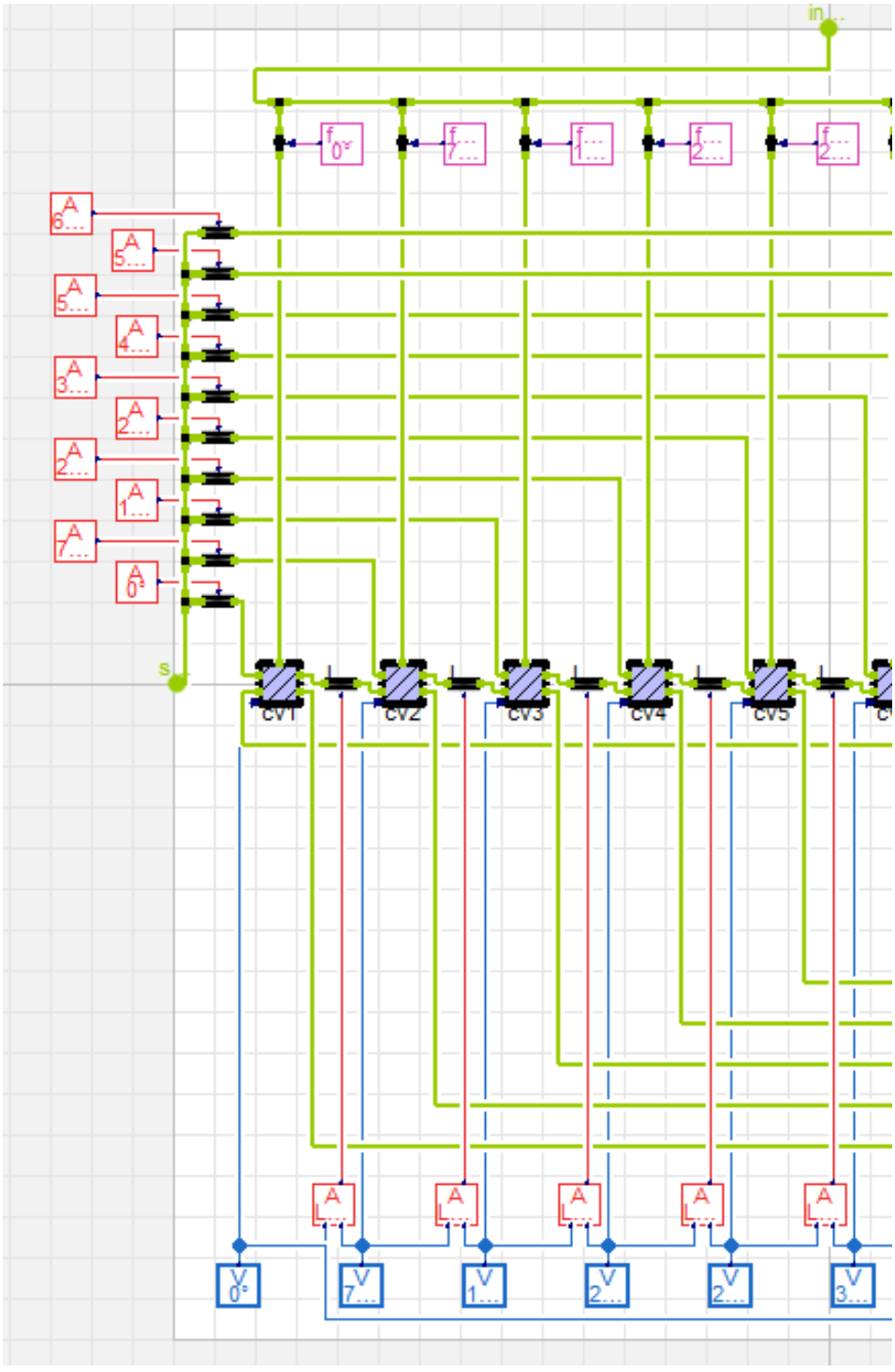

Figure D.1 left side of Modelica diagram

D.2 Right side of the model diagram

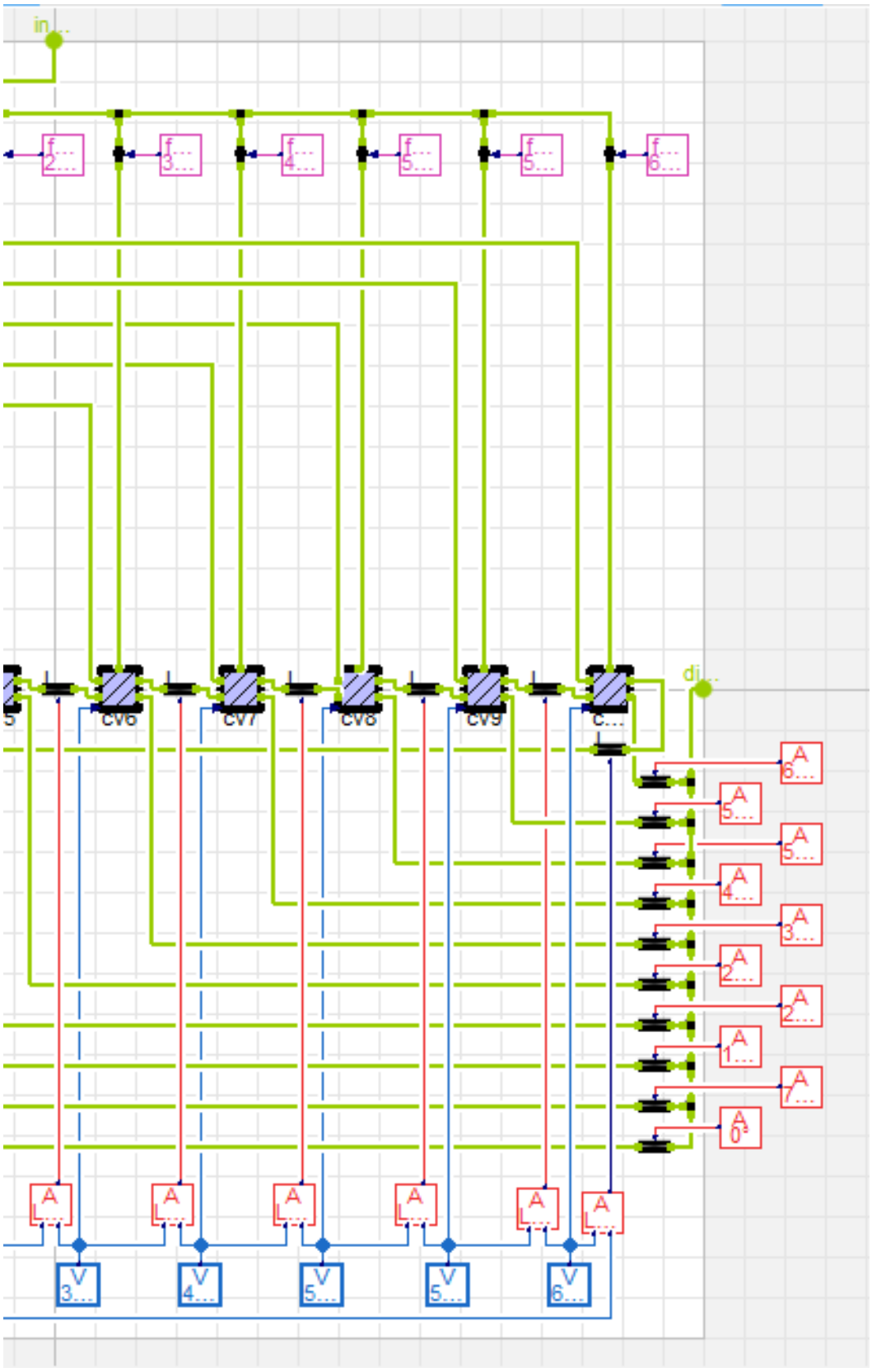

Figure D.2 Right side of Modelica diagram

D.3 Screw compressor code

```
model ScrewCompressor_10Chambers_v1
  "Screw compressor model with 10 control volumes"

  /*SIM*/
  outer TIL.SystemInformationManager sim "System information manager";

  /*Working fluid type*/
  inner TILMedia.VLEFluidTypes.BaseVLEFluid vleFluidType = sim.vleFluidType1 "VLE fluid
type";

  /*Compressor features*/
  parameter Modelica.SIunits.Frequency f = 5000/60 "Operational frequency of the compres
sor";

  parameter Real Max_cav = 1 "Maximum cavity volume coefficient";

  inner Modelica.SIunits.AngularVelocity w = 2*Modelica.Constants.pi*f "*VoleffAngular v
elocity";

  inner parameter Modelica.SIunits.Angle thetaCycle = 12.566370614359 "Total rotation fo
r one compression cycle";

  inner Modelica.SIunits.Time tCycle = thetaCycle/w "Duration of one compression cycle";

  inner parameter Modelica.SIunits.Volume Vmax = 0.001255*Max_cav "Maximum cavity volume
";

  parameter Real Vi = 4.2 "Built-in volume ratio";

  inner parameter Real Cleak = 0 "Leakage flow coefficient";

  inner parameter Modelica.SIunits.Area Asuction = 0.005 "Maximum effective flow area of
 suction path";

  inner parameter Modelica.SIunits.Area Adischarge = 0.001 "Maximum effective flow area
of discharge path";

  inner Modelica.SIunits.Time tDischargeOpen = V1.t4 + ((Vmax - V1.dVdt*(V1.t4-
V1.t3)/2)-Vmax/Vi)/V1.dVdt "Point in time when the discharge port opens";

  inner Modelica.SIunits.Angle thetaDischargeOpen = thetaCycle*tDischargeOpen/tCycle "Ro
tational angle where discharge begins";

  inner parameter Modelica.SIunits.Angle injectionAngle = 6.49663 "Rotational angle wher
e injection begins";

  inner parameter Modelica.SIunits.Angle injectionAngle2 = 8.52884 "Rotational angle whe
re injection begins";

  inner parameter Modelica.SIunits.Angle injectionAngle3 = 10.56105 "Rotational angle wh
ere injection begins";

  inner parameter Modelica.SIunits.MassFlowRate mDotInjection = 0 "Injection mass flow r
ate";

  inner parameter Modelica.SIunits.MassFlowRate mDotInjection2 = 0 "Injection mass flow
rate";

  inner parameter Modelica.SIunits.MassFlowRate mDotInjection3 = 0 "Injection mass flow
rate";

  inner parameter Modelica.SIunits.CoefficientOfHeatTransfer alpha = 0 "Heat transfer co
efficient";

  inner parameter Modelica.SIunits.Temperature Tbody = 373.15 "Average compressor body t
emperature";

  /*Suction properties*/
  inner Modelica.SIunits.AbsolutePressure pSuction = suctionPort.p "Pressure in suction
line";
```

```
  inner Modelica.SIunits.SpecificEnthalpy hSuction = inStream(suctionPort.h_outflow) "Sp
ecific enthalpy in suction line";

  inner Modelica.SIunits.MassFraction[vleFluidType.nc-
1] xiSuction = inStream(suctionPort.xi_outflow) "Mass fraction in suction line";

  /*Start values*/
  parameter Modelica.SIunits.AbsolutePressure pSuctionStart = 500000 "Start value for su
ction pressure"
    annotation(Dialog(group="Pressure", tab="Start values"));

  parameter Modelica.SIunits.AbsolutePressure pStart_cv5 = 500000 "Start value for press
ure in control volume 5"
    annotation(Dialog(group="Pressure", tab="Start values"));

  parameter Modelica.SIunits.AbsolutePressure pStart_cv6 = 653000 "Start value for press
ure in control volume 6"
    annotation(Dialog(group="Pressure", tab="Start values"));

  parameter Modelica.SIunits.AbsolutePressure pStart_cv7 = 1213000 "Start value for pres
sure in control volume 7"
    annotation(Dialog(group="Pressure", tab="Start values"));

  parameter Modelica.SIunits.AbsolutePressure pStart_cv8 = 1213000 "Start value for pres
sure in control volume 8"
    annotation(Dialog(group="Pressure", tab="Start values"));
                          /*new add*/

  parameter Modelica.SIunits.AbsolutePressure pStart_cv9 = 1213000 "Start value for pres
sure in control volume 9"
    annotation(Dialog(group="Pressure", tab="Start values"));
                          /*new add*/

  parameter Modelica.SIunits.AbsolutePressure pDischargeStart = 2500000 "Start value for
 discharge pressure"
    annotation(Dialog(group="Pressure", tab="Start values"));

  parameter Modelica.SIunits.SpecificEnthalpy hSuctionStart = 1737e3 "Start value for sp
ecific enthalpy at suction"
    annotation(Dialog(group="Specific enthalpy", tab="Start values"));

  parameter Modelica.SIunits.SpecificEnthalpy hStart_cv5 = 1737e3 "Start value for speci
fic enthalpy in control volume 5"
    annotation(Dialog(group="Specific enthalpy", tab="Start values"));

  parameter Modelica.SIunits.SpecificEnthalpy hStart_cv6 = 1779e3 "Start value for speci
fic enthalpy in control volume 6"
    annotation(Dialog(group="Specific enthalpy", tab="Start values"));

  parameter Modelica.SIunits.SpecificEnthalpy hStart_cv7 = 1888e3 "Start value for speci
fic enthalpy in control volume 7"
    annotation(Dialog(group="Specific enthalpy", tab="Start values"));

  parameter Modelica.SIunits.SpecificEnthalpy hStart_cv8 = 1888e3 "Start value for speci
fic enthalpy in control volume 8"
    annotation(Dialog(group="Specific enthalpy", tab="Start values"));
                                  /*new add*/

  parameter Modelica.SIunits.SpecificEnthalpy hStart_cv9 = 1888e3 "Start value for speci
fic enthalpy in control volume 9"
    annotation(Dialog(group="Specific enthalpy", tab="Start values"));
                                  /*new add*/

  parameter Modelica.SIunits.SpecificEnthalpy hDischargeStart = 2034e3 "Start value for
specific enthalpy at discharge"
    annotation(Dialog(group="Specific enthalpy", tab="Start values"));

  parameter Modelica.SIunits.SpecificEnthalpy hInjectionStart = 1737e3 "Start value for
specific enthalpy of injection fluid"
    annotation(Dialog(group="Specific enthalpy", tab="Start values"));
```

```
  parameter Modelica.SIunits.MassFraction[vleFluidType.nc-
1] xiSuctionStart = zeros(vleFluidType.nc-1) "Start value for suction mass fraction"
    annotation(Dialog(group="Mass fraction", tab="Start values"));

  parameter Modelica.SIunits.MassFraction[vleFluidType.nc-
1] xiStart_cv5 = zeros(vleFluidType.nc-
1) "Start value for mass fraction in control volume 5"
    annotation(Dialog(group="Mass fraction", tab="Start values"));

  parameter Modelica.SIunits.MassFraction[vleFluidType.nc-
1] xiStart_cv6 = zeros(vleFluidType.nc-
1) "Start value for mass fraction in control volume 6"
    annotation(Dialog(group="Mass fraction", tab="Start values"));

  parameter Modelica.SIunits.MassFraction[vleFluidType.nc-
1] xiStart_cv7 = zeros(vleFluidType.nc-
1) "Start value for mass fraction in control volume 7"
    annotation(Dialog(group="Mass fraction", tab="Start values"));

  parameter Modelica.SIunits.MassFraction[vleFluidType.nc-
1] xiStart_cv8 = zeros(vleFluidType.nc-
1) "Start value for mass fraction in control volume 8"
    annotation(Dialog(group="Mass fraction", tab="Start values"));
                                                              /*new add*/

  parameter Modelica.SIunits.MassFraction[vleFluidType.nc-
1] xiStart_cv9 = zeros(vleFluidType.nc-
1) "Start value for mass fraction in control volume 9"
    annotation(Dialog(group="Mass fraction", tab="Start values"));
                                                              /*new add*/

  parameter Modelica.SIunits.MassFraction[vleFluidType.nc-
1] xiDischargeStart = zeros(vleFluidType.nc-1) "Start value for discharge mass fraction"
    annotation(Dialog(group="Mass fraction", tab="Start values"));

  parameter Modelica.SIunits.MassFraction[vleFluidType.nc-
1] xiInjectionStart = zeros(vleFluidType.nc-1) "Start value for injection mass fraction"
    annotation(Dialog(group="Mass fraction", tab="Start values"));

  /*Additional variables for calculation of compressor characteristics*/
  Modelica.SIunits.Mass mSucked_total "Total mass sucked in by the compressor";

  Modelica.SIunits.Work W_total "Total compression work";

  /*Control volumes*/
  ScrewCompressorPackage_Water_theo.Components.ControlVolume cv1(
    pStart=pSuctionStart,
    hStart=hSuctionStart,
    xiStart=xiSuctionStart) "Control volume 1"
    annotation (Placement(transformation(extent={{-278,-10},{-258,10}})));
  ScrewCompressorPackage_Water_theo.Components.ControlVolume cv2(
    pStart=pSuctionStart,
    hStart=hSuctionStart,
    xiStart=xiSuctionStart) "Control volume 2"
    annotation (Placement(transformation(extent={{-218,-10},{-198,10}})));
  ScrewCompressorPackage_Water_theo.Components.ControlVolume cv3(
    pStart=pSuctionStart,
    hStart=hSuctionStart,
    xiStart=xiSuctionStart) "Control volume 3"
    annotation (Placement(transformation(extent={{-158,-10},{-138,10}})));
  ScrewCompressorPackage_Water_theo.Components.ControlVolume cv4(
    pStart=pSuctionStart,
    hStart=hSuctionStart,
    xiStart=xiSuctionStart) "Control volume 4"
    annotation (Placement(transformation(extent={{-98,-10},{-78,10}})));
  ScrewCompressorPackage_Water_theo.Components.ControlVolume cv5(
    pStart=pStart_cv5,
    hStart=hStart_cv5,
    xiStart=xiStart_cv5) "Control volume 5"
    annotation (Placement(transformation(extent={{-38,-10},{-18,10}})));
  ScrewCompressorPackage_Water_theo.Components.ControlVolume cv6(
    pStart=pStart_cv6,
```

```
    hStart=hStart_cv6,
    xiStart=xiStart_cv6) "Control volume 6"
    annotation (Placement(transformation(extent={{22,-10},{42,10}})));
  ScrewCompressorPackage_Water_theo.Components.ControlVolume cv7(
    pStart=pStart_cv7,
    hStart=hStart_cv7,
    xiStart=xiStart_cv7) "Control volume 7"
    annotation (Placement(transformation(extent={{82,-10},{102,10}})));
  ScrewCompressorPackage_Water_theo.Components.ControlVolume cv8(
    pStart=pStart_cv8,
    hStart=hStart_cv8,
    xiStart=xiStart_cv8) "Control volume 8"
    annotation (Placement(transformation(extent={{140,-
10},{160,10}})));                                                    /*new add*/
  ScrewCompressorPackage_Water_theo.Components.ControlVolume cv9(
    pStart=pStart_cv9,
    hStart=hStart_cv9,
    xiStart=xiStart_cv9) "Control volume 9"
    annotation (Placement(transformation(extent={{202,-
10},{222,10}})));                                                    /*new add*/
  ScrewCompressorPackage_Water_theo.Components.ControlVolume cv10(
    pStart=pDischargeStart,
    hStart=hDischargeStart,
    xiStart=xiDischargeStart) "Control volume 10"
    annotation (Placement(transformation(extent={{264,-
10},{284,10}})));                                                    /*new add*/

  /*Volume functions*/
  ScrewCompressorPackage_Water_theo.Functions.VolumeFunction V1(thetaStart=0)
    "Volume function 1"
    annotation (Placement(transformation(extent={{-298,-304},{-278,-284}})));
  ScrewCompressorPackage_Water_theo.Functions.VolumeFunction V2(thetaStart=
        1.2793263417118) "Volume function 2"
    annotation (Placement(transformation(extent={{-238,-304},{-218,-284}})));
  ScrewCompressorPackage_Water_theo.Functions.VolumeFunction V3(thetaStart=
        2.5586526834237) "Volume function 3"
    annotation (Placement(transformation(extent={{-178,-304},{-158,-284}})));
  ScrewCompressorPackage_Water_theo.Functions.VolumeFunction V4(thetaStart=
        3.8379790251355) "Volume function 4"
    annotation (Placement(transformation(extent={{-118,-304},{-98,-284}})));
  ScrewCompressorPackage_Water_theo.Functions.VolumeFunction V5(thetaStart=
        5.1173053668474) "Volume function 5"
    annotation (Placement(transformation(extent={{-58,-304},{-38,-284}})));
  ScrewCompressorPackage_Water_theo.Functions.VolumeFunction V6(thetaStart=
        6.3966317085592) "Volume function 6"
    annotation (Placement(transformation(extent={{2,-304},{22,-284}})));
  ScrewCompressorPackage_Water_theo.Functions.VolumeFunction V7(thetaStart=
        7.6759580502711) "Volume function 7"
    annotation (Placement(transformation(extent={{62,-304},{82,-284}})));
  ScrewCompressorPackage_Water_theo.Functions.VolumeFunction V8(thetaStart=
        8.9552843919829) "Volume function 8"
    annotation (Placement(transformation(extent={{122,-304},{142,-284}})));
  ScrewCompressorPackage_Water_theo.Functions.VolumeFunction V9(thetaStart=
        10.234610733695) "Volume function 9"
    annotation (Placement(transformation(extent={{184,-304},{204,-
284}})));
  ScrewCompressorPackage_Water_theo.Functions.VolumeFunction V10(thetaStart=
        11.513937075407) "Volume function 10"
    annotation (Placement(transformation(extent={{244,-304},{264,-
284}})));

  /*Connection ports*/
  TIL.Connectors.VLEFluidPort suctionPort(final vleFluidType=vleFluidType) "The compress
or's suction port"
    annotation (Placement(transformation(extent={{-328,-10},{-308,10}})));
  TIL.Connectors.VLEFluidPort dischargePort(final vleFluidType=vleFluidType) "The compre
ssor's discharge port"
    annotation (Placement(transformation(extent={{310,-10},{330,10}})));
  TIL.Connectors.VLEFluidPort injectionPort(final vleFluidType=vleFluidType) "The compre
ssor's injection port"
    annotation (Placement(transformation(extent={{-10,310},{10,330}})));
```

```
  /*Leakage paths*/
  Components.FlowRestrictor leak21 "Leakage from control volume 2 to 1"
    annotation (Placement(transformation(extent={{-8,-4},{8,4}},rotation=180,origin={-
238,0})));
  Components.FlowRestrictor leak32 "Leakage from control volume 3 to 2"
    annotation (Placement(transformation(extent={{-8,-4},{8,4}},rotation=180,origin={-
178,0})));
  Components.FlowRestrictor leak43 "Leakage from control volume 4 to 3"
    annotation (Placement(transformation(extent={{-8,-4},{8,4}},rotation=180,origin={-
118,0})));
  Components.FlowRestrictor leak54 "Leakage from control volume 5 to 4"
    annotation (Placement(transformation(extent={{-8,-4},{8,4}},rotation=180,origin={-
58,0})));
  Components.FlowRestrictor leak65 "Leakage from control volume 6 to 5"
    annotation (Placement(transformation(extent={{-8,-
4},{8,4}},rotation=180,origin={2,0})));
  Components.FlowRestrictor leak76 "Leakage from control volume 7 to 6"
    annotation (Placement(transformation(extent={{-8,-
4},{8,4}},rotation=180,origin={62,0})));
  Components.FlowRestrictor leak87 "Leakage from control volume 8 to 7"
    annotation (Placement(transformation(extent={{-8,-
4},{8,4}},rotation=180,origin={122,0})));
  Components.FlowRestrictor leak110 "Leakage from control volume 1 to 10"
    annotation (Placement(transformation(
        extent={{-8,4},{8,-4}},
        rotation=0,
        origin={274,-30})));
  Components.FlowRestrictor leak98 "Leakage from control volume 9 to 8"
    annotation (Placement(transformation(
        extent={{-8,-4},{8,4}},
        rotation=180,
        origin={182,0})));
  Components.FlowRestrictor leak109 "Leakage from control volume 10 to 9"
    annotation (Placement(transformation(
        extent={{-8,-4},{8,4}},
        rotation=180,
        origin={242,0})));

  /*Leakage area functions*/
  Functions.LeakageAreaFunction leakageAreaFunction21 "Effective flow area of leak21"
    annotation (Placement(transformation(extent={{-252,-264},{-232,-244}})));
  Functions.LeakageAreaFunction leakageAreaFunction32 "Effective flow area of leak32"
    annotation (Placement(transformation(extent={{-192,-264},{-172,-244}})));
  Functions.LeakageAreaFunction leakageAreaFunction43 "Effective flow area of leak43"
    annotation (Placement(transformation(extent={{-132,-264},{-112,-244}})));
  Functions.LeakageAreaFunction leakageAreaFunction54 "Effective flow area of leak54"
    annotation (Placement(transformation(extent={{-72,-264},{-52,-244}})));
  Functions.LeakageAreaFunction leakageAreaFunction65 "Effective flow area of leak65"
    annotation (Placement(transformation(extent={{-12,-264},{8,-244}})));
  Functions.LeakageAreaFunction leakageAreaFunction76 "Effective flow area of leak76"
    annotation (Placement(transformation(extent={{48,-264},{68,-244}})));
  Functions.LeakageAreaFunction leakageAreaFunction87 "Effective flow area of leak87"
    annotation (Placement(transformation(extent={{108,-264},{128,-244}})));
  Functions.LeakageAreaFunction leakageAreaFunction98 "Effective flow area of leak 98"
    annotation (Placement(transformation(extent={{168,-264},{188,-244}})));
  Functions.LeakageAreaFunction leakageAreaFunction109
    "Effective flow area of leak109"
    annotation (Placement(transformation(extent={{228,-266},{248,-246}})));
  Functions.LeakageAreaFunction leakageAreaFunction110
    "Effective flow area of leak110"
    annotation (Placement(transformation(extent={{260,-268},{280,-248}})));

  /*Suction paths*/
  Components.FlowRestrictor suctionPath1 "Suction path to control volume 1"
    annotation (Placement(transformation(extent={{-306,36},{-290,44}})));
  Components.FlowRestrictor suctionPath2 "Suction path to control volume 2"
    annotation (Placement(transformation(extent={{-306,56},{-290,64}})));
  Components.FlowRestrictor suctionPath3 "Suction path to control volume 3"
    annotation (Placement(transformation(extent={{-306,76},{-290,84}})));
  Components.FlowRestrictor suctionPath4 "Suction path to control volume 4"
    annotation (Placement(transformation(extent={{-306,96},{-290,104}})));
  Components.FlowRestrictor suctionPath5 "Suction path to control volume 5"
```

```
    annotation (Placement(transformation(extent={{-306,116},{-290,124}})));
  Components.FlowRestrictor suctionPath6 "Suction path to control volume 6"
    annotation (Placement(transformation(extent={{-306,136},{-290,144}})));
  Components.FlowRestrictor suctionPath7 "Suction path to control volume 7"
    annotation (Placement(transformation(extent={{-306,156},{-290,164}})));
  Components.FlowRestrictor suctionPath8 "Suction path to control volume 8"
    annotation (Placement(transformation(extent={{-306,176},{-290,184}})));
 Components.FlowRestrictor suctionPath9 "Suction path to control volume 8"
    annotation (Placement(transformation(extent={{-306,196},{-290,204}})));
  Components.FlowRestrictor suctionPath10
                                        "Suction path to control volume 8"
    annotation (Placement(transformation(extent={{-306,216},{-290,224}})));

  /*Suction area functions*/
  Functions.SuctionAreaFunction suctionAreaFunction1(thetaStart=0) "Effective flow area
of suction path 1"
    annotation (Placement(transformation(extent={{-348,40},{-328,60}})));
  Functions.SuctionAreaFunction suctionAreaFunction2(thetaStart=
        1.2793263417118)                                                    "Effect
ive flow area of suction path 2"
    annotation (Placement(transformation(extent={{-378,60},{-358,80}})));
  Functions.SuctionAreaFunction suctionAreaFunction3(thetaStart=
        2.5586526834237)                                                    "Effect
ive flow area of suction path 3"
    annotation (Placement(transformation(extent={{-348,80},{-328,100}})));
  Functions.SuctionAreaFunction suctionAreaFunction4(thetaStart=
        3.8379790251355)                                                    "Effect
ive flow area of suction path 4"
    annotation (Placement(transformation(extent={{-378,100},{-358,120}})));
  Functions.SuctionAreaFunction suctionAreaFunction5(thetaStart=
        5.1173053668474)                                                    "Effect
ive flow area of suction path 5"
    annotation (Placement(transformation(extent={{-348,120},{-328,140}})));
  Functions.SuctionAreaFunction suctionAreaFunction6(thetaStart=
        6.3966317085592)                                                    "Effect
ive flow area of suction path 6"
    annotation (Placement(transformation(extent={{-378,140},{-358,160}})));
  Functions.SuctionAreaFunction suctionAreaFunction7(thetaStart=
        7.6759580502711)                                                    "Effect
ive flow area of suction path 7"
    annotation (Placement(transformation(extent={{-348,160},{-328,180}})));
  Functions.SuctionAreaFunction suctionAreaFunction8(thetaStart=
        8.9552843919829)                                                    "Effect
ive flow area of suction path 8"
    annotation (Placement(transformation(extent={{-378,180},{-358,200}})));
  Functions.SuctionAreaFunction suctionAreaFunction9(thetaStart=
        10.234610733695)                                                    "Effect
ive flow area of suction path 8"
    annotation (Placement(transformation(extent={{-350,202},{-330,222}})));
  Functions.SuctionAreaFunction suctionAreaFunction10(thetaStart=
        11.513937075407)                                                    "Effect
ive flow area of suction path 8"
    annotation (Placement(transformation(extent={{-380,220},{-360,240}})));

  /*Discharge paths*/
  Components.FlowRestrictor dischargePath1 "Discharge path for control volume 1"
    annotation (Placement(transformation(extent={{288,-230},{304,-222}})));
  Components.FlowRestrictor dischargePath2 "Discharge path for control volume 2"
    annotation (Placement(transformation(extent={{288,-210},{304,-202}})));
  Components.FlowRestrictor dischargePath3 "Discharge path for control volume 3"
    annotation (Placement(transformation(extent={{288,-190},{304,-182}})));
  Components.FlowRestrictor dischargePath4 "Discharge path for control volume 4"
    annotation (Placement(transformation(extent={{288,-170},{304,-162}})));
  Components.FlowRestrictor dischargePath5 "Discharge path for control volume 5"
    annotation (Placement(transformation(extent={{288,-150},{304,-142}})));
  Components.FlowRestrictor dischargePath6 "Discharge path for control volume 6"
    annotation (Placement(transformation(extent={{288,-130},{304,-122}})));
  Components.FlowRestrictor dischargePath7 "Discharge path for control volume 7"
    annotation (Placement(transformation(extent={{288,-110},{304,-102}})));
  Components.FlowRestrictor dischargePath8 "Discharge path for control volume 8"
    annotation (Placement(transformation(extent={{288,-90},{304,-82}})));
  Components.FlowRestrictor dischargePath9
```

```
    "Discharge path for control volume 9"
    annotation (Placement(transformation(extent={{288,-70},{304,-62}})));
  Components.FlowRestrictor dischargePath10
    "Discharge path for control volume 10"
    annotation (Placement(transformation(extent={{288,-50},{304,-42}})));

  /*Discharge area functions*/
  Functions.DischargeAreaFunction dischargeAreaFunction1(thetaStart=0) "Effective flow a
rea of discharge path 1"
    annotation (Placement(transformation(extent={{328,-226},{348,-206}})));
  Functions.DischargeAreaFunction dischargeAreaFunction2(thetaStart=
        1.2793263417118)                                                    "Ef
fective flow area of discharge path 2"
    annotation (Placement(transformation(extent={{358,-206},{378,-186}})));
  Functions.DischargeAreaFunction dischargeAreaFunction3(thetaStart=
        2.5586526834237)                                                    "Ef
fective flow area of discharge path 3"
    annotation (Placement(transformation(extent={{328,-186},{348,-166}})));
  Functions.DischargeAreaFunction dischargeAreaFunction4(thetaStart=
        3.8379790251355)                                                    "Ef
fective flow area of discharge path 4"
    annotation (Placement(transformation(extent={{358,-166},{378,-146}})));
  Functions.DischargeAreaFunction dischargeAreaFunction5(thetaStart=
        5.1173053668474)                                                    "Ef
fective flow area of discharge path 5"
    annotation (Placement(transformation(extent={{328,-146},{348,-126}})));
  Functions.DischargeAreaFunction dischargeAreaFunction6(thetaStart=
        6.3966317085592)                                                    "Ef
fective flow area of discharge path 6"
    annotation (Placement(transformation(extent={{358,-126},{378,-106}})));
  Functions.DischargeAreaFunction dischargeAreaFunction7(thetaStart=
        7.6759580502711)                                                    "Ef
fective flow area of discharge path 7"
    annotation (Placement(transformation(extent={{328,-106},{348,-86}})));
  Functions.DischargeAreaFunction dischargeAreaFunction8(thetaStart=
        8.9552843919829)                                                    "Ef
fective flow area of discharge path 8"
    annotation (Placement(transformation(extent={{358,-86},{378,-66}})));
  Functions.DischargeAreaFunction dischargeAreaFunction10(thetaStart=
        11.513937075407)                                                    "Ef
fective flow area of discharge path 10"
    annotation (Placement(transformation(extent={{358,-46},{378,-26}})));
  Functions.DischargeAreaFunction dischargeAreaFunction9(thetaStart=10.234610733695)
    "Effective flow area of discharge path 9"
    annotation (Placement(transformation(extent={{328,-66},{348,-46}})));

  /*Injection paths*/
  Components.Injector injector1 "Injection path to control volume 1"
    annotation (Placement(transformation(extent={{-278,254},{-258,274}})));
  Components.Injector injector2 "Injection path to control volume 2"
    annotation (Placement(transformation(extent={{-218,254},{-198,274}})));
  Components.Injector injector3 "Injection path to control volume 3"
    annotation (Placement(transformation(extent={{-158,254},{-138,274}})));
  Components.Injector injector4 "Injection path to control volume 4"
    annotation (Placement(transformation(extent={{-98,254},{-78,274}})));
  Components.Injector injector5 "Injection path to control volume 5"
    annotation (Placement(transformation(extent={{-38,254},{-18,274}})));
  Components.Injector injector6 "Injection path to control volume 6"
    annotation (Placement(transformation(extent={{22,254},{42,274}})));
  Components.Injector injector7 "Injection path to control volume 7"
    annotation (Placement(transformation(extent={{82,254},{102,274}})));
  Components.Injector injector8 "Injection path to control volume 8"
    annotation (Placement(transformation(extent={{142,254},{162,274}})));
 Components.Injector injector9 "Injection path to control volume 8"
    annotation (Placement(transformation(extent={{202,254},{222,274}})));
  Components.Injector injector10
                                "Injection path to control volume 8"
    annotation (Placement(transformation(extent={{264,254},{284,274}})));

  /*Injection flow functions*/
  Functions.InjectionFlowFunction injectionFlowFunction1(thetaStart=0) "Mass flow throug
h injector 1"
```

```
    annotation (Placement(transformation(extent={{-248,254},{-228,274}})));
  Functions.InjectionFlowFunction injectionFlowFunction2(thetaStart=
        1.2793263417118)                                                    "Ma
ss flow through injector 2"
    annotation (Placement(transformation(extent={{-188,254},{-168,274}})));
  Functions.InjectionFlowFunction injectionFlowFunction3(thetaStart=
        2.5586526834237)                                                    "Ma
ss flow through injector 3"
    annotation (Placement(transformation(extent={{-126,254},{-106,274}})));
  Functions.InjectionFlowFunction injectionFlowFunction4(thetaStart=
        3.8379790251355)                                                    "Ma
ss flow through injector 4"
    annotation (Placement(transformation(extent={{-68,254},{-48,274}})));
  Functions.InjectionFlowFunction injectionFlowFunction5(thetaStart=
        5.1173053668474)                                                    "Ma
ss flow through injector 5"
    annotation (Placement(transformation(extent={{-6,254},{14,274}})));
  Functions.InjectionFlowFunction injectionFlowFunction6(thetaStart=
        6.3966317085592)                                                    "Ma
ss flow through injector 6"
    annotation (Placement(transformation(extent={{52,254},{72,274}})));
  Functions.InjectionFlowFunction injectionFlowFunction7(thetaStart=
        7.6759580502711)                                                    "Ma
ss flow through injector 7"
    annotation (Placement(transformation(extent={{112,254},{132,274}})));
  Functions.InjectionFlowFunction injectionFlowFunction8(thetaStart=
        8.9552843919829)                                                    "Ma
ss flow through injector 8"
    annotation (Placement(transformation(extent={{170,254},{190,274}})));
  Functions.InjectionFlowFunction injectionFlowFunction9(thetaStart=
        10.234610733695)                                                    "Ma
ss flow through injector 8"
    annotation (Placement(transformation(extent={{230,254},{250,274}})));
  Functions.InjectionFlowFunction injectionFlowFunction10(thetaStart=
        11.513937075407)                                                     "M
ass flow through injector 8"
    annotation (Placement(transformation(extent={{292,254},{312,274}})));

  /*Suction junctions*/
  Components.Junction suctionJunction1(hStart=hSuctionStart, xiStart=xiSuctionStart) "Se
parate suction flow 1"
    annotation (Placement(transformation(extent={{-10,-
10},{10,10}},rotation=180,origin={-314,40})));
  Components.Junction suctionJunction2(hStart=hSuctionStart, xiStart=xiSuctionStart) "Se
parate suction flow 2"
    annotation (Placement(transformation(extent={{-10,-
10},{10,10}},rotation=180,origin={-314,60})));
  Components.Junction suctionJunction3(hStart=hSuctionStart, xiStart=xiSuctionStart) "Se
parate suction flow 3"
    annotation (Placement(transformation(extent={{-10,-
10},{10,10}},rotation=180,origin={-314,80})));
  Components.Junction suctionJunction4(hStart=hSuctionStart, xiStart=xiSuctionStart) "Se
parate suction flow 4"
    annotation (Placement(transformation(extent={{-10,-
10},{10,10}},rotation=180,origin={-314,100})));
  Components.Junction suctionJunction5(hStart=hSuctionStart, xiStart=xiSuctionStart) "Se
parate suction flow 5"
    annotation (Placement(transformation(extent={{-10,-
10},{10,10}},rotation=180,origin={-314,120})));
  Components.Junction suctionJunction6(hStart=hSuctionStart, xiStart=xiSuctionStart) "Se
parate suction flow 6"
    annotation (Placement(transformation(extent={{-10,-
10},{10,10}},rotation=180,origin={-314,140})));
  Components.Junction suctionJunction7(hStart=hSuctionStart, xiStart=xiSuctionStart) "Se
parate suction flow 7"
    annotation (Placement(transformation(extent={{-10,-
10},{10,10}},rotation=180,origin={-314,160})));
  Components.Junction suctionJunction8(hStart=hSuctionStart, xiStart=
        xiSuctionStart)                                                     "Se
parate suction flow 7"
    annotation (Placement(transformation(extent={{-10,-
10},{10,10}},rotation=180,origin={-314,180})));
```

```
  Components.Junction suctionJunction9(hStart=hSuctionStart, xiStart=
        xiSuctionStart)                                                    "Se
parate suction flow 7"
    annotation (Placement(transformation(extent={{-10,-
10},{10,10}},rotation=180,origin={-314,200})));
  /*Discharge junctions*/

  Components.Junction dischargeJunction1(hStart=hDischargeStart, xiStart=xiDischargeStar
t)
    "Merge discharge flow 2"
    annotation (Placement(transformation(extent={{-10,-
10},{10,10}},rotation=0,origin={314,-206})));
  Components.Junction dischargeJunction2(hStart=hDischargeStart, xiStart=xiDischargeStar
t)
    "Merge discharge flow 3"
    annotation (Placement(transformation(extent={{-10,-
10},{10,10}},rotation=0,origin={314,-186})));
  Components.Junction dischargeJunction3(hStart=hDischargeStart, xiStart=xiDischargeStar
t)
    "Merge discharge flow 4"
    annotation (Placement(transformation(extent={{-10,-
10},{10,10}},rotation=0,origin={314,-166})));
  Components.Junction dischargeJunction4(hStart=hDischargeStart, xiStart=xiDischargeStar
t)
    "Merge discharge flow 5"
    annotation (Placement(transformation(extent={{-10,-
10},{10,10}},rotation=0,origin={314,-146})));
  Components.Junction dischargeJunction5(hStart=hDischargeStart, xiStart=xiDischargeStar
t)
    "Merge discharge flow 6"
    annotation (Placement(transformation(extent={{-10,-
10},{10,10}},rotation=0,origin={314,-126})));
  Components.Junction dischargeJunction6(hStart=hDischargeStart, xiStart=xiDischargeStar
t)
    "Merge discharge flow 7"
    annotation (Placement(transformation(extent={{-10,-
10},{10,10}},rotation=0,origin={314,-106})));
  Components.Junction dischargeJunction7(hStart=hDischargeStart, xiStart=xiDischargeStar
t)
    "Merge discharge flow 8"
    annotation (Placement(transformation(extent={{-10,-
10},{10,10}},rotation=0,origin={314,-86})));
  Components.Junction dischargeJunction9(hStart=hDischargeStart, xiStart=
        xiDischargeStart) "Merge discharge flow 10" annotation (Placement(
        transformation(
        extent={{-10,-10},{10,10}},
        rotation=0,
        origin={314,-46})));
  Components.Junction dischargeJunction8(hStart=hDischargeStart, xiStart=
        xiDischargeStart) "Merge discharge flow 9" annotation (Placement(
        transformation(
        extent={{-10,-10},{10,10}},
        rotation=0,
        origin={314,-66})));

  /*Injection junctions*/
  Components.Junction injectionJunction1(hStart=hInjectionStart, xiStart=xiInjectionStar
t) "Separate injection flow 1"
    annotation (Placement(transformation(extent={{-10,-
10},{10,10}},rotation=90,origin={-268,284})));
  Components.Junction injectionJunction2(hStart=hInjectionStart, xiStart=xiInjectionStar
t) "Separate injection flow 2"
    annotation (Placement(transformation(extent={{-10,-
10},{10,10}},rotation=90,origin={-208,284})));
  Components.Junction injectionJunction3(hStart=hInjectionStart, xiStart=xiInjectionStar
t) "Separate injection flow 3"
    annotation (Placement(transformation(extent={{-10,-
10},{10,10}},rotation=90,origin={-148,284})));
  Components.Junction injectionJunction4(hStart=hInjectionStart, xiStart=xiInjectionStar
t) "Separate injection flow 4"
    annotation (Placement(transformation(extent={{-10,-
10},{10,10}},rotation=90,origin={-88,284})));
```

```
  Components.Junction injectionJunction5(hStart=hInjectionStart, xiStart=xiInjectionStar
t) "Separate injection flow 5"
    annotation (Placement(transformation(extent={{-10,-
10},{10,10}},rotation=90,origin={-28,284})));
  Components.Junction injectionJunction6(hStart=hInjectionStart, xiStart=xiInjectionStar
t) "Separate injection flow 6"
    annotation (Placement(transformation(extent={{-10,-
10},{10,10}},rotation=90,origin={32,284})));
  Components.Junction injectionJunction7(hStart=hInjectionStart, xiStart=xiInjectionStar
t) "Separate injection flow 7"
    annotation (Placement(transformation(extent={{-10,-
10},{10,10}},rotation=90,origin={92,284})));
  Components.Junction injectionJunction8(hStart=hInjectionStart, xiStart=xiInjectionStar
t) "Separate injection flow 8"
    annotation (Placement(transformation(extent={{-10,-
10},{10,10}},rotation=90,origin={152,284})));                    /*new add*/
  Components.Junction injectionJunction9(hStart=hInjectionStart, xiStart=xiInjectionStar
t) "Separate injection flow 9"
    annotation (Placement(transformation(extent={{-10,-
10},{10,10}},rotation=90,origin={212,284})));                    /*new add*/

  /*Initial equations*/
initial equation
  mSucked_total = 0;

  W_total = 0;

    /*Equations*/
equation
  der(mSucked_total) = suctionPort.m_flow;

  der(W_total) = cv1.Wdot + cv2.Wdot + cv3.Wdot + cv4.Wdot + cv5.Wdot + cv6.Wdot + cv7.W
dot + cv8.Wdot + cv9.Wdot + cv10.Wdot; /*add 9 and 10*/

  /*Connections*/
  connect(V1.y, cv1.volumeInput) annotation (Line(points={{-288,-283.4},{-288,-9},
          {-280,-9}},           color={28,108,200}));
  connect(V2.y, cv2.volumeInput) annotation (Line(points={{-228,-283.4},{-228,-9},
          {-220,-9}},           color={28,108,200}));
  connect(V3.y, cv3.volumeInput) annotation (Line(points={{-168,-283.4},{-168,-9},
          {-160,-9}},           color={28,108,200}));
  connect(V8.y, cv8.volumeInput) annotation (Line(points={{132,-283.4},{132,-9},
          {138,-9}},          color={28,108,200}));
  connect(V4.y, cv4.volumeInput) annotation (Line(points={{-108,-283.4},{-108,-9},
          {-100,-9}},         color={28,108,200}));
  connect(V5.y, cv5.volumeInput) annotation (Line(points={{-48,-283.4},{-48,-9},
          {-40,-9}},    color={28,108,200}));
  connect(V7.y, cv7.volumeInput) annotation (Line(points={{72,-283.4},{72,-9},{80,
          -9}},               color={28,108,200}));
  connect(V6.y, cv6.volumeInput) annotation (Line(points={{12,-283.4},{12,-9},{20,
          -9}},             color={28,108,200}));

  connect(leakageAreaFunction21.x1, cv1.volumeInput) annotation (Line(points={{-246,
          -264.4},{-246,-274},{-288,-274},{-288,-9},{-280,-9}},
                                          color={28,108,200}));
  connect(leakageAreaFunction21.x2, cv2.volumeInput) annotation (Line(points={{-238,
          -264.4},{-238,-274},{-228,-274},{-228,-9},{-220,-9}},
                                          color={28,108,200}));
  connect(leakageAreaFunction32.x1, cv2.volumeInput) annotation (Line(points={{-186,
          -264.4},{-186,-274},{-228,-274},{-228,-9},{-220,-9}},
                                          color={28,108,200}));
  connect(leakageAreaFunction32.x2, cv3.volumeInput) annotation (Line(points={{-178,
          -264.4},{-178,-274},{-168,-274},{-168,-9},{-160,-9}},
                                          color={28,108,200}));
  connect(leakageAreaFunction43.x1, cv3.volumeInput) annotation (Line(points={{-126,
          -264.4},{-126,-274},{-168,-274},{-168,-9},{-160,-9}},
                                    color={28,108,200}));
  connect(leakageAreaFunction43.x2, cv4.volumeInput) annotation (Line(points={{-118,
          -264.4},{-118,-274},{-108,-274},{-108,-9},{-100,-9}},
                                  color={28,108,200}));
  connect(leakageAreaFunction76.x1, cv6.volumeInput) annotation (Line(points={{54,
          -264.4},{54,-274},{12,-274},{12,-9},{20,-9}},
```

```
                                color={28,108,200}));
connect(leakageAreaFunction76.x2, cv7.volumeInput) annotation (Line(points={{62,
        -264.4},{62,-274},{72,-274},{72,-9},{80,-9}},
                                  color={28,108,200}));
connect(leakageAreaFunction87.x1, cv7.volumeInput) annotation (Line(points={{114,
        -264.4},{114,-274},{72,-274},{72,-9},{80,-9}},
                                  color={28,108,200}));

connect(leak21.portB, cv1.leakInPort) annotation (Line(
    points={{-246,0},{-252,0},{-252,4},{-258,4}},
    color={153,204,0},
    thickness=0.5));
connect(cv2.leakOutPort, leak21.portA) annotation (Line(
    points={{-218,-4},{-224,-4},{-224,0},{-230,0}},
    color={153,204,0},
    thickness=0.5));
connect(leak32.portB, cv2.leakInPort) annotation (Line(
    points={{-186,0},{-192,0},{-192,4},{-198,4}},
    color={153,204,0},
    thickness=0.5));
connect(cv3.leakOutPort, leak32.portA) annotation (Line(
    points={{-158,-4},{-164,-4},{-164,0},{-170,0}},
    color={153,204,0},
    thickness=0.5));
connect(leak43.portB, cv3.leakInPort) annotation (Line(
    points={{-126,0},{-132,0},{-132,4},{-138,4}},
    color={153,204,0},
    thickness=0.5));
connect(cv4.leakOutPort, leak43.portA) annotation (Line(
    points={{-98,-4},{-104,-4},{-104,0},{-110,0}},
    color={153,204,0},
    thickness=0.5));
connect(leak54.portB, cv4.leakInPort) annotation (Line(
    points={{-66,0},{-72,0},{-72,4},{-78,4}},
    color={153,204,0},
    thickness=0.5));
connect(leak65.portB, cv5.leakInPort) annotation (Line(
    points={{-6,0},{-12,0},{-12,4},{-18,4}},
    color={153,204,0},
    thickness=0.5));
connect(cv6.leakOutPort, leak65.portA) annotation (Line(
    points={{22,-4},{16,-4},{16,0},{10,0}},
    color={153,204,0},
    thickness=0.5));
connect(leak76.portB, cv6.leakInPort) annotation (Line(
    points={{54,0},{48,0},{48,4},{42,4}},
    color={153,204,0},
    thickness=0.5));
connect(cv7.leakOutPort, leak76.portA) annotation (Line(
    points={{82,-4},{76,-4},{76,0},{70,0}},
    color={153,204,0},
    thickness=0.5));
connect(cv5.leakOutPort, leak54.portA) annotation (Line(
    points={{-38,-4},{-42,-4},{-42,0},{-50,0}},
    color={153,204,0},
    thickness=0.5));
connect(leak87.portB, cv7.leakInPort) annotation (Line(
    points={{114,0},{108,0},{108,4},{102,4}},
    color={153,204,0},
    thickness=0.5));
connect(cv8.leakOutPort, leak87.portA) annotation (Line(
    points={{140,-4},{140,0},{130,0}},
    color={153,204,0},
    thickness=0.5));
connect(leak110.portA, cv1.leakOutPort) annotation (Line(
    points={{266,-30},{-286,-30},{-286,-4},{-278,-4}},
    color={153,204,0},
    thickness=0.5));
connect(suctionPath1.portB, cv1.suctionPort) annotation (Line(
    points={{-290,40},{-286,40},{-286,4},{-278,4}},
    color={153,204,0},
    thickness=0.5));
```

```
connect(suctionPath2.portB, cv2.suctionPort) annotation (Line(
    points={{-290,60},{-222,60},{-222,4},{-218,4}},
    color={153,204,0},
    thickness=0.5));
connect(suctionPath3.portB, cv3.suctionPort) annotation (Line(
    points={{-290,80},{-162,80},{-162,4},{-158,4}},
    color={153,204,0},
    thickness=0.5));
connect(suctionPath4.portB, cv4.suctionPort) annotation (Line(
    points={{-290,100},{-102,100},{-102,4},{-98,4}},
    color={153,204,0},
    thickness=0.5));
connect(suctionPath5.portB, cv5.suctionPort) annotation (Line(
    points={{-290,120},{-40,120},{-40,4},{-38,4}},
    color={153,204,0},
    thickness=0.5));
connect(suctionPath6.portB, cv6.suctionPort) annotation (Line(
    points={{-290,140},{18,140},{18,4},{22,4}},
    color={153,204,0},
    thickness=0.5));
connect(suctionPath7.portB, cv7.suctionPort) annotation (Line(
    points={{-290,160},{78,160},{78,4},{82,4}},
    color={153,204,0},
    thickness=0.5));
connect(suctionPath8.portB, cv8.suctionPort) annotation (Line(
    points={{-290,180},{140,180},{140,4}},
    color={153,204,0},
    thickness=0.5));
connect(cv8.dischargePort, dischargePath8.portA)
  annotation (Line(
    points={{160,-4},{168,-4},{168,-86},{288,-86}},
    color={153,204,0},
    thickness=0.5));
connect(cv7.dischargePort, dischargePath7.portA)
  annotation (Line(
    points={{102,-4},{108,-4},{108,-106},{288,-106}},
    color={153,204,0},
    thickness=0.5));
connect(cv6.dischargePort, dischargePath6.portA)
  annotation (Line(
    points={{42,-4},{48,-4},{48,-126},{288,-126}},
    color={153,204,0},
    thickness=0.5));
connect(cv5.dischargePort, dischargePath5.portA)
  annotation (Line(
    points={{-18,-4},{-12,-4},{-12,-146},{288,-146}},
    color={153,204,0},
    thickness=0.5));
connect(cv4.dischargePort, dischargePath4.portA)
  annotation (Line(
    points={{-78,-4},{-72,-4},{-72,-166},{288,-166}},
    color={153,204,0},
    thickness=0.5));
connect(cv3.dischargePort, dischargePath3.portA)
  annotation (Line(
    points={{-138,-4},{-132,-4},{-132,-186},{288,-186}},
    color={153,204,0},
    thickness=0.5));
connect(cv2.dischargePort, dischargePath2.portA)
  annotation (Line(
    points={{-198,-4},{-192,-4},{-192,-206},{288,-206}},
    color={153,204,0},
    thickness=0.5));
connect(cv1.dischargePort, dischargePath1.portA)
  annotation (Line(
    points={{-258,-4},{-252,-4},{-252,-226},{288,-226}},
    color={153,204,0},
    thickness=0.5));
connect(dischargePath1.portB, dischargeJunction1.separatePort2)
  annotation (Line(
    points={{304,-226},{314,-226},{314,-210}},
    color={153,204,0},
```

```
    thickness=0.5));
connect(dischargePath2.portB, dischargeJunction1.separatePort1)
  annotation (Line(
    points={{304,-206},{310,-206}},
    color={153,204,0},
    thickness=0.5));
connect(dischargeJunction1.mergePort, dischargeJunction2.separatePort2)
  annotation (Line(
    points={{314,-202},{314,-190}},
    color={153,204,0},
    thickness=0.5));
connect(dischargePath3.portB, dischargeJunction2.separatePort1)
  annotation (Line(
    points={{304,-186},{310,-186}},
    color={153,204,0},
    thickness=0.5));
connect(dischargeJunction2.mergePort, dischargeJunction3.separatePort2)
  annotation (Line(
    points={{314,-182},{314,-170}},
    color={153,204,0},
    thickness=0.5));
connect(dischargePath4.portB, dischargeJunction3.separatePort1)
  annotation (Line(
    points={{304,-166},{310,-166}},
    color={153,204,0},
    thickness=0.5));
connect(dischargeJunction3.mergePort, dischargeJunction4.separatePort2)
  annotation (Line(
    points={{314,-162},{314,-150}},
    color={153,204,0},
    thickness=0.5));
connect(dischargePath5.portB, dischargeJunction4.separatePort1)
  annotation (Line(
    points={{304,-146},{310,-146}},
    color={153,204,0},
    thickness=0.5));
connect(dischargeJunction4.mergePort, dischargeJunction5.separatePort2)
  annotation (Line(
    points={{314,-142},{314,-130}},
    color={153,204,0},
    thickness=0.5));
connect(dischargePath6.portB, dischargeJunction5.separatePort1)
  annotation (Line(
    points={{304,-126},{310,-126}},
    color={153,204,0},
    thickness=0.5));
connect(dischargeJunction5.mergePort, dischargeJunction6.separatePort2)
  annotation (Line(
    points={{314,-122},{314,-110}},
    color={153,204,0},
    thickness=0.5));
connect(dischargePath7.portB, dischargeJunction6.separatePort1)
  annotation (Line(
    points={{304,-106},{310,-106}},
    color={153,204,0},
    thickness=0.5));
connect(dischargeJunction6.mergePort, dischargeJunction7.separatePort2)
  annotation (Line(
    points={{314,-102},{314,-90}},
    color={153,204,0},
    thickness=0.5));
connect(dischargePath8.portB, dischargeJunction7.separatePort1)
  annotation (Line(
    points={{304,-86},{310,-86}},
    color={153,204,0},
    thickness=0.5));
connect(injectionJunction1.mergePort, injectionPort)
  annotation (Line(
    points={{-272,284},{-280,284},{-280,300},{0,300},{0,320}},
    color={153,204,0},
    thickness=0.5));
connect(injectionJunction1.separatePort2, injectionJunction2.mergePort)
```

```
  annotation (Line(
    points={{-264,284},{-212,284}},
    color={153,204,0},
    thickness=0.5));
connect(injectionJunction2.separatePort2, injectionJunction3.mergePort)
  annotation (Line(
    points={{-204,284},{-152,284}},
    color={153,204,0},
    thickness=0.5));
connect(injectionJunction3.separatePort2, injectionJunction4.mergePort)
  annotation (Line(
    points={{-144,284},{-92,284}},
    color={153,204,0},
    thickness=0.5));
connect(injectionJunction4.separatePort2, injectionJunction5.mergePort)
  annotation (Line(
    points={{-84,284},{-32,284}},
    color={153,204,0},
    thickness=0.5));
connect(injectionJunction5.separatePort2, injectionJunction6.mergePort)
  annotation (Line(
    points={{-24,284},{28,284}},
    color={153,204,0},
    thickness=0.5));
connect(injectionJunction6.separatePort2, injectionJunction7.mergePort)
  annotation (Line(
    points={{36,284},{88,284}},
    color={153,204,0},
    thickness=0.5));
connect(leakageAreaFunction21.y, leak21.effectiveFlowAreaInput)
  annotation (Line(points={{-238,-243.4},{-238,-5}}, color={238,46,47}));
connect(leakageAreaFunction32.y, leak32.effectiveFlowAreaInput)
  annotation (Line(points={{-178,-243.4},{-178,-5}}, color={238,46,47}));
connect(leakageAreaFunction43.y, leak43.effectiveFlowAreaInput)
  annotation (Line(points={{-118,-243.4},{-118,-5}},
                                                  color={238,46,47}));
connect(leakageAreaFunction54.y, leak54.effectiveFlowAreaInput)
  annotation (Line(points={{-58,-243.4},{-58,-5}},
                                                color={238,46,47}));
connect(leakageAreaFunction65.y, leak65.effectiveFlowAreaInput)
  annotation (Line(points={{2,-243.4},{2,-5}},   color={238,46,47}));
connect(leakageAreaFunction76.y, leak76.effectiveFlowAreaInput)
  annotation (Line(points={{62,-243.4},{62,-5}},   color={238,46,47}));
connect(leakageAreaFunction87.y, leak87.effectiveFlowAreaInput)
  annotation (Line(points={{122,-243.4},{122,-5}}, color={238,46,47}));
connect(suctionAreaFunction1.y, suctionPath1.effectiveFlowAreaInput)
  annotation (Line(points={{-327.4,50},{-298,50},{-298,45}}, color={238,46,47}));
connect(suctionAreaFunction2.y, suctionPath2.effectiveFlowAreaInput)
  annotation (Line(points={{-357.4,70},{-298,70},{-298,65}}, color={238,46,47}));
connect(suctionAreaFunction3.y, suctionPath3.effectiveFlowAreaInput)
  annotation (Line(points={{-327.4,90},{-298,90},{-298,85}}, color={238,46,47}));
connect(suctionAreaFunction4.y, suctionPath4.effectiveFlowAreaInput)
  annotation (Line(points={{-357.4,110},{-298,110},{-298,105}}, color={238,46,
      47}));
connect(suctionAreaFunction5.y, suctionPath5.effectiveFlowAreaInput)
  annotation (Line(points={{-327.4,130},{-298,130},{-298,125}}, color={238,46,
      47}));
connect(suctionAreaFunction6.y, suctionPath6.effectiveFlowAreaInput)
  annotation (Line(points={{-357.4,150},{-298,150},{-298,145}}, color={238,46,
      47}));
connect(suctionAreaFunction7.y, suctionPath7.effectiveFlowAreaInput)
  annotation (Line(points={{-327.4,170},{-298,170},{-298,165}}, color={238,46,
      47}));
connect(suctionAreaFunction8.y, suctionPath8.effectiveFlowAreaInput)
  annotation (Line(points={{-357.4,190},{-298,190},{-298,185}}, color={238,46,
      47}));
connect(dischargeAreaFunction1.y, dischargePath1.effectiveFlowAreaInput)
  annotation (Line(points={{327.4,-216},{296,-216},{296,-221}}, color={238,46,
      47}));
connect(dischargeAreaFunction2.y, dischargePath2.effectiveFlowAreaInput)
  annotation (Line(points={{357.4,-196},{296,-196},{296,-201}}, color={238,46,
      47}));
```

```
connect(dischargeAreaFunction3.y, dischargePath3.effectiveFlowAreaInput)
  annotation (Line(points={{327.4,-176},{296,-176},{296,-181}}, color={238,46,
        47}));
connect(dischargeAreaFunction4.y, dischargePath4.effectiveFlowAreaInput)
  annotation (Line(points={{357.4,-156},{296,-156},{296,-161}}, color={238,46,
        47}));
connect(dischargeAreaFunction5.y, dischargePath5.effectiveFlowAreaInput)
  annotation (Line(points={{327.4,-136},{296,-136},{296,-141}},
                                                         color={238,46,47}));
connect(dischargeAreaFunction6.y, dischargePath6.effectiveFlowAreaInput)
  annotation (Line(points={{357.4,-116},{296,-116},{296,-121}},
                                                         color={238,46,47}));
connect(dischargeAreaFunction7.y, dischargePath7.effectiveFlowAreaInput)
  annotation (Line(points={{327.4,-96},{296,-96},{296,-101}},color={238,46,47}));
connect(dischargeAreaFunction8.y, dischargePath8.effectiveFlowAreaInput)
  annotation (Line(points={{357.4,-76},{296,-76},{296,-81}}, color={238,46,47}));
connect(injector1.outPort, cv1.injectionPort) annotation (Line(
    points={{-268,258},{-268,10}},
    color={153,204,0},
    thickness=0.5));
connect(injector2.outPort, cv2.injectionPort) annotation (Line(
    points={{-208,258},{-208,10}},
    color={153,204,0},
    thickness=0.5));
connect(injector3.outPort, cv3.injectionPort) annotation (Line(
    points={{-148,258},{-148,10}},
    color={153,204,0},
    thickness=0.5));
connect(injector4.outPort, cv4.injectionPort) annotation (Line(
    points={{-88,258},{-88,10}},
    color={153,204,0},
    thickness=0.5));
connect(injector5.outPort, cv5.injectionPort) annotation (Line(
    points={{-28,258},{-28,10}},
    color={153,204,0},
    thickness=0.5));
connect(injector6.outPort, cv6.injectionPort) annotation (Line(
    points={{32,258},{32,10}},
    color={153,204,0},
    thickness=0.5));
connect(injector7.outPort, cv7.injectionPort) annotation (Line(
    points={{92,258},{92,10}},
    color={153,204,0},
    thickness=0.5));
connect(injector8.outPort, cv8.injectionPort) annotation (Line(
    points={{152,258},{152,10},{150,10}},
    color={153,204,0},
    thickness=0.5));
connect(injectionJunction1.separatePort1, injector1.inPort) annotation (Line(
    points={{-268,280},{-268,270}},
    color={153,204,0},
    thickness=0.5));
connect(injectionJunction2.separatePort1, injector2.inPort) annotation (Line(
    points={{-208,280},{-208,270}},
    color={153,204,0},
    thickness=0.5));
connect(injectionJunction3.separatePort1, injector3.inPort) annotation (Line(
    points={{-148,280},{-148,270}},
    color={153,204,0},
    thickness=0.5));
connect(injectionJunction4.separatePort1, injector4.inPort) annotation (Line(
    points={{-88,280},{-88,270}},
    color={153,204,0},
    thickness=0.5));
connect(injectionJunction5.separatePort1, injector5.inPort) annotation (Line(
    points={{-28,280},{-28,270}},
    color={153,204,0},
    thickness=0.5));
connect(injectionJunction6.separatePort1, injector6.inPort) annotation (Line(
    points={{32,280},{32,270}},
    color={153,204,0},
    thickness=0.5));
```

```
connect(injectionJunction7.separatePort1, injector7.inPort) annotation (Line(
    points={{92,280},{92,270}},
    color={153,204,0},
    thickness=0.5));
connect(injectionFlowFunction1.y, injector1.m_flowInput)
  annotation (Line(points={{-248.6,264},{-263,264}}, color={217,67,180}));
connect(injectionFlowFunction2.y, injector2.m_flowInput)
  annotation (Line(points={{-188.6,264},{-203,264}}, color={217,67,180}));
connect(injectionFlowFunction3.y, injector3.m_flowInput)
  annotation (Line(points={{-126.6,264},{-143,264}},
                                                    color={217,67,180}));
connect(injectionFlowFunction4.y, injector4.m_flowInput)
  annotation (Line(points={{-68.6,264},{-83,264}}, color={217,67,180}));
connect(injectionFlowFunction5.y, injector5.m_flowInput)
  annotation (Line(points={{-6.6,264},{-23,264}},color={217,67,180}));
connect(injectionFlowFunction6.y, injector6.m_flowInput)
  annotation (Line(points={{51.4,264},{37,264}},  color={217,67,180}));
connect(injectionFlowFunction7.y, injector7.m_flowInput)
  annotation (Line(points={{111.4,264},{97,264}},  color={217,67,180}));
connect(injectionFlowFunction8.y, injector8.m_flowInput)
  annotation (Line(points={{169.4,264},{157,264}}, color={217,67,180}));
connect(leakageAreaFunction54.x1, V4.y) annotation (Line(points={{-66,-264.4},
        {-66,-274},{-108,-274},{-108,-283.4}},
                                              color={28,108,200}));
connect(leakageAreaFunction54.x2, V5.y) annotation (Line(points={{-58,-264.4},
        {-58,-274},{-48,-274},{-48,-283.4}},
                                           color={28,108,200}));
connect(leakageAreaFunction65.x1, V5.y) annotation (Line(points={{-6,-264.4},{
        -6,-274},{-48,-274},{-48,-283.4}},
                                            color={28,108,200}));
connect(leakageAreaFunction65.x2, V6.y) annotation (Line(points={{2,-264.4},{2,
        -274},{12,-274},{12,-283.4}},    color={28,108,200}));
connect(suctionJunction1.mergePort, suctionPort) annotation (Line(
    points={{-314,36},{-314,0},{-318,0}},
    color={153,204,0},
    thickness=0.5));
connect(suctionJunction1.separatePort1, suctionPath1.portA) annotation (Line(
    points={{-310,40},{-306,40}},
    color={153,204,0},
    thickness=0.5));
connect(suctionJunction1.separatePort2, suctionJunction2.mergePort)
  annotation (Line(
    points={{-314,44},{-314,56}},
    color={153,204,0},
    thickness=0.5));
connect(suctionJunction2.separatePort1, suctionPath2.portA) annotation (Line(
    points={{-310,60},{-306,60}},
    color={153,204,0},
    thickness=0.5));
connect(suctionJunction2.separatePort2, suctionJunction3.mergePort)
  annotation (Line(
    points={{-314,64},{-314,76}},
    color={153,204,0},
    thickness=0.5));
connect(suctionJunction3.separatePort1, suctionPath3.portA) annotation (Line(
    points={{-310,80},{-306,80}},
    color={153,204,0},
    thickness=0.5));
connect(suctionJunction3.separatePort2, suctionJunction4.mergePort)
  annotation (Line(
    points={{-314,84},{-314,96}},
    color={153,204,0},
    thickness=0.5));
connect(suctionJunction4.separatePort1, suctionPath4.portA) annotation (Line(
    points={{-310,100},{-306,100}},
    color={153,204,0},
    thickness=0.5));
connect(suctionJunction4.separatePort2, suctionJunction5.mergePort)
  annotation (Line(
    points={{-314,104},{-314,116}},
    color={153,204,0},
    thickness=0.5));
```

```
connect(suctionJunction5.separatePort1, suctionPath5.portA) annotation (Line(
    points={{-310,120},{-306,120}},
    color={153,204,0},
    thickness=0.5));
connect(suctionJunction5.separatePort2, suctionJunction6.mergePort)
  annotation (Line(
    points={{-314,124},{-314,136}},
    color={153,204,0},
    thickness=0.5));
connect(suctionJunction6.separatePort1, suctionPath6.portA) annotation (Line(
    points={{-310,140},{-306,140}},
    color={153,204,0},
    thickness=0.5));
connect(suctionJunction6.separatePort2, suctionJunction7.mergePort)
  annotation (Line(
    points={{-314,144},{-314,156}},
    color={153,204,0},
    thickness=0.5));
connect(suctionJunction7.separatePort1, suctionPath7.portA) annotation (Line(
    points={{-310,160},{-306,160}},
    color={153,204,0},
    thickness=0.5));

/*Screw compressor model icon*/
connect(dischargeJunction9.mergePort, dischargePort) annotation (Line(
    points={{314,-42},{314,0},{320,0}},
    color={153,204,0},
    thickness=0.5));
connect(dischargeJunction9.separatePort2, dischargeJunction8.mergePort)
  annotation (Line(
    points={{314,-50},{314,-62}},
    color={153,204,0},
    thickness=0.5));
connect(dischargeJunction7.mergePort,dischargeJunction8. separatePort2)
  annotation (Line(
    points={{314,-82},{314,-70}},
    color={153,204,0},
    thickness=0.5));
connect(cv8.leakInPort, leak98.portB) annotation (Line(
    points={{160,4},{168,4},{168,0},{174,0}},
    color={153,204,0},
    thickness=0.5));
connect(leak98.portA, cv9.leakOutPort) annotation (Line(
    points={{190,-8.88178e-16},{196,-8.88178e-16},{196,-4},{202,-4}},
    color={153,204,0},
    thickness=0.5));
connect(cv9.leakInPort, leak109.portB) annotation (Line(
    points={{222,4},{228,4},{228,0},{234,0}},
    color={153,204,0},
    thickness=0.5));
connect(leak109.portA, cv10.leakOutPort) annotation (Line(
    points={{250,0},{256,0},{256,-4},{264,-4}},
    color={153,204,0},
    thickness=0.5));
connect(leakageAreaFunction98.y, leak98.effectiveFlowAreaInput)
  annotation (Line(points={{182,-243.4},{182,-5}}, color={238,46,47}));
connect(leakageAreaFunction109.y, leak109.effectiveFlowAreaInput)
  annotation (Line(points={{242,-245.4},{242,-5}}, color={238,46,47}));
connect(V9.y, cv9.volumeInput) annotation (Line(points={{194,-283.4},{194,-9},
        {200,-9}}, color={28,108,200}));
connect(V9.y, leakageAreaFunction98.x2) annotation (Line(points={{194,-283.4},
        {194,-274},{182,-274},{182,-264.4}}, color={28,108,200}));
connect(leakageAreaFunction109.x1, V9.y) annotation (Line(points={{234,-266.4},
        {234,-274},{194,-274},{194,-283.4}}, color={28,108,200}));
connect(dischargeAreaFunction9.y, dischargePath9.effectiveFlowAreaInput)
  annotation (Line(points={{327.4,-56},{296,-56},{296,-61}}, color={238,46,47}));
connect(dischargeJunction8.separatePort1, dischargePath9.portB) annotation (
    Line(
    points={{310,-66},{304,-66}},
    color={153,204,0},
    thickness=0.5));
connect(dischargeAreaFunction10.y, dischargePath10.effectiveFlowAreaInput)
```

```
  annotation (Line(points={{357.4,-36},{296,-36},{296,-41}}, color={238,46,47}));
connect(dischargeJunction9.separatePort1, dischargePath10.portB) annotation (
    Line(
    points={{310,-46},{304,-46}},
    color={153,204,0},
    thickness=0.5));
connect(cv9.dischargePort, dischargePath9.portA) annotation (Line(
    points={{222,-4},{226,-4},{226,-66},{288,-66}},
    color={153,204,0},
    thickness=0.5));
connect(cv10.dischargePort, dischargePath10.portA) annotation (Line(
    points={{284,-4},{286,-4},{286,-46},{288,-46}},
    color={153,204,0},
    thickness=0.5));
connect(cv10.leakInPort, leak110.portB) annotation (Line(
    points={{284,4},{300,4},{300,-30},{282,-30}},
    color={153,204,0},
    thickness=0.5));
connect(V10.y, cv10.volumeInput) annotation (Line(points={{254,-283.4},{254,-9},
        {262,-9}}, color={28,108,200}));
connect(leakageAreaFunction109.x2, V10.y) annotation (Line(points={{242,-266.4},
        {242,-274},{254,-274},{254,-283.4}}, color={28,108,200}));
connect(leakageAreaFunction110.x1, V10.y) annotation (Line(points={{266,-268.4},
        {266,-274},{254,-274},{254,-283.4}}, color={28,108,200}));
connect(V1.y, leakageAreaFunction110.x2) annotation (Line(points={{-288,-283.4},
        {-288,-274},{-246,-274},{-246,-310},{274,-310},{274,-268.4}}, color={28,
        108,200}));
connect(leakageAreaFunction110.y, leak110.effectiveFlowAreaInput)
  annotation (Line(points={{274,-247.4},{274,-35}}, color={0,0,127}));
connect(injector9.outPort, cv9.injectionPort) annotation (Line(
    points={{212,258},{212,10}},
    color={153,204,0},
    thickness=0.5));
connect(injector10.outPort, cv10.injectionPort) annotation (Line(
    points={{274,258},{274,10}},
    color={153,204,0},
    thickness=0.5));
connect(injectionFlowFunction9.y, injector9.m_flowInput)
  annotation (Line(points={{229.4,264},{217,264}}, color={217,67,180}));
connect(injectionFlowFunction10.y, injector10.m_flowInput)
  annotation (Line(points={{291.4,264},{279,264}}, color={217,67,180}));
connect(injectionJunction9.separatePort1, injector9.inPort) annotation (Line(
    points={{212,280},{212,270}},
    color={153,204,0},
    thickness=0.5));
connect(injectionJunction8.separatePort1, injector8.inPort) annotation (Line(
    points={{152,280},{152,270}},
    color={153,204,0},
    thickness=0.5));
connect(injectionJunction7.separatePort2, injectionJunction8.mergePort)
  annotation (Line(
    points={{96,284},{148,284}},
    color={153,204,0},
    thickness=0.5));
connect(injectionJunction8.separatePort2, injectionJunction9.mergePort)
  annotation (Line(
    points={{156,284},{208,284}},
    color={153,204,0},
    thickness=0.5));
connect(injectionJunction9.separatePort2, injector10.inPort) annotation (Line(
    points={{216,284},{274,284},{274,270}},
    color={153,204,0},
    thickness=0.5));
connect(suctionAreaFunction9.y, suctionPath9.effectiveFlowAreaInput)
  annotation (Line(points={{-329.4,212},{-298,212},{-298,205}}, color={238,46,
        47}));
connect(suctionAreaFunction10.y, suctionPath10.effectiveFlowAreaInput)
  annotation (Line(points={{-359.4,230},{-298,230},{-298,225}}, color={238,46,
        47}));
connect(suctionJunction8.mergePort, suctionJunction7.separatePort2)
  annotation (Line(
    points={{-314,176},{-314,164}},
```

```
      color={153,204,0},
      thickness=0.5));
  connect(suctionJunction8.separatePort1, suctionPath8.portA) annotation (Line(
      points={{-310,180},{-306,180}},
      color={153,204,0},
      thickness=0.5));
  connect(suctionJunction8.separatePort2, suctionJunction9.mergePort)
    annotation (Line(
      points={{-314,184},{-314,196}},
      color={153,204,0},
      thickness=0.5));
  connect(suctionJunction9.separatePort1, suctionPath9.portA) annotation (Line(
      points={{-310,200},{-306,200}},
      color={153,204,0},
      thickness=0.5));
  connect(suctionJunction9.separatePort2, suctionPath10.portA) annotation (Line(
      points={{-314,204},{-314,220},{-306,220}},
      color={153,204,0},
      thickness=0.5));
  connect(suctionPath10.portB, cv10.suctionPort) annotation (Line(
      points={{-290,220},{258,220},{258,4},{264,4}},
      color={153,204,0},
      thickness=0.5));
  connect(suctionPath9.portB, cv9.suctionPort) annotation (Line(
      points={{-290,200},{198,200},{198,4},{202,4}},
      color={153,204,0},
      thickness=0.5));
  connect(V8.y, leakageAreaFunction87.x2) annotation (Line(points={{132,-283.4},
        {132,-274},{122,-274},{122,-264.4}}, color={28,108,200}));
  connect(V8.y, leakageAreaFunction98.x1) annotation (Line(points={{132,-283.4},
        {132,-274},{174,-274},{174,-264.4}}, color={28,108,200}));
  annotation (Icon(coordinateSystem(preserveAspectRatio=false, extent={{-320,-320},
          {320,320}}),
                  graphics={
        Ellipse(
          extent={{-318,318},{320,-320}},
          lineColor={0,0,0},
          fillColor={255,255,255},
          fillPattern=FillPattern.Solid,
          lineThickness=0.5),
        Line(
          points={{-220,230},{308,80}},
          color={0,0,0},
          thickness=0.5),
        Line(
          points={{-218,-230},{308,-80}},
          color={0,0,0},
          thickness=0.5)}),                                        Diagram(
        coordinateSystem(preserveAspectRatio=false, extent={{-320,-320},{320,320}})),
    experiment(__Dymola_NumberOfIntervals=1000, __Dymola_Algorithm="Esdirk45a"));
end ScrewCompressor_10Chambers_v1;
```

D.4 Control volume component

```
model ControlVolume "Control volume, representing the volume of one cavity"

  /*Working fluid type*/
  outer TILMedia.VLEFluidTypes.BaseVLEFluid vleFluidType "VLE fluid type";

  /*Working fluid model*/
  TILMedia.VLEFluid_ph workingFluid(
    final p=p,
    final h=h,
    final xi=xi,
    final vleFluidType=vleFluidType) "Working fluid model"
    annotation (Placement(transformation(extent={{-10,-12},{10,8}})));

  /*Connection ports*/
  TIL.Connectors.VLEFluidPort suctionPort(final vleFluidType = vleFluidType) "The cv's s
uction port"
    annotation (Placement(transformation(extent={{-110,30},{-90,50}})));
  TIL.Connectors.VLEFluidPort dischargePort(final vleFluidType = vleFluidType) "The cv's
 discharge port"
    annotation (Placement(transformation(extent={{90,-50},{110,-30}})));
  TIL.Connectors.VLEFluidPort injectionPort(final vleFluidType = vleFluidType) "The cv's
 injection port"
    annotation (Placement(transformation(extent={{-10,90},{10,110}})));
  TIL.Connectors.VLEFluidPort leakInPort(final vleFluidType = vleFluidType) "The cv's le
ak-in port"
    annotation (Placement(transformation(extent={{90,30},{110,50}})));
  TIL.Connectors.VLEFluidPort leakOutPort(final vleFluidType = vleFluidType) "The cv's l
eak-out port"
    annotation (Placement(transformation(extent={{-110,-50},{-90,-30}})));

  /*Volume input*/
  Modelica.Blocks.Interfaces.RealInput volumeInput[3] "Volume input: {V, dVdt, theta}"
    annotation (Placement(transformation(extent={{-140,-110},{-100,-70}})));

  /*Start values*/
  parameter Modelica.SIunits.AbsolutePressure pStart "Start value for pressure";

  parameter Modelica.SIunits.SpecificEnthalpy hStart "Start value for specific enthalpy"
;

  parameter Modelica.SIunits.MassFraction[vleFluidType.nc-
1] xiStart = zeros(vleFluidType.nc-1) "Start value for mass fraction";

  /*Control volume properties*/
  Modelica.SIunits.Volume V = volumeInput[1] "Volume of control volume";

  Real dVdt = volumeInput[2] "Time derivative of volume";

  Modelica.SIunits.Angle theta = volumeInput[3] "Rotational angle";

  Modelica.SIunits.Mass m "Total fluid mass in control volume";

  Modelica.SIunits.AbsolutePressure p "Pressure in control volume";

  Modelica.SIunits.SpecificEnthalpy h "Specific enthalpy in control volume";

  Modelica.SIunits.MassFraction[vleFluidType.nc-
1] xi "Mass fraction of fluid component i";

  Modelica.SIunits.SpecificInternalEnergy u "Specific internal energy in control volume"
;

  /*Suction properties*/
  outer Modelica.SIunits.AbsolutePressure pSuction "Pressure in suction line";

  outer Modelica.SIunits.SpecificEnthalpy hSuction "Specific enthalpy in suction line";

  outer Modelica.SIunits.MassFraction[vleFluidType.nc-
1] xiSuction "Mass fraction in suction line";
```

```
  /*Compressor features*/
  outer Modelica.SIunits.Angle thetaCycle "Total rotation for one compression cycle";

  outer Modelica.SIunits.CoefficientOfHeatTransfer alpha "Heat transfer coefficient";

  outer Modelica.SIunits.Temperature Tbody "Average compressor body temperature";

  Modelica.SIunits.Power Wdot "Compression work rate";

  Modelica.SIunits.HeatFlowRate QdotBody "Heat flow rate from the working fluid to the c
ompressor body";

  /*Initial equations*/
initial equation
  p = pStart "Pressure initialization";

  h = hStart "Specific enthalpy initialization";

  xi = xiStart "Mass fraction initialization";

  /*Equations*/
equation
  m = workingFluid.d*V "Mass given by density and volume";

  h = u + p/workingFluid.d "The definition of specific enthalpy";

  Wdot = -p*dVdt "Work rate";

  QdotBody = alpha*V^(2/3)*(workingFluid.T - Tbody) "Heat loss rate";

  der(m*u) = Wdot - QdotBody + noEvent(suctionPort.m_flow*actualStream(suctionPort.h_out
flow) + dischargePort.m_flow*actualStream(dischargePort.h_outflow)
   + injectionPort.m_flow*actualStream(injectionPort.h_outflow) + leakInPort.m_flow*actu
alStream(leakInPort.h_outflow)
   + leakOutPort.m_flow*actualStream(leakOutPort.h_outflow)) "Energy balance";

  der(m) = suctionPort.m_flow + dischargePort.m_flow + injectionPort.m_flow + leakInPort
.m_flow + leakOutPort.m_flow "Total mass balance";

  der(m*xi) = noEvent(suctionPort.m_flow*actualStream(suctionPort.xi_outflow) + discharg
ePort.m_flow*actualStream(dischargePort.xi_outflow)
   + injectionPort.m_flow*actualStream(injectionPort.xi_outflow) + leakInPort.m_flow*act
ualStream(leakInPort.xi_outflow)
   + leakOutPort.m_flow*actualStream(leakOutPort.xi_outflow)) "Mass balance for componen
t i";

  p = suctionPort.p;
  p = dischargePort.p;
  p = injectionPort.p;
  p = leakInPort.p;
  p = leakOutPort.p; //Homogeneous pressure in the control volume

  h = suctionPort.h_outflow;
  h = dischargePort.h_outflow;
  h = injectionPort.h_outflow;
  h = leakInPort.h_outflow;
  h = leakOutPort.h_outflow; //Homogeneous specific enthalpy in the control volume

  xi = suctionPort.xi_outflow;
  xi = dischargePort.xi_outflow;
  xi = injectionPort.xi_outflow;
  xi = leakInPort.xi_outflow;
  xi = leakOutPort.xi_outflow; //Homogeneous mass fraction in the control volume

  when (theta < thetaCycle/2) then
    reinit(p, pSuction);
    reinit(h, hSuction);
    if (vleFluidType.nc > 1) then
      reinit(xi, xiSuction);
    end if;
  end when "Re-initialize when compression cycle starts over";
```

```
  suctionPort.h_limit = -1e6;
  dischargePort.h_limit = -1e6;
  injectionPort.h_limit = -1e6;
  leakInPort.h_limit = -1e6;
  leakOutPort.h_limit = -1e6; //Unused limit parameters

  /*Control volume model icon*/
  annotation (Icon(coordinateSystem(preserveAspectRatio=false), graphics={
          Rectangle(
          extent={{-100,100},{100,-100}},
          lineColor={0,0,0},
          lineThickness=1,
          fillColor={188,189,255},
          fillPattern=FillPattern.Backward), Text(
          extent={{-60,60},{60,-60}},
          lineColor={0,0,0},
          lineThickness=1,
          fillColor={188,189,255},
          fillPattern=FillPattern.Solid,
          textString="CV"),
        Text(
          extent={{-100,-120},{100,-160}},
          lineColor={0,0,0},
          lineThickness=0.5,
          fillColor={0,0,0},
          fillPattern=FillPattern.Solid,
          textString="%name")}),                                    Diagram(
        coordinateSystem(preserveAspectRatio=false)));
end ControlVolume;
```

D.5 Flow restrictor component

```
model FlowRestrictor "Component for closing and opening of flow paths"

  /*Working fluid type*/
  outer TILMedia.VLEFluidTypes.BaseVLEFluid vleFluidType "VLE fluid type";

  /*Area input*/
  Modelica.Blocks.Interfaces.RealInput effectiveFlowAreaInput "Effective flow area input
"
    annotation (Placement(transformation(
        origin={0,50},
        extent={{-10,-10},{10,10}},
        rotation=270)));

  Modelica.SIunits.Area AreaEff = effectiveFlowAreaInput "Effective flow area";

  /*Connection ports*/
  TIL.Connectors.VLEFluidPort portA(final vleFluidType = vleFluidType) "portA"
    annotation (Placement(transformation(extent={{-90,-10},{-70,10}}, rotation=
            0)));
  TIL.Connectors.VLEFluidPort portB(final vleFluidType = vleFluidType) "portB"
    annotation (Placement(transformation(extent={{70,-10},{90,10}}, rotation=0)));

  /*Fluid models*/
  TILMedia.VLEFluid_ph vleFluidA(
    p=portA.p, h=inStream(portA.h_outflow),
    xi = inStream(portA.xi_outflow),
    final vleFluidType = vleFluidType)
    annotation (Placement(transformation(extent={{-100,20},{-80,40}}, rotation=0)));
  TILMedia.VLEFluid_ph vleFluidB(
    p=portB.p,
    h=inStream(portB.h_outflow),
    xi = inStream(portB.xi_outflow),
    final vleFluidType = vleFluidType)
    annotation (Placement(transformation(extent={{80,20},{100,40}}, rotation=0)));

  /*Equations*/
equation
  portA.xi_outflow = inStream(portB.xi_outflow);
  portB.xi_outflow = inStream(portA.xi_outflow); //Mass fraction

  portA.h_outflow = inStream(portB.h_outflow);
  portB.h_outflow = inStream(portA.h_outflow); //Specific enthalpy

  portA.h_limit = -1e6;
  portB.h_limit = -1e6; //Unused limit parameters

  portB.m_flow + portA.m_flow = 0 "Mass balance";

  if noEvent(portA.p > portB.p) then
    portA.m_flow = AreaEff*TIL.Utilities.Numerics.squareRootFunction(2*vleFluidA.d*(port
A.p - portB.p), 1e-6);
    //Flow direction A to B, sqrtFunction approximation below sqrt(1e-6)
  else
    portA.m_flow = AreaEff*TIL.Utilities.Numerics.squareRootFunction(2*vleFluidB.d*(port
A.p - portB.p), 1e-6);
    //Flow direction B to A, sqrtFunction returns negative value
  end if;

  /*Flow restrictor model icon*/
  annotation (defaultComponentName="flowRestrictor",Icon(coordinateSystem(
          preserveAspectRatio=true, extent={{-80,-40},{80,40}}),
                                                graphics={
        Polygon(
          points={{-10,60},{10,60},{0,40},{-10,60}},
          lineColor={0,0,255},
          pattern=LinePattern.None,
          fillColor={175,175,175},
          fillPattern=FillPattern.Solid),
        Rectangle(
          extent={{-80,20},{80,-20}},
```

```
          lineColor={0,0,0},
          lineThickness=0.5),
        Ellipse(
          extent={{-80,32},{80,8}},
          lineColor={0,0,0},
          lineThickness=0.5,
          startAngle=0,
          endAngle=180,
          fillColor={0,0,0},
          fillPattern=FillPattern.Solid),
        Ellipse(
          extent={{-80,-32},{80,-8}},
          lineColor={0,0,0},
          lineThickness=0.5,
          startAngle=0,
          endAngle=180,
          fillColor={0,0,0},
          fillPattern=FillPattern.Solid),
        Text(
          extent={{-80,-40},{80,-60}},
          lineColor={0,0,0},
          lineThickness=0.5,
          fillColor={0,0,0},
          fillPattern=FillPattern.Solid,
          textString="%name")}),
    Diagram(coordinateSystem(preserveAspectRatio=true, extent={{-100,-100},{100,
          100}})));
end FlowRestrictor;
```

D.6 Junction component

```
model Junction "Component used to merge or separate flows"

  /*Working fluid type*/
  outer TILMedia.VLEFluidTypes.BaseVLEFluid vleFluidType "VLE fluid type";

  /*Connection ports*/
  TIL.Connectors.VLEFluidPort mergePort(final vleFluidType = vleFluidType) "Port for mer
ged flow"
    annotation (Placement(transformation(extent={{-10,30},{10,50}})));
  TIL.Connectors.VLEFluidPort separatePort1(final vleFluidType=vleFluidType) "Port for s
eparate flow 1"
    annotation (Placement(transformation(extent={{-50,-10},{-30,10}})));
  TIL.Connectors.VLEFluidPort separatePort2(final vleFluidType=vleFluidType) "Port for s
eparate flow 2"
    annotation (Placement(transformation(extent={{-10,-50},{10,-30}})));

  /*Start values*/
  parameter Modelica.SIunits.SpecificEnthalpy hStart "Start value for specific enthalpy"
;

  parameter Modelica.SIunits.MassFraction[vleFluidType.nc-
1] xiStart = zeros(vleFluidType.nc-1) "Start value for mass fraction";

  /*Junction properties*/
  Modelica.SIunits.Mass m = 1e-8 "Fluid mass in junction";

  Modelica.SIunits.SpecificEnthalpy h "Specific enthalpy in junction";

  Modelica.SIunits.MassFraction[vleFluidType.nc-
1] xi "Mass fraction of fluid component i";

  /*Initial equations*/
initial equation
  h = hStart "Specific enthalpy initialization";

  xi = xiStart "Mass fraction initialization";

  /*Equations*/
equation
  separatePort1.m_flow + separatePort2.m_flow + mergePort.m_flow = 0 "Total mass balance
";

  m*der(xi) = noEvent(separatePort1.m_flow*actualStream(separatePort1.xi_outflow) + sepa
ratePort2.m_flow*actualStream(separatePort2.xi_outflow)
    + mergePort.m_flow*actualStream(mergePort.xi_outflow)) "Mass balance for component i
";

  m*der(h) = noEvent(separatePort1.m_flow*actualStream(separatePort1.h_outflow) + separa
tePort2.m_flow*actualStream(separatePort2.h_outflow)
    + mergePort.m_flow*actualStream(mergePort.h_outflow)) "Energy balance";

  mergePort.p = separatePort1.p;
  mergePort.p = separatePort2.p; //Pressure

  xi = separatePort1.xi_outflow;
  xi = separatePort2.xi_outflow;
  xi = mergePort.xi_outflow; //Mass fraction

  h = separatePort1.h_outflow;
  h = separatePort2.h_outflow;
  h = mergePort.h_outflow; //Specific enthalpy

  separatePort1.h_limit = -1e6;
  separatePort2.h_limit = -1e6;
  mergePort.h_limit = -1e6; //Unused limit parameters

  /*Junction model icon*/
  annotation (Icon(coordinateSystem(preserveAspectRatio=false, extent={{-100,-
100},{100,100}}), graphics={Ellipse(
          extent={{-80,80},{0,0}},
```

```
          lineColor={0,0,0},
          lineThickness=1,
          startAngle=0,
          endAngle=90,
          closure=EllipseClosure.None), Line(
          points={{0,40},{0,-40}},
          color={0,0,0},
          thickness=1)}),                                    Diagram(coordinateSyste
m(preserveAspectRatio=false, extent={{-100,-100},{100,100}})));
end Junction;
```

D.7 Injector component

```
model Injector "Component used to regulate the injection mass flow rate"

  /*Working fluid type*/
  outer TILMedia.VLEFluidTypes.BaseVLEFluid vleFluidType "VLE fluid type";

  /*Connection ports*/
  TIL.Connectors.VLEFluidPort inPort(final vleFluidType=vleFluidType)
    "Port where fluid flows in from the injection line"
    annotation (Placement(transformation(extent={{-10,50},{10,70}}),
        iconTransformation(extent={{-10,50},{10,70}})));
  TIL.Connectors.VLEFluidPort outPort(final vleFluidType=vleFluidType)
    "Port where fluid flows out to the control volume"
    annotation (Placement(transformation(extent={{-10,-70},{10,-50}}),
        iconTransformation(extent={{-10,-70},{10,-50}})));

  /*Flow input*/
  Modelica.Blocks.Interfaces.RealInput m_flowInput "Mass flow rate input"
    annotation (Placement(transformation(extent={{70,-20},{30,20}})));

  Modelica.SIunits.MassFlowRate m_flow = m_flowInput "Mass flow rate";

  /*Equations*/
equation
  inPort.m_flow = m_flow;
  outPort.m_flow = -inPort.m_flow; //Mass flow rate

  inPort.xi_outflow = inStream(outPort.xi_outflow);
  outPort.xi_outflow = inStream(inPort.xi_outflow); //Mass fraction

  inPort.h_outflow = inStream(outPort.h_outflow);
  outPort.h_outflow = inStream(inPort.h_outflow); //Specific enthalpy

  inPort.h_limit = -1e6;
  outPort.h_limit = -1e6; //Unused limit parameters

  /*Injector model icon*/
  annotation (Icon(coordinateSystem(preserveAspectRatio=false, extent={{-100,-
100},{100,100}}), graphics={
                                        Line(
          points={{0,60},{0,-60}},
          color={0,0,0},
          thickness=1),
        Line(
          points={{0,-20},{20,20}},
          color={0,0,0},
          thickness=1),
        Line(
          points={{0,-20},{-20,20}},
          color={0,0,0},
          thickness=1),
        Text(
          extent={{-60,20},{60,-20}},
          lineColor={0,0,0},
          lineThickness=1,
          textString="%name",
          origin={-60,-7.10543e-15},
          rotation=-
90)}),                                        Diagram(coordinateSystem(preserveAspectRati
o=false, extent={{-100,-100},{100,100}})));
end Injector;
```

D.8 Volume function

```
model VolumeFunction "Function for the volume of a cavity"

  Modelica.Blocks.Interfaces.RealOutput[3] y = {V, derV, theta} "Volume output"
    annotation (Placement(transformation(extent={{-10,-10},{10,10}},
        rotation=90,
        origin={0,106})));

  parameter Modelica.SIunits.Angle thetaStart = 1.5707963267949 "Start value for rotatio
nal angle";

  outer Modelica.SIunits.Angle thetaCycle "Total rotation for one compression cycle";

  outer Modelica.SIunits.AngularVelocity w "Angular velocity";

  outer Modelica.SIunits.Time tCycle "Duration of one compression cycle";

  outer Modelica.SIunits.Volume Vmax "Maximum cavity volume";

  Modelica.SIunits.Volume Vmin = 1e-8 "Minimum cavity volume";

  Modelica.SIunits.Volume V "Cavity volume";

  Real derV "Time derivative of cavity volume";

  Modelica.SIunits.Angle theta "Rotational angle";

  Modelica.SIunits.Angle theta1 = thetaCycle/10;

  Modelica.SIunits.Angle theta2 = 4*thetaCycle/10;

  Modelica.SIunits.Angle theta3 = 5*thetaCycle/10;

  Modelica.SIunits.Angle theta4 = 6*thetaCycle/10;

  Modelica.SIunits.Angle theta5 = 9*thetaCycle/10;

  Modelica.SIunits.Time t = tCycle*theta/thetaCycle "Time since beginning of compression
 cycle";

  Modelica.SIunits.Time t1 = tCycle*theta1/thetaCycle;

  Modelica.SIunits.Time t2 = tCycle*theta2/thetaCycle;

  Modelica.SIunits.Time t3 = tCycle*theta3/thetaCycle;

  Modelica.SIunits.Time t4 = tCycle*theta4/thetaCycle;

  Modelica.SIunits.Time t5 = tCycle*theta5/thetaCycle;

  Real dVdt = 2*Vmax/(-t1+t2+t3) "Time derivative of volume in the linear region";

initial equation
  theta = thetaStart "Angle initialization";

equation
  der(theta) = w "Time derivative of theta";

  when (theta >= thetaCycle) then
    reinit(theta, 0);
  end when;

  V = smooth(1,
    if (theta < theta1) then dVdt*t^(2)/(2*t1) + Vmin
    else if (theta < theta2) then dVdt*w*(t1)^(2)/(2*theta1) + dVdt*(t-t1) + Vmin
    else if (theta < theta4) then dVdt*w*(t1)^(2)/(2*theta1) + dVdt*(t2-
t1) + dVdt*(t3*t-t^(2)/2-t3*t2+t2^(2)/2)/(t3-t2) + Vmin
    else if (theta < theta5) then Vmax - dVdt*(t4^(2)/2-t3*t4+t3^(2)/2)/(t4-
t3) - dVdt*(t-t4) + Vmin
    else Vmax - dVdt*(t4^(2)/2-t3*t4+t3^(2)/2)/(t4-t3) - dVdt*(t5-t4) - dVdt*(tCycle*t-
t^(2)/2-tCycle*t5+t5^(2)/2)/(tCycle-t5) + Vmin);
```

```
  //Smooth used to specify that V is continous and continously differentiable up to orde
r 1

  derV = smooth(0,
    if (theta < theta1) then dVdt*t/t1
    else if (theta < theta2) then dVdt
    else if (theta < theta4) then dVdt*(t3-t)/(t3-t2)
    else if (theta < theta5) then -dVdt
    else -dVdt*(tCycle-t)/(tCycle-t5));

  annotation (Icon(coordinateSystem(preserveAspectRatio=false), graphics={
          Rectangle(extent={{-100,100},{100,-100}},
                                              lineColor={28,108,200},
          fillColor={255,255,255},
          fillPattern=FillPattern.Solid,
          lineThickness=0.5),                                          Text(
          extent={{-40,80},{40,0}},
          lineColor={28,108,200},
          textString="V"),
        Text(
          extent={{-100,-20},{100,-60}},
          lineColor={28,108,200},
          textString="%thetaStart")}),                                     Diagram(
        coordinateSystem(preserveAspectRatio=false)),
    experiment(StopTime=2));
end VolumeFunction;
```

D.9 Leakage area function

```
model LeakageAreaFunction "Function for the effective flow area of a leakage path"

  Modelica.Blocks.Interfaces.RealInput x1[3] "Volume input 1: {V, dVdt, theta}"
    annotation (Placement(transformation(extent={{-10,-10},{10,10}},
        rotation=90,
        origin={-40,-104})));
  Modelica.Blocks.Interfaces.RealInput x2[3] "Volume input 2: {V, dVdt, theta}"
    annotation (Placement(transformation(extent={{-10,-10},{10,10}},
        rotation=90,
        origin={40,-104})));
  Modelica.Blocks.Interfaces.RealOutput y = Aeff "Effective flow area output"
    annotation (Placement(transformation(extent={{-10,-10},{10,10}},
        rotation=90,
        origin={40,106})));

  Modelica.SIunits.Volume V1 = x1[1] "Volume of control volume 1";

  Real derV1 = x1[2] "Time derivative of volume 1";

  Modelica.SIunits.Angle theta1 = x1[3] "Rotational angle of control volume 1";

  Modelica.SIunits.Volume V2 = x2[1] "Volume of control volume 2";

  Real derV2 = x2[2] "Time derivative of volume 2";

  outer Real Cleak "Leakage flow coefficient";

  Real Cleak2 = Cleak "leakage flow coefficent path 2";

  outer Modelica.SIunits.Angle thetaDischargeOpen "Rotational angle where discharge begi
ns";

  Modelica.SIunits.Area Aeff "Effective flow area of leakage path";

  Real Aeff1 "effective leakage area path 1";

  Real Aeff2 "effective leakage area path 2";

  Real Aeff2max = Cleak *10e-5 "maximum effective leakage area path2";

equation
  if noEvent((derV2 < 0) and (theta1 < thetaDischargeOpen)) then
    Aeff1 = Cleak*min(V1, V2);
    //Leakage from cv2 to cv1 when cv2 is in the compression/discharge phase AND cv1 has
 not reached the discharge phase yet
  else
    Aeff1 = 0;
  end if;

  if noEvent((derV2 > 0) and (derV1 > 0) and (Cleak2*min(V1, V2)*2 < Aeff2max) or (derV2
 < 0) and (derV1 < 0) and (Cleak2*min(V1, V2)*2 < Aeff2max)) then
    Aeff2 = Cleak2*min(V1, V2)*2;
  elseif noEvent((derV2 > 0) and (derV1 > 0) and (Cleak2*min(V1, V2)*2 > Aeff2max) or (d
erV2 < 0) and (derV1 < 0) and (Cleak2*min(V1, V2)*2 > Aeff2max)) then
    Aeff2 = Aeff2max;
  else
    Aeff2 = 0;
  end if;

  Aeff = Aeff1 + Aeff2;
  annotation (Icon(coordinateSystem(preserveAspectRatio=false), graphics={
          Rectangle(extent={{-100,100},{100,-100}},
                                                   lineColor={238,46,47},
          fillColor={255,255,255},
          fillPattern=FillPattern.Solid),                                  Text(
          extent={{-40,80},{40,0}},
          lineColor={238,46,47},
          textString="A"),
        Text(
          extent={{-100,-20},{100,-60}},
```

```
          lineColor={238,46,47},
          textString="Leak")}),                                                    Diagram(
        coordinateSystem(preserveAspectRatio=false)),
    experiment(StopTime=2));
end LeakageAreaFunction;
```

D.10 Suction Area Function

```
model SuctionAreaFunction "Function for the effective flow area of a suction path"

  Modelica.Blocks.Interfaces.RealOutput y = Aeff
    annotation (Placement(transformation(extent={{-10,-10},{10,10}},
        rotation=0,
        origin={106,0})));

  parameter Modelica.SIunits.Angle thetaStart = 0 "Start value for rotational angle";

  outer Modelica.SIunits.Angle thetaCycle "Total rotation for one compression cycle";

  outer Modelica.SIunits.AngularVelocity w "Angular velocity";

  outer Modelica.SIunits.Time tCycle "Duration of one compression cycle";

  outer Modelica.SIunits.Area Asuction "Maximum effective flow area of suction path";

  Modelica.SIunits.Area Aeff "Effective flow area of suction path";

  Modelica.SIunits.Angle theta "Rotational angle";

  Modelica.SIunits.Angle theta1 = thetaCycle*t1/tCycle;

  Modelica.SIunits.Angle theta2 = thetaCycle*t2/tCycle;

  Modelica.SIunits.Angle theta3 = thetaCycle*t3/tCycle;

  Modelica.SIunits.Angle theta4 = thetaCycle*t4/tCycle;

  Modelica.SIunits.Angle theta5 = thetaCycle*t5/tCycle;

  Modelica.SIunits.Time t = tCycle*theta/thetaCycle "Time since beginning of compression
 cycle";

  Modelica.SIunits.Time t1 = 0.5*tCycle/20;

  Modelica.SIunits.Time t2 = 2*tCycle/20;

  Modelica.SIunits.Time t3 = 2.5*tCycle/20;

  Modelica.SIunits.Time t4 = 9*tCycle/20;

  Modelica.SIunits.Time t5 = 10*tCycle/20;

  Real dAdt = 2*Asuction/(-t1+t2+t3) "Time derivative of area in the linear region";

initial equation
  theta = thetaStart "Angle initialization";

equation
  der(theta) = w "Time derivative of theta";

  when (theta >= thetaCycle) then
    reinit(theta, 0);
  end when;

  if noEvent(theta < theta1) then
    Aeff = dAdt*t^(2)/(2*t1);
  elseif noEvent(theta < theta2) then
    Aeff = dAdt*t1/2 + dAdt*(t-t1);
  elseif noEvent(theta < theta3) then
    Aeff = dAdt*t1/2 + dAdt*(t2-t1) + dAdt*(t3*t-t^(2)/2-t3*t2+t2^(2)/2)/(t3-t2);
  elseif noEvent(theta < theta4) then
    Aeff = Asuction;
  elseif noEvent(theta < theta5) then
    Aeff = Asuction*(1-(t-t4)/(t5-t4));
  else
    Aeff = 0;
  end if;
```

```
  annotation (Icon(coordinateSystem(preserveAspectRatio=false), graphics={
          Rectangle(extent={{-100,100},{100,-100}},
                                                lineColor={238,46,47},
          fillColor={255,255,255},
          fillPattern=FillPattern.Solid),                                  Text(
          extent={{-40,80},{40,0}},
          lineColor={238,46,47},
          textString="A"),
        Text(
          extent={{-100,-20},{100,-60}},
          lineColor={238,46,47},
          textString="%thetaStart"),                                       Text(
          extent={{4,42},{100,10}},
          lineColor={238,46,47},
          textString="suc")}),                                                 Diagram(
        coordinateSystem(preserveAspectRatio=false)),
    experiment(StopTime=2));
end SuctionAreaFunction;
```

D.11 Discharge area function

```
model DischargeAreaFunction "Function for the effective flow area of a discharge path"

  Modelica.Blocks.Interfaces.RealOutput y = Aeff
    annotation (Placement(transformation(extent={{10,-10},{-10,10}},
        rotation=0,
        origin={-106,0})));

  parameter Modelica.SIunits.Angle thetaStart = 0 "Start value for rotational angle";

  outer Modelica.SIunits.Angle thetaCycle "Total rotation for one compression cycle";

  outer Modelica.SIunits.AngularVelocity w "Angular velocity";

  outer Modelica.SIunits.Time tCycle "Duration of one compression cycle";

  outer Modelica.SIunits.Area Adischarge "Maximum effective flow area of discharge path"
;

  outer Modelica.SIunits.Time tDischargeOpen "Point in time when the discharge port open
s";

  Modelica.SIunits.Area Aeff "Effective flow area of suction path";

  Modelica.SIunits.Angle theta "Rotational angle";

  Modelica.SIunits.Angle theta1 = thetaCycle*tDischargeOpen/tCycle;

  Modelica.SIunits.Angle theta2 = thetaCycle*t2/tCycle;

  Modelica.SIunits.Angle theta3 = thetaCycle*t3/tCycle;

  Modelica.SIunits.Angle theta4 = thetaCycle*t4/tCycle;

  Modelica.SIunits.Time t = tCycle*theta/thetaCycle "Time since beginning of compression
 cycle";

  Modelica.SIunits.Time t2 = tDischargeOpen+0.4*(tCycle-tDischargeOpen);

  Modelica.SIunits.Time t3 = tDischargeOpen+0.5*(tCycle-tDischargeOpen);

  Modelica.SIunits.Time t4 = tDischargeOpen+0.6*(tCycle-tDischargeOpen);

  Real dAdt = 2*Adischarge/(-
2*tDischargeOpen+t2+t3) "Time derivative of area in the linear region";

initial equation
  theta = thetaStart "Angle initialization";

equation
  der(theta) = w "Time derivative of theta";

  when (theta >= thetaCycle) then
    reinit(theta, 0);
  end when;

  if noEvent(theta < theta1) then
    Aeff = 0;
  elseif noEvent(theta < theta2) then
    Aeff = dAdt*(t-tDischargeOpen);
  elseif noEvent(theta < theta4) then
    Aeff = dAdt*(t2-tDischargeOpen) + dAdt*(t3*t-t^(2)/2-t3*t2+t2^(2)/2)/(t3-t2);
  else
    Aeff = dAdt*(t2-tDischargeOpen) - dAdt*(t-t4);
  end if;

  annotation (Icon(coordinateSystem(preserveAspectRatio=false), graphics={
          Rectangle(extent={{-100,100},{100,-100}},
                                                   lineColor={238,46,47},
          fillColor={255,255,255},
          fillPattern=FillPattern.Solid),                                  Text(
```

```
          extent={{-40,80},{40,0}},
          lineColor={238,46,47},
          textString="A"),
        Text(
          extent={{-100,-20},{100,-60}},
          lineColor={238,46,47},
          textString="%thetaStart"),                                    Text(
          extent={{4,42},{100,10}},
          lineColor={238,46,47},
          textString="dis")}),                                              Diagram(
        coordinateSystem(preserveAspectRatio=false)),
    experiment(StopTime=2));
end DischargeAreaFunction;
```

D.12 Injection flow function

```
model InjectionFlowFunction "Function for the injection mass flow rate"

  Modelica.Blocks.Interfaces.RealOutput y = mDot "Mass flow rate output"
    annotation (Placement(transformation(extent={{10,-10},{-10,10}},
        rotation=0,
        origin={-106,0})));

  parameter Modelica.SIunits.Angle thetaStart = 0 "Start value for rotational angle";

  outer Modelica.SIunits.Angle thetaCycle "Total rotation for one compression cycle";

  outer Modelica.SIunits.AngularVelocity w "Angular velocity";

  outer Modelica.SIunits.Time tCycle "Duration of one compression cycle";

  outer Modelica.SIunits.MassFlowRate mDotInjection "Injection mass flow rate";

  outer Modelica.SIunits.MassFlowRate mDotInjection2 "Injection mass flow rate";

  outer Modelica.SIunits.MassFlowRate mDotInjection3 "Injection mass flow rate";

  outer Modelica.SIunits.Angle injectionAngle "Rotational angle where injection begins";

  outer Modelica.SIunits.Angle injectionAngle2  "Rotatinal angle where the second inject
ion begins";

  outer Modelica.SIunits.Angle injectionAngle3 "Rotational angle where the third injecti
on begins";

  Modelica.SIunits.MassFlowRate mDot "Mass flow rate";

  Modelica.SIunits.Angle theta "Rotational angle";

  Modelica.SIunits.Angle theta2 = injectionAngle + 0.02;

  Modelica.SIunits.Angle theta3 = injectionAngle + 0.04;

  Modelica.SIunits.Angle theta4 = theta6 - 0.04;

  Modelica.SIunits.Angle theta5 = theta6 - 0.02;

  Modelica.SIunits.Angle theta6 = injectionAngle+thetaCycle/10 + 0.04;

  Modelica.SIunits.Angle theta2_2 = injectionAngle2 + 0.02;

  Modelica.SIunits.Angle theta3_2 = injectionAngle2 + 0.04;

  Modelica.SIunits.Angle theta4_2 = theta6_2 - 0.03;

  Modelica.SIunits.Angle theta5_2 = theta6_2 - 0.02;

  Modelica.SIunits.Angle theta6_2 = injectionAngle2 + thetaCycle /10 + 0.04;

  Modelica.SIunits.Angle theta2_3 = injectionAngle3 + 0.03;

  Modelica.SIunits.Angle theta3_3 = injectionAngle3 + 0.04;

  Modelica.SIunits.Angle theta4_3 = theta6_3 - 0.04;

  Modelica.SIunits.Angle theta5_3 = theta6_3 - 0.02;

  Modelica.SIunits.Angle theta6_3 = injectionAngle3 + thetaCycle /10 + 0.04;

  Modelica.SIunits.Time t = tCycle*theta/thetaCycle "Time since beginning of compression
 cycle";

  Modelica.SIunits.Time t1 = tCycle*injectionAngle/thetaCycle;

  Modelica.SIunits.Time t2 = tCycle*theta2/thetaCycle;
```

```
  Modelica.SIunits.Time t3 = tCycle*theta3/thetaCycle;

  Modelica.SIunits.Time t4 = tCycle*theta4/thetaCycle;

  Modelica.SIunits.Time t5 = tCycle*theta5/thetaCycle;

  Modelica.SIunits.Time t6 = tCycle*theta6/thetaCycle;

  Modelica.SIunits.Time t1_2 = tCycle*injectionAngle2/thetaCycle;

  Modelica.SIunits.Time t2_2 = tCycle*theta2_2/thetaCycle;

  Modelica.SIunits.Time t3_2 = tCycle*theta3_2/thetaCycle;

  Modelica.SIunits.Time t4_2 = tCycle*theta4_2/thetaCycle;

  Modelica.SIunits.Time t5_2 = tCycle*theta5_2/thetaCycle;

  Modelica.SIunits.Time t6_2 = tCycle*theta6_2/thetaCycle;

  Modelica.SIunits.Time t1_3 = tCycle*injectionAngle3/thetaCycle;

  Modelica.SIunits.Time t2_3 = tCycle*theta2_3/thetaCycle;

  Modelica.SIunits.Time t3_3 = tCycle*theta3_3/thetaCycle;

  Modelica.SIunits.Time t4_3 = tCycle*theta4_3/thetaCycle;

  Modelica.SIunits.Time t5_3 = tCycle*theta5_3/thetaCycle;

  Modelica.SIunits.Time t6_3 = tCycle*theta6_3/thetaCycle;

  Real dmDotdt = 2*mDotInjection/(t3-
t1) "Time derivative of mass flow rate at maximum slope";

initial equation
  theta = thetaStart "Angle initialization";

equation
  der(theta) = w "Time derivative of theta";

  when (theta >= thetaCycle) then
    reinit(theta, 0);
  end when;

  mDot = smooth(1,
    if (theta < injectionAngle) then 0
    else if (theta < theta2) then dmDotdt*(t^(2)/2 - t1*t + t1^(2)/2)/(t2-t1)
    else if (theta < theta3) then mDotInjection/2 + dmDotdt*(t3*t - t^(2)/2 - t3*t2 + t2
^(2)/2)/(t3-t2)
    else if (theta < theta4) then mDotInjection
    else if (theta < theta5) then mDotInjection - dmDotdt*(t^(2)/2 - t4*t + t4^(2)/2)/(t
5-t4)
    else if (theta < theta6) then mDotInjection/2 - dmDotdt*(t6*t - t^(2)/2 - t6*t5 + t5
^(2)/2)/(t6-t5)
    else if (theta < injectionAngle2) then 0
    else if (theta < theta2_2) then dmDotdt*(t^(2)/2 - t1_2*t + t1_2^(2)/2)/(t2_2-t1_2)
    else if (theta < theta3_2) then mDotInjection2/2 + dmDotdt*(t3_2*t - t^(2)/2 - t3_2*
t2_2 + t2_2^(2)/2)/(t3_2-t2_2)
    else if (theta < theta4_2) then mDotInjection2
    else if (theta < theta5_2) then mDotInjection2 - dmDotdt*(t^(2)/2 - t4_2*t + t4_2^(2
)/2)/(t5_2-t4_2)
    else if (theta < theta6_2) then mDotInjection2/2 - dmDotdt*(t6_2*t - t^(2)/2 - t6_2*
t5_2 + t5_2^(2)/2)/(t6_2-t5_2)
    else if (theta < injectionAngle3) then 0
    else if (theta < theta2_3) then dmDotdt*(t^(2)/2 - t1_3*t + t1_3^(2)/2)/(t2_3-t1_3)
    else if (theta < theta3_3) then mDotInjection3/2 + dmDotdt*(t3_3*t - t^(2)/2 - t3_3*
t2_3 + t2_3^(2)/2)/(t3_3-t2_3)
    else if (theta < theta4_3) then mDotInjection3
    else if (theta < theta5_3) then mDotInjection3 - dmDotdt*(t^(2)/2 - t4_3*t + t4_3^(2
)/2)/(t5_3-t4_3)
```

```
    else if (theta < theta6_3) then mDotInjection3/2 - dmDotdt*(t6_3*t - t^(2)/2 - t6_3*
t5_3 + t5_3^(2)/2)/(t6_3-t5_3)
    else 0);

  annotation (Icon(coordinateSystem(preserveAspectRatio=false), graphics={
          Rectangle(extent={{-100,100},{100,-100}},
                                                lineColor={217,67,180},
          fillColor={255,255,255},
          fillPattern=FillPattern.Solid),                                  Text(
          extent={{-80,80},{80,0}},
          lineColor={217,67,180},
          textString="flow"),
        Text(
          extent={{-100,-20},{100,-60}},
          lineColor={217,67,180},
          textString="%thetaStart")}),                                        Diagram(
        coordinateSystem(preserveAspectRatio=false)),
    experiment(StopTime=2));
end InjectionFlowFunction;
```

D.13 Sim model code

```
model SimModel_10Chambers_evap80dish135 "Screw compressor simulation"
  inner TIL.SystemInformationManager sim(redeclare
      TILMedia.VLEFluidTypes.TILMedia_Water vleFluidType1)
    annotation (Placement(transformation(extent={{70,70},{90,90}})));
  TIL.VLEFluidComponents.Boundaries.Boundary suctionBoundary(
    streamVariablesInputType="T",
    hFixed=2644e3,
    TFixed=356.14,
    mixingRatioFixed={1},
    boundaryType="p",
    pFixed=48000)
    annotation (Placement(transformation(extent={{-84,-10},{-76,10}})));
  TIL.VLEFluidComponents.Boundaries.Boundary dischargeBoundary(
    streamVariablesInputType="T",
    hFixed=2724e3,
    TFixed=408.263,
    mixingRatioFixed={1},
    boundaryType="p",
    pFixed=292900)
    annotation (Placement(transformation(extent={{76,-10},{84,10}})));
  TIL.VLEFluidComponents.Boundaries.Boundary injectionBoundary(
    streamVariablesInputType="T",
    hFixed=72e3,
    TFixed=290.2978,
    mixingRatioFixed={1},
    boundaryType="p",
    pFixed=181960,
    m_flowFixed=-0.002)
    annotation (Placement(transformation(extent={{-24,70},{-16,90}})));
  ScrewCompressor_10Chambers_v1 screwCompressor_10Chambers_v1_1(
    f=5000/60,
    Max_cav=0.466,
    thetaCycle(displayUnit="deg") = 12.793263417118,
    Vi=4.2,
    Cleak=0.098,
    injectionAngle(displayUnit="deg") = 6.49663,
    mDotInjection=0.002,
    mDotInjection2=0.002,
    mDotInjection3=0.002,
    Tbody(displayUnit="degC") = 383.15,
    pSuctionStart=64000,
    pStart_cv5=64000,
    pStart_cv6=75000,
    pStart_cv7=80000,
    pStart_cv8=100000,
    pStart_cv9=120000,
    pDischargeStart=195000,
    hSuctionStart=2662e3,
    hStart_cv5=2662e3,
    hStart_cv6=2670e3,
    hStart_cv7=2675e3,
    hStart_cv8=2680e3,
    hStart_cv9=2695e3,
    hDischargeStart=2706e3,
    hInjectionStart=63e3,
    xiSuctionStart=zeros(0),
    xiStart_cv5=zeros(0),
    xiStart_cv6=zeros(0),
    xiStart_cv7=zeros(0),
    xiStart_cv8=zeros(0),
    xiStart_cv9=zeros(0),
    xiDischargeStart=zeros(0),
    xiInjectionStart=zeros(0))
    annotation (Placement(transformation(extent={{-32,-32},{32,32}})));
  Modelica.Blocks.Sources.RealExpression real_mflow_dis(y=dischargeBoundary.summary.m_fl
ow)
    annotation (Placement(transformation(extent={{-320,58},{-192,88}})));
  Modelica.Blocks.Math.Mean mean_mflow_dis(f(displayUnit="Hz")=
      screwCompressor_10Chambers_v1_1.f/2, yGreaterOrEqualZero=false)
    annotation (Placement(transformation(extent={{-160,62},{-138,84}})));
```

```
  Modelica.Blocks.Sources.RealExpression real_Vflow_dis(y=dischargeBoundary.summary.V_fl
ow)
    annotation (Placement(transformation(extent={{-320,24},{-192,54}})));
  Modelica.Blocks.Math.Mean mean_Vflow_dis(f(displayUnit="Hz")=
      screwCompressor_10Chambers_v1_1.f/2, yGreaterOrEqualZero=false)
    annotation (Placement(transformation(extent={{-160,28},{-138,50}})));
  Modelica.Blocks.Sources.RealExpression real_mflow_suc(y=suctionBoundary.summary.m_flow
)
    annotation (Placement(transformation(extent={{-320,-14},{-192,16}})));
  Modelica.Blocks.Math.Mean mean_mflow_suc(f(displayUnit="Hz")=
      screwCompressor_10Chambers_v1_1.f/2, yGreaterOrEqualZero=false)
    annotation (Placement(transformation(extent={{-160,-10},{-138,12}})));
  Modelica.Blocks.Sources.RealExpression real_Vflow_suc(y=suctionBoundary.summary.V_flow
)
    annotation (Placement(transformation(extent={{-320,-48},{-192,-18}})));
  Modelica.Blocks.Math.Mean mean_Vflow_suc(f(displayUnit="Hz")=
      screwCompressor_10Chambers_v1_1.f/2, yGreaterOrEqualZero=false)
    annotation (Placement(transformation(extent={{-160,-44},{-138,-22}})));
  Modelica.Blocks.Sources.RealExpression real_mflow_inj(y=injectionBoundary.summary.m_fl
ow)
    annotation (Placement(transformation(extent={{-322,-82},{-194,-52}})));
  Modelica.Blocks.Math.Mean mean_mflow_inj(f(displayUnit="Hz")=
      screwCompressor_10Chambers_v1_1.f/2, yGreaterOrEqualZero=false)
    annotation (Placement(transformation(extent={{-160,-78},{-138,-56}})));
  Modelica.Blocks.Sources.RealExpression real_Vflow_inj(y=injectionBoundary.summary.V_fl
ow)
    annotation (Placement(transformation(extent={{-322,-116},{-194,-86}})));
  Modelica.Blocks.Math.Mean mean_Vflow_inj(f(displayUnit="Hz")=
      screwCompressor_10Chambers_v1_1.f/2, yGreaterOrEqualZero=false)
    annotation (Placement(transformation(extent={{-160,-112},{-138,-90}})));
  Modelica.Blocks.Math.Add3 add3_1
    annotation (Placement(transformation(extent={{-112,-10},{-92,10}})));
  Modelica.Blocks.Math.Gain gain(k=60)
    annotation (Placement(transformation(extent={{-104,30},{-84,50}})));
  Modelica.Blocks.Sources.RealExpression wdot_cv110(y=
        screwCompressor_10Chambers_v1_1.cv1.Wdot +
        screwCompressor_10Chambers_v1_1.cv2.Wdot +
        screwCompressor_10Chambers_v1_1.cv3.Wdot +
        screwCompressor_10Chambers_v1_1.cv4.Wdot +
        screwCompressor_10Chambers_v1_1.cv5.Wdot +
        screwCompressor_10Chambers_v1_1.cv6.Wdot +
        screwCompressor_10Chambers_v1_1.cv7.Wdot +
        screwCompressor_10Chambers_v1_1.cv8.Wdot +
        screwCompressor_10Chambers_v1_1.cv9.Wdot +
        screwCompressor_10Chambers_v1_1.cv10.Wdot)
    annotation (Placement(transformation(extent={{-322,-156},{-194,-126}})));
  Modelica.Blocks.Math.Mean mean_Wdot_cv110(f(displayUnit="Hz")=
      screwCompressor_10Chambers_v1_1.f/2, yGreaterOrEqualZero=false)
    annotation (Placement(transformation(extent={{-158,-152},{-136,-130}})));
equation
  connect(suctionBoundary.port, screwCompressor_10Chambers_v1_1.suctionPort)
    annotation (Line(
      points={{-80,0},{-31.8,0}},
      color={153,204,0},
      thickness=0.5));
  connect(screwCompressor_10Chambers_v1_1.dischargePort, dischargeBoundary.port)
    annotation (Line(
      points={{32,0},{80,0}},
      color={153,204,0},
      thickness=0.5));
  connect(injectionBoundary.port, screwCompressor_10Chambers_v1_1.injectionPort)
    annotation (Line(
      points={{-20,80},{0,80},{0,32}},
      color={153,204,0},
      thickness=0.5));
  connect(real_mflow_dis.y, mean_mflow_dis.u)
    annotation (Line(points={{-185.6,73},{-162.2,73}}, color={0,0,127}));
  connect(real_mflow_suc.y, mean_mflow_suc.u)
    annotation (Line(points={{-185.6,1},{-162.2,1}}, color={0,0,127}));
  connect(real_Vflow_dis.y, mean_Vflow_dis.u)
    annotation (Line(points={{-185.6,39},{-162.2,39}}, color={0,0,127}));
  connect(real_Vflow_suc.y, mean_Vflow_suc.u)
```

```
    annotation (Line(points={{-185.6,-33},{-162.2,-33}}, color={0,0,127}));
  connect(real_mflow_inj.y, mean_mflow_inj.u)
    annotation (Line(points={{-187.6,-67},{-162.2,-67}}, color={0,0,127}));
  connect(real_Vflow_inj.y, mean_Vflow_inj.u)
    annotation (Line(points={{-187.6,-101},{-162.2,-101}}, color={0,0,127}));
  connect(mean_mflow_dis.y, add3_1.u1) annotation (Line(points={{-136.9,73},{
          -120,73},{-120,8},{-114,8}}, color={0,0,127}));
  connect(mean_mflow_suc.y, add3_1.u2) annotation (Line(points={{-136.9,1},{
          -120,1},{-120,0},{-114,0}}, color={0,0,127}));
  connect(mean_mflow_inj.y, add3_1.u3) annotation (Line(points={{-136.9,-67},
          {-122,-67},{-122,-8},{-114,-8}}, color={0,0,127}));
  connect(mean_Vflow_dis.y, gain.u) annotation (Line(points={{-136.9,39},{
          -108,39},{-108,40},{-106,40}}, color={0,0,127}));
  connect(wdot_cv110.y, mean_Wdot_cv110.u) annotation (Line(points={{-187.6,
          -141},{-173.8,-141},{-173.8,-141},{-160.2,-141}}, color={0,0,127}));
  annotation (Icon(coordinateSystem(preserveAspectRatio=false), graphics={
          Rectangle(
          extent={{-60,40},{60,-40}},
          lineColor={28,108,200},
          lineThickness=0.5), Text(
          extent={{-50,30},{50,-30}},
          lineColor={28,108,200},
          textString="SIM")}),                                    Diagram(
        coordinateSystem(preserveAspectRatio=false)),
    experiment(
      StopTime=0.08,
      __Dymola_NumberOfIntervals=1000,
      __Dymola_Algorithm="Esdirk23a"));
end SimModel_10Chambers_evap80dish135;
```

D.14 Comparison between integration methods

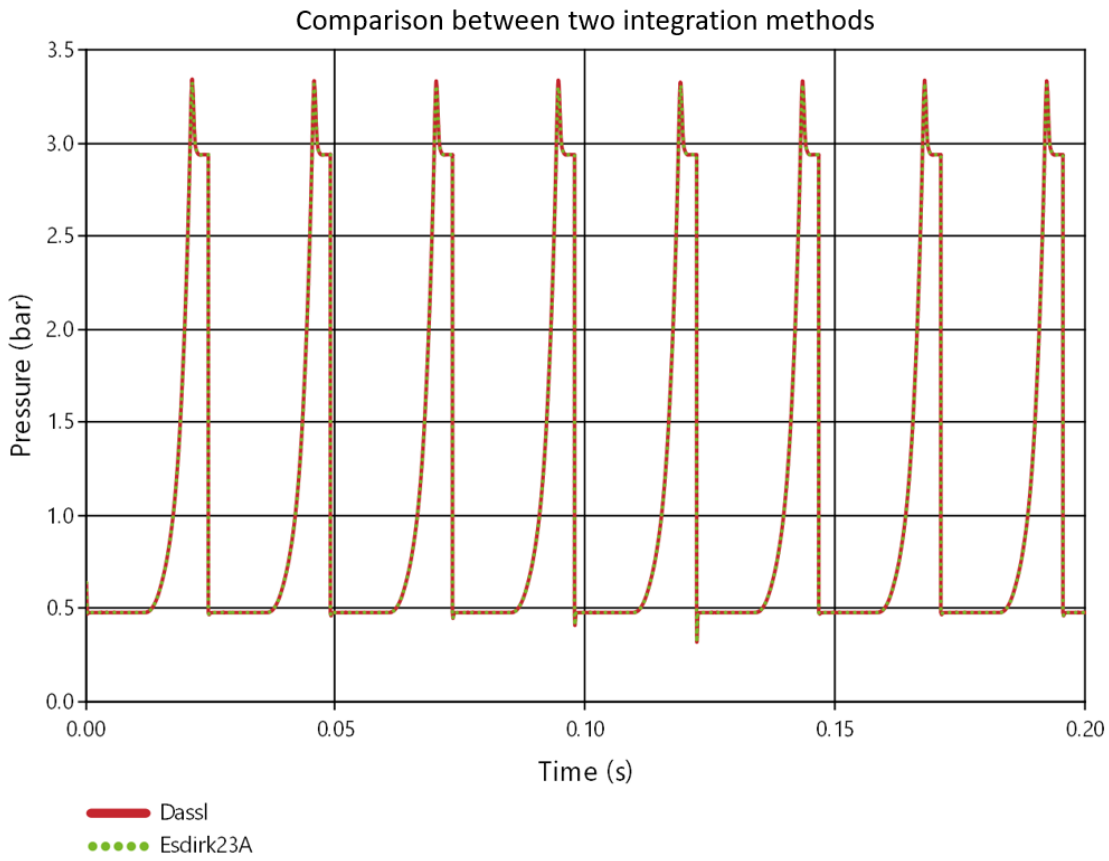

Figure D.3 Comparison between integration methods

Appendix E: Scientific Paper

Thermodynamic modelling of a water-injected twin-screw compressor used in VHTHP range

Martin Klevjer[1,2], Marcel U. Ahrens[1], Bin Hu[2], Trygve M. Eikevik[1] and R.Z Wang[2]

[1] Department of Energy and Process Engineering, Norwegian University of Science and Technology, Trondheim, Norway
[2] Institute of Refrigeration and Cryogenics, Shanghai Jiao Tong University, Shanghai, China

E-mail: xxx@xxx.xx

Received xxxxxx
Accepted for publication xxxxxx
Published xxxxxx

Abstract

High temperature heat pumps (HTHPs) are predicted to be an intergral part of a more energy-efficienct indsutry sector in the future. One of the contributions to this research is a water-injected twin-screw compressor used in very high temperature heat pump operation developed in Shanghai, China. The main challenge faced in HTHP/VHTHP research is to find a reliable, efficient compressor that can operate with low-GWP and low-ODP refrigerants. The twin-screw compressor with water injection shows good promise, and a thermodynamic model is developed to optimize the operation of the compressor. A study on the optimum amount of liquid injected, along with the distribution of liquid injected on three injection nozzles has been conducted. The thermodynamic model was developed in the modelica programming language. It has been based on another model used for an ammonia-water compressor. This makes the model more adaptable, and allows for further modifications to fit other applications. The model was then validated against experimental data before the liquid-injection optimization study was conducted. The results indicate that when the compressor is looked at as an individual component, a higher amount of liquid injected leads to less compressor work. On the other hand when the entire system is taken into consideration it is clear that there are some downsides to liquid injection that are not represented in this model. Furthermore, the study indicates that the compressor performance increases with a higher amount of liquid injection early in the process.

Keywords: Thermodynamic model, water-vapor refrigerant, high temperature heat pump, water injection

1. Introduction

Global energy demand is on the rise [1], and at the same time, climate change is becoming more and more prominent. The need for energy effective solutions is a focus in all energy-consuming sectors. Heat demand represents about 50% of the energy end-use, larger than any other category. Over half of this is consumed in the industry; process heat, drying, and industrial hot water are some examples of heat used in industry [2]. Keeping in mind that energy production accounts for 72% of greenhouse gas emissions[3], increasing energy efficiency in the industrial sector will have a major impact on greenhouse gas emissions. Heat pumps are the most energy-efficient heat providing technology on the market today. Almost 80% of heat provided comes from fossil-fuel or less efficient conventional electric heating while heat pumps cover only 5% of the heat demand. According to IEA [2] heat pumps should cover 22% of the heating demand in 2030 to stay on track with

the sustainable development scenario. Consequently, heat pump technology must be further developed so the market share increases.

Another reason to implement heat pumps in the industry is that most green and renewable energy resources create electrical energy (solar PV, wind, and hydro). This will lead to an increase in the overall efficiency of the electrically driven heat pumps. In today's fossil-fuelled society, a lot of energy is lost in the process of creating electricity from fossil fuel. The average coal-based power plants operate with an efficiency of under 40% [4]. Renewable power plants like wind-, hydro-, and solar PV plants produce electricity directly, which indicates that heat pump technology will become even more desirable when implemented with green renewable energy sources. Heat pumps are already integrated into residential buildings all around the world. In recent times the research on high-temperature heat pumps(HTHPs) for industrial purposes has received a lot of attention, but there are still some challenges that need to be solved before heat pumps become the go-to heating technology in most industrial applications.

Technical improvements must be made to ensure safe, reliable, and efficient operation of heat pumps. Economically viable components must be developed to handle the high temperatures and pressures that are required for HTHP-operation. The component with the highest power consumption and also the highest potential for energy savings in a heat pump system is the compressor [5]. One step in the process of improving today's compressor technology is to investigate the thermodynamic operation of cutting edge HTHP-application compressors. In this thesis, a thermodynamic model of a water-injected twin-screw compressor with water vapor will be developed and verified against experimental data. This will increase the understanding of the operating challenges in the compressor. Furthermore, the model can be used as a cheap and efficient measure to optimize the operation of said compressor.

In the past couple of years, liquid injected twin-screw compressors has earned attention in the research field of HTHP. In 2011 a dynamic model of a twin-screw compressor using water as the refrigerant was presented [6]. The main challenges for the twin-screw compressor were identified as sub-atmospheric pressure in the evaporation side, high volumetric flow rate, and high superheat at the compressor outlet. The proposed solutions to the challenges were a purging system to avoid gas in the system, a twin-screw compressor that is compliant with high volumetric flow rates, and liquid injection to limit the superheat. The dynamic model was a part of the development of a screw compressor developed by Svenska Rotor Maskiner which was presented in 2013 [7]. Along with the new compressor, a mathematical model and simulation of the compressor were made. This model was created using the object-oriented programming language Modelica. The model was used to prove the advantages of liquid injection, which included lower power consumption of the compressor, and lower superheat, which in turn prevented failure of the equipment. The project was concluded with a paper reporting a system delivering a condensation temperature up to 145°C from waste heat of 85-95°C. The COP was dependent on the waste heat temperature and was measured as high as 5.9 [8].

In 2016 a double effect desalination system with a water-injected twin-screw compressor was developed. The system was designed and constructed by the Institute of Seawater Desalination and Multipurpose Utilization in Tianjin China. The compressor speed varied from 2000-3000 rpm and performed at high volumetric and isentropic efficiencies throughout the process. The pressure ratio was 2.74 with compressor inlet temperatures of 77.5°C and 79°C. The analysis of the experiment showed that the compressor work increased approximately linearly with an increasing operational speed of the compressor. This is expected as the volumetric flow rate should increase linearly under these conditions. Furthermore, the compressor power consumption increases with an increased inlet temperature, with a constant pressure ratio, this is expected as a result of the increase of the specific volume. The effect of the liquid injection is also presented in the report. The consequences of an increased amount of liquid injected are higher isentropic efficiency as a result of lower superheat and discharge temperature [9].

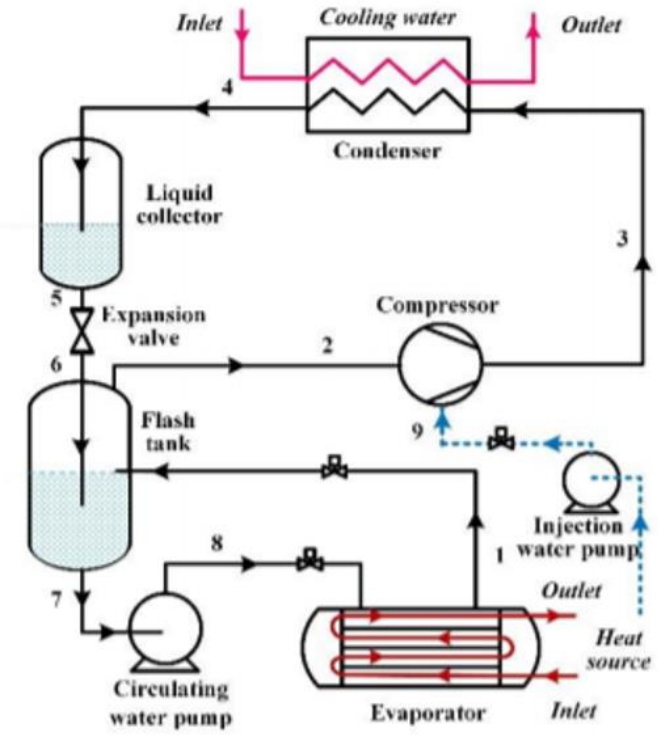

Figure 1 Schematic of VHTHP with a water-injection twin-screw compressor [10]

2. Water vapor twin-screw compressor with liquid injection for VHTHP operation

2.1 Experimental setup

The experimental setup has been explained in previous literature [6] and [7], the schematics of the system can be seen in Figure 1 with the corresponding *p-h* diagram in Figure 2. The system consists of the following components: a falling film evaporator, a flash tank, a compressor, a condenser, a liquid collector, an expansion valve, and a circulating water pump. Liquid is injected into the compressor through three nozzles on both sides of the male and female rotor, and the liquid water is provided from an outside tank and pumped into the system using an injection water pump.

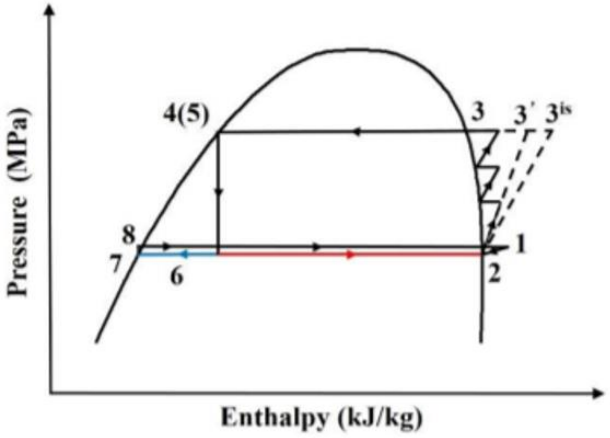

Figure 2 Log p-h diagram of VHTHP with a water-injection twin-screw compressor [10]

The compressor was constructed by Shanghai Hanbell Precise Machinery co LTD,. The compressor itself was modified from an air compressor. The compressor chamber has no lubricating oil, and liquid water is the only fluid injected. There is naturally lubricating oil for the bearings and gears. The compressor has a male to female lobe ratio of 5:7. It is run at 5000 rpm, with an internal compression ratio of 7.

The working principle of the system is built on the well-known VCC (vapor compression cycle). From the evaporator, water vapor (state 1) flows into a flash tank. Pure vapor (state 2) is sucked into the twin-screw compressor where the water vapor is compressed up to the desired condensation pressure (state 3). Liquid water is injected in the compressor to cool down the compressed water vapor to limit the superheat and therefore the compressor work. The high-pressure water vapor then goes through a condenser where heat is provided to a heat sink. The purity of the liquid is guaranteed in a liquid collector (state 5) before the liquid is expanded to a pressure lower than the evaporation pressure (state 6). The expanded water goes through the flash tank, and liquid (state 7) is pumped up to the evaporation pressure (state 8) and into the evaporator, where heat is absorbed from the heat source.

High performance indicators along with a safe and reliable operation with a low GWP and zero ODP refrigerant have caught the attention of researchers around the world. The concept is viewed as one of the most promising VHTHP concepts in the field.

2.2 Thermodynamic model

A thermodynamic model of the abovementioned system was developed using the object-oriented programming language Modelica. A shell from a model of a twin-screw compressor using ammonia-water [8] was used as a starting point. The model is a quasi-one-dimensional numerical model. There are 10 control volumes, where each control volume represents a cavity in the prototype. The control volumes change in size, similarly to the cavities in the prototype, as a function of rotational angle which again is dependent on time and speed of the compressor. As the control volume goes through one complete cycle of suction, compression, and discharge, there are three injection points and two different leakage functions. Mass and energy conservation equations are implemented in each control volume. The thermodynamic state of each control volume is continuously calculated using libraries from TILMedia. The conditions inside each control volume are assumed to be homogenous. However, this is not realistic in an actual compressor cavity, especially when liquid is injected at three different times during the compression process.

3. Results and discussion

3.1 Validation against experimental data

To validate the thermodynamic model, a linear function was made to predict what input parameters should be used for the operating conditions. The prediction function was made to fit 20 out of 22 data points from the experiments. The reason only 20 data points were considered is that if all 22 points were to be considered the overall accuracy of the model would decrease. The two points that are disregarded in the function are the points with the lowest pressure ratio out of the experiments with an evaporation temperature of 85°C. A consequence of elimintating these two data points is that the range where the model is considered valid is limited. The input parameters in the model are the volumetric efficiency, along with the thermodynamic condition of suction-, injection-, and discharge mass flow rate. The outputs are mass flow rate at the suction-, injection-, and discharge port and power consumption of the compressor.

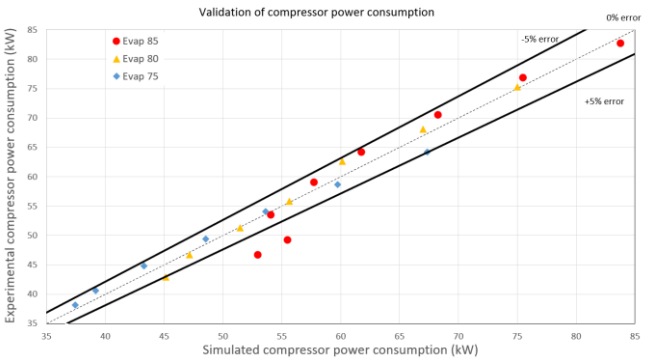

Figure 3 Validation of compressor power consumption

All 22 data points from the experimental investigation of the twin-screw compressor are shown in Figure 3, the two data points outside of the +-5% error range are the two points not included in the prediction function for the inputs. An error of +-5% is an acceptable error, and when considering the uncertainty in the experimental data as well as the fluctuations in the simulations, it is unrealistic to get a more precise outcome than what is presented here.

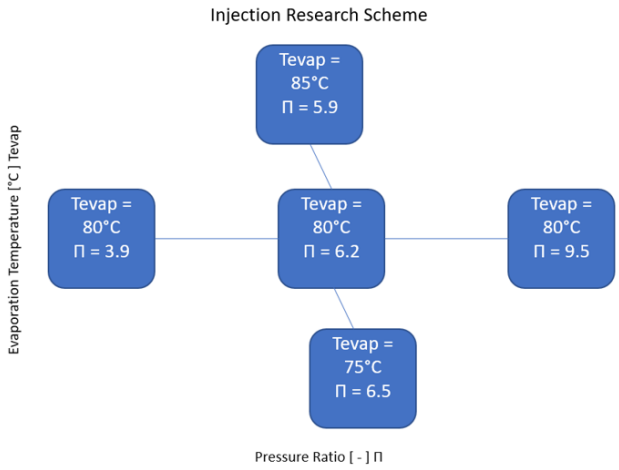

Figure 4 Operating conditions considered for liquid injection optimization study

3.2 Liquid-injection optimization studies

Optimizing the liquid injection in a water-vapor twin-screw compressor is an efficient way of improving the thermodynamic performance of the compressor. Adjusting or implementing injection nozzles can be done without adding much complexity or cost. One of the advantages of making a thermodynamic model of a compressor is that various conditions can be simulated and its thermodynamic performance can be analyzed without going through expensive and time-consuming experimental investigation.

Two different variants of liquid injection study were carried out to optimize the liquid injection to make the compressor operate efficiently from a thermodynamic point of view. First, the amount of liquid injection was studied, then the distribution of the injection was investigated.

Five different operating conditions were tested. Pressure ratio and evaporation temperature were varied in each case to get a representative view of the operating conditions from the experimental data. The cases studies are shown graphically in Figure 4

3.2.1 Injected mass flow rate optimization study

As previously mentioned, the injection in the experiment was done through three nozzles, where the distribution was equally weighted. Based on Figure 5, it appears that more liquid injection leads to less compressor work. For small amounts of liquid injection, the change is significant, likely as a result of the limitation of superheat. If too much liquid is injected, the discharged fluid will be inside the saturation dome and the decrease in compressor power consumption will slow down. To see if the compressor power consumption would increase if there was enough liquid injected, an additional test was done with an injection amount 27 times higher than the injection in the experimental case. It was expected that the amount of mass pumped through the system would lead to an increase in power consumption larger than the effect of a lower enthalpy of the discharged fluid. However, the simulation showed a continuing trend that power consumption continuously decreased with more liquid injected. The mass injection amount at which the effect of limiting the superheat is outweighed by the decerase in enthalpy is dependent on the pressure ratio and evaporation temperature. These can be seen graphically as the the elbow of the data points vary between the 5 operating conditions studied.

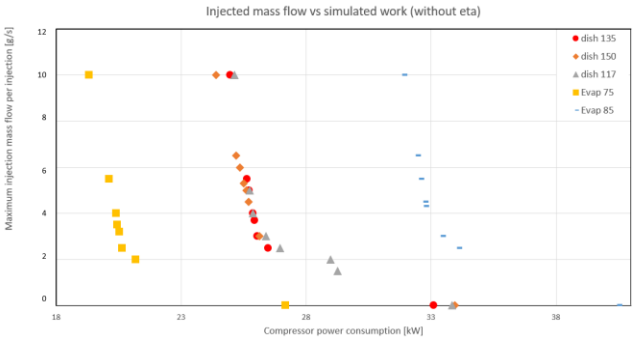

Figure 5 Injected mass flow vs simulated compressor power consumption

The compressor power consumption keeps decreasing as the amount of liquid injected in the simulation increases. To understand why this is not beneficial for the actual operation of the compressor, an investigation of the pressure, temperature, and enthalpy development was conducted (see Figure 6 and Figure 7). It is evident in Figure 6b that liquid inection is beneficial, even in small quantities. In the case without any liquid injection, it is impossible to keep the

discharge temperature below 250°C. In a real application, this discharge temperature would require some changes in material selection to prohibit any damage to the equipment. The highest temperature in the compression phase is close to 330°C according to the simulation. Because the superheat in this case exceeds 200°C the isentropic efficiency of the compressor will be low. There simulation show over-compression at this point, which is indicate wasted compressor power consumption. Thie low pressure rato case is the most sensitive for liquid injection as the built-in compressor ratio is significantly larger than the desired pressure ratio, and over-compression can easily occur.

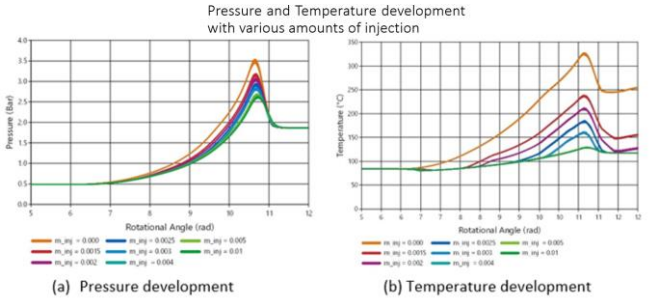

Figure 6 Pressure (a) and temperature (b) development of the compressor simulated at a low-pressure ratio with various amounts of injection

To further study the ideal amount of injection, the development of the enthalpy was investigated. After the enthalpy values of the discharge phase were gathered, they were plotted in a log p-h diagram. This was done to see if the discharge fluid was inside or outside the saturation line. Ideally, the discharge fluid should barely be outside of the saturation line, to ensure vapor condition without redundant superheat. It was found that the discharge fluid was inside the saturation dome when liquid was injected. However, the thermodynamic model assumes instant evaporation of the liquid, as the fluid inside of the compression chamber is homogenous at any instant. The liquid leakage between the chambers is therefore not accounted for. As the fluid in the compression and discharge chamber is a bio-phasic mixture, there is reason to believe the majority of the fluid is in vapor phase, even though the average enthalpy is inside the saturation dome.

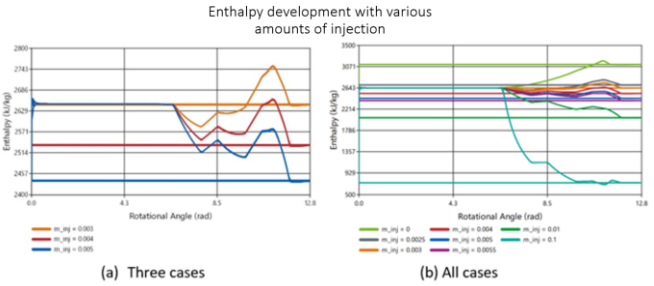

Figure 7 Enthalpy development with various amounts of injection for an evaporation temperature of 85°C (suction pressure of 0.47 bar) and a discharge pressure set to 2.93 bar. (a) shows the three most relevant cases. (b) shows all amounts tested

The downside of too much liquid injection is clear when enthalpy development is evaluated. As seen in Figure 7, several cases with large injection amounts have unreasonable low enthalpy values for the discharge flow, which would mean that the flow is far inside of the saturation dome. When the majority of the fluid in the discharge phase is liquid, the latent heat of condensation is small. With a small latent heat of condensation, the heat provided to the heat sink decreases, and the overall performance of the system is reduced.

3.2.2 Distribution of liquid injection optimization study

The second part of the injection study investigated how the liquid injection could be distributed differently at the three injection nozzles and how this affected the performance of the compressor and heat pump system. The same 5 operating conditions were taken into consideration for this optimization study. 5 new distributions of the liquid injection were considered in addition to the equal distribution case already simulated. All the distributions were conducted for 3 different injection mass flow rates for each operating condition considered.

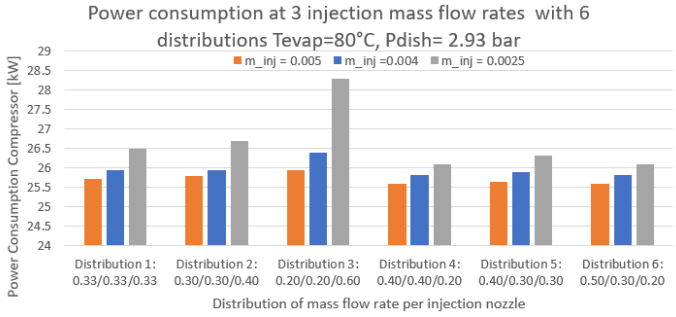

Figure 8 Power consumption at 3 different liquid injection mass flow rates with 6 distributions per mass flow rate (Tevap = 80°C, Pdish = 2.929)

As seen in Figure 8, it is beneficial to inject a larger share of the liquid early in the compression process. Distribution 6 had the lowest amount of compressor work, while distribution 3 had the highest. A higher injection mass flow rate led to

higher compressor power consumption, as expected based on previous results.

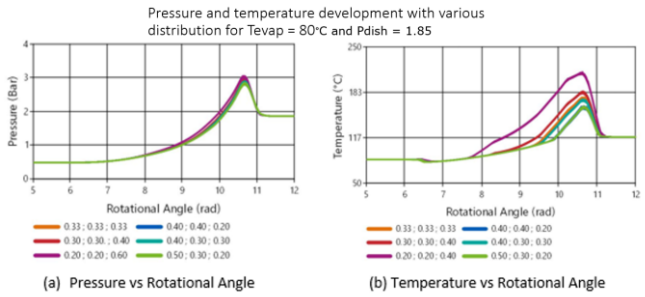

Figure 9 Pressure and temperature graphs of various distributions of m_inj at Tevap 80°C and Pdish = 1.85 with a total liquid injection of 0.008 kg/s

When the temperature and pressure development of the different distributions are considered (see Figure 9) it can be seen that the isentropic efficiency of the compressor should be higher at distributions with more liquid injected earlier in the compression process. This is a result of limited superheat and over-compression.

To further optimize the liquid injection both the enthalpy of the discharged fluid and the compressor work must be taken into consideration. After finding a suitable amount of liquid injection, modifying the distribution can be used to further optimize the performance. In Figure 10 an injection amount that originally seemed too small was tested with different distributions and ended up with a discharged fluid on the saturation line. Even though the compressor work was highest with the distribution that ended up at the saturation line, the gained latent heat of condensation is reason to believe that the overall performance of the system is highest at that condition.

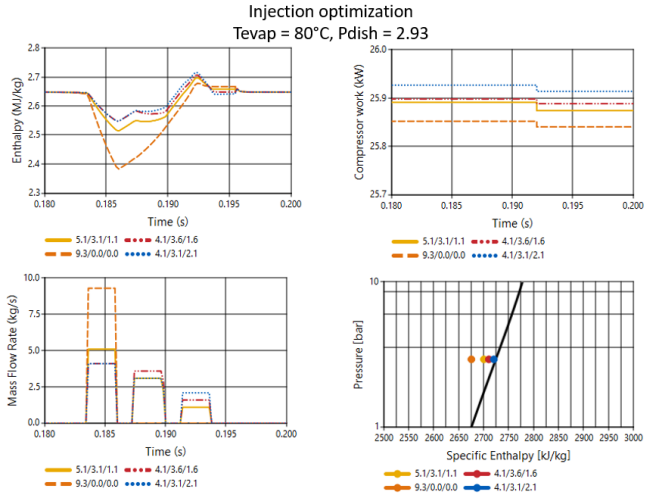

Figure 10 Injection optimization

To increase the reliability of the injection optimization studies, the assumption of the homogenous distribution of temperature and pressure, and therefore a mono-phasic fluid, should be changed. One way of doing this is to model a working chamber as two separate control volumes, where there are mass and energy transfer between the two control volumes which together represent one cavity. If this is done and verified satisfyingly, several other factors of the liquid injection can be challenged. Further research on the optimum temperature and pressure of the liquid injected, the size of the nozzle, implementation of an atomizer in the nozzles, and placement of nozzles can all be performed to further optimize the operation of a water-injected twin-screw compressor in very high-temperature heat pump range.

4. Conclusion

A thermodynamic model of a water-injected twin-screw compressor was developed from an ammonia-water injection compressor. The model was then verified against experimental data provided by Shanghai Jiao Tong University. After the verification, the model was used to study liquid injection, to see how this can be adjusted to optimize the thermodynamic performance of the compressor.

The major findings from the liquid injection optimization study were:

- The model showed that the compressor power consumption decreased with an increased amount of liquid injection. However, through a thermodynamic analysis of the discharged fluid it was concluded that when the enthalpy was lower than the saturation line for the discharge pressure, the overall performance of the system would decrease significantly.
- Furthermore, it was noted that injecting a large amount of liquid early in the compression process decreased the superheat, and therefore the compressor power consumption. When the enthalpy of the discharged fluid was taken into consideration, it was seen that there is a thermodynamic benefit to a more even distribution.
- Each operating condition should be evaluated separately, and the optimal distribution is dependent on the amount of liquid injected and vice-versa.
- To further challenge more factors in the liquid-injection the reliability of the model should be further developed and validated against experimental data for the evaporation of the liquid.

Acknowledgments

This research work was funded by the Chinese-Norwegian collaboration project on Energy(ChiNoZEN) and National Key R&D Program of China (SQ2019YFE010256). The authors also gratefully acknowledge the financial support from the Research Council of Norway and user partners of High EFF (Centre for an Energy Efficient and Competitive

Industry for the Future, an 8-year Research Centre under the FME-scheme).

References

[1] Equinor ASA, "Energy Perspectives 2019," Equinor, Stavanger, 2019.

[2] IEA, "Fuels and technologies - heating," International Energy Agency, 2020.

[3] World Resources Institute, "climate Analysis Indicators Tool," 2017. [Online]. Available: http://cait.wri.org/.

[4] LLC, "Power: News & Technology for the global energy industry," 31 Mars 2017. [Online]. Available: https://www.powermag.com/who-has-the-worlds-most-efficient-coal-power-plant-fleet/. [Accessed February 2020].

[5] K. Haugland, Undersøkelse av Skruekompressorens Arbeidsprocess, Trondheim : NTH - Institutt for kuldeteknikk, 1993.

[6] M. Chamoun, R. Rulliere, P. Haberschill and J. F. Berail, "Dynamic model of an industrial heat pump using water as refrigerant," *International Journal of Refrigeration,* pp. 1080-1091, 2012.

[7] M. Chamoun, R. Rulliere, P. Haberschill and J. Peureux, "Modela-based modeling and simulation of a twin screw compressor for heat pump applications," *Applied Thermal Engineering,* pp. 479-489, 2013.

[8] Chamoun, Rulliere, Haberschill and Peureux, "Experimental and numerical investigations of a new high temperature heat pump for industrial heat recovery using water as refrigerant," *International Journal of Refrigeration,* pp. 177-188, 2014.

[9] J. Shen, Z. Xing, K. Zhang, Z. He and X. Wang, "Development of a water-injected twin-screw compressor for mechanical vapor desalination system," *Applied Thermal Engineering,* pp. 125-135, 2016.

[10] D. Wu, B. Hu and R. Wang, "Theoretical and Experiemental Investigation on a Very High Temperature Heat Pump with Water Refrigerant," in *The 25th IIR International Congress of Refrigeration*, Montreal, 2019.

[11] D. Wu, J. Jiang, B. Hu and R. Wang, "Experimental investigation on the performance of a very high temperature heat pump with water refrigerant," *Energy,* 2020.

[12] E. K. Tønsberg, "Modeling Approach for a Liquid-Injected NH3-H20 Screw Compressor," NTNU, Norway, 2020.

[13] International Energy Agency, "Heating without global warming - market overview, state of the art, research status, refrigerants and application potensials," IEA, Paris, 2014.

[14] World Resources institute, "climate Analysis Indicators Tool," 2017. [Online]. Available: http://cait.wri.org/.

[15] D. Wu, B. Hu, R. Wang, H. Fan and R. Wang, "The performance comparison of high temperature heat pump among R718 and other refrgierants," *Renewable Energy,* pp. 715-722, 2020.

NTNU

Norwegian University of
Science and Technology